An EMG-Driven Cervical Spine Model for the Investigation of Joint Kinetics:
With Application to a Helicopter Pilot Population

by

Jeffery Matthew Barrett

A thesis
presented to the University of Waterloo
in fulfillment of the
thesis requirement for the degree of
Master of Science
in
Kinesiology

Waterloo, Ontario, Canada, 2016

I hereby declare that I am the sole author of this thesis. This is a true copy of the thesis, including any required final revisions, as accepted by my examiners.

I understand that my thesis may be made electronically available to the public.

Abstract

As the workforce has been shifting from manufacturing to office work, reports of neck pain have been on the rise. Unfortunately, the mechanism for the development of chronic neck pain still remains disputed. Most current cervical spine biomechanical models are aimed at the simulation of whiplash and are forward models employing the finite element method or multibody dynamics that are ill-equipped for incorporating motion capture data, with even fewer models capable of interfacing with electromyography (EMG) data. Therefore, there is a considerable opportunity to develop an inverse dynamic model that can drive muscle forces using EMG with the goal of determining the joint mechanics that could lend insight to the loading patterns and injury mechanics in the cervical spine.

The current model is an inverse dynamic multi-body model of the whole cervical spine, head, and thorax. It was created entirely in Python, using anatomical data obtained from the Anatomography project, which were rescaled to match dimensions from a 50^{th} percentile male. Constitutive expressions for ligaments are described by nonlinear springs, while the disc and facet joints are lumped into exponential rotational springs. Active muscle forces are estimated from EMG using a Hill-type muscle modeling framework.

The model has endured a rigorous validation procedure comparing its predicted compression and shear values to a previously published model. The gains for each muscle were analyzed to evaluate how well muscle forces are being predicted from EMG. Finally, a sensitivity analysis was conducted to identify if the outputs of the model were overly dependent on the numeric value of a specific parameter. Overall, compression and mediolateral shear values were in good agreement with the previous model, while anteroposterior shear values were significantly smaller in magnitude. Despite this, muscle gains were, in some cases, alarmingly high. Finally, the sensitivity analysis revealed that the model is somewhat sensitive to ligament and muscle slack lengths, albeit to a much lesser extent than previously published models.

The model was used to evaluate the change in joint kinetics with a flexed posture compared to a neutral one. With 45° of flexion, compressive forces increased twofold throughout the cervical spine. In addition, anteroposterior shear tended to increase fourfold in the upper cervical spine, however, equalized with a neutral posture around the C4-C5 level. These findings may have implications for injury mechanisms, as a flexed posture under compression has been strongly associated with the development of posterior disc prolapse.

In addition, the model was used to assess the joint kinetics from an existing data set on helicopter pilots who are required to wear night vision goggles during night flights. The classic solution to the anteriorly placed weight of the night vision goggles has been to counterbalance it with a posterior counterweight. While this works theoretically in a neutral posture, once a deviated posture is assumed, joint kinetics correspondingly increase. Adding a helmet increased the compression at C5-C6 from 204 N to 258 N, a 26% increase. Furthermore, adding night vision goggles and a counterweight increased it by 60%. Increasing the mass of the head-segment leads to an increase of compression.

Acknowledgements

I am grateful for the encouragement, guidance and insight of my supervisor, Dr. Jack Callaghan. I doubt that words could express how grateful I am for your mentorship throughout my undergraduate and graduate studies. Although, I would like to apologize for the times I, tired and defeated, meandered my way into your office following a particularly challenging all-nighter, only to unload a fusillade of vaguely coherent complaints in your direction.

I am appreciative of my committee members, Drs. Andrew Laing and Clark Dickerson, for their valuable insight in finalizing the document and asking the hard questions. Both the quality of this work, and myself, are better for it.

I would like to thank Dr. Stacey Acker, who, many years ago now, hired me for a co-op position in her lab. Were it not for this position, I would have never considered research or graduate school, much less pursued subsequent co-op jobs in Dr. Callaghan's lab.

My fellow lab members who were always there to offer encouragement and support, this would have been an abysmal failure without you: David Kingston, Daniel Viggiani, Maureen Riddell, Colin McKinnon, Kayla Fewster, Michał Glinka, Johnny Park, Graham Mayberry, Kristina Gruevski, and Mamiko Noguchi. I would also like to acknowledge the acknowledgment section of Daniel Viggiani's master's thesis for inspiring this acknowledgments section. In addition, a handful of individuals outside my lab who were also there to endure the ramblings of sleep-deprived Jeff: Dr. Ed Cambridge, Frederick Goh, Dan Martel, and Taylor Winberg. In particular, the Scotsman Jordan Cannon, whose insight in scientific discussion, company on the frequent coffee runs, and provision of hilarious stories was always appreciated.

From outside kinesiology, in sociology, my good friends, Alexander Graham and Pierson Browne, whose wise counsel belies their years. Lastly, Gregory Metcalfe, a geographer and good friend who has put up with me as a roommate since undergrad.

Denise Hay, Margaret Burnett and Cheryl Kieswetter took care of the many thankless administrative jobs, which made the entire experience seamless.

I've been fortunate to have had the financial support of the National Sciences and Engineering Research Council of Canada (NSERC). I hope it was put to good use!

Lastly, my loving family: my wonderful parents, Michael and Rosemary, for their unconditional support and understanding when I was away for vast stretches of time; my brothers, Nicholas, Jacob, and Darin, for your antics; and my sisters, Rebecca and Lorabeth, for being generally supportve; and my (mother's) dog, Misty.

Thank you.

Table of Contents

List of Tables

List of Figures

Chapter 1

Introduction

1.1 Epidemiology of Chronic Neck Pain

As employment shifts from manufacturing to office work, the prevalence of musculoskeletal disorders, such as back and neck pain, has been on the rise in Canada, with an annual incidence of 13.2% (Côté et al., 2004). In Québec, there is an estimated 47.8% annual prevalence of neck pain (Holm et al., 2008). In Saskatchewan, two-thirds of the population are expected to experience neck pain at some point in their lives; and in Ontario, neck pain constitutes 3 – 12% of total lost time claims (Côté et al., 2009, 1998). Sadly, most individuals who suffer neck pain do not experience complete remission of their symptoms and disability (Côté et al., 2004; Vasseljen et al., 2013). Therefore, there is considerable benefit to the primary prevention of neck pain from work, both in counteracting its economic burden and halting its deleterious impact on the quality of life of those suffering.

Unfortunately, the underlying mechanism explaining the cause of chronic neck pain remains elusive. Recently, a possible mechanism has been proposed linking chronic neck pain to what is considered maladaptive muscle activity (Falla et al., 2007, 2004). These investigators have reported aberrant muscle control in the 'agonistic' muscles during upper limb tasks, most notably the upper trapezius and anterior scalene muscles, which they believe to be related to their patients' neck pain. Specifically, an increase in co-contraction in these superficial muscles, with a marked decrease in activation of the deep cervical spine muscles, is associated with neck pain (Jull, 2000). A musculoskeletal cervical spine model is well suited for investigating the implications of these authors' claims and uncovering potential injury mechanisms. Furthermore, a musculoskeletal model of the cervical spine may help inform ergonomic efforts, similar to prior low-back and shoulder modelling approaches (Dickerson et al., 2007; McGill, 1992).

Neck pain is disproportionately high among air force personnel, most notably helicopter pilots, where the prevalence of neck pain is between 43 and 97% (Adam, 2004; Lange et al., 2011; van den Oord et al., 2010; Bridger et al., 2002). Visibility is critically important for this occupation, where pilots need to navigate, control, and land a six degree-of-freedom aerial vehicle. Night flying is made possible by the use of night vision goggles, which enable the pilot to see light into the near-infrared spectrum, but at the cost of dramatically reducing their peripheral vision and increasing the weight of their helmets. The anteriorly placed mass from the night vision goggles naturally induces a flexion moment which the neck extensors need to actively combat. As they are military personnel, they are required to wear ballistically certified helmets while on the job, which conflates the already problematic

muscular demands of the neck. The combination of awkward postures, high load, and repetition are a perfect storm for the development of musculoskeletal disorders. Preliminary work has quantified the neuromuscular and mechanical demands of the job (Callaghan et al., 2014; Forde et al., 2011). However, these investigations have, thus far, fallen short of quantifying the loads experienced at the level of the intervertebral joints once muscular forces have been accounted for. The model presented in this paper is capable of quantifying the compression and shear forces in the intervertebral joints.

1.2 Modelling Philosophy

1.2.1 What is a Model?

Models are simplified abstractions of phenomena, but can be used to gain insight into its behaviour under certain conditions (Alexander, 2003; Sargent, 1998), a sentiment eloquently summarized in George Box's famous quote, "*All models are wrong; but some are useful*" (Box and Draper, 1987).

There are many types of models, but broadly speaking, they can be categorized as physical, mathematical, or conceptual (Alexander, 2003). A physical model is a physical recreation of the system of interest with simplified parts. A conceptual model is a simplification of a complicated phenomenon into a series of simpler ones often by analogy (Alexander, 2003). In contrast, mathematical models are quantitative descriptions of the system of interest, sometimes predicting how it will evolve in time (Alexander, 2003; Basmadjian, 1999; Hicks et al., 2014; Sargent, 1998). For example, Newton (1687) noticed

that the product of mass and velocity is a conserved quantity, which he called *momentum*. He noticed that objects could interact with each other to increase or decrease their momentum, and he called these interactions *forces*. He summarized these observations with his famous Second Law of Motion:

$$\frac{d}{dt}\left(m\frac{dx}{dt}\right) = F \tag{1.1}$$

Where m is the object's mass, dx/dt is the velocity, and F represents the sum of all forces acting on the object. This is a differential equation in the position of the object, however, it is not a closed equation – it is one equation in several unknowns: the particle's position as well as all forces acting on it. In order to solve for the position of the object, knowledge of how the forces depend (if at all) on the current state of the system are required. These models relating quantities in a system are known as *constitutive equations* or *auxiliary relations* (Basmadjian, 1999). For example, in his Principia Mathematica, Newton (1687) proposed a constitutive equation for the gravitational force:

$$\frac{d}{dt}\left(m\frac{dx}{dt}\right) = -\frac{GMm}{(R+x)^2} \tag{1.2}$$

Where G is Newton's Gravitational Constant, M is the mass of the Earth, R is the radius of the Earth, and x is the distance of the object above the surface of the Earth. Like most models, it has no analytic solution[1] (Basmadjian, 1999). Generally speaking, there are two ways to deal with this: (i) resort to numerical techniques to give an approximation to the solution of this differential equation, in which case the model can be sub-classed

[1] i.e. It is not possible to write down a closed-form expression for $x(t)$.

as a *computational model* (Sargent, 1998) or (*ii*) make a simplification of the equations of motion so that they can be solved. In this case, the assumption that the x on the right hand side is negligible compared to the radius of the Earth yields the *projectile motion model*:

$$\frac{d}{dt}\left(m\frac{dx}{dt}\right) = -\frac{GMm}{R^2} = -mg \tag{1.3}$$

Where $g = \frac{GM}{R^2} = 9.81\frac{\mathrm{m}}{\mathrm{s}^2}$ is the acceleration due to gravity. This is a much simpler equation of motion, only valid when x is much smaller than R. Transparency about assumptions like this is extremely important, since it would be inappropriate to use model 1.3 when x is large – applying it to the motion of the moon relative to Earth, for instance, would violate that assumption and output poor results.

Although Newtonian gravity (equation 1.2) was able to accurately predict the motion of celestial bodies, it did not give much explanation for exactly how gravity works (Feynman, 1963). Such a mathematical model is termed a *phenomenological model* to distinguish it from *mechanistic models* which begin with a description of how a process works first, then mesh it with the appropriate model equations (Frigg and Hartmann, 2012).

Another notion in the philosophy of modelling is *simulation* (Sargent, 1998). The act of simulating a phenomenon is using a model to map initial conditions and parameters onto the corresponding outputs.

1.2.2 Verification and Validation

Two important concepts in modelling are *verification* and *validation*. Intuitively, verification asks if one is solving the equations correctly; while validation asks if one is solving the correct equations (Babuska and Oden, 2004; Hicks et al., 2014; Popper, 1959; Sargent, 1998).

Verification of a computational model involves evaluating if the algorithms used to solve a problem are actually solving the problem, and whether the implementation of these algorithms are correct (Babuska and Oden, 2004; Sargent, 1998). This requires comparing model outputs to known standards, or matching the output of another verified model. Because of the difficulty of this step, it is often recommended to use commercial software for modelling, since commercial software is likely to have endured rigorous verification tests (Hicks et al., 2014).

Validation is a much more complicated process since there are many types of validity with no relationship between them (Babuska and Oden, 2004; Sargent, 1998).

1. *Content Validity*: the degree to which the model includes all of the necessary components of the system.

2. *Operational or Criterion Validity*: the degree to which the model outputs agree with experimental results.

3. *Face Validity*: the degree to which experts in the field accept the reasonableness of a model prior to formal validation.

Models can exhibit some or all types of validity. For instance, a statistical regression model may have excellent operational validity, but lack any governing mechanism and therefore have very little content validity. Conversely, a model could include the minutest features of a physical system and still disagree with experiment.

By far the most common use of the word validity in modelling is that of operational or criterion validity. The standard procedure for evaluating this is to provide the model similar initial conditions or forcing terms to those seen in nature, and comparing the outputs of the model to what is observed. To account for variability, there is usually a corridor for which the model's performance is considered allowable – within a 95% confidence interval, for example (Sargent, 1998).

1.3 Global Thesis Questions and Hypotheses

Given the degree of debilitation observed in those with chronic neck pain juxtaposed with the small probability of remission, there is a considerable benefit to preventing its onset. The catalyst for chronic neck pain is believed to be mechanical in nature, justifying the biomechanical modeling approach taken in this thesis. Since the problem is exacerbated in helicopter pilots, likely due to the combination of helmet and night-vision goggles, it may be useful from an ergonomic point-of-view to understand the underlying joint kinetics. Such improved resolution of mechanical information may help inform future designs of equipment.

1.3.1 Does Flexion Impact the Loads on the Cerivcal Spine?

Ariens et al. (2000) flagged a prolonged, flexed cervical spine posture as a major risk factor for the development of chronic neck pain. In addition, Tampier et al. (2007) has presented a compelling biomechanical mechanism linking repeated flexion to the initiation and presentation of disc herniation. Because of this plausible pathway leading from repeated flexion to chronic neck pain, the question remains how adopting a flexed posture directly affects the compression and shear forces acting on the intervertebral joints in the cervical spine. To examine this, bone-on-bone forces predicted from a neutral posture can be compared to that of a flexed posture.

In a flexed posture, the center of mass of the head is positioned anteriorly to the trunk, inducing a flexor moment throughout the cervical spine that must be balanced by the extensor musculature on the posterior neck. This observation has been verified before (Bonney and Corlett, 2002; Snijders et al., 1991), and an informal calculation suggests that the joint moment scales with the sine of the flexion angle, mass of the head, length of the neck, and magnitude of gravity. More subtly, in a flexed posture, the gravitational force acts to shear vertebrae relative to one-another, which requires muscular involvement to buttress against (McGill and Norman, 1986). Therefore, the magnitude of the muscular recruitment should scale more dramatically than what is required to balance the external gravitational moment. A cervical spine model is well suited to test this hypothesis by computing the joint kinetics required to hold static postures and, with the aid of electromyography, deduce what the net compression and shear forces are on the vertebrae. If results from the proposed model refute this hypothesis, then the net joint moment needed to balance the external

load and/or buttress the shearing forces may come from the passive constituents of muscle, or from the ligaments. This argument motivates the following hypothesis:

Hypothesis One: Posture will magnify the bone-on-bone loads in the cervical spine, which will also be higher at the C4-C5, C5-C6 and C6-C7 levels. The rationale for singling out these levels comes from the studies of Kelsey et al. (1984), who reported that the site of intervertebral disc herniation in the cervical spine is highest at the C6-C7 level, followed closely by the C5-C6 level; and that of Matsumoto et al. (1998), who reported the highest levels of posterior disc prolapse to be at the C5-C6 level, followed closely by the C6-C7 and C4-C5 levels.

1.3.2 Does Helmet Use Impact the Joint Mechanics in the Neck?

The increased mass of the head and helmet system should, naturally, increase the force of gravity acting on the entire cervical spine. Because of this, a neutral posture should experience more compressive forces when a helmet is present. Similarly, if there are effects of posture on the kinetics of the cervical spine, as hypothesized earlier, then these effects should be magnified when a participant is helmeted. Previous investigations found only modest interactions between helmeted participants and posture on neck muscular activity (Thuresson et al., 2003; Callaghan et al., 2014), which seems to imply that kinetics might not be very different with or without a helmet. Conversely, a similar investigation found that a novel elastic helmet strap which provided a supplementary extensor moment had a substantial impact on electromyography collected from cervical spine extensors (Dibblee et al., 2015). The supplemental extensor moment from the elastic strap alleviates the role

of the musculature in providing a counter-moment against the helmet's weight. In either case, there has yet to be a detailed analysis of the resulting kinetics of the cervical spine.

As discussed earlier, the gravitational force acting on the night vision goggles naturally induce a flexor moment which the neck extensors need to negate. The classic solution to this problem has been the adoption of a counter-weight placed posteriorly on the helmet. This counter-weight supplies a supplementary extensor moment, which, theoretically, reduces the required extensor moment from the cervical musculature when the spine is neutral and the head is upright. However, once the spine deviates from neutral, the increased mass may serve to dramatically increase the muscular demand in order to balance this gravitational moment.

Hypothesis Two: Helmet-use will be associated with larger magnitudes of compression and shear, which will further increase with the use of night-vision goggles. Of course, this hypothesis is motivated by the above mechanical reasoning. In addition, the suspiciously high prevalence of chronic neck pain among helicopter pilots speaks to a mechanical catalyst looming in the background. It stands to reason that the joint mechanics would be altered by the use of a helmet and night vision goggles.

1.3.3 Objectives

To test the above hypotheses, the goal of this project was to develop a computational model of a 50^{th} percentile male human cervical spine in order to assess the joint kinetics of the neck in simulated helicopter helmet wearing tasks. Briefly, the model uses inverse dynamics to compute the net joint moments and forces required to produce the external

motions, and then partitions the net joint moments amongst the muscles at each joint in an EMG-driven manner. More formally, the objectives of the proposed research are:

1. To develop and validate a model of the cervical spine.
2. To provide visual and numerical representations of cervical spine joint kinematics.
3. To design the model in a way that makes it programmatically easy to adapt to different musculoskeletal geometries, add different anatomical features not considered in the base-model, and apply it to different situations and studies.
4. To use the model to evaluate the loads on the cervical spine in frequently encountered postures.

Chapter 2

Literature Review

"If I have seen further, it is by standing on the shoulders of giants."

– Sir Isaac Newton

Before starting this review, I knew creating a biomechanical model of a cervical spine would be a challenging, yet possible, task. Upon starting, I was immediately struck with a sense of *where to start?* Over the last four decades, biomechanists have made leaps and bounds in the understanding of cervical spine injury in car accidents, tensile loading, and fringe impact scenarios – it goes without saying that the cervical spine literature is immense. Additionally, since the early twentieth century, biophysicists and physiologists were devising methods for the modelling of skeletal muscle tissue, which has progressively evolved into the detailed models used today. These are the giants whose shoulders I will be standing on.

This review begins where anyone modelling a part of the body should begin: with the anatomy. While the anatomy will describe, geometrically, the structures that should be included in a model, the next section describes, in detail, the mechanical properties of those structures with a focus on the cervical spine: from ligaments to the functional spinal unit. The third section revolves around the modelling of both the activation and contraction dynamics of muscular tissues. Following this, there is a discussion on the trials and tribulations of the past forty years of neck modelling. The review wraps up with a section addressing the current gaps in the literature.

2.1 Anatomy of the Cervical Spine

The neck is the anatomical region which spans the thoracic inlet to the base of the skull. It houses the respiratory, gastrointestinal, nervous, arterial, and venous pathways between the head and the thorax; the thyroid and parathyroid endocrine glands; the larynx and the vocal cords; and some muscles of facial expression. In addition to its role as conduit for all of these structures, it also affords an impressive range of motion, for which it is outfitted with a complex musculature and highly specialized osteoligamentous structures. This section describes this complicated anatomy from bones, to ligaments, and finally muscles.

2.1.1 Osseous Members

The human cervical spine is composed of seven vertebrae, labelled C1 through C7. Because of the different morphological characteristics of the cervical vertebrae they are

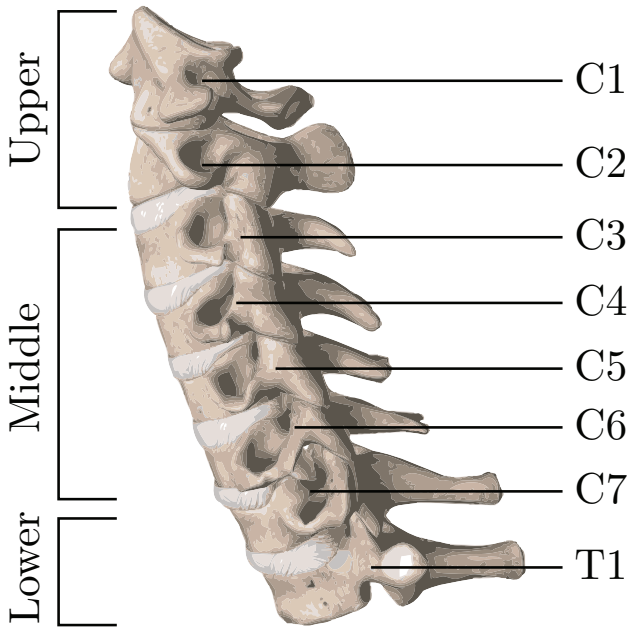

Figure 2.1: Regions of the cervical spine. Image adapted from Essential Anatomy (3D4Medical Inc., San Diego, CA).

subdivided (Figure 2.1) into the upper, C1 and C2, middle, C3 to C6, and the lower cervical spine, C7 to T1; here T1 is the first thoracic vertebra, included in the last section as an honorary member of the cervical spine (Benzel et al., 2004). Another distinction is that of typical versus atypical vertebrae, where the typical vertebrae (C3 to C6) conform to the same morphology while the atypical vertebrae (C1, C2 and C7) do not.

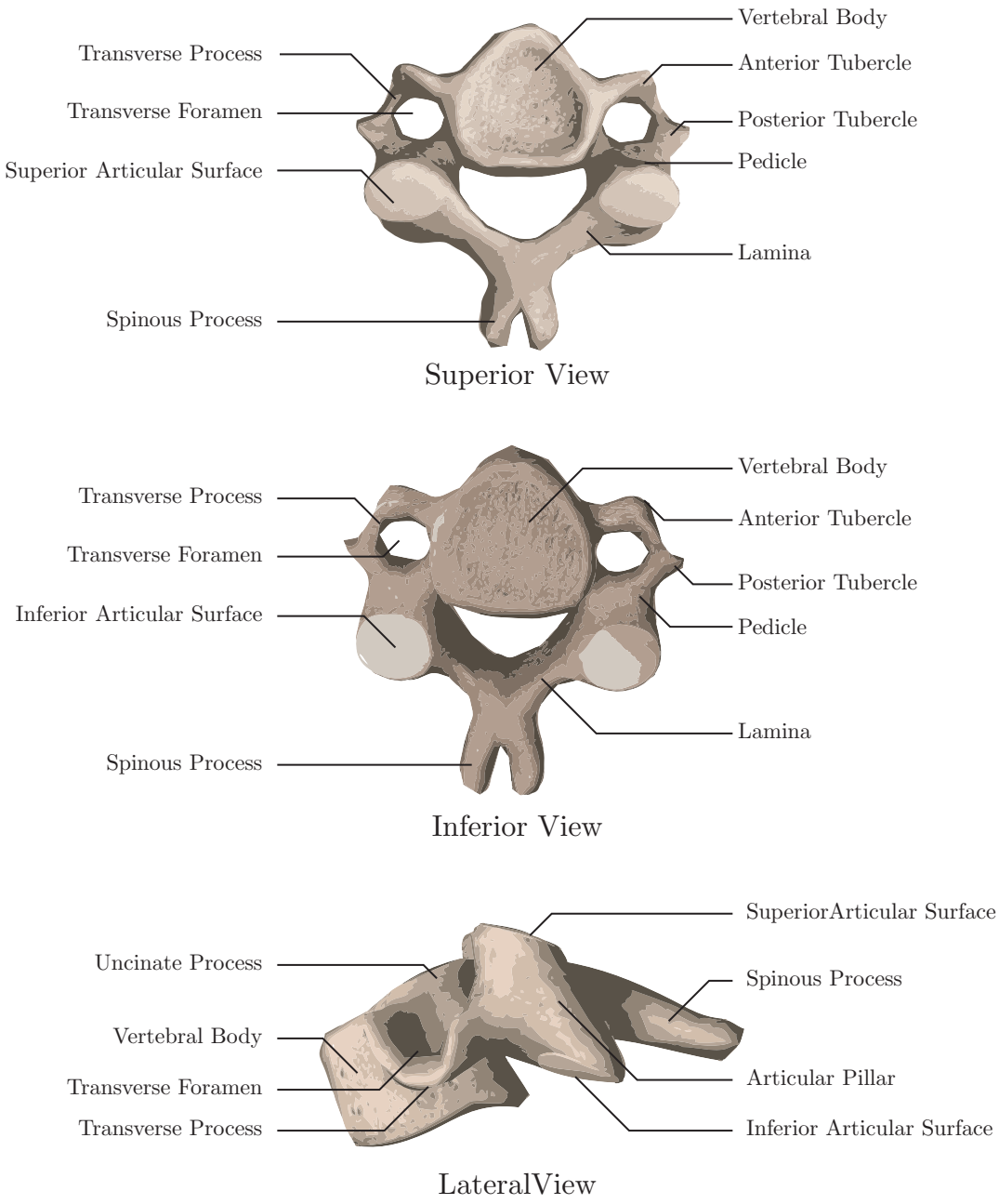

Figure 2.2: A typical cervical vertebra (C5) and the anatomical landmarks on it from a superior (top), inferior (middle) and lateral (bottom) view. Image adapted from Essential Anatomy (3D4Medical Inc., San Diego, CA).

The typical cervical vertebrae (Figure 2.2) have a cylindrically shaped vertebral body, with an interior consisting of an elaborate network of trabecular bone, and its boundary coated with a thin (0.40 — 0.70 mm thick) layer of strong cortical bone (Panjabi et al., 2001a). Both the superior and inferior surfaces of the vertebral bodies have a saddle shape: the superior surface being convex in the anterior-posterior direction while concave in the mediolateral direction and vice-versa for the inferior surface (Benzel et al., 2004). This concavity is particularly notable on the posterior-lateral borders of the superior surface, where a bony process projects superiorly known as the uncus (or hook), which overlap with the caudal vertebrae forming the uncovertebral joint (formerly known as the Joints of Luschka) (Benzel et al., 2004). The articulating surfaces of the vertebral bodies are coated by a thin layer of hyaline cartilage known as the end-plate, which transitions to the intervertebral disc (Standring, 2008).

Projecting laterally from the vertebral body are the transverse processes, which divide into an anterior and posterior tubercles for muscle attachment. The anterior tubercle of the sixth cervical vertebra (C6) is particularly pronounced, and anatomically occurs where the vertebral artery diverges from the common carotid artery (Benzel et al., 2004). Because of this it is known as the carotid tubercle, although it also goes by its archaic name of Chassaignac's tubercle. Through the center of the transverse process is the foramen transversarium (or transverse foramen), which acts as a channel for the vertebral artery and vein. Posterior to the transverse processes is the articular pillar, which houses articulating surfaces on its superior and inferior sides which will form the zygopophyseal joints (or facet joints) with the corresponding superior or inferior vertebrae respectively (Benzel et al., 2004). Between the two articulating vertebrae are small menisci, and the entire joint

is encased in a ligamentous joint capsule (Mercer and Bogduk, 1993). The facet joints in the upper cervical spine are oriented approximately 45 degrees from the transverse plane, and gradually become more vertical as they transition to thoracic vertebrae (Francis, 1955; Panjabi et al., 1991a). The pedicles project posteromedially to form the lamina, until it meets with the contralateral lamina to form a bifurcated spinous process.

The vertebral body of caudal vertebrae are generally wider and taller than more cranial ones, owing to the biomechanical demand imposed on them from bearing more mass (Gilad and Nissan, 1986; Nissan and Gilad, 1984; Panjabi et al., 1991e). The typical height is between 13 and 15 mm, with a width of approximately 20 mm (Gilad and Nissan, 1986; Pooni et al., 1986). Males generally have larger vertebrae than females, although the scaling is not constant across all dimensions, unlike the appendicular skeleton (Gilsanz et al., 1997; Vasavada et al., 2008). Typical vertebrae dimensions are summarized in Table 2.1 for the dimensions specified in Figure 2.3.

Table 2.1: Summary of vertebral body dimensions, means (standard deviations) from C2 to C7. Adapted from Panjabi et al. (1991a), Nissan and Gilad (1984), and Gilad and Nissan (1986). Dimensions are as specified on the row-heading. Dimensions are labelled in Figure 2.3

Item	**C2**	**C3**	**C4**	**C5**	**C6**	**C7**
SBD (mm)	12.6 (2.1)	14.8 (1.5)	15.5 (1.7)	15.5 (1.7)	16.0 (1.7)	16.4 (1.4)
IBD (mm)	15.3 (1.6)	15.6 (1.5)	15.8 (1.5)	16.1 (1.5)	16.6 (1.4)	16.3 (1.4)
ABH (mm)	19.0 (3.2)	14.1 (1.3)	13.4 (1.3)	12.7 (1.3)	13.0 (1.3)	14.6 (1.4)
PBH (mm)	16.6 (2.5)	14.5 (1.4)	13.9 (1.2)	13.8 (1.4)	13.9 (1.6)	14.9 (1.4)
SBW (mm)		15.8 (0.46)	17.2 (0.66)	17.5 (0.58)	18.5 (0.55)	21.8 (0.66)
IBW (mm)	17.5 (0.52)	17.2 (0.29)	17.0 (0.49)	19.4 (0.40)	22.0 (0.75)	23.4 (0.98)
SPL (mm)	33.7 (1.39)	29.6 (0.78)	30.3 (1.07)	28.5 (0.98)	34.2 (1.88)	45.7 (0.84)
SPA (°)	10.7	14.4	12.1	6.1	3.8	7.3
TPW (mm)	52.6 (2.08)	50.3 (1.62)	48.5 (2.14)	46.4 (2.97)	49.5 (2.11)	66.6 (1.13)

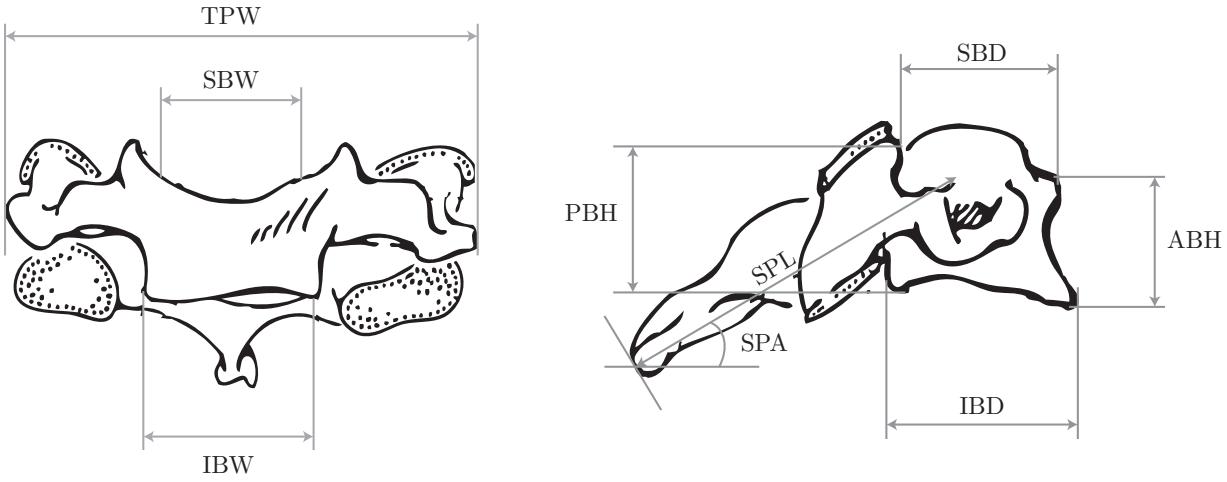

Figure 2.3: Dimension legend for the measurements in Table 2.1, images adapted from Panjabi et al. (1991a).

The first cervical vertebrae, C1, is also called the atlas. The atlas is a very unique vertebra anatomically as it lacks a vertebral body, giving it a characteristic ring-like shape (Figure 2.4). On the anterior arch of the ring is a distinct anterior tubercle, whereas a small posterior tubercle projects out of the posterior arch where a spinous process would normally be present. The ring extends laterally into prominent transverse processes, which, like the typical vertebrae, contain the transverse foramen, a conduit for the vertebral arteries and veins (Moore and Dalley, 2005). These prominent transverse processes make the atlas the widest vertebra (Doherty and Heggeness, 1994). It articulates superiorly with the occipital bone of the skull with two kidney-shaped concave articulating surfaces wherein the convex occipital condyles rest to form the Atlanto-occipital joints (OCC-C1). Inferiorly, it articulates with C2 through two circular convex articulating surfaces on the inferior side of the vertebrae forming the atlanto-axial joint (C1-C2) (Benzel et al., 2004). Unlike the rest of the vertebral column, neither the atlanto-occipetal nor the atlanto-axial

joints possess an intervertebral disc (Benzel et al., 2004; Moore and Dalley, 2005; White and Panjabi, 1990). Typical dimensions for the atlas are summarized in Table 2.2.

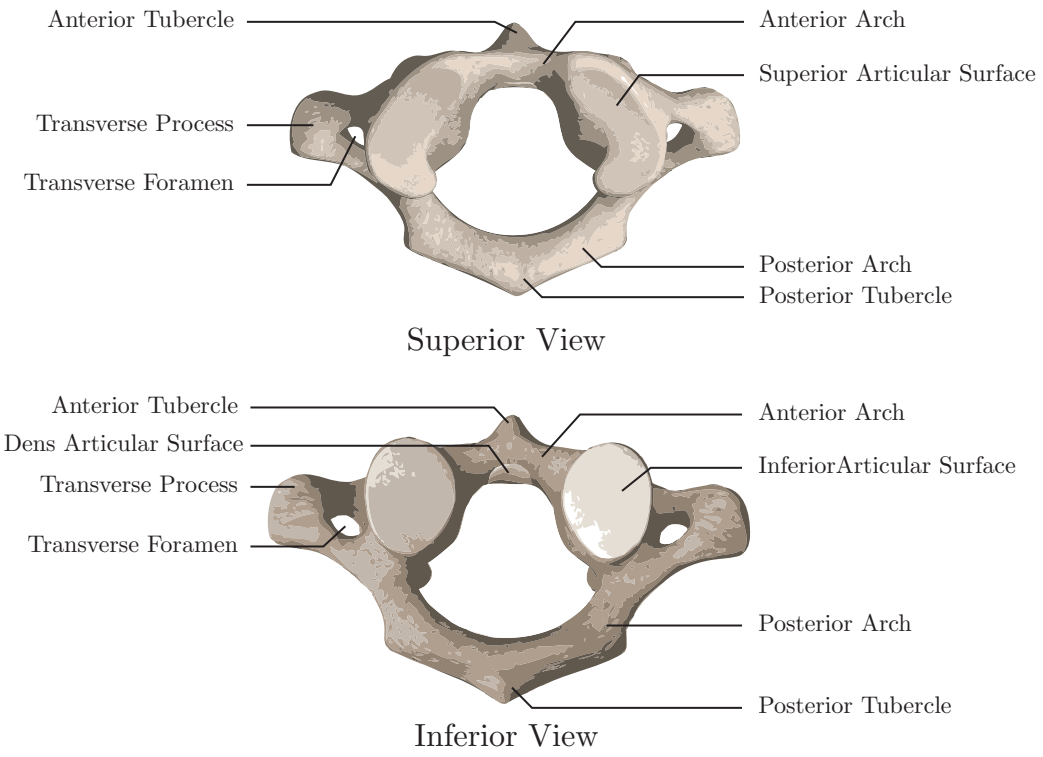

Figure 2.4: Atlas from a Superior View (Above) and from an Inferior view (below). Image adapted from Essential Anatomy (3D4Medical Inc., San Diego, CA)

The second vertebra has four common aliases: C2, the epistropheus, vertebrae dentata, and, most commonly, the axis (Benzel et al., 2004). Its appearance is very similar to a typical cervical vertebra, only lacking an anterior tubercle on the transverse processes (Figure 2.5). The most notable anatomical distinction of the axis is the presence of the odontoid process (or dens) which projects superiorly from its vertebral body, providing a hinge for the atlas to pivot upon in rotation (Doherty and Heggeness, 1995). On either

Table 2.2: Summary of atlas dimensions (mean (standard deviation)), adapted from Doherty and Heggeness (1994).

Dimension		**Mean (SD)**
Vertebral Foramen Diameter (mm)	Mediolateral	32.2 (2.3)
	Anterior-Posterior	31.7 (2.2)
Overall Height (mm)	Anterior	15.4 (3.2)
	Posterior	10.0 (1.8)
Overall Width (mm)		78.6 (8.1)
Overall Length (mm)		45.8 (2.9)
Anterior Tubercle Length (mm)		6.4 (1.0)
Posterior Tubercle Length (mm)		8.0 (2.1)

side of the dens are large, convex articulating surfaces which meet with the convex inferior articulating surfaces of atlas. On the posterior aspect of C2 are the convex inferior articulating surfaces, which connect with the superior articulating surfaces of the third cervical vertebra. The anatomy of the axis is different between males and females and has been used to forensically sex skeletal remains (Bethard and Seet, 2013; Heller et al., 1992; Marlow and Pastor, 2011), where male axis tend to be taller and longer, but have similar sized vertebral canals and odontoid processes. Typical dimensions of the axis are summarized in Table 2.3.

The diameter of the dens at its base near the vertebral body is narrower than toward the top (Doherty and Heggeness, 1994), with articular surfaces on its anterior and posterior borders. The anterior border articulates with the atlas, while the posterior border provides a groove for the transverse ligament to attach.

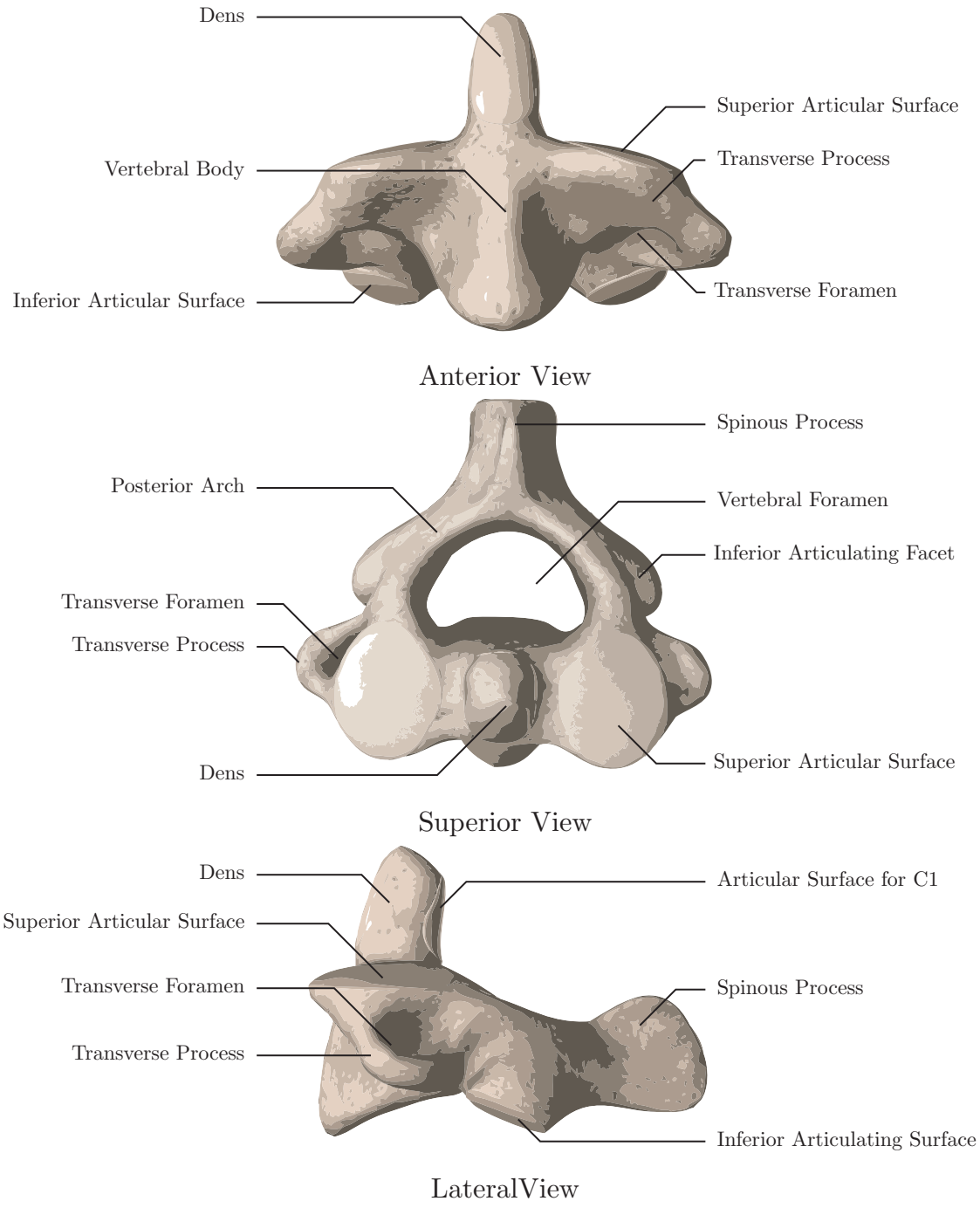

Figure 2.5: Axis from an anterior view (above), from a superior view (middle), and from an Inferior view (below). Image adapted from Essential Anatomy (3D4Medical Inc., San Diego, CA)

Table 2.3: Summary of axis dimensions.

Dimension	**Doherty and Heggeness (1995)**	**Marlow and Pastor (2011)**		**Heller et al. (1992)**	
		Males	Females	Males	Females
Vertebral Body Height (mm)	23.3 (1.9)				
Dens Height (mm)	16.6 (2.5)				
Total Height (mm)	39.9 (3.0)	38.97 (2.26)	36.18 (2.09)	39.0 (2.3)	36.5 (2.8)
Total Length (mm)		50.22 (2.45)	46.50 (2.72)		
Dens Upper AP Diameter (mm)	11.2 (1.0)	11.86 (0.81)	11.20 (0.67)		
Dens Upper ML Diameter (mm)	10.8 (1.0)	10.65 (0.78)	10.05 (0.89)		
Dens Lower AP Diameter (mm)	10.8 (1.0)			6.5 (1.2)	5.8 (0.9)
Dens Upper ML Diameter (mm)	9.9 (1.3)			4.6 (1.1)	4.3 (1.4)
Dens Angle w.r.t Sagittal (°)	13 (9.0)				
Foramen AP Diameter (mm)	16.5 (1.7)	16.54 (1.94)	15.77 (1.47)		
Foramen ML Diameter (mm)	23.6 (1.6)	23.34 (1.33)	23.12 (1.48)		

The seventh cervical vertebra, C7 is also called vertebra prominens, because of its prominent, unified spinous process (Moore and Dalley, 2005). Like the typical vertebrae it has transverse processes with a transverse foramen. However these structures lack anterior tubercles (Standring, 2008). The transverse processes contain a transverse foramen which houses the vertebral vein, but not the vertebral artery (Standring, 2008). Orientation of the facets at C7 are vertical and smoothly transition with the thoracic spine.

The hyoid bone is a U-shaped bone suspended in the mid-neck, at the C3-level, by muscular attachments and articulations with the thyroid cartilage, unique in the sense that it does not articulate with any other bone. The body of the hyoid bone projects laterally and posteriorly in the greater horns, while the lesser horn projects superiorly. It has a functioning role in swallowing and provides a movable origin point for the tongue, although it does not appear to play a critical role in the moment generating capacity of the cervical spine (Moore and Dalley, 2005).

2.1.2 Ligamentous Members

Ligaments in the cervical spine can be broadly subcategorized into two distinct groups: those of the upper cervical spine and those of the lower (and middle) cervical spine. The upper cervical spine possesses many of the same ligamentous structures as the middle and lower regions of the cervical spine, in addition to specialized ligaments to stabilize the interactions between the occiput, atlas, and axis. While the upper cervical spine is highly specialized to permit axial rotation, the middle and lower cervical spine functions in a similar manner to the rest of the vertebral column. Therefore, it is not surprising to find

similar ligamentous structures in this region as in the rest of the column, possessing the anterior and posterior longitudinal ligaments, the ligamenta flava, and the interspinous ligaments.

Ligaments of the Middle and Lower Cervical Spine

The anterior longitudinal ligament (ALL) is continuous along the anterior side of the vertebral bodies (Figure 2.6) over the entire vertebral column beginning at the occiput (Kapandji, 2008). Together with the posterior longitudinal ligament (PLL), which connect the posterior aspects of the vertebral bodies, these ligaments limit the rotational range of motion in the sagittal plane (Standring, 2008). Specifically, the ALL restricts hyper-extensive motions, while the PLL prohibits excessive flexion. The PLL is generally larger than the ALL, both in terms of width and cross-sectional area (Panjabi et al., 1991e; Przybylski et al., 1998; Yoganandan et al., 2000).

The ligamenta flava (singular: ligamentum flavum) (LF) are ligamentous bands which connect the lamina of two adjacent vertebrae, beginning at the C2-C3 level (Standring, 2008). The LF are composed of more elastin than collagen, which makes them much more flexible than other ligaments (Nachemson and Evans, 1968).

The interspinous and intertransverse ligaments present in the thoracic and lumbar regions of the spine are almost non-existent in the cervical spine (Bogduk and Mercer, 2000). The cervical spine primarily relies on the intertransversaii and interspinalis muscles to provide a similar function to these ligaments.

The nuchal ligament (NL) is a fibrous membrane that spans the superior nuchal line of

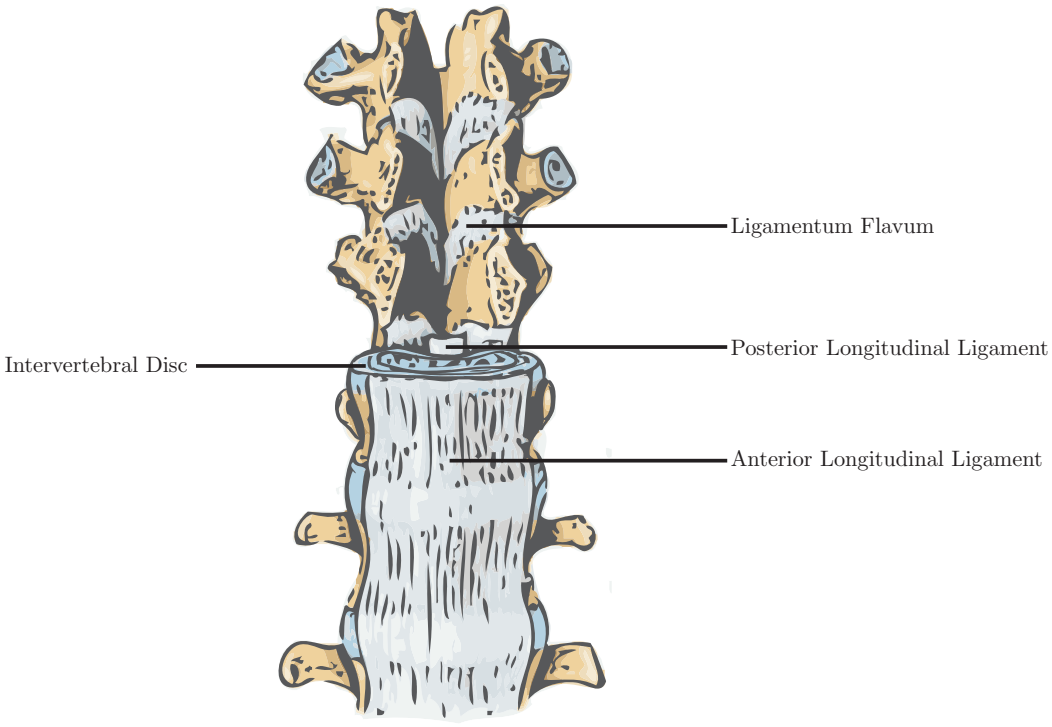

Figure 2.6: Anterior view of the anterior and posterior longitudinal ligaments, the ligamentum flavum, and an intervertebral disc. Image adapted from Moore and Dalley (2005).

the occiput to the spinous processes of all the cervical vertebrae (Figure 2.7). It has two histologically distinct regions: a funicular section, a fibrous band constituting the posterior edge of the ligament; and a lamellar section, which communicates the funicular section to the spinous processes of the vertebrae (Fielding et al., 1976; Johnson et al., 2000). With the largest moment arm in the sagittal plane of all the ligaments, it has a substantial capacity to aid in restraining cervical spine flexion (Takeshita et al., 2004b), while also serving as connective tissue for the attachment of the trapezius, rhomboids minor, and the splenius capitis muscles (Johnson et al., 2000).

The capsular ligaments (CL) encase each of the facet joints in the cervical spine. These

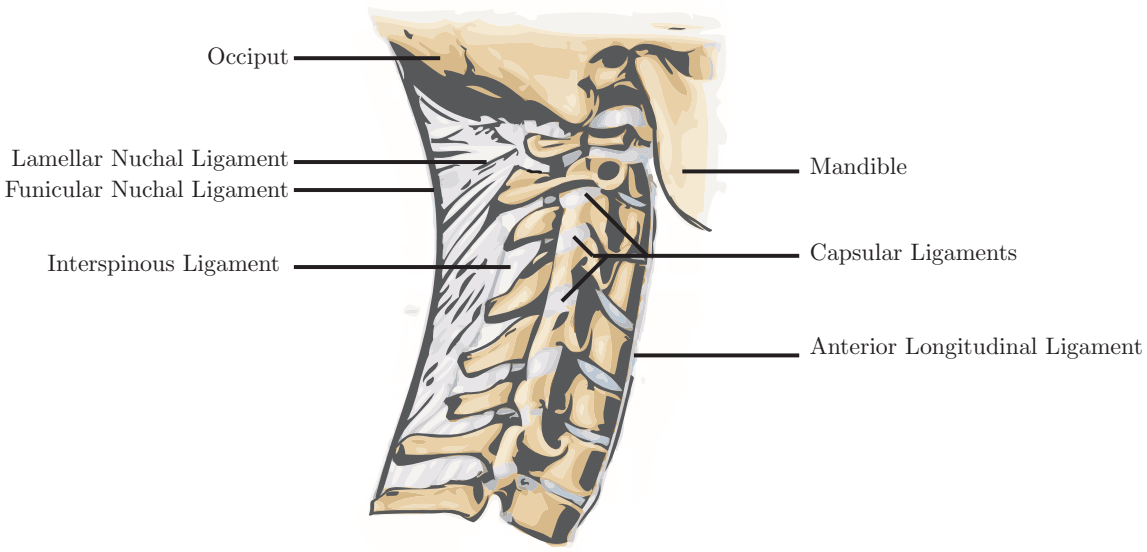

Figure 2.7: Lateral view of the ligaments of the cervical spine. Image adapted from Moore and Dalley (2005).

are thin ligamentous tissues that attach the articular pillars of two adjacent vertebrae and resist motion in the sagittal plane (Winkelstein et al., 2000). Damage to the capsular ligaments has been implicated as a possible source of chronic neck pain, as they contain an abundance of nociceptors, nerves that sense painful stimuli (Cavanaugh et al., 1996; Lu et al., 2005). Typical morphological characteristics for ligaments in the middle and lower cervical spine are given in Table 2.4.

Table 2.4: Summary of ligament dimensions, mean (standard deviation) for the middle and lower cervical spine.

study	Level	ALL		PLL		LF		CL		ISL
		Length (mm)	Width (mm)	Length (mm)	Width (mm)	Length (mm)	Width (mm)	Length (mm)	Width (mm)	Length (mm)
Panjabi et al. (1991e)	C12	23.1 (5.1)	3.8 (2.4)	30.7 (3.3)	3.7 (1.0)					12.0 (3.9)
	C23	14.6 (1.2)	5.6 (1.5)	13.4 (3.3)	6.2 (1.0)	5.2 (1.4)	4.7 (1.6)	8.4 (1.5)	6.7 (1.9)	9.8 (2.2)
	C34	13.5 (1.8)	7.5 (2.1)	10.1 (1.7)	7.1 (1.6)	6.2 (1.6)	5.2 (2.0)	8.8 (2.1)	8.3 (3.0)	9.8 (2.7)
	C45	12.3 (2.1)	7.8 (1.8)	12.0 (2.3)	8.9 (1.9)	6.2 (1.3)	5.4 (1.4)	9.0 (1.8)	7.4 (3.3)	11.2 (2.3)
	C56	11.5 (2.9)	7.3 (1.9)	11.7 (2.1)	7.6 (1.4)	6.5 (1.6)	5.5 (0.7)	9.0 (2.0)	5.5 (2.8)	12.3 (2.6)
	C67	13.7 (2.5)	7.6 (3.0)	13.3 (3.9)	7.4 (3.4)	7.7 (1.6)	5.3 (1.6)	8.6 (1.8)	8.0 (2.2)	16.1 (6.2)
	C7T1	13.3 (3.0)	7.4 (0.6)	15.0 (2.7)	7.5 (1.8)	8.8 (2.1)	5.2 (2.1)			
Przybylski et al. (1998)	C23	5.8 (1.7)	7.3 (2.4)	4.3 (0.9)	8.5 (2.0)					
	C34	5.8 (1.2)	9.0 (2.7)	4.7 (2.6)	9.6 (4.9)					
	C45	5.7 (1.3)	9.6 (2.8)	5.0 (1.3)	10.7 (5.3)					
	C56	5.2 (1.0)	9.6 (3.0)	5.2 (1.5)	11.3 (5.6)					
	C67	5.4 (1.0)	9.6 (2.9)	5.3 (0.9)	10.8 (4.9)					
Yoganandan et al. (2001)	C2-C5	18.8 (1.04)		19.0 (1.04)		8.45 (0.85)		6.92 (0.68)		10.4 (0.77)
	C5-T1	18.3 (0.5)		17.9 (0.54)		10.6 (0.64)		6.72 (0.45)		9.87 (0.69)
Mattucci (2011)	C12									
	C23	4.5 (0.3)		4.2 (0.8)		7.3 (0.9)		3.8 (1.2)		10.7 (1.6)
	C34	4.3 (1.5)		4.3 (1.1)		7.4 (1.1)		3.9 (0.6)		8.9 (1.7)
	C45	5.2 (1.2)		4.3 (0.8)		8.3 (1.1)		4.5 (1.1)		9.7 (1.1)
	C56	4.2 (1.4)		3.8 (0.9)		8.4 (1.1)		4.4 (1.1)		10.3 (1.6)
	C67	4.1 (0.7)		4.5 (0.4)		9.7 (2.1)		3.7 (0.3)		11.7 (2.5)
	C7T1	3.5 (0.8)		3.5 (0.8)		9.6 (1.0)		4.1 (0.8)		12.54 (2.28)

Ligaments of the Upper Cervical Spine

Approximately 80 — 90% of the total twisting range-of-motion of the cervical spine comes from the specialized interaction between the anterior arch of the atlas and the dens of the axis (Goel et al., 1988a; Penning and Wilmink, 1987; Villas et al., 1999). To stabilize this complex articulation between the atlas, axis, and occiput, the upper cervical spine possesses of a number of specialized ligaments (Panjabi et al., 1991d).

The dens of the axis is encircled anteriorly by the atlas and posteriorly by the transverse ligament (TL), which functions in limiting the anterior displacement of atlas by pressing the dens firmly against the articular surface. It is the largest and strongest ligament in the upper cervical spine (Panjabi et al., 1998). In some individuals, the cruciate ligament is formed by small bands, which extend from the transverse ligament superiorly to the occiput and inferiorly to the body of C2 from the center of the TL, forming a cross-like structure when viewed from a posterior view (Figure 2.8) (Goel et al., 1988a; Standring, 2008). The fibres that run superiorly form the transverso-occipital ligament (also known as the superior cruciform ligament), while those that run inferiorly form the transverso-axial ligament (sometimes called the inferior cruciform ligament) (Kapandji, 2008; Standring, 2008). These ligaments are pictured in Figures 2.8 and 2.9.

Posterior to the transverse ligament, extending from the body of the axis to the foramen magnum, are the occipito-axial ligaments connecting the occiput to the axis, typically subdivided into two lateral bands and a medial one (Figure 2.9). Just posterior to the occipito-axial ligaments is the posterior longitudinal ligament, where it spans to its origin on the inner side of the occiput (Benzel et al., 2004).

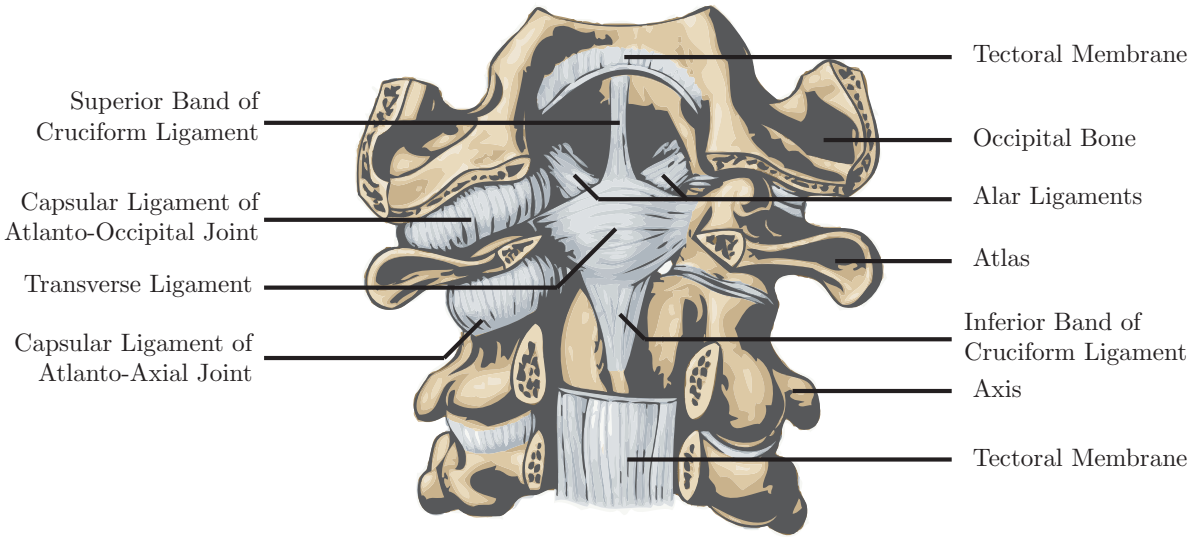

Figure 2.8: Posterior view of the deep ligaments of the cervical spine. Image adapted from Standring (2008).

The alar ligaments are a pair of ligaments originating from the apex of the dens and inserting onto the occipital condyles of the occiput, where they limit axial rotation of the occiput with respect to C2 (Crisco et al., 1991; Panjabi et al., 1991b). There is some evidence to suggest that the alar ligaments have an attachment on the atlas as well (Dvorak et al., 1987). In addition, the apical ligament of the dens extends from the apex of the dens to the anterior margin of the foramen magnum, where it is believed to stabilize the translation of the occiput relative to C2 (Maak et al., 2006; Tubbs et al., 2000). Posterior to the apical and alar ligaments, the tectorial membrane (TM), a band of fibrous tissue, connects the axis to the basilar groove on the occiput (Kapandji, 2008).

Encasing this intricate network of ligaments anteriorly is the anterior atlanto-axial membrane (AAAM), which connects the anterior arch of the atlas, as well as the anterior surface of the dens, to the anterior border of the foramen magnus (the basilar process)

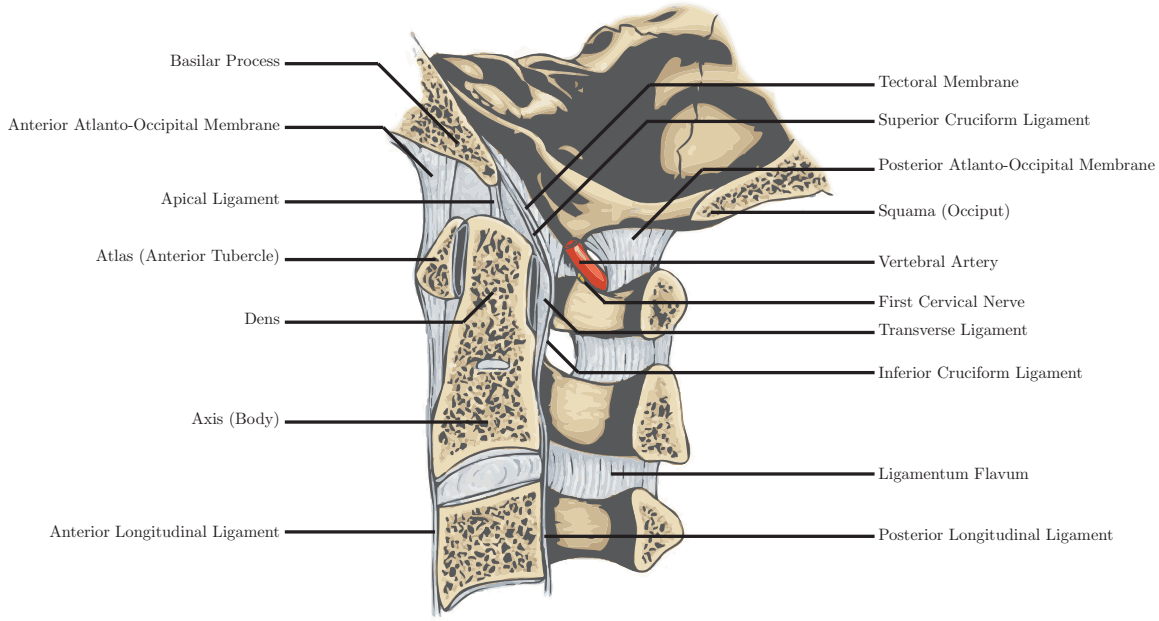

Figure 2.9: Lateral view of the ligamentous structure of the cervical spine. Adapted from Standring (2008).

of the occiput, running just deep to the ALL (Benzel et al., 2004; Kapandji, 2008). Deep fibres of the AAAM that run from the atlas to the occiput are sometimes called the anterior atlanto-occipetal membrane (AAOM) (Kapandji, 2008). Posteriorly, where the ligamentum flavum would normally be on C1, the posterior atlanto-axial membrane (PAAM) extends from the posterior arch of the atlas to the posterior border of the foramen magnus (the squama) of the occipital bone. These ligaments can be seen in Figures 2.10 and 2.11, while a summary of ligament morphologies is provided in Table 2.5.

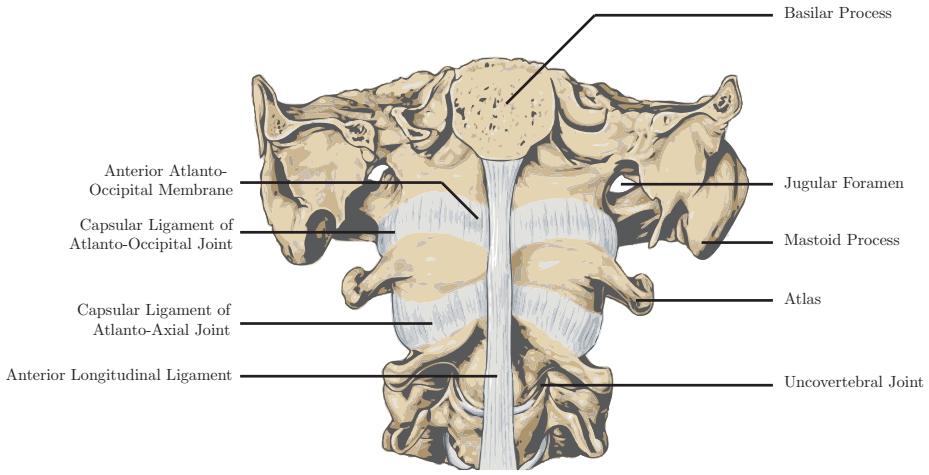

Figure 2.10: Ligaments of the anterior upper cervical spine. Image adapted from Standring (2008).

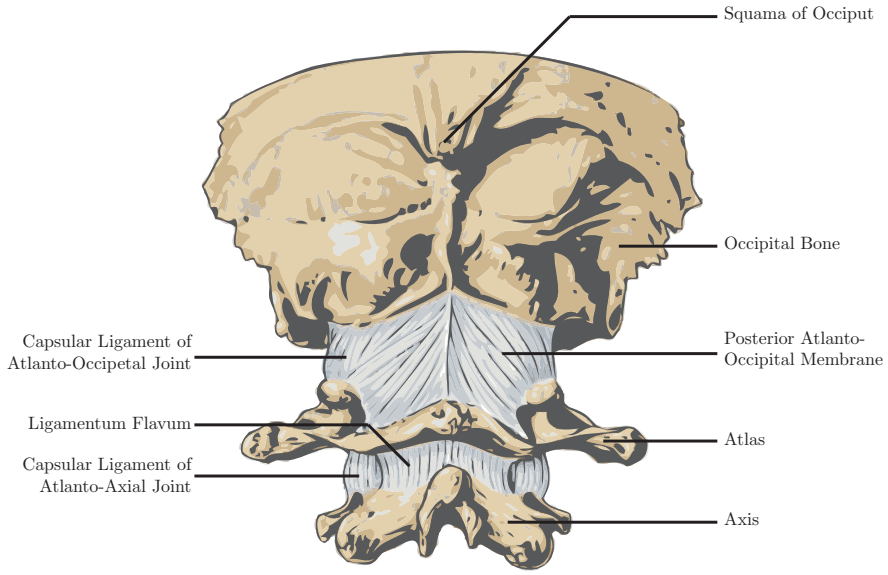

Figure 2.11: Ligaments of the posterior upper cervical spine. Image adapted from Standring (2008).

Table 2.5: Summary of morphological studies, mean (standard deviation), of the upper cervical spine ligaments.

Study	Ligament	Length (mm)	Width (mm)	Area mm^2
Panjabi et al. (1991d)	Apical	23.5 (3.8)		
	Transverse	21.9 (3.7)		
	Left Alar	9.5 (2.1)		
	Right Alar	11.0 (1.8)		
Tubbs et al. (2000)	Apical	7.33(2.46)	4.9 (2.90)	
Dvorak et al. (1987)	Alar	12 (2.1)	3.2(0.8)	
Maak et al. (2006)	Apical	23.1 (3.6)		
	Transverse	21.6 (1.5)		
	Left Alar	12.9 (1.4)		
	Right Alar	12.9 (1.5)		
Mattucci (2011)	Tectoral Membrane	18.92 (3.88)		33.02 (5.46)
	Transverse	20.79 (3.48)		18.89 (3.05)
	AAOM	12.51 (2.16)		87.03 (28.38)
	PAOM	13.92 (3.28)		48.84 (10.85)
	AAAM	12.47		50.34
	PAAM	15.72		21.55

2.1.3 The Intervertebral Disc

The intervertebral disc is a fibro-cartilaginous structure positioned between two adjacent vertebrae which functions to both transmit force between them while affording an appreciable degree of flexibility (Humzah and Soames, 1988; White and Panjabi, 1990). The human spine has at least 25 intervertebral discs, accounting for one third of the total height of the vertebral column (White and Panjabi, 1990). There are six in the cervical region, 12 in the thoracic, and six in the lumbar region, and one between the sacrum and coccyx, in addition to any unfused discs in the sacral region (Humzah and Soames, 1988).

The discs are generally smaller cranially than caudally (Anderst et al., 2015; Pooni et al., 1986), and exist between any two vertebrae, with the exception of the atlas and axis. The cervical spine is lordotic, like the lumbar spine, which is due to the wedge-like shape of the discs where the posterior intervertebral disc height is only 60% of the anterior (Pooni et al., 1986; Przybylski et al., 1998) (Table 2.6).

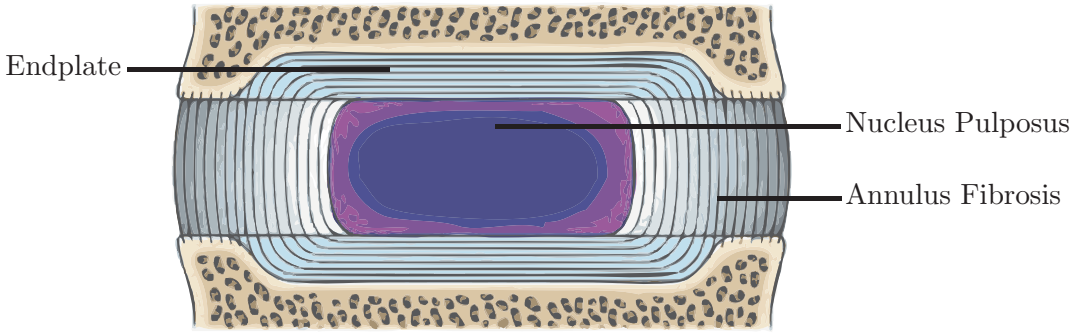

Figure 2.12: General anatomy of an intervertebral disc positioned between two vertebrae. Image adapted from Standring (2008).

Table 2.6: Summary of the means (standard deviations) of intervertebral disc heights (IVDH) and cross sectional areas (CSA).

Study		**C2-C3**	**C3-C4**	**C4-C5**	**C5-C6**	**C6-C7**	**C7-T1**
Przybylski et al. (1998)	Anterior IVDH (mm) Posterior IVDH (mm)	5.2 (1.4) 3.4 (1.0)	5.3 (1.3) 3.4 (1.6)	5.2 (1.5) 3.7 (0.9)	4.6 (1.3) 3.9 (1.0)	4.9 (1.1) 4.3 (1.0)	
Gilad and Nissan (1986)	Anterior IVDH (mm) Posterior IVDH (mm)	4.8 (1.0) 3.4 (1.0)	5.3 (0.9) 3.3 (0.9)	5.5 (1.0) 3.0 (1.0)	5.4 (1.0) 3.0 (0.9)	5.2 (1.0) 3.3 (1.0)	4.7 (1.2) 3.5 (1.2)
Pooni et al. (1986)	Middle IVDH (mm) Disc CSA (mm^2)	3.8 5.8 108 262	4.5 6.0 98 442	4.6 6.5 118 332	4.2 7.2 129 440	5.0 7.5 168 502	4.5 7.2 188 482
Anderst et al. (2015)	Average IVDH		2.6 mm	2.4 mm	2.5 mm	2.9 mm	

There are three histologically distinct regions in the intervertebral disc (Figure 2.12): an

inner nucleus pulposus, radially encased by the annulus fibrosis, both sandwiched between two cartilaginous endplates (Sivan et al., 2014; Urban and Roberts, 2003). The nucleus pulposus is usually described as a jelly-like substance, and accounts for between one and two thirds of the total cross-section of the disc (Iatridis et al., 1996; Inoue, 1981; Pooni et al., 1986). It is mostly composed of water, which constitutes 90% of the disc at birth, decreasing to approximately 70% by age 60 (Oda et al., 1988; Roughley, 2004). In addition, the nucleus pulposus houses a small population of several types of chondrocytes, which manage the turnover and manufacture of the proteoglycans and collagen fibres (type II, IV, IX, and XI) that aggregate the extracellular matrix, with type II collagen being the most abundant (Bruehlmann et al., 2002; Hayes et al., 2001; Kandel et al., 2007; Roberts et al., 1991; Sivan et al., 2014).

Unlike the loose collection of collagen and proteoglycans in the nucleus pulposus, the annulus fibrosis is comprised of 25 to 30 organized concentric annular layers of collagen (Figure 2.13), each oriented approximately 60 degrees from the previous layer (Cassidy et al., 1989; Marchand and Ahmed, 1990; Mengoni et al., 2015; Tampier et al., 2007; Wagner and Lotz, 2004). Like the nucleus, it is mostly water, which makes up 70% of its weight (Urban and Roberts, 2003), supplemented with collagen fibres and a small amount of elastin (Hayes et al., 2001; Yu et al., 2005). Collagen content varies as a function of layer in the annulus, with the outer layers of annular tissue being composed primarily of type I collagen fibres, which smoothly transition to type II in the innermost layers (Sivan et al., 2014). The strands of collagen and elastin within the IVD have also been shown to, in some cases, span multiple annular layers, which impede layers from shearing past one another (Schollum et al., 2008; Yu et al., 2007). On the anterior and posterior sides,

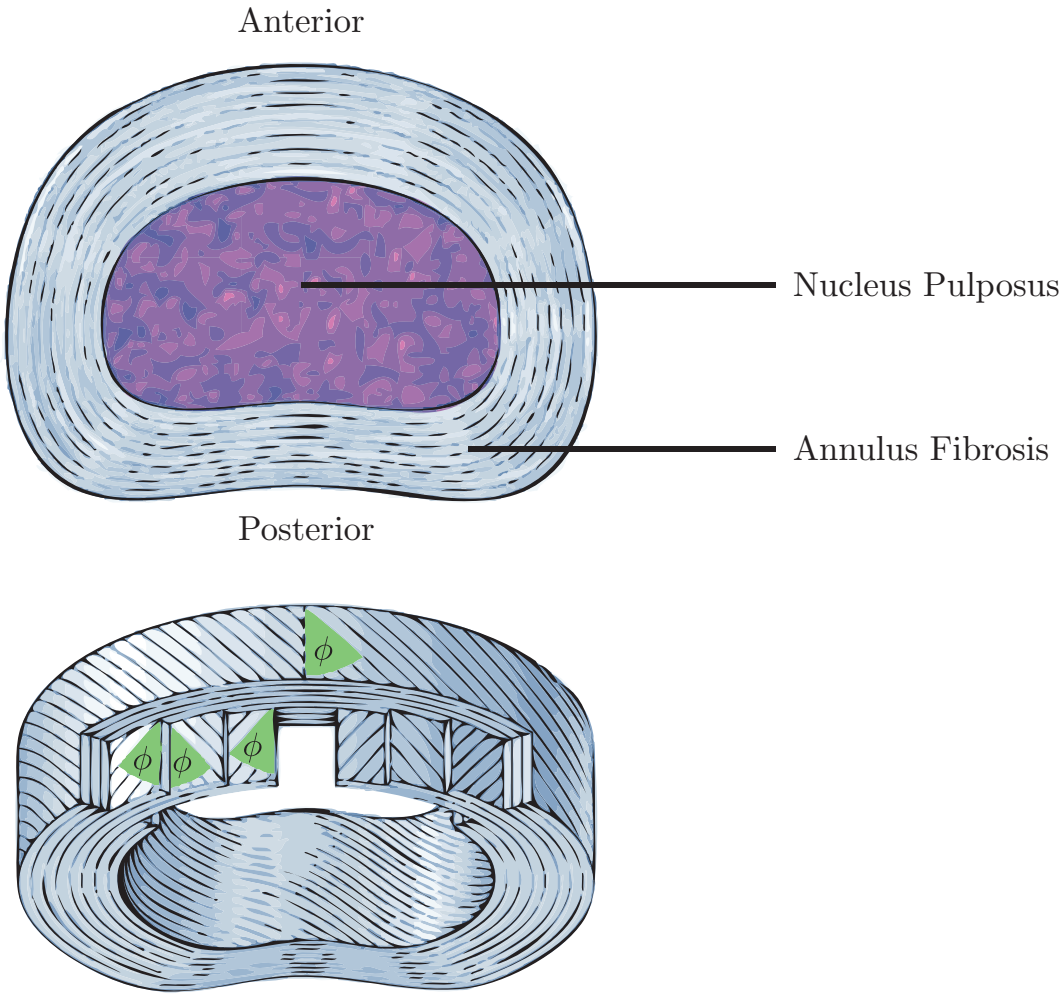

Figure 2.13: The intervertebral disc showcasing the concentric ring-like structure of the annulus fibrosis, each oriented at an angle of 30° from the previous later (i.e. $\phi = 30°$). Image adapted from Standring (2008).

the intervertebral disc is continuous with the anterior-longitudinal ligament and posterior longitudinal ligaments respectively (Benzel et al., 2004; Bogduk and Mercer, 2000).

On the superior and inferior edges of the nucleus pulposus and annulus are thin layers of hyaline cartilage known as endplates. Like the annulus and nucleus, the endplates are

primarily composed of water, collagen, and proteoglycans (Roberts et al., 1989). The adherence of the annulus to the endplate is accomplished by means of Sharpey's fibres: strands of collagen or elastin which originate in the endplate and project into the concentric structure of the annulus fibrosis (Johnson et al., 1982). There is some experimental evidence to suggest that similar fibres exist between the nucleus pulposus and the endplate as well, and even between the nucleus pulposus and the annulus fibrosis (Wade et al., 2012). Normal dimensions of the end plate are summarized in Table 2.7.

Table 2.7: Summary of end plate Dimension means (standard deviations), adapted from Panjabi et al. (1991a). Units are specified under each row heading.

Dimension		**C2**	**C3**	**C4**	**C5**	**C6**	**C7**
Endplate Width (mm)	(superior)		15.8 (0.46)	17.2 (0.66)	17.5 (0.58)	18.5 (0.55)	21.8 (0.66)
	(inferior)	17.5 (0.52)	17.2 (0.29)	17.0 (0.49)	19.4 (0.40)	22.0 (0.75)	23.4 (0.98)
Endplate Depth (mm)	(superior)		15.0 (0.55)	15.3 (0.75)	15.2 (0.35)	16.4 (0.52)	18.1 (0.66)
	(inferior)	15.6 (0.58)	15.6 (0.40)	15.9 (0.38)	17.9 (0.52)	18.5 (0.69)	16.8 (0.32)
Endplate Area (mm^2)	(superior)		169.4 (8.8)	183.0 (9.3)	182.9 (7.8)	221.2 (7.6)	278.3 (12.9)
	(inferior)	194.4 (9.6)	190.7 (5.7)	199.2 (7.3)	246.2 (12.1)	289.9 (16.5)	280.3 (13.7)

Together, the annulus fibrosis and endplate contain the nucleus pulposus in a way analogous to a pressure vessel (Kapandji, 2008). When a compressive force acts on the annulus fibrosis, the nucleus pulposus bulges radially, stretching the annular collagen fibres and loading them in tension (Holzapfel et al., 2005; White and Panjabi, 1990). The now pressurized nucleus pulposus acts as a conduit for compressive load to pass between the endplates of adjacent vertebra, providing a mechanism for resisting compression. The pressurized nucleus also acts a ball (Figure 2.14), which the superior vertebra can pivot upon, allowing the IVD to accommodate bending as well (White and Panjabi, 1990). Consistent with beam theory, annular fibres on the side of the bend are loaded in compression while on the opposite side, they are loaded in tension (White and Panjabi, 1990).

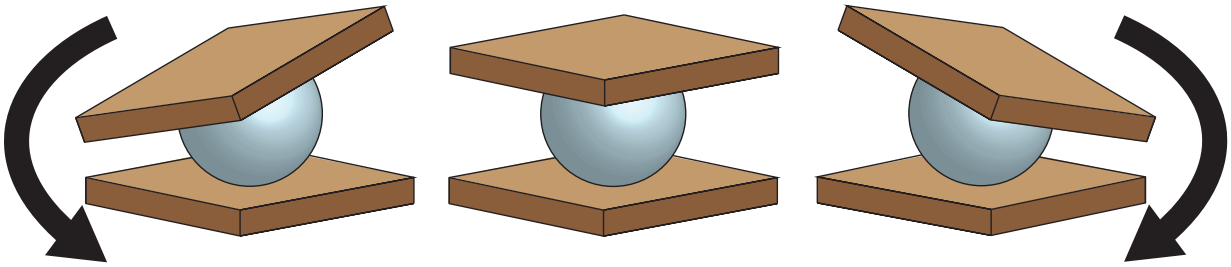

Figure 2.14: The roughly spherical nucleus pulposus acts as a swivel for the vertebrae to pivot upon. Adapted from Kapandji (2008).

The collagen fibres of the annulus fibrosis are responsible for bearing load while in tension, and since they are not aligned with the tensile axis, the intervertebral disc showcases less stiffness in tension than in compression (White and Panjabi, 1990; Lin et al., 1978). Similarly, in torsion, only half of the collagen fibres are engaged, rendering the disc particularly weak in this mode of loading (White and Panjabi, 1990).

2.1.4 Muscles

There are 38 muscles that span the neck (summarized in Table 2.8), each mirrored bilaterally about the sagittal plane (Gray, 1918). While systems of organization vary between sources (Gray, 1918; Kamibayashi and Richmond, 1998; Kapandji, 2008; Moore and Dalley, 2005), the cervical spine muscles are generally categorized into six groups: the suprahyoid, infrahyoid, anterior, lateral, suboccipital, and posterior muscle groups. Together, the anterior and lateral muscles are a subset of the prevertebral muscles, while the infrahyoid and suprahyoid constitute the hyoid group of muscles.

Superficial Muscles and the Hyoid Group

The largest muscle in the cervical spine is the trapezius which is positioned on the posterior surface of the neck. The most prominent muscle on the anterior side of the neck is the sternocleidomastoid (SCM) muscle, which subdivides the neck into the anterior and lateral triangles. Similarly, the most superficial neck muscle is platysma – a loose arrangement of muscle tissue within the subcutaneous fat region of the anterior neck, responsible for some facial expressions (Moore and Dalley, 2005). These can be seen in Figure 2.16.

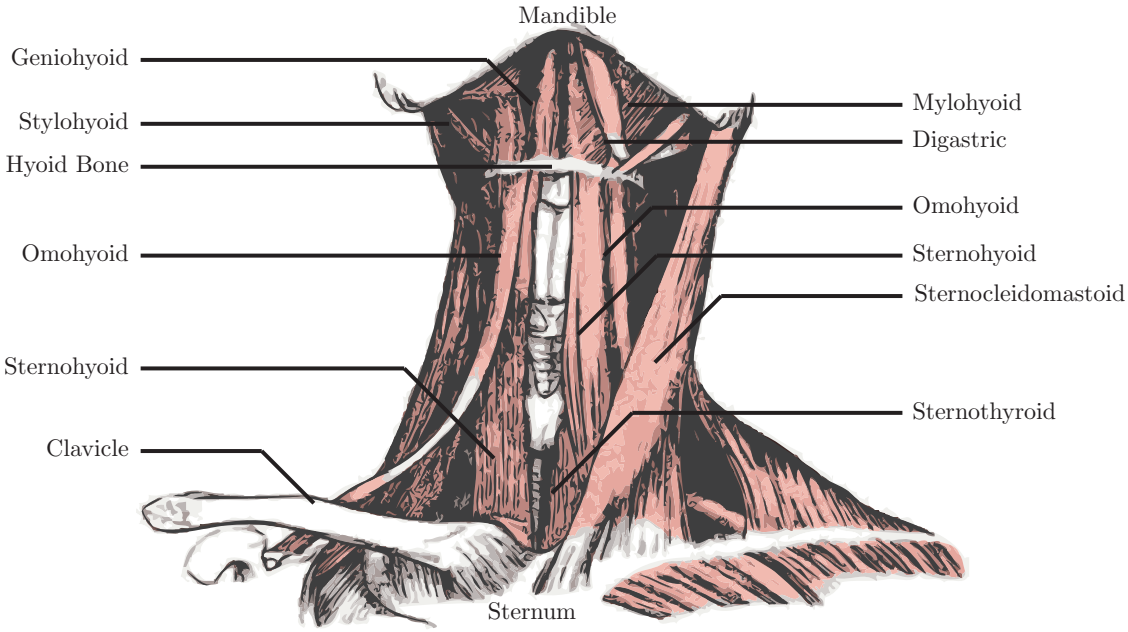

Figure 2.15: The hyoid muscle group of the anterior neck. Image adapted from Gray (1918).

The hyoid group of muscles constitute the anterior triangle and consists of those muscles on the anterior neck which attach to the hyoid bone (Figure 2.15). All of these muscles

are small and play a role in the control of the hyoid bone during swallowing. They are further subdivided into the suprahyoid and infrahyoid muscles; the suprahyoid group consists of the stylohyoid, digastric, mylohyoid, hypoglossus, and geniohyoid muscles, while sternohyoid, omohyoid, thyrohyoid and sternothyroid constitute the infrahyoid muscles (Moore and Dalley, 2005). The suprahyoid muscles provide tension on the hyoid bone which acts to translate it superiorly, whereas the infrahyoid muscles pull it inferiorly. Neither the suprahyoid nor infrahyoid muscles are believed to play a major role in neck movement (Pearson et al., 2010), although they have been shown to exhibit increased amplitude electromyography during head extension, suggesting a possible role as sagittal plane stabilizers (Forsberg et al., 1985).

The lateral triangle is bordered anteriorly by the SCM, posteriorly by the trapezius, and inferiorly by the clavicle. Muscles in this region include the scalenes (anterior, middle, and posterior), and the levator scapula.

Prevertebral Muscles

The prevertebral muscles (Figure 2.17) are subdivided into the anterior and lateral vertebral muscles. The anterior vertebral muscles lie posterior to the retropharyngeal space – a small anatomical region posterior to the esophagus – and consist of the longus colli and capitus, the rectus capitis anterior, and the anterior scalene muscles (Kapandji, 2008). The rectus capitus anterior (and lateralis, discussed later) are small muscles that connect the atlas to the occiput, and are involved primarily in rotation and lateral bending. The longus colli, sometimes called the deep flexor of the neck, is a long muscle that is typically partitioned into three sections: an oblique descending part, an oblique ascending part,

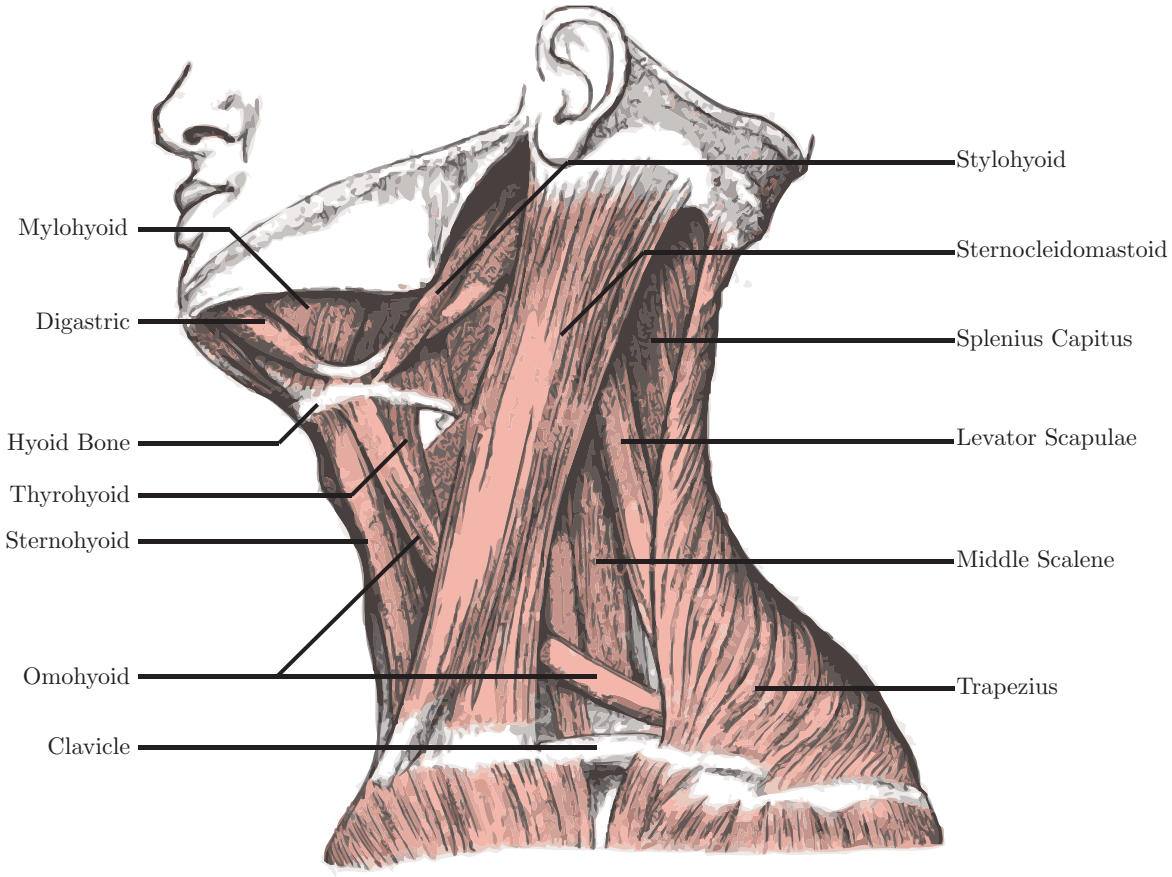

Figure 2.16: Lateral view of the middle musculature of the cervical spine. Image adapted from Gray (1918).

and a longitudinal part (Jull et al., 2008). The anterior vertebral muscles are separated from the lateral vertebral muscles by the brachial plexus and subclavian arteries, which are sometimes called the neurovascular plane of the neck (Moore and Dalley, 2005). The lateral vertebral muscles includes the rectus capitis lateralis, splenius capitis, levator scapulae, and middle and posterior scalene muscles. The omohyoid, a two-bellied muscle that originates on the hyoid bone and inserts on the superior surface of the scapula, passes through this region, and is sometimes included in the lateral vertebral muscles.

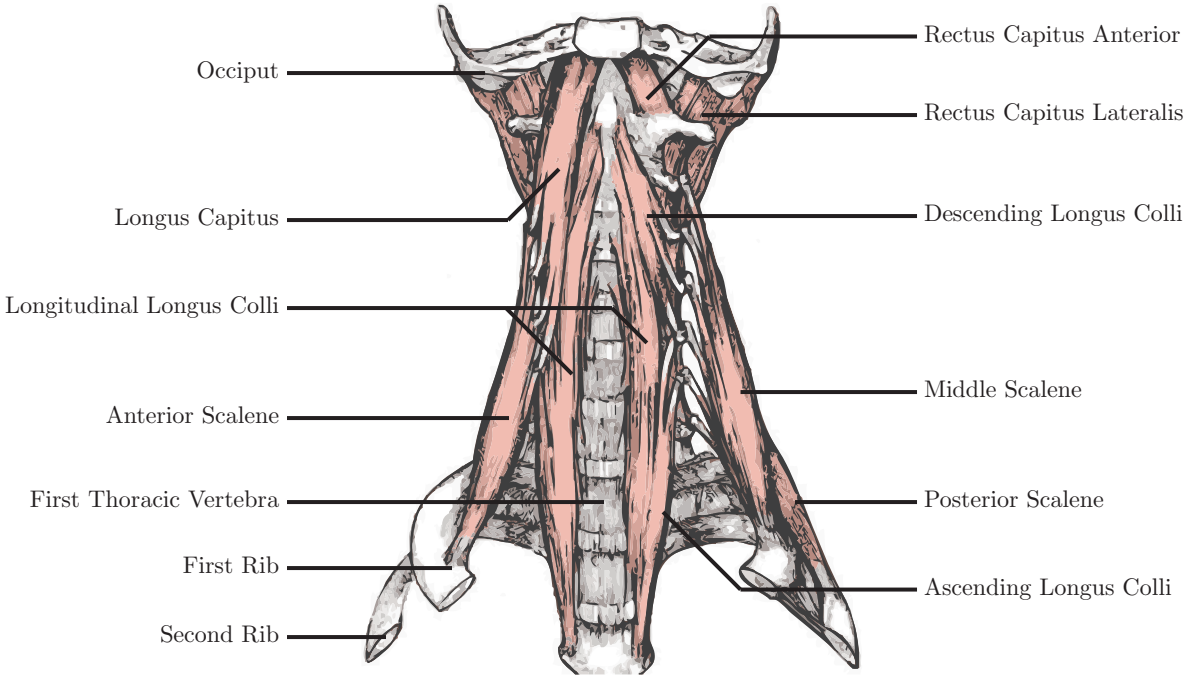

Figure 2.17: The deep anterior muscles of the cervical spine. Image adapted from Gray (1918).

The Posterior Neck Muscles

The posterior muscles of the neck are partitioned into four muscle planes: the deep plane, the plane of semispinalis capitis, the plane of the splenius and levator scapulae, and the superficial plane (Kapandji, 2008). The deep plane contains the intrinsic muscles of the upper cervical spine (Figure 2.18), also called the suboccipetal muscles, consisting of the rectus capitis posterior major and minor, the obliquus capitis inferior and the obliquus capitis superior, in addition to the small interspinalis and intertransversaii muscles that move down the spinal column. The plane of the semispinalis contains the semispinalis capitis, the longissimus capitis, and, more laterally, the illiocostalis cervicis. The plane of

the splenius and levator scapulae contains, as the name suggests, the splenius capitis and cervices and the levator scapulae. This layer contains the covering muscles of the posterior neck – namely the splenius muscles. Finally the superficial plane consists of the trapezius and sternocleidomastoid (Figure 2.19).

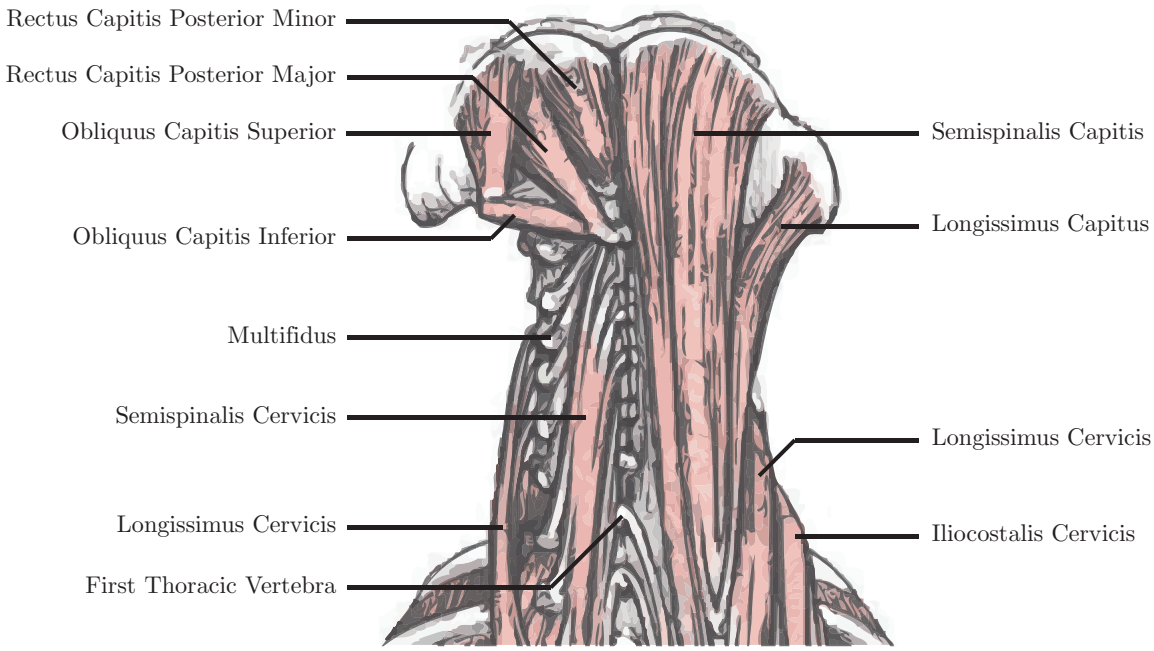

Figure 2.18: Posterior musculature of the cervical spine. Adapted from Gray (1918).

With the exception of the deep plane, the posterior muscles of the neck produce extension (Figure 2.18), rotation, and lateral bending of the cervical spine. On the other hand, the muscles of the superficial plane act directly on the head, producing extension movements. The suboccipetal muscles are fine-tuning muscles that act to stabilize the

occiput-atlas-axis complex during flexion, extension, and twisting (Kapandji, 2008).

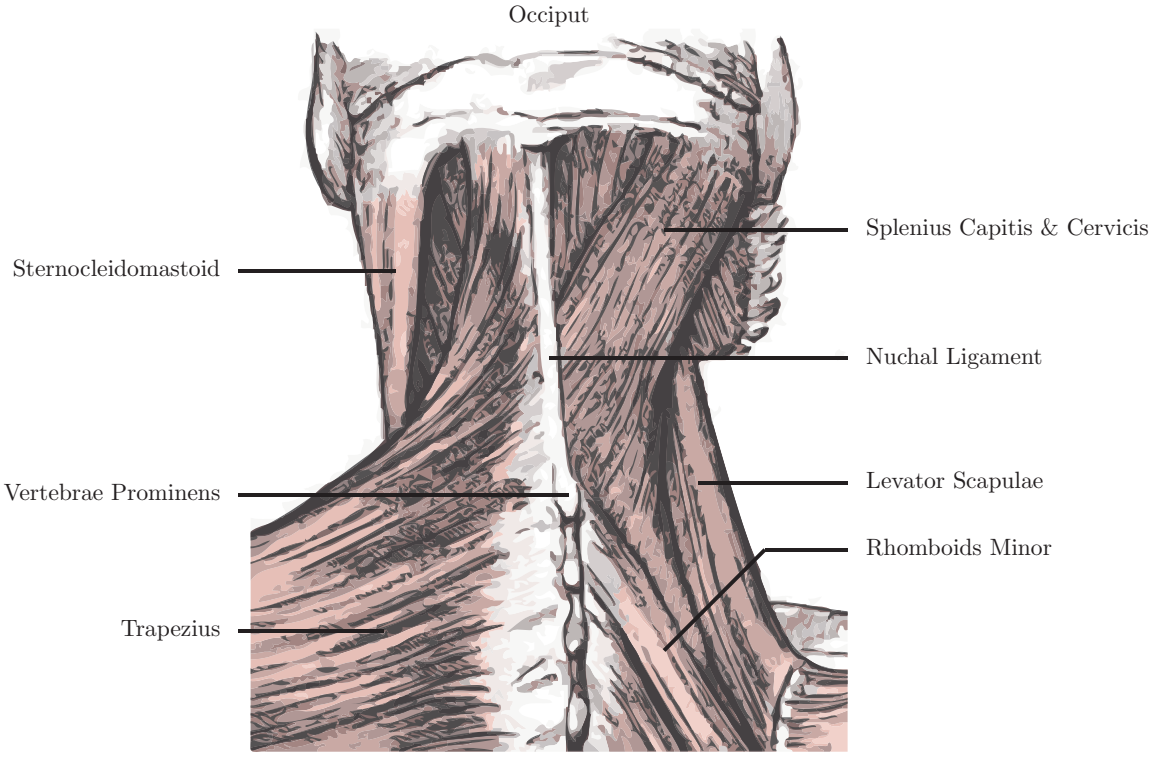

Figure 2.19: Superficial posterior musculature of the cervical spine. Image adapted from Gray (1918).

Table 2.8: Summary of the anatomy of the muscles of the cervical spine. Summarized from Kamibayashi and Richmond (1998); Van Ee et al. (2000); and Pearson et al. (2010). Here AP means Articular Process; TP means Transverse Process; SP means Spinous Process; VB means Vertebral Body; SCT means subcutaneous tissue.

Muscle	**Muscle Group**	**Origin**	**Insertion**	**Action**	**Nerve**	**PCSA (cm^2)**
Obliquus Capitis Inferior	Suboccipetal	C2 (SP)	C1 (TP)	Rotation	Suboccipital Nerve	1.95
Obliquus Capitis Superior	Suboccipetal	C1 (TP)	Inf. Nuchal Line (occiput)	Lat. Bending; Extension	Suboccipital Nerve	0.88
Rectus Capitus Posterior Major	Suboccipetal	C2 (SP)	Inf. Nuchal Line (occiput)	Rotation; Extension	Suboccipital Nerve	1.68
Rectus Capitus Posterior Minor	Suboccipetal	C1 (posterior arch)	Inf. Nuchal Line (occiput)	Extension; stabilizer	Suboccipital Nerve	0.92
Platysma	Anterior	SCT of Anterior Neck	Base of mandible	Frowning	Facial nerve	
Longus Capitis	Anterior	C3 – C6 (TP)	Basilar process (occiput)	Flexion	C1 – C3/C4	1.37
Longus Colli (oblique, descending)	Anterior	C3 – C6 (TP)	C1 (AT)	Rotation; Flexion; Lat. Bending	C2 – C6 (Spinal nerve)	0.69
Longus Colli (oblique, ascending)	Anterior	C4 – C7 (TP)	T2 and T3 (VB)	Rotation; Flexion; Lat. Bending	C2 – C6 (Spinal nerve)	0.69
Longus Colli (longidutinal)	Anterior	C2 – C7 (VB)	T1 – T3 (VB)	Rotation; Flexion; Lat. Bending	C2 – C6 (Spinal nerve)	1.37
Rectus Capitis Anterior	Anterior	C1 (TP)	Basilar process (occiput)	Flexion	Ventral Rami C1 – C2	
Rectus Capitis Lateralis	Lateral	C1 (TP)	Jugular process (occiput)	Flexion; Lat. Bending	C1 – C2	
Anterior Scalene	Lateral	C3 – C6 (TP)	1st Rib	Lat. Bending; Flexion	C3 – C6 (Spinal nerve)	1.88
Middle Scalene	Lateral	C2 – C7 (TP)	1st Rib	Lat. Bending; Flexion	C3 – C6 (Spinal nerve)	1.36
Posterior Scalene	Lateral	C5 – C7 (TP)	2nd Rib	Lat. Bending; Flexion	C6 – C8 (Spinal nerve)	1.05
Sternocleidomastoid	Lateral	Manubrium; Clavicle	Mastoid process	Lat. Bending; Rotation; Flexion	Accessory Nerve	4.92
Levator Scapula	Lateral	C1 – C4 (TP)	Sup. Med. Scapula	Elevate scapula; rotate scapula	Dorsal Scapular nerve	3.12
Digastric	Suprahyoid	Mandible; Mastoid	Hyoid	Deglutition	Trigeminal	0.60
Geniohyoid	Suprahyoid	Mandible	Hyoid	Deglutition	C1; Hypoglossal	0.46
Mylohyoid	Suprahyoid	Mandible	Hyoid	Deglutition	Mandibular nerve	0.63
Stylohyoid	Suprahyoid	Styloid process	Hyoid	Deglutition	Facial Nerve	0.27
Omohyoid	Infrahyoid	Scapula	Hyoid	Deglutition	Ansa cervicalis (C1 – C3)	0.75
Sternohyoid	Infrahyoid	Manubrium	Hyoid	Deglutition	Ansa cervicalis (C1 – C3)	0.58
Sternothyroid	Infrahyoid	Manubrium	Thyroid Cartilage	Depress thyroid cartilage	Ansa cervicalis (C1 – C3)	0.65
Thyrohyoid	Infrahyoid	Thyroid Cartilage	Hyoid	Elevate Thyroid	C1; Hypoglossal	
Iliocostalis Cervicis	Posterior	3rd, 4th, 5th Rib	C4 – C6 (TP)	Lat. Bending; Extension	Spinal nerve	1.04
Longissimus Capitis	Posterior	C5 – T5 (TP)	C3 – C6 (TP); Mastoid	Lat Bending; Extension	Spinal Nerve	0.98
Longissimus Cervicis	Posterior	T1 – T5 (TP)	C2 – C6 (AP)	Lat. Bending; Extension	Spinal Nerve	1.49
Semispinalis Capitis	Posterior	C4 – T6 (TP)	Nuchal line	Rotation; Extension	Greater Occipital Nerve	5.52
Semispinalis Cervicis	Posterior	T1 – T6 (TP)	C2 – C5 (TP)	Rotation; Extension	Spinal Nerve	3.06
Splenius Capitis	Posterior	C7 – T4 (SP); Nuchal Lig.	Mastoid	Rotation; Extension	Spinal Nerve (C3 – C4)	3.09
Splenius Cervicis	Posterior	T3 – T6 (SP)	C1 – C3 (TP)	Extend; Lat. Bending; Rotation	Spinal Nerve	1.43
Rhomboid Minor	Posterior	C7 – T1 (SP); Nuchal Lig.	Med. Scapula	Retract scapula	Dorsal Scapular nerve	1.02
Rhomboid Major	Posterior	T2 – T5 (SP)	Med. Scapula	Retract Scapula	Dorsal Scapular nerve	
Trapezius (upper portion)	Posterior	C0 – T12 (SP)	Scapula Spine; Clavicle	Rotation; Retract Scapula	Accessory Nerve	13.73
Multifidus	Deep Posterior	C4 – T1 (AP)	C2 – C6 (SP)	Proprioception; Extension	Spinal Nerve	
Intertransversarii	Deep Posterior	C1–C7 (TP)	C0 – C6 (TP) adjacent vertebra	Lat. Bending	Spinal Nerve	
Interspinales	Deep Posterior	C2 – C7 (SP)	C1 – C6 (SP) adjacent vertebra	Extension	Spinal Nerve	

2.1.5 Intervertebral Joints

The cervical vertebral column consists of seven segments, with at least three joints between each (Mercer and Bogduk, 2001). The unit of two cervical vertebrae and their intervening intervertebral disc is referred to as a functional spinal unit (FSU) or motion segment. The typical vertebrae motion segments have two facet and uncovertebral joints for every vertebral level, while the upper cervical spine consists of the joints that make up the atlanto-axial-occipital complex.

The Zygopophyseal Joints

The zygopophyseal joints, or facet joints, are synovial joints formed from the articulation of the cranial vertebra's inferior articular surface with the caudal vertebra's superior articular surface (Figure 2.20). The joints are wrapped in capsular ligaments, with lubricating synovial fluid, small cartilaginous menisci contained in the joint-space (Figure 2.21) (Jaumard et al., 2011; Mercer and Bogduk, 1993; Yu et al., 1987).

The size, shape, and orientation of the facet joints play a role, with the uncovertebral joints, in the kinematics of the cervical spine (Francis, 1955; Pal, 2001; Panjabi et al., 1993; Yoganandan et al., 2003). The orientation of the facets to the transverse plane being at approximately 40° at the atlanto-occipetal joint, and smoothly transitions to roughly 60° at C7; on the other hand, the angle they form with the sagittal plane is typically between 0° and 15° (Table 2.9). The facet joints play an important role in the transmission of load between vertebrae, bearing approximately 12% of the compressive load (Goel and Clausen, 1998). They also play an important role in the kinematics of the joint (Penning, 1978).

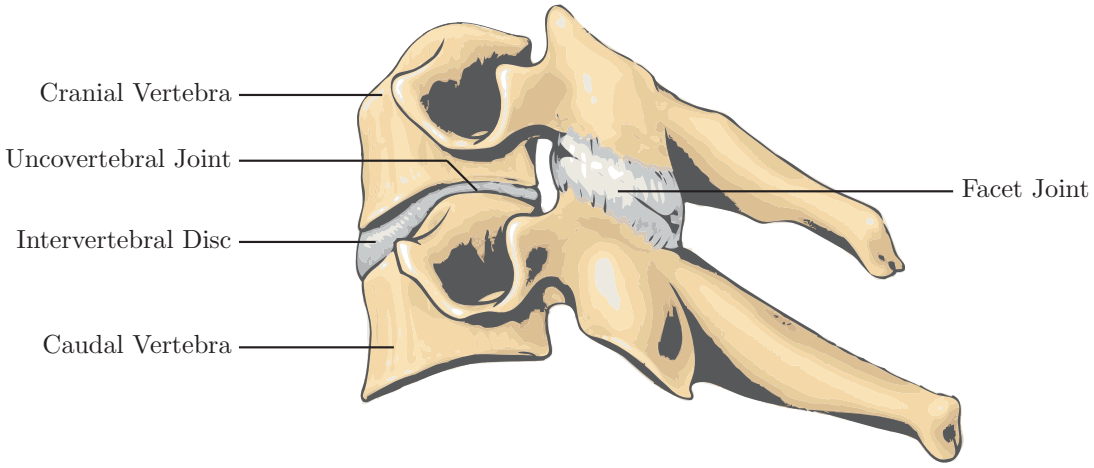

Figure 2.20: A Motion Segment consisting of two typical vertebrae and their intervening intervertebral disc, adapted from Moore and Dalley (2005).

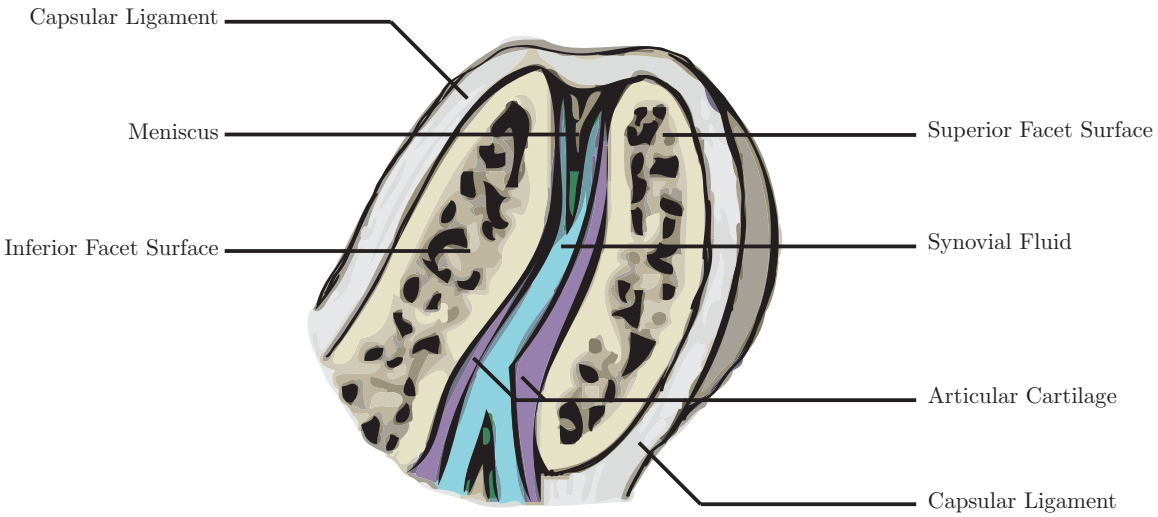

Figure 2.21: Cross-section of a facet joint, adapted from Jaumard et al. (2011).

Because of the angle they form with the transverse plane, axial rotation is coupled with lateral flexion and vice-versa (Bogduk and Mercer, 2000). If one of these motions were to occur, the facet joints on that side collide and begin sliding past one another, inducing

the other motion (Clausen et al., 1997; Penning, 1978). The net result is that there is no true axial rotation or lateral flexion in the cervical spine, rather a rotation about an axis perpendicular to the surface of the facet joints (Bogduk and Mercer, 2000; Penning, 1988).

The Uncovertebral Joints

The uncovertebral joints are small joints formed from the articulation between the uncus of the inferior vertebra with the vertebral body of the superior vertebra – similar to facet joints (Kumaresan et al., 1999b). They prohibit axial rotation (Goel and Clausen, 1998), and contribute to the coupling of axial rotation movements with lateral bending (Clausen et al., 1997). Their orientation with respect to the frontal plane increases from about 75° at C3 to 115° at C7; while the orientation with respect to the sagittal plane is generally between 35° and 40° (Panjabi et al., 1991a)(Table 2.10).

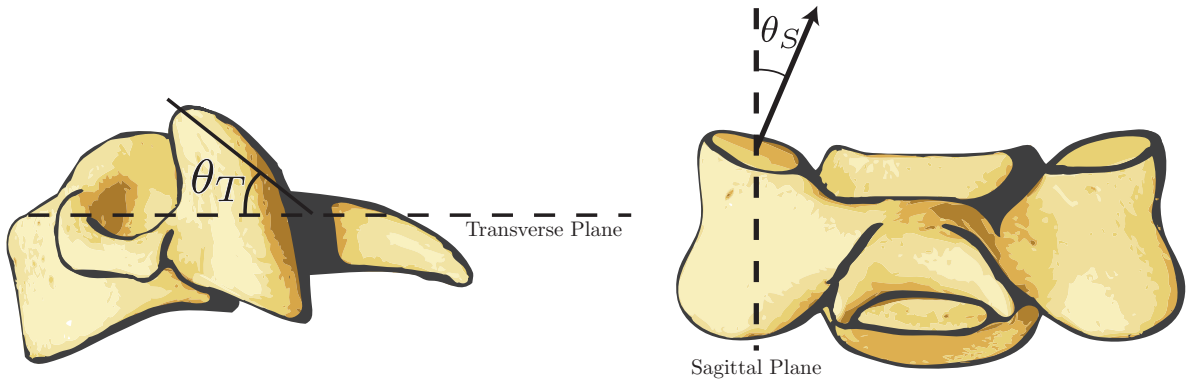

Figure 2.22: Angle definitions for the orientation of the facet joints in Table 2.9.

Table 2.9: Size and orientation of the facet joints of the cervical spine. For angle definitions consult Figure 2.22

Study	Level	Superior Surface Width	Superior Surface Height	Superior Surface θ_T	Superior Surface θ_S	Inferior Surface Width	Inferior Surface Height	Inferior Surface θ_T	Inferior Surface θ_S
Francis (1955)	C1	11.6 mm	23.4 mm			17.2 mm	18.0 mm		
	C2	17.7 mm	19.0 mm			11.8 mm	11.4 mm		
	C3	11.8 mm	11.3 mm			12.2 mm	11.5 mm		
	C4	12.2 mm	11.5 mm			12.7 mm	11.4 mm		
	C5	12.6 mm	11.2 mm			13.2 mm	11.2 mm		
	C6	13.1 mm	10.8 mm			13.6 mm	11.0 mm		
	C7	14.0 mm	10.2 mm			14.8 mm	12.4 mm		
Panjabi et al. (1993)	C2	16.4 mm	17.9 mm	37.1°	-23.6°	10.9 mm	12.4 mm	33.8°	17.4°
	C3	11.1 mm	11.6 mm	52.0°	15.8°	11.4 mm	12.4 mm	42.6°	12.7°
	C4	11.5 mm	12.2 mm	48.4°	5.4°	11.6 mm	12.3 mm	42.6°	15.3°
	C5	12.1 mm	11.6 mm	45.6°	6.4°	11.7 mm	11.2 mm	51.7°	16.4°
	C6	12.4 mm	11.0 mm	47.6°	11.0°	12.9 mm	12.3 mm	54.9°	7.6°
	C7	12.6 mm	11.4 mm	55.5°	7.1°	13.3 mm	12.7 mm	49.5°	8.7°
	T1	13.7 mm	12.6 mm	60.0°	4.1°	12.6 mm	12.9 mm	64.3°	14.5°
Pal (2001)	C3	10.3 mm	10.0 mm	45.8°	20.1°				
	C4	10.8 mm	10.7 mm	50.8°	8.3°				
	C5	11.3 mm	9.7 mm	52.3°	-1.0°				
	C6	12.3 mm	9.0 mm	56.0°	-5.7°				
	C7	13.6 mm	8.6 mm	64.7°	-4.1°				
	T1	14.3 mm	8.8 mm	68.8°	-9.3°				
Yoganandan et al. (2003)	C0						18.6 mm		
	C1		18.6 mm				16.7 mm		
	C2		16.7 mm				11.5 mm		
	C3		11.5 mm				11.6 mm		
	C4		11.9 mm				10.6 mm		
	C5		10.6 mm				10.8 mm		
	C6		10.8 mm				11.1 mm		
	C7		11.1 mm				12.4 mm		
	T1		12.4 mm						

Table 2.10: Summary of sizes, mean (standard deviations), and orientation of uncovertebral articulations. Adapted from Panjabi et al. (1991a)

Level	Superior Uncovertebral Joint θ_F (°)	Superior Uncovertebral Joint θ_S (°)	Superior Uncovertebral Joint Area (mm^2)	Inferior Uncovertebral Joint θ_F (°)	Inferior Uncovertebral Joint θ_S (°)	Inferior Uncovertebral Joint Area (mm^2)
C2				78.4 (3.20)	63.7 (5.05)	18.75 (3.11)
C3	76.6 (2.22)	38.7 (3.87)	43.6 (4.11)	81.6 (1.59)	47.8 (4.01)	22.5 (2.71)
C4	76.2 (2.45)	40.0 (2.89)	39.9 (3.30)	83.5 (1.39)	47.8 (3.46)	24.5 (2.70)
C5	82.7 (1.44)	34.5 (2.08)	42.9 (5.45)	84.9 (1.10)	45.0 (3.03)	28.9 (3.42)
C6	104.0 (2.40)	40.8 (3.52)	53.5 (5.77)	106.2 (2.28)	49.2 (4.33)	24.8 (2.27)
C7	115.6 (2.68)	47.3 (3.00)	42.2 (3.51)	113.4 (2.17)	59.8 (4.47)	21.2 (2.86)

The Upper Cervical Spine

The upper cervical spine consists of roughly five joints: the two facet joints between the axis and atlas (the lateral atlanto-axial joints); the articulation between the odontoid process of C2 with C1 (the median atlanto-axial joint); the two atlanto-occipital joints between the atlas and the occiput; and, debatably, the articulation between the dens and the occiput.

The bulk of the rotational range of motion in the cervical spine comes from the median atlanto-axial joint – the complicated articulation between the atlas and the dens of the axis (Figure 2.23) (Goel et al., 1988a). The atlas is able to pivot on the dens relatively unimpeded, held in place by the transverse ligament (White and Panjabi, 1990). Indeed, the isolated joint is capable of almost 180° of rotation, which accounts for nine-tenths of the total rotational range of motion in the cervical spine (Goel et al., 1988a).

Because there is no disc between the atlas and axis, the facet joints are responsible for transferring all of the compressive load between these two vertebrae. The facet joints in this region are particularly unique since they are biconvex – both the inferior articular surface of the atlas and the superior articular surface of the axis are convex (Koebke and Brade, 1982). In a neutral posture, the apex of the atlas facets rest on the summit of the superior articular surfaces of the axis; however, rotation requires the anterior displacement of one of the lateral masses of the atlas and posterior displacement of the opposite one. When this occurs, the ipsilateral facet of the atlas slides down the posterior surface of the axial facet surface while the contralateral facet slides down the anterior surface (Bogduk and Mercer, 2000; Mercer and Bogduk, 2001).

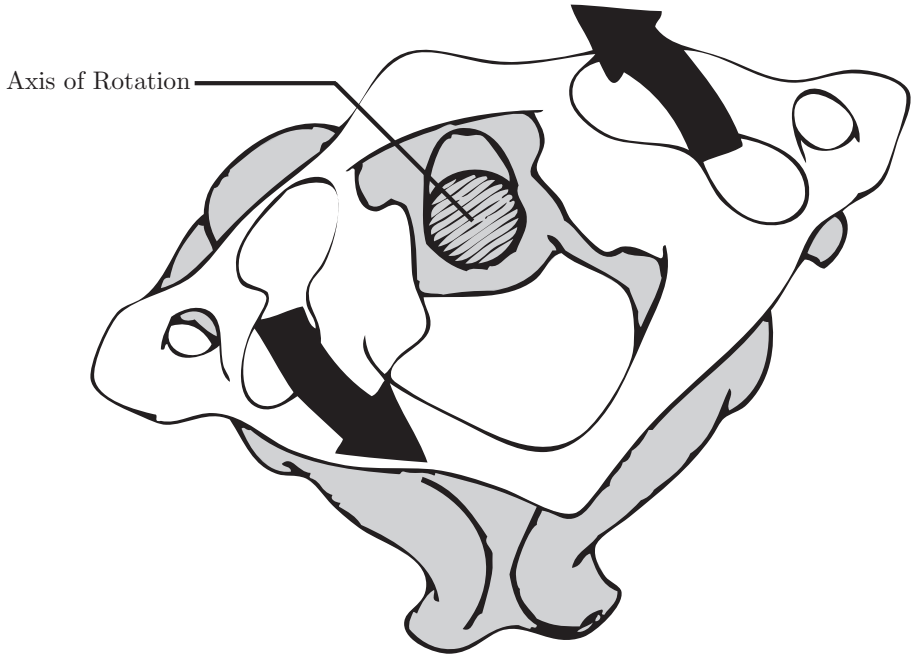

Figure 2.23: The odontoid articulation between the axis and atlas. Adapted from White and Panjabi (1990).

The biconvex nature of these facet joints is also believed to contribute to the paradoxical motion of the atlanto-axial joint in flexion, where, in a fully flexed cervical spine, the atlas can, and usually does, extend (Bogduk and Mercer, 2000). Of the muscles that attach to the atlas, only the descending longus colli directly acts to move the atlas in flexion. Other muscles use C1 as a vantage point to act on other regions, the levator scapulae for instance, while it attaches to the transverse tubercle of the atlas, has a primary function of elevating the scapula (Bogduk and Mercer, 2000). The motion of the atlas is therefore passively determined as a by-product of musculature acting directly on the occiput. Ultimately, whether the atlas flexes or extends is dictated by the position of the net compressive force relative to the facet position: if the force is directed anteriorly, the atlas will flex; conversely if directed posteriorly it will extend (Bogduk and Mercer, 2000) (Figure 2.24).

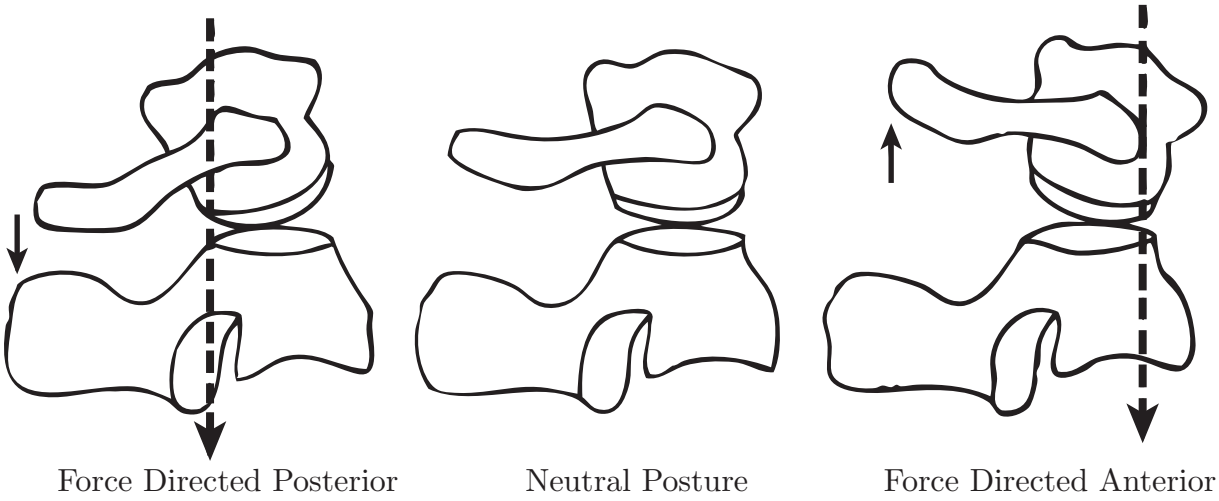

Figure 2.24: The mechanism of the kinematic paradox for the atlas. When the force is directed posteriorly, the facet of the atlas will pivot, causing extension. Conversely when it is directed anteriorly, the pivot of the atlas will cause flexion. Image adapted from Bogduk and Mercer (2000).

The atlanto-occipital joint is formed by the articulation of the two concave superior articular surfaces of the atlas with the convex occipital condyles. Like facet joints, the atlanto-occipital joints are synovial joints encased in a capsular ligament (Mercer and Bogduk, 2001). Unlike the facet joints, they rarely contain a meniscus (Mercer and Bogduk, 1993). The fibrous compartment of these joints, combined with the particularly deep socket in the atlas, do not allow for translation of the occiput relative to the atlas and consequently prohibit rotation as well. The only physiological motion afforded by these joints is flexion-extension (Bogduk and Mercer, 2000).

2.2 Tissue Mechanics

Tissue mechanics refers to the study of the mechanics of tissues, often done through the examination of *stress* and *strain* in tissues (Kenedi et al., 1975). Stress (σ) is a physical quantity expressing the amount of force acting on an object over a given area, whereas strain (ε) quantifies the change in deformation in a body relative to the original dimension (Lautrup, 2005). Tissues, in this document, refer to biological tissues, which is a population of related cells and their extra-cellular matrix.

2.2.1 Ligaments

Ligaments are fibrous connective tissues that adhere bones to bones. They transmit only uniaxial tensile forces, although the position and orientation of the ligament ultimately dictates which loading modes it resists best. Ligaments are composite materials of primarily two types of proteins: collagen and elastin (Chazal et al., 1985). Generally speaking, ligaments which are abundant in collagen, such as the alar ligaments, are stiffer and break at lower magnitudes of strain, while those rich in elastin, like the ligamenta flava, are more pliant and resistant to damage (Yoganandan et al., 2000, 1989). Ligaments exhibit a characteristic sigmoidal stress-strain curve (Figure 2.25), showcasing a flexible toe region before an abrupt increase in stiffness signifying the beginning of a linear region. At high strains, there is a decrease in stiffness before failure (Shim et al., 2006). The toe region of the ligament is believed to be due to the stepwise involvement of collagen fibres as the ligament stretches, sometimes termed *uncrimping* (Chazal et al., 1985; Rigby et al., 1959).

The linear region begins once all of the collagen fibres are engaged, ceasing any subsequent contribution to the stiffness of the ligament. Prior to ultimate failure there is a decrease in ligament stiffness termed the sub-failure region, caused by breaking of individual collagen fibres (Panjabi et al., 1998). Supporting this, loading in the sub-failure region is associated with plastic deformation, tissue damage, and an increase in the length of the toe region (Provenzano et al., 2002).

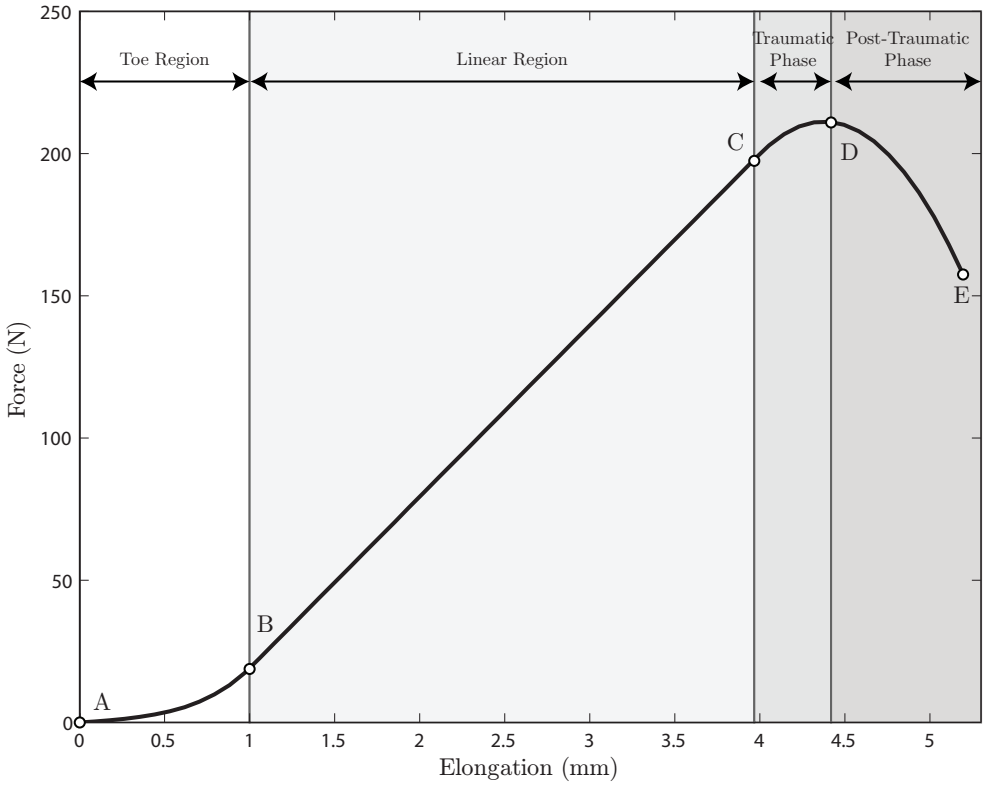

Figure 2.25: Typical force-deflection curve for a ligament exhibits a toe region (AB), a linear region (BC), a traumatic phase (or pretraumatic phase) (CD), and a traumatic phase (DE). Figure adapted from Przybylski et al. (1996).

Spinal ligaments exhibit viscoelastic behaviour like strain-rate dependent stiffness, creep, and stress-relaxation (Chazal et al., 1985; Little and Khalsa, 2005; Lucas et al.,

2009; Nachemson and Evans, 1968; Panjabi et al., 1998; Provenzano et al., 2001; Troyer and Puttlitz, 2011). Typically, tensile tests of ligaments load them in tension until failure, and report descriptive metrics of the shape of their force-deflection curves such as the stiffness, failure force, failure elongation, or ordered pairs representing the points outlined in Figure 2.25. Currently, there is contention in the literature on whether it is more appropriate to report stiffness values as the ratio of the failure force over the amount it was lengthened (Przybylski et al., 1996; Shim et al., 2006), the slope in the linear region (Bass et al., 2007; Chazal et al., 1985; Trajkovski et al., 2014; Yoganandan et al., 1989), or to report a bilinear response where the slope changes at a prescribed displacement to account for the toe region (Chandrashekar et al., 2008; Yoganandan et al., 2000). Of these three methods, it is clear that reporting bilinear slopes will yield a more accurate description of the ligament's stress strain behaviour, although common to all methods is the exclusion of viscoelastic effects, such as rate-dependence (Mattucci et al., 2013). To account for this, the rate-of-strain used in the experiment is reported alongside the stress-strain curve obtained. From a modelling perspective, these studies are consolidated by scaling stress-strain properties from one strain-rate to another (Ahn, 2005; Panzer et al., 2011; Mattucci et al., 2012). A summary of failure properties of ligaments are provided in Tables 2.11, and 2.12.

More recent efforts have attempted to fit the viscoelastic behaviour of cervical ligaments to a viscoelastic model (Lucas et al., 2009; Troyer and Puttlitz, 2011). Traditionally this requires either a creep test, where a ligament is under constant load and the elongation is measured, or a relaxation test, where a ligament is under constant elongation and the force is measured. Although common practice for Quasi-Linear viscoelastic (QLV) or non-linear

viscoelastic tests is to cyclically load the specimens and least-squares fit model predictions to experiment.

More recently, detailed force-deflection curves for all of the cervical spine ligaments were reported alongside methods for scaling the stress-strain curves depending on spinal level, age, and sex (Mattucci, 2011; Mattucci et al., 2013, 2012). These curves are based on failure tests from an impressive 261 human cadaveric ligament specimens.

Table 2.11: Summary of failure characteristics for the upper and middle cervical spine ligaments. Here d_f is the failure elongation in mm unless otherwise specified (note that Przybylski et al. (1996) reports strain in %), and F_f is the failure force. The stiffness reported in these studies is the ultimate failure force over the ultimate strain.

study	Level	Rate (mm/s)	ALL			PLL			LF			CL			ISL		
			d_f (mm)	F_f (N)	K (N/mm)	d_f (mm)	F_f (N)	K (N/mm)	d_f (mm)	F_f (N)	K (N/mm)	d_f (mm)	F_f (N)	K (N/mm)	d_f (mm)	F_f (N)	K (N/mm)
Chazal et al. (1985)	C2-C3	1				2.3	220	95.6									
	C3-C4	1	2.4	140	58.3												
Yoganandan et al. (1989)	C2-T1	9	7.48 (2.15)	120.58 (13.76)	16.4 (0.92)				7.55 (0.49)	131 (12.9)	18.2 (2.4)						
		25	5.53 (1.13)	122.36 (24.27)	26.9 (8.87)				5.65 (0.39)	118 (12.8)	22.1 (3.2)						
		250	6.40 (0.37)	166.39 (31.34)	25.5 (3.98)				6.29 (0.82)	180 (13.1)	32.6 (5.6)						
		2500	6.34 (0.59)	349.48 (44.85)	56.3 (6.34)				7.95 (0.67)	335 (28.0)	42.5 (2.4)						
Myklebust et al. (1988)	C2-C3	9	8.7 (3.8)	207 (98)		9.6 (9.3)	84 (81)		5.8 (0.8)	86 (61)		8.9 (4.6)	211 (130)		7.0 (1.6)	37 (2)	
	C3-C4	9	4.2 (1.8)	47 (14)		7.4 (7.1)	82 (66)		3.7 (1.5)	75 (8)		8.7 (2.2)	224 (60)		6.6 (6.1)	33 (2)	
	C4-C5	9	4.8 (2.9)	47 (13)		3.4 (1.4)	47 (11)		12.8 (7.3)	56 (17)		9.1 (6.0)	170 (20)		6.9 (2.9)	26 (24)	
	C5-C6	9	5.0 (1.7)	89 (67)		4.8 (2.0)	85 (50)		8.0 (4.4)	89 (48)		8.7 (7.9)	144 (36)		5.5 (3.1)	33 (15)	
	C6-C7	9	13.7 (5.7)	176 (25)		5.0 (1.6)	102 (29)		7.7 (0.4)	160 (38)		10.0 (3.9)	277 (147)		9.2 (6.6)	31 (12)	
	C7-T1	9	7.6 (3.8)	97 (28)		6.4 (1.6)	95 (23)		9.9 (6.0)	221 (67)		6.8 (2.8)	264 (88)		8.7 (5.9)	45 (32)	
Przybylski et al. (1996)	C2-C3	0.33	33 % (11)	66 (37)	43 (29)	41 % (7)	150 (71)	78 (36)									
	C3-C4	0.33	43 % (18)	104 (99)	37 (31)	45 % (17)	111 (49)	54 (25)									
	C4-C5	0.33	42 % (17)	106 (61)	54 (27)	33 % (12)	102 (67)	90 (84)									
	C5-C6	0.33	36 % (9)	104 (54)	57 (30)	33 % (10)	89 (42)	65 (33)									
	C6-C7	0.33	39 % (13)	105 (44)	48 (19)	43 % (18)	95 (65)	55 (37)									
Yoganandan et al. (2000)	C2-C5	9	5.80 (0.94)	92.8 (19.5)	16.0 (2.7)	3.46 (0.61)	71.1 (25.8)	25.4 (7.2)	6.51 (1.09)	121 (36.3)	25.0 (7.04)	10.2 (1.97)	239 (62.0)	33.6 (5.53)	6.33 (1.16)	38.6 (9.88)	7.74 (1.61)
	C5-T1	9	6.48 (1.1)	145 (17.0)	17.9 (3.44)	6.10 (1.57)	188 (49.7)	23.0 (2.39)	9.37 (1.39)	129 (16.6)	21.6 (3.65)	7.80 (1.32)	364 (62.9)	36.9 (6.06)	6.72 (1.36)	38.6 (9.92)	6.36 (0.69)
Bass et al. (2007)	C3-C4	627 (M)	1.36 (0.81)	494 (359)		1.05 (0.48)	462 (356)		1.06 (0.53)	315 (97.9)							
	C3-C4	627 (F)	0.97 (0.13)	294 (194)		1.53 (1.01)	587 (640)		1.78 (1.41)	134 (21.4)							
	C5-C6	627 (M)	1.87 (1.04)	326 (116)		1.57 (0.87)	375 (122)		1.05 (0.48)	270 (143)							
	C5-C6	627 (F)	1.41 (0.88)	284 (170)		1.10 (0.80)	358 (158)		1.90 (0.60)	136 (45.0)							
	C7-T1	627 (M)	1.12 (0.35)	355 (242)		1.35 (0.56)	415 (90.4)		0.61 (0.37)	177 (137)							
	C7-T1	627 (F)	1.29 (0.15)	673 (104)		0.95 (0.33)	431 (192)		3.09 (3.03)	303 (98.2)							

Table 2.12: Summary of ligament properties for the upper cervical spine.

Study	Rate (mm/s)	TM			TL			Apical			Alar			LF		
		d_f (mm)	F_f (N)	K (N/mm)	d_f (mm)	F_f (N)	K (N/mm)	d_f (mm)	F_f (N)	K (N/mm)	d_f (mm)	F_f (N)	K (N/mm)	d_f (mm)	F_f (N)	K (N/mm)
Dvorak et al. (1988)						354 (168) 354 (168)			L: 212 (81) R: 216 (60)							
Myklebust et al. (1988)	9	11.9 (2.5)	76 (44)					11.5 (10.5)	214 (115)		14.1 (7.2)	357 (220)		25.2 (14.6)	436 (69)	
Panjabi et al. (1998)	0.1						96.1 (16.5)						80.1 (9.4)			
	920				0.42 (0.17)	436 (54.6)	1472 (691)				0.35 (0.14)	367 (83.2)	2316 (888)			

2.2.2 Intervertebral Disc

The intervertebral disc (IVD) is a composite of three histologically dissimilar regions (the annulus fibrosis, nucleus pulposis, and cartilaginous endplate), inescapably linking the structural properties of the whole disc to the material properties of the individual components. There have been many studies investigating the mechanical properties of each of these constituents, implicating how they contribute to the mechanics of the whole disc.

The mechanical response of the annulus fibrosis to load is the result of the interactions between collagen fibres of the annulus with each other and their surrounding extra-cellular matrix (Wagner and Lotz, 2004). Because of this, individual annular layers are considered the monad for the study of the mechanical properties of the annulus fibrosis. When loaded in tension, the stress-strain relationship of a single annular layer resembles that of a ligament (Figure 2.26): a toe region with a subsequent linear region (Holzapfel et al., 2005). The toe region, like that of ligaments, is believed to be due to the progressive stepwise engagement of collagen fibres during an uncrimping phase (Elliott and Setton, 2001; Schollum et al., 2010). This nonlinear behaviour manifests itself to multilayer specimens under circumferential, axial, and shear loading (Ebara et al., 1996; Elliott and Setton, 2001; Galante, 1967; Green et al., 1993; Gregory et al., 2011; Gregory and Callaghan, 2011; Wu and Yao, 1976). In addition, the stress-strain characteristics of annular layers are dependent on position within the annulus fibrosis. Specifically, the outer annulus fibrosis is stiffer than the inner layers (Holzapfel et al., 2005), thought to be due to local differences in collagen composition (type I versus type II). To complicate matters further, the annulus

exhibits the viscoelastic behaviour stereotypical of biological tissues (Holzapfel et al., 2005; Iatridis et al., 1998).

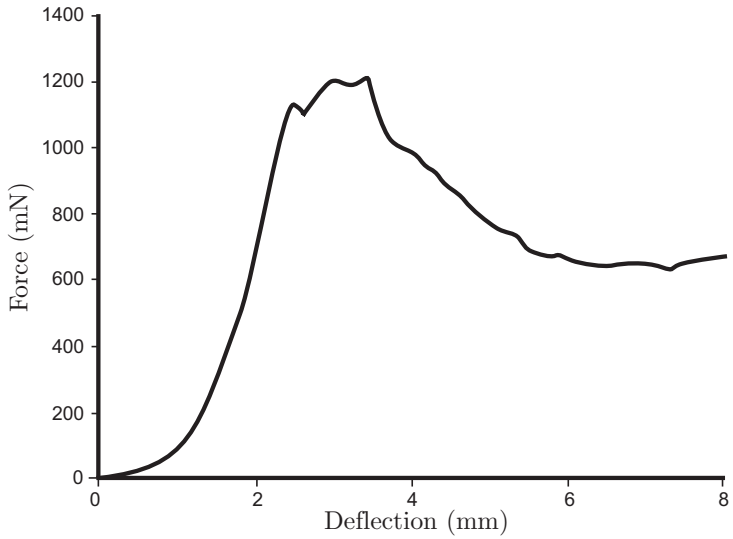

Figure 2.26: Typical force-deflection curve for a multilayer annular specimen loaded in shear. Adapted from Gregory et al. (2011).

The nucleus pulposus had long been considered an incompressible fluid until the mid-1990s when a series of studies tested the responses of isolated nucleus pulposus samples to applied shear stresses (Belytschko et al., 1974; Broberg, 1993; Iatridis et al., 1997a,b, 1996; Lin et al., 1978; Spilker et al., 1986). Until that time, the mechanical behaviour of the nucleus pulposus was inferred based on measurements of pressure on whole inter-vertebral disc specimens, precluding it from any detailed analysis of its load-deformation characteristics (Iatridis et al., 1996). From these studies, it became clear that the nucleus pulposus behaved as a viscoelastic fluid at low strain-rates and like a viscoelastic solid at high strain-rates, which could be well explained with Fung's Quasilinear Viscoelastic (QLV) theory (Fung, 1967; Iatridis et al., 1996).

The endplate is comprised of hyaline cartilage which is viscoelastic in nature (Hayes and Mockros, 1971). Unlike ligaments and annulus fibrosis, the mechanism behind cartilage viscoelasticity is thought to be the flow of fluids through its porous media (Mow and Guo, 2002). Because of this, it is common to use a poroelastic model for cartilage rather than a viscoelastic one (DiSilvestro and Suh, 2001; Panzer et al., 2011). Briefly, a poroelastic model treats a material as consisting of two phases: an elastic solid phase which houses a population of pores (unoccupied volume inside it), and fluid substance which occupy the space in the pores – much like a saturated sponge holding water. The interaction between the two phases allows a material to exhibit viscoelastic-like properties, with the added feature of dependence on the geometry of the body (Carter and Wong, 2003; Mow and Guo, 2002; Wang et al., 2014). Poroelasticity is a continuum model (Mow and Guo, 2002), and is more appropriate for use in finite element formulations than multibody simulations. It will not be discussed further.

Despite extensive research into the viscoelastic properties of the constituents of the IVD, such detailed research on whole cervical disc specimens is limited (Moroney et al., 1988b; Yoganandan et al., 2001, 1996) (Table 2.13). While the elastic response of the disc has been studied in detail, the viscous contributions have been largely ignored. It seems that the most comprehensive analysis of the viscoelastic properties of the cervical spine intervertebral disc was done by Lucas et al. (2006), and went unpublished; it is only available as a conference preceding.

Intervertebral discs are typically modelled as *bushing elements* (Christophy et al., 2013; Karajan et al., 2013), which is a generalized 6 degree of freedom Voigt model. Specifically, the forces and moments exerted by the intervertebral discs are given by:

Table 2.13: Summary of Stiffness values for isolated intervertebral discs (motion segments with posterior elements removed).

Study	Level	Compression (N/mm)	Tension (N/mm)	Shear (N/mm)	Flexion (Nm/deg)	Extension (Nm/deg)	Bending (Nm/deg)	Torsion (Nm/deg)
Moroney et al. (1988b)		492 (472)		Ant: 62 (63) Post: 50(36) Lat: 73(62)	0.21 (0.14)	0.32 (0.15)	0.33 (0.18)	0.42 (0.17)
Yoganandan et al. (2001)	C2-C3	637.5						
	C3-C4	765.3						
	C4-C5	784.6						
	C5-C6	800.2						
	C6-C7	829.7						
	C7-T1	973.6						
Yoganandan et al. (1996)	C2-C3		63.5					
	C3-C4		69.8					
	C4-C5		66.8					
	C5-C6		22.0					
	C6-C7		69.0					
	C7-T1		82.2					

$$\vec{F} = \mathbf{K}\vec{q} + \mathbf{C}\dot{\vec{q}} \tag{2.1}$$

Here, $\mathbf{K}$ is a 6×6 stiffness matrix, and $\mathbf{C}$ is a 6×6 viscosity matrix; $\vec{F}$ is a 6×1 vector containing the forces and moments, and $\vec{q}$ is a 6×1 vector of the generalized coordinates. Usually only the main diagonals of each of these matrices are considered (de Jager et al., 1996; van der Horst et al., 1997; van Lopik and Acar, 2007), but doing this ignores the coupling of motions that occurs due to the intervertebral disc (Moroney et al., 1988b). Some authors have even criticised the linearity of such a relationship (Karajan et al., 2013).

2.2.3 Mechanical Properties of Motion Segments

Despite the lack of literature on the stress-strain properties of individual discs, there are plenty of data on motion segments (Goel et al., 1988a,b, 1984; Nightingale et al., 2002; Panjabi et al., 1991c; Schulte et al., 1989; Voo et al., 1998). Since the motion segment is

comprised of the entire osteoligamentous structure surrounding the disc, it is not surprising that the force-deflection and moment-angle relationships resemble that of ligaments and isolated disc specimens: featuring an exponential toe region, linear region, and subsequent failure. In addition, many studies have examined the range of motion of FSUs in flexion-extension, axial rotation, and lateral bending (Camacho et al., 1997; Dvorak et al., 1987; Ivancic, 2013; Nightingale et al., 2007; Panjabi and Courtney, 2001; Panjabi et al., 1988; Puttlitz et al., 2004; Wheeldon et al., 2006) which are summarized in Tables 2.14, 2.15, and 2.16.

Table 2.14: Summary of range of motions of cervical motion segments, in degrees mean (standard deviation), in flexion/extension.

Study	Load (Nm)	C0-C1	C1-C2	C2-C3	C3-C4	C4-C5	C5-C6	C6-C7	C7-T1
Goel et al. (1984)	0.3						10.1 (2.3)		
Goel et al. (1988a)	0.3	23.0 (2.0)	10.1 (2.5)						
Goel et al. (1988b)	0.3				6.4 (1.2)	6.2 (1.2)	5.2 (1.1)	5.7 (1.3)	2.3 (0.7)
Moroney et al. (1988b)	1.8			9.1 (1.9)	9.1 (1.9)	9.1 (1.9)	9.1 (1.9)	9.1 (1.9)	9.1 (1.9)
Panjabi et al. (1988)	1.5	24.5 (1.4)	22.4 (1.6)						
Schulte et al. (1989)	0.45					6.5 (1.6)	4.5 (1.8)	4.4 (1.5)	5.2 (1.7)
Panjabi et al. (1991c)	1.5	28.8 (3.2)	33.2 (4.2)						
Wen et al. (1993)			23.8 (4.9)	11.1 (3.0)	12.0 (4.0)	13.3 (3.5)	11.9 (4.4)	11.6 (5.0)	
Camacho et al. (1997)	1.5	28.3	11.8	10.4	10.6	10.8	8.3	5.9	
Richter et al. (2000)	2.5						13.4 (3.1)		
Winkelstein et al. (2000)	1.5				11.6 (2.0)		9.8 (1.2)		
Panjabi and Courtney (2001)	1.0	27.4 (3.7)	24.4 (4.8)	6.2 (1.2)	7.7 (2.5)	10.1 (2.5)	9.9 (2.7)	7.1 (2.0)	
Nightingale et al. (2002)	1.5	58.4 (10.7)	20.8 (3.0)	22.8 (2.3)		13.8 (2.8)			
Puttlitz et al. (2004)	1.0					9.4 (2.2)			
Wheeldon et al. (2006)	2.0			14.1	12.9	12.7	14.5	14.3	7.60
Nightingale et al. (2007)	1.5	51.4 (9.3)	17.3 (3.9)	14.6 (5.8)					
Ivancic (2013)	1.5	18.6 (5.9)	12.0 (4.3)	6.4 (4.4)	7.9 (4.5)	8.1 (2.1)	9.9 (4.1)	8.8 (2.7)	5.3 (1.3)

Table 2.15: Summary of range of motions of cervical motion segments, in degrees mean (standard deviation), in axial rotation.

Study	Load (Nm)	C0-C1	C1-C2	C2-C3	C3-C4	C4-C5	C5-C6	C6-C7	C7-T1
Goel et al. (1984)	0.3					3.6 (1.3)	2.8 (0.8)		
Goel et al. (1988a)	0.3	4.8 (1.2)	46.6 (11.2)						
Goel et al. (1988b)	0.3				4.6 (1.8)	4.6 (1.3)	4.6 (1.0)	3.4 (1.4)	2.8 (0.8)
Moroney et al. (1988a)	1.8				8.4 (1.38)	8.4 (1.38)	8.4 (1.38)	8.4 (1.38)	8.4 (1.38)
Panjabi et al. (1988)	1.5	14.5 (0.7)	77.8 (1.7)						
Schulte et al. (1989)	0.45					5.0 (1.8)	2.6 (0.8)	2.2 (0.9)	4.2 (1.6)
Panjabi et al. (1991b)	1.5	9.3 (3.6)	71.4 (9.4)						
Chang et al. (1992)	2.0		74.8 (5.9)						
Wen et al. (1993)			75.9 (8.3)	11.1 (2.9)	12.2 (4.4)	15.5 (4.7)	11.0 (3.6)	9.8 (4.3)	
Richter et al. (2000)	2.5						8.6 (2.4)		
Panjabi and Courtney (2001)	1.0	9.9 (3.0)	56.7 (4.8)	3.3 (0.8)	5.1 (1.2)	6.8 (1.3)	5.0 (1.0)	2.9 (0.8)	
Puttlitz et al. (2004)	1.0					9.9 (2.1)			
Ivancic (2013)	1.5	10.2 (4.0)	62.9 (13.1)	5.8 (4.1)	7.4 (5.7)	7.5 (2.6)	7.2 (2.3)	6.1 (3.0)	6.6 (3.6)

Table 2.16: Summary of range of motions of cervical motion segments, in degrees mean (standard deviation), in lateral bending.

Study	Load (Nm)	C0-C1	C1-C2	C2-C3	C3-C4	C4-C5	C5-C6	C6-C7	C7-T1
Goel et al. (1984)	0.3					5.4 (1.1)	4.6 (1.4)		
Goel et al. (1988a)	0.3	6.8 (2.8)	8.4 (2.8)						
Goel et al. (1988b)	0.3				6.4 (1.8)	7.2 (2.4)	4.8 (1.3)	3.6 (1.1)	3.0 (0.9)
Moroney et al. (1988a)	1.8			9.4 (3.0)	9.4 (3.0)	9.4 (3.0)	9.4 (3.0)	9.4 (3.0)	9.4 (3.0)
Panjabi et al. (1988)	1.5	11.0 (0.9)	13.4 (1.5)						
Schulte et al. (1989)	0.45					6.0 (1.6)	2.4 (0.9)	2.8 (0.9)	3.6 (0.9)
Panjabi et al. (1991c)	1.5	10.7 (2.5)	10.5(5.8)						
Wen et al. (1993)			8.3 (2.2)	11.6 (2.2)	10.8 (3.4)	10.5 (4.1)	10.0 (3.3)	9.8 (3.7)	
Richter et al. (2000)	2.5						9.9 (2.4)		
Panjabi et al. (2001b)	1.0	9.1 (1.5)	6.5 (2.3)	9.6 (1.8)	9.0 (1.9)	9.3 (1.7)	6.5 (1.5)	5.4 (1.5)	
Puttlitz et al. (2004)	1.0					13.0 (3.6)			
Ivancic (2013)	1.5	6.8 (2.3)	6.2 (4.6)	4.6 (3.4)	4.0 (2.8)	4.5 (1.6)	3.9 (1.8)	4.0 (2.0)	4.5 (2.0)

2.3 Muscle Modelling

The formal scientific study of muscle tissue is roughly as old as calculus is: beginning in the mid-to-late seventeenth century with the pioneering microscope studies of Antonie van Leeuwenhoek, the microscope's inventor, and William Croone, a founding member of the British Royal Society (Martonosi, 2000). However, it was Archibald Hill, three-hundred years later, who formally reconciled calculus with the study of muscular tissue (Hill, 1938). Since that time, the problem of muscle mechanics has been broken up into two sub-problems: modelling of muscular activation, and modelling of muscle force production (Figure 2.27).

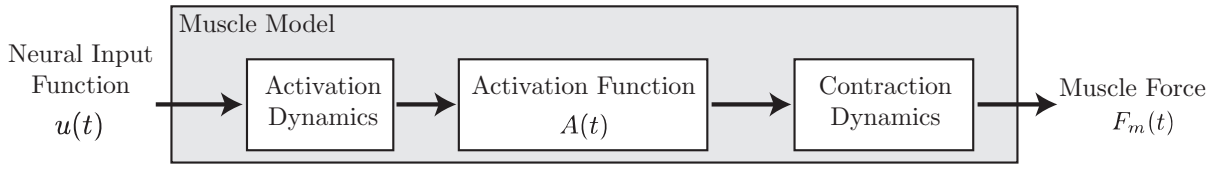

Figure 2.27: Conceptualization of how activation and contraction dynamics make up a muscle model.

Muscle modelling naturally arises in biomechanics from the problem of indeterminacy (Figure 2.28) in inverse dynamics (Winter, 1990). Briefly, standard Newtonian mechanics provides six equations of motion per segment; however, since muscle forces are unknown, the resulting system has more unknowns than equations. Such a system is algebraically underdetermined with no unique solution – so the question is, of the set of muscle forces which solve Newton's equations, which one is realized in nature?

This problem has been 'solved' in three different ways with varying levels of success. The first method is the most simplistic. It treats the joint as only having one muscle crossing it –

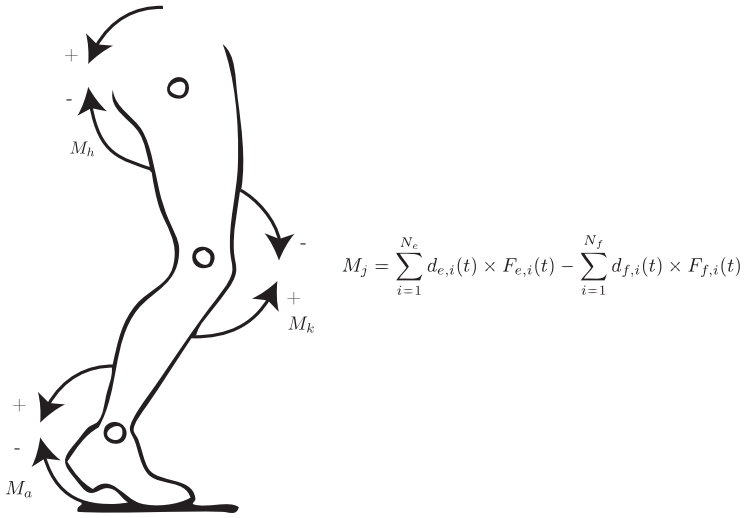

Figure 2.28: The problem of indeterminacy: there are N_e extensors and N_f flexors at each joint, each with their own moment arms, and only three net-joint moment equations to work with. Adapted from Winter (1990).

a method called the *single muscle equivalent*. With this one unknown, Newton's equations can be solved and the muscle force can be obtained. The downside is that any claim about physiology or co-contraction loses credibility, since to balance the net joint moment, the muscle must be able to push. A better solution, *optimization*, is to assume that, of the set of muscle forces which solve Newton's equations, the one realized in nature minimizes some cost function (Crowninshield and Brand, 1981; Delp et al., 2007; Dickerson et al., 2007; Lin et al., 2010; Moroney et al., 1988b). The final method, an *electromyography driven model*, is to use an electromyogram as an approximation of neural commands into a detailed biomechanical model of the muscle (Cholewicki and McGill, 1996; Lloyd and Besier, 2003). In this method, the process of muscle modelling can be considered the process of converting a neural input function $u(t)$ into the muscle force, $F_M(t)$, typically with the existence of an intermediate function $A(t)$ representing the amount of muscle in

the 'active state' – a loosely defined term coined by Hill (1949) to describe the onset of force generation in muscles. The process of obtaining $A(t)$ is called *activation dynamics*, while the process of obtaining $F_M(t)$ is *contraction dynamics* (Zajac, 1989).

2.3.1 Activation Dynamics

The term activation dynamics encompasses the events in muscular force production from the action potential of a motor-neuron to the calcium-troponin dynamics that take place in the sarcomere. Mathematically, the process begins with the definition of a neural input function, $u(t)$, which is meant to represent the arrival of action potentials to the surface of the myocyte cell membrane. The acquisition of such a function is non-trivial, sometimes done through electromyography (Cholewicki and McGill, 1996; McGill and Brown, 1992; Olney and Winter, 1985; Shao et al., 2009), an educated guess about the system (Brolin et al., 2008; de Jager et al., 1996; Panzer et al., 2011; van Lopik and Acar, 2007), optimization (Delp et al., 2007), or a combination of the above (Cholewicki and McGill, 1996; Lloyd and Besier, 2003). Once the neural input function is obtained, it is used as an input into the activation dynamics model.

Electromyography

The electrochemical events in muscle recruitment are complex: a motor neuron initially discharges an action potential to its motor unit, the muscle fibres of which subsequently propagate their own action potentials down their respective sarcolemma (Fuglevand et al., 1993; Milner-Brown et al., 1973). A recording electrode in the vicinity of the myocyte will

detect a change in the electrical potential due to the rapid movement of ions through the cell membranes of the cells involved (De Luca, 1979). The time-series acquired by this electrode is called the *electromyogram*, and the study of the electromyogram is *electromyography* (EMG) (Winter, 1990). Since muscle modelling begins with a description of the activation dynamics of the muscle cell, and because EMG effectively measures a superposition of action potentials from the underlying muscle, it stands to reason that it may be a good candidate for the neural input function (Farina and Negro, 2012).

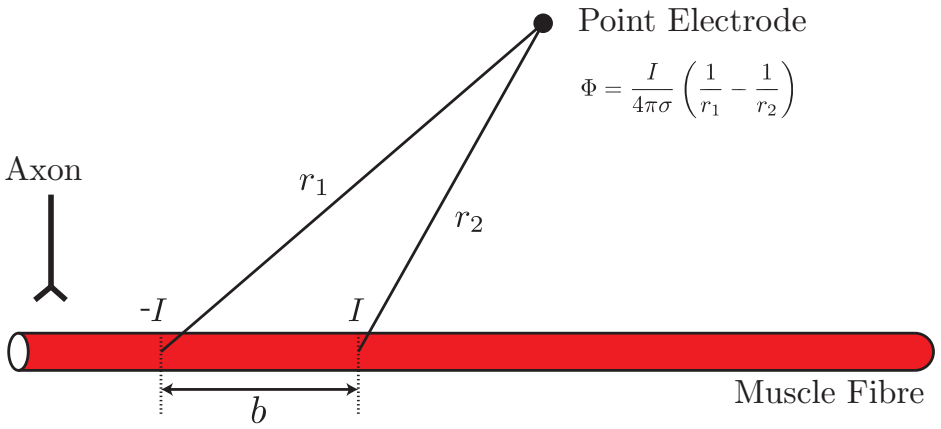

Figure 2.29: The dipole model of the action potential's effect on EMG. Adapted from Fuglevand et al. (1992).

Generally speaking, there are two types of electrodes commonly used in biomechanics: surface and in-dwelling (Winter, 1990). Surface EMG electrodes rest on the skin over the muscle, while in-dwelling electrodes are attached to a hypodermic needle and inserted into the muscle of interest. Surface electrodes contain a metal material, typically silver-silver chloride, and the size, shape, and orientation of the electrodes has an influence on the nature of the EMG signal obtained (Winter, 1990). Fuglevand et al. (1992) used a dipole model (Figure 2.29) to explain a number of phenomena commonly seen with EMG.

Firstly, the vast majority of the EMG signal came from muscle fibres located only within 10 -- 12 mm of the electrode, which seemed to be independent of the electrode's size. Secondly, Fuglevand noticed that the inter-electrode distance effectively band-pass filtered the resulting EMG, with a larger spacing correlating with a shorter pass-band. Finally, the best results for the shape of the electrode was a lengthened electrode aligned with the orientation of the fibres.

Activation Models

Hatze (1977) presented a very detailed mechanistic model which extrapolates an analysis of a single muscle fibre to the entire muscle. Hatze embarked on a lengthy derivation a differential system to model the activation dynamics of muscle, taking the form of the initial value problem (IVP):

$$\dot{\gamma} = m(cv - \gamma) \qquad \gamma(0) = 0 \qquad (2.2)$$

$$\dot{A} = m\mu(cv - \gamma) \qquad A(0) = q_0 \qquad (2.3)$$

$$\dot{\mu} = m(cv - \gamma)[r_1(\xi)(1 - q_0)u + q_0 - A) - r_2(\xi)\mu] \qquad \mu(0) = 0 \qquad (2.4)$$

Here γ is the concentration of intracellular calcium ions. A is the activation function, which Hatze took to be the number of bound actin-myosin cross-bridges. And μ is the average active state rate, which describes how the active-state changes with variations in the calcium concentration. The constants, m, c, are parameters obtained through the simplification of the membrane dynamics from two coupled second order ordinary differential equations, to a single first order one. q_0 represents the number of bound cross-bridges when

the muscle is at rest. Hatze reasoned that r_1 and r_2, functions which describe the affinity of an actin-myosin bond to form, should be dependent on the length of the muscle, as:

$$r_1(\xi) = r\left(1 - \left(\frac{n}{\xi}\right)^2\right) \tag{2.5}$$

$$r_2(\xi) = 4\varrho^2 r_1(\xi) \tag{2.6}$$

Where r, s and ϱ are parameters which define the relationship of a muscle's length to its capacity to generate actin-myosin bonds. In Equations 2.2 —2.4, u and v, which Hatze called control parameters, represent the proportion of recruited motor units and average firing rate of the muscle respectively. A downside of Hatze's modelling paradigm is that it does not explicitly utilize the neural input function, which renders it difficult to reconcile with EMG.

In a four-part series, Hof and Van den Berg (1981a,b,c,d) proposed and validated a processing method to convert the electrical potential measured with EMG to force with the aid of a Hill-type muscle model. To obtain the neural input function, $u(t)$, the raw EMG is band-pass filtered from 30 to 600 Hz, full-wave rectified, and smoothed with a moving averaging filter with a period of $\tau_1 = 25$ ms. The conversion to the active state, defined here as the number of bound cross-bridges, is accomplished by:

$$A(t) = \max_{\Delta t} \begin{cases} u(t - \Delta t) & 0 \leq \Delta t < \tau_2 \\ u(t - \Delta t) \exp\left(-\frac{\Delta t - \tau_2}{\tau_3}\right) & \tau_2 \leq \Delta t \end{cases} \tag{2.7}$$

Here, τ_2 and τ_3 are constants dictating the window-width and decay time of the activation function, manually inducing the electromechanical delay of the muscle – the delay

between the arrival of the action potential and the maximum force developed from a twitch (Corcos et al., 1992). This activation model follows rises and plateaus in the full-wave rectified EMG exactly, and exponentially decays if the EMG abruptly decreases. This technique establishes a plausible activation function, which Hof and Van den Berg then used as an input into a Hill type muscle model.

Like Hof and Van den Berg (1981a), Winter (1976) uses the full-wave rectified band-passed filtered EMG as the neural input function, and the active state is (implicitly) defined to be related to the number of bound actin-myosin cross-bridges. Unlike Hof and Van den Berg (1981a), Olney and Winter (1985) low pass filter the full-wave rectified EMG with a filter whose transfer function mimics that of a twitch response. The twitch response has been well described by a critically damped second order system (Milner-Brown et al., 1973), so a second-order single-pass critically damped digital filter is applied to the full-wave rectified EMG, although a Butterworth filter is sometimes used (Cholewicki and McGill, 1996; Robertson and Dowling, 2003). Using a single pass filter will induce a time-shift in the time-series, which can be exploited to account for the electromechanical delay of the muscle. Specifically, if a muscle's twitch-time, T, is known, then an appropriate cut-off frequency for the filter is determined by:

$$f_c = \frac{1}{2\pi T} \tag{2.8}$$

The resulting waveform is known as the linear envelope. Strong correlations have been reported in the literature between linear enveloped waveforms and force (Calvert and Chapman, 1977; Crosby, 1978), with a mixture of researchers reporting linear (Lippold, 1952) and non-linear relationships (Fuglevand et al., 1993; Guimaraes et al., 1995; Herzog

et al., 1998; Zuniga and Simons, 1969).

Zajac (1989) proposed an activation-dynamic model where activation levels are related to the neural input by a single bilinear first order system. Zajac insists that the excitation dynamics are governed by a first order system, even claiming that it would be a misnomer to use the term *musculotendon contraction dynamics* otherwise. In this method (Equation 2.9), the neural input acts as both a modulator on the relaxation constant of the system as well as a forcing term.

$$\frac{dA}{dt} + \left(\frac{1}{\tau_{\text{act}}} \left(\beta + (1-\beta)u(t) \right) \right) A(t) = \frac{1}{\tau_{\text{act}}} u(t) \tag{2.9}$$

Here β is a constant that determines how the idealized neural input will affect the time-parameter for the first order system. For $u = 0$, no neural drive, the relaxation time constant is β/τ_{act}; conversely for $u = 1$, indicating full neural drive, the activation time is $1/\tau_{\text{act}}$. If EMG is to be used as an input, then $u(t)$ would be the linear enveloped EMG (Zajac, 1989). Since its inception, Equation 2.9 has been revised and packaged in the open source biomechanical software package OpenSim (Simbios, NIH Center for Biomedical Computation at Stanford University, Stanford, CA), which uses the differential equation (Delp et al., 2007):

$$\frac{dA}{dt} = \begin{cases} (u - A)\left(\frac{u}{\tau_a} + \frac{1-u}{\tau_d} \right) & u \geq A \\ \frac{u-A}{\tau_d} & u < A \end{cases} \tag{2.10}$$

Where τ_a and τ_d are the activation and deactivation time-constants for this first-order system. Both Zajac (1989) and OpenSim (Delp et al., 2007) advocate coupling these activation dynamic schemes with a Hill type muscle model.

Winters and Stark (1985) hypothesized a different activation scheme. By taking the number of bound cross-bridges as the active state, and introducing an intermediate excitation function $E(t)$, Winters and Stark proposed the coupled linear system:

$$\frac{dE}{dt} = \frac{u(t) - E(t)}{\tau_d} \tag{2.11}$$

$$\frac{dA}{dt} = \frac{E(t) - A(t)}{\tau_a} \tag{2.12}$$

Where τ_a and τ_d are the activation and deactivation time-constants respectively. When $u > E$, the system is in a state of excitation, and E will increase. Similarly, when $E > A$, the system is in a state of activation, and $A(t)$ will increase. With some routine manipulations, this system can be written as a second order equation in $A(t)$:

$$\tau_a \tau_d \frac{d^2A}{dt^2} + (\tau_a + \tau_d)\frac{dA}{dt} + A = u(t) \tag{2.13}$$

If $u(t)$ is taken to be the rectified EMG, then this is equivalent to filtering it with a second order system. Moreover, if $\tau_a = \tau_d$, then Equation 2.13 is critically damped, rendering this approach equivalent to Winter (1976). In this way, Winter's approach is a special case of Winters and Stark's where the activation and relaxation time-constants are the same.

A more recent development is that of Buchanan et al. (2014). This method, like Winter's, was designed to operate on EMG to obtain activation state, and it begins, similar to Winter's, by obtaining a 'linear envelope'[1] of the EMG through full-wave rectification,

[1]Caveat: Buchanan et al. (2014) is using a dual-pass filter rather than single-pass.

dual-pass low-pass Butterworth filtering (cut-off frequency of 2 – 6 Hz), and normalization of EMG, denoted $e(t)$. The neural input function is then obtained from the linear enveloped EMG by use of the second order system, typically computed through the digital filter (Buchanan et al., 2014; Lloyd and Besier, 2003):

$$\text{Analog: } u = M\frac{d^2e}{dt^2} + B\frac{de}{dt} + Ke \tag{2.14}$$

$$\text{Digital: } u_i = \alpha e_{i-d} - \beta_1 u_{i-1} - \beta_2 u_{i-2} \tag{2.15}$$

Where M, is the mass, B is the damping and K is the stiffness of the analog second order system. For the digital system, d is the electromechanical delay (in frames), and $\alpha = \beta_1 + \beta_2 + 1$ with $\beta_1 = \gamma_1 + \gamma_2$, $\beta_2 = \gamma_1\gamma_2$, subject to $|\gamma_1| < 1$ and $|\gamma_2| < 1$, are requirements for the numeric stability of the filter (Buchanan et al., 2014). Finally, the activation, $A(t)$ is obtained from the neural input function by one of the nonlinear functions:

$$A(t) = \begin{cases} d\ln(cu(t)+1) & 0 \le u(t) < 0.3 \\ mu(t) + b & 0.3 \le u(t) < 1 \end{cases} \tag{2.16}$$

or:

$$A(t) = \frac{e^{\kappa u(t)} - 1}{e^{\kappa} - 1} \tag{2.17}$$

Where d, c, m, κ, and b are parameters that characterize the nonlinearity between neural activation and muscle activation. This highly convolved method is far removed from the phenomenology of a muscle twitch resembling a second-order system, effectively running

the rectified EMG through a sixth order system in addition to a non-linear transformation at the end.

Summary of Activation Models

There is a great diversity in the choice of activation dynamic model although each showcase similar end-results after processing: all of which resemble the response of a first-order system (e.g. Figure 2.30). Of all of the methods, Winter's has the most utility, employing a transfer function that is reminiscent of a muscle's twitch response while also being the easiest to drive with EMG. The other methods seem to be more effort computationally, with a similar end result, and no underlying biological reasoning. An exception might be Buchanan's processing method, which was markedly different from the others, adhering to the original shape of the input signal but inducing a noticeable phase-lag (see bottom graph in Figure 2.30). To be fair to this approach, the input function, in this case a box-function, would have been processed with a dual pass fourth order Butterworth filter previously with a cut-off frequency of 6 Hz. Unfortunately, the resulting overshoot from processing data in this way makes it very hard to justify physiologically, and it seems to dramatically over-process the data.

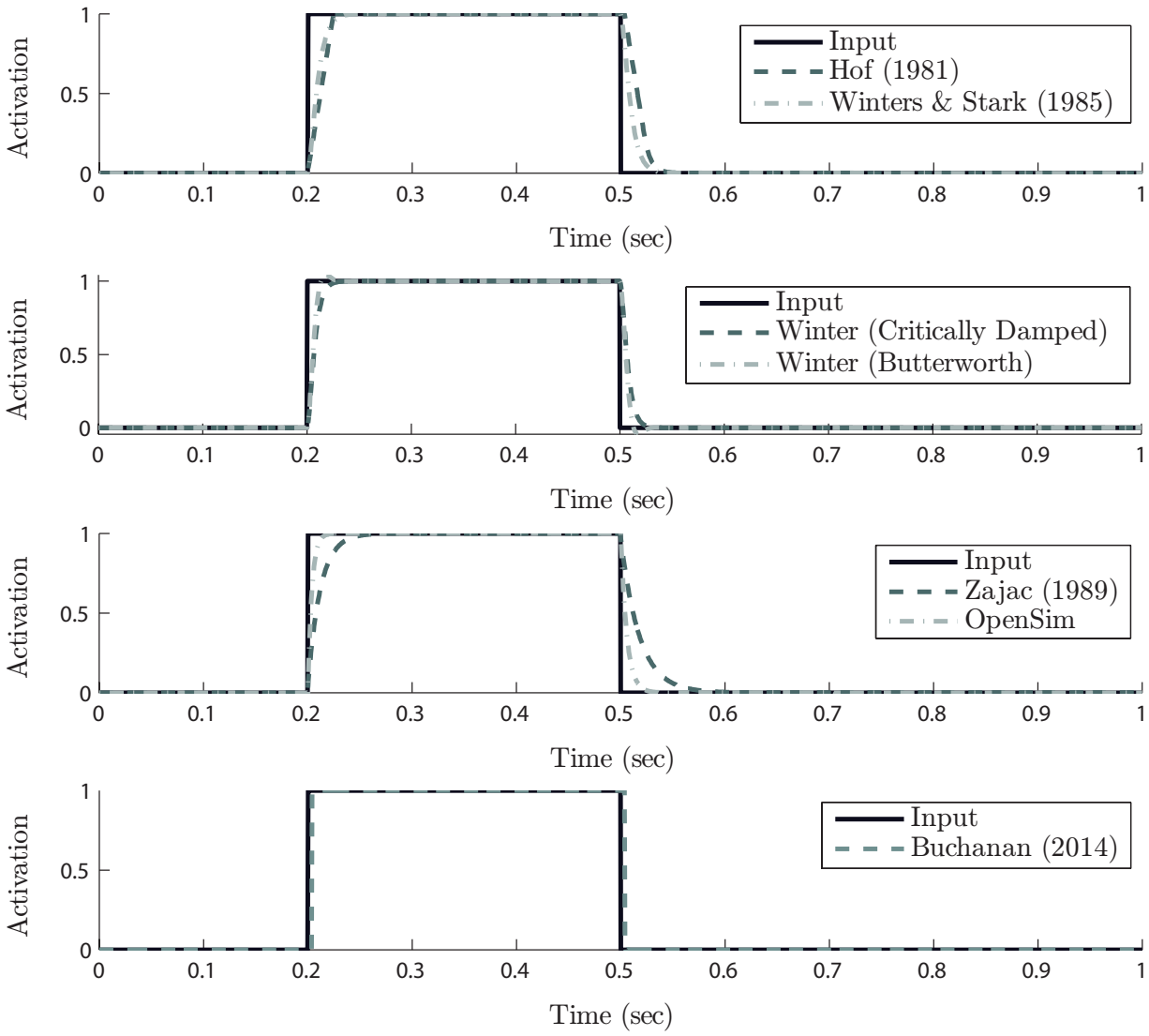

Figure 2.30: Comparison of the response of the activation dynamic models to a box-function input. Hof and Van den Berg (1981a,b,c,d), Winter (1990) and Buchanan et al. (2014) were implemented as per their description. Zajac (1989) and Winters and Stark (1985) methods were implemented using the Backward Euler method, while the OpenSim method was simulated using a forward Euler numerical method.

2.3.2 Contraction Dynamics

There are three main types of muscle model in biomechanics: the Hill type muscle model, the Huxley muscle model and the Distribution Moment Model. The Hill-type muscle model is the most widely adapted in biomechanics (Winters, 1990). It is a phenomenological model, inheriting from the early work of Hill (1938). The Huxley model is a mechanistic model, more commonly used in biophysics than larger scale biomechanics (Winters, 1990). Finally, the distribution moment model is a simplification of Huxley's model, which reduces it from a partial differential equation to a series of ordinary differential equation. These models are described in great detail below.

The Hill Muscle Model

The Hill type muscle model was developed from observations made by Nobel Laureate Archibald Hill (Hill, 1938). Hill originally derived an expression relating the amount of force in muscle to its shortening velocity, however modern implementations of the model include the relationship between force and muscle fibre length discovered by Huxley (Gordon et al., 1966; Hill, 1938). The muscle is partitioned into a contractile element, a series (considered the tendon) elastic element, and a parallel elastic element (Figure 2.31), each of which with its own constitutive expression relating the muscle's length to its force output. The force in the tendon, is then given by:

$$F_T = (F_{CE} + F_{PE}) \cos\theta \tag{2.18}$$

Where F_{CE} is the force in the contractile element, θ is the pennation angle, F_{PE} is the

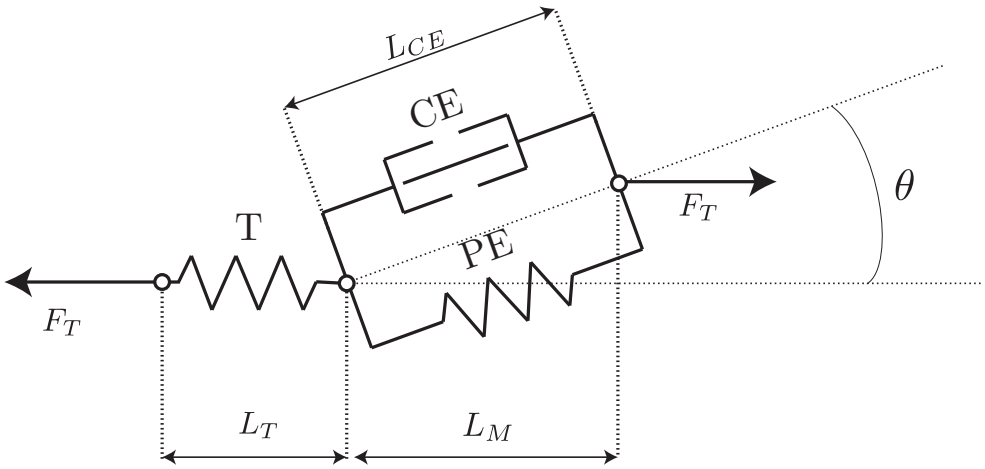

Figure 2.31: The Hill-type muscle model. PE is the parallel elastic component, CE is the contractile element, T is the tendon, and the angle θ is the pennation angle. F_T is the force in the tendon (and therefore related to the muscle).

force in the parallel element and F_T is the force in the tendon. The passive components of muscle has been observed to be nonlinear and viscoelastic (Hatze, 1977; Van Ee et al., 2000; Zatsiorsky and Prilutsky, 2002), and are typically modelled as exponential springs with constitutive expression:

$$F_{PE} = \frac{F_k}{e^{k_T \varepsilon_k} - 1} \left(e^{k_T \varepsilon} - 1 \right) \tag{2.19}$$

Where F_{PE} is the force in the parallel element, k_T is the exponential stiffness of the tissue, and ε, is the strain and the ordered pair (ε_k, F_k) is a reference point on the stress-strain[2] curve. The contractile element in Hill's model has a force generating capacity that obeys two empirical observations: the *force-length* and *force-velocity* relationships. The force-velocity relationship was originally described by Hill (1938), who derived the hyperbolic relationship:

[2]With the proper adjustments, this can also be taken from a force-deflection curve.

$$(F + a)(v + b) = (F_0 + a)b \tag{2.20}$$

Where F is the force, F_0 is the maximum force, and v is the velocity, and the parameters a and b define the shape of the relationship. The hyperbolic relationship predicts a decrease in the force-generating capacity of muscle tissue with increasing shortening velocity (Figure 2.32). Unfortunately, Hill's original derivation is not extendible to eccentric contractions, and other empirically derived fits to force-velocity data are used.

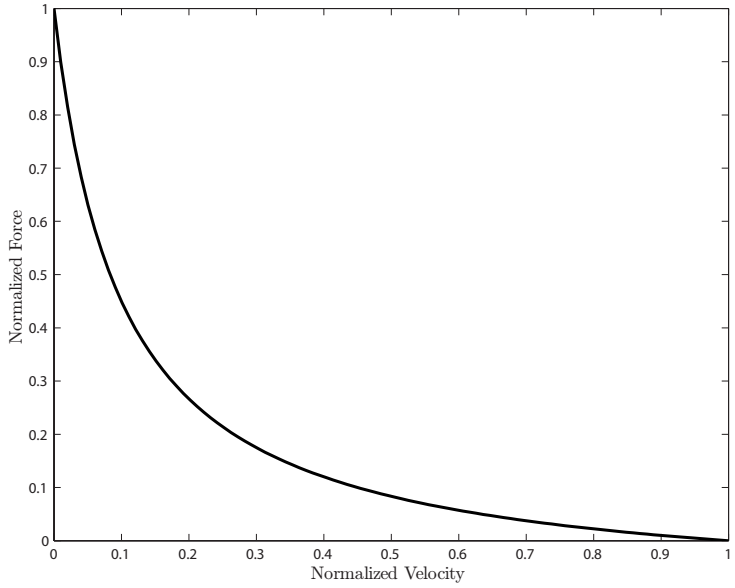

Figure 2.32: The force-velocity relationship for $F_0 = 1$, $a = b = 1/2$, where the axis have been normalized.

Gordon et al. (1966) observed that the force-generating capacity of a sarcomere seemed to change with the length of the sarcomere. In particular, sarcomeres have an optimal length for force generating potential that decays as they are lengthened or shortened. These observations were accompanied with a mechanism that Huxley termed the *sliding*

filament theory (Huxley and Simmons, 1971). Both the force-velocity and force-length relationships, together with the active-state of the muscle are combined in a multiplicative fashion to yield the Hill-type muscle model, an expression for the force-development in the contractile element (Equation 2.21).

$$F_{CE} = F_{\max} A(t) f_\ell(L_{CE}) f_v(\dot{L}_{CE}) \tag{2.21}$$

Where f_ℓ describes the force-length relationship (Figures 2.33 and 2.34), f_v denotes the force-velocity relationship, $A(t)$ is the active state of the muscle, and $F_{\max}$ is the maximum muscle force; sometimes represented $F_{\max} = \sigma_{\max} A_{\text{phys}}$, where $\sigma_{\max}$ is the specific muscle tension and A_{phys} is the physiological cross-sectional area (PCSA) (Zatsiorsky and Prilutsky, 2002). The specific tension of muscles is the subject of some scrutiny of the model because of the wide range of values reported in the literature (35 – 137 N/cm^2) (Buchanan, 1995; Thelen, 2003). Taken together, the entire muscle model is written:

$$F_T = \Big(F_{\max} A(t) f_\ell(L_{CE}) f_v(\dot{L}_{CE}) + F_{PE} \Big) \cos\theta \tag{2.22}$$

The Hill-type muscle model is the most widely used muscle model in biomechanics (Winters, 1990), despite its phenomenological nature. The model has been criticized on the basis of being *too simple* since it fails to reproduce some experimental results on isolated muscles. Additionally, being overly complex as more empirical relationships are added to it (Winters, 1990). For example, during eccentric muscle contraction at low activation there is a notable decrease in the force generating capacity of the muscle, which is not accounted for in models using the original force-velocity relationship (termed 'muscle yielding' in

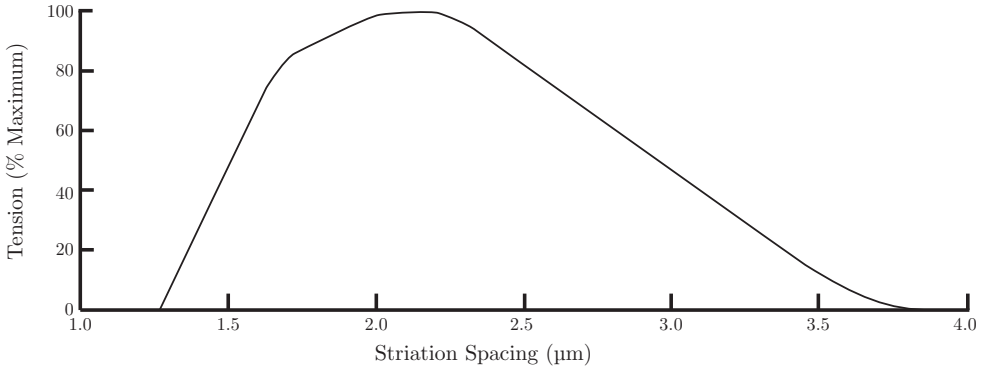

Figure 2.33: The force-length relationship, adapted from Gordon et al. (1966)

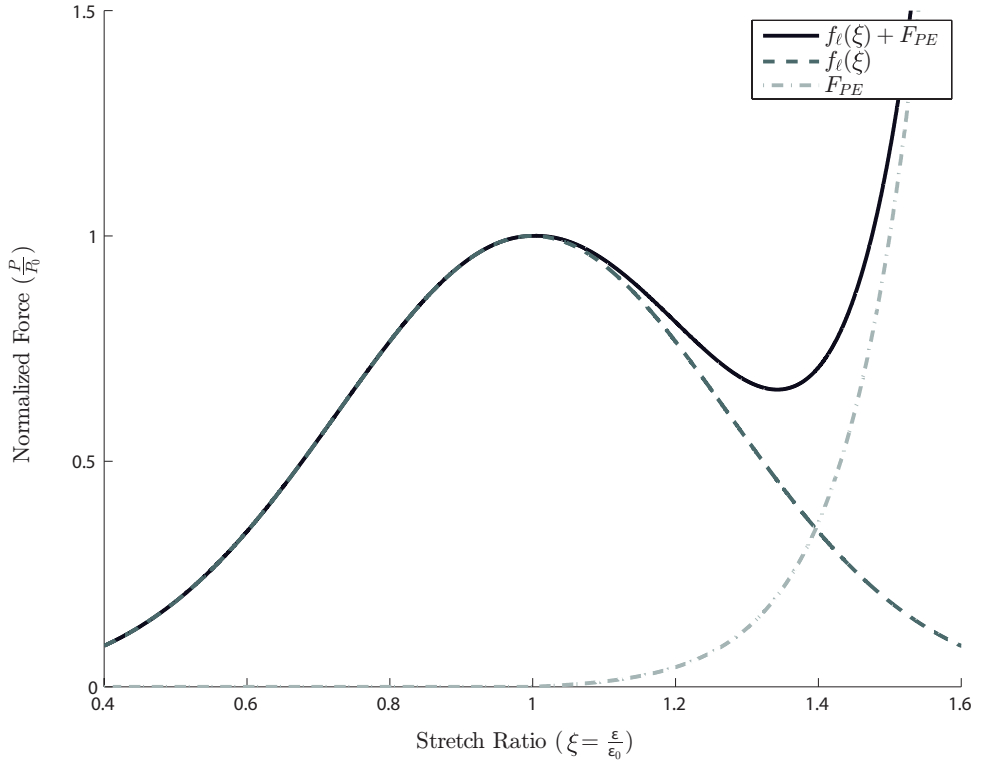

Figure 2.34: Force-length relationship for both the active and passive elements of the muscle. Functions obtained from Thelen (2003). The variance of the Gaussian used by Thelen is exaggerated here for clarity; normally, the active muscle component has a much wider range to operate on.

Figure 2.35) (Joyce and Rack, 1969). To explicitly program this into the Hill model would require force-velocity curves at every possible activation level, or a force-velocity model that scales non-linearly with the activation level.

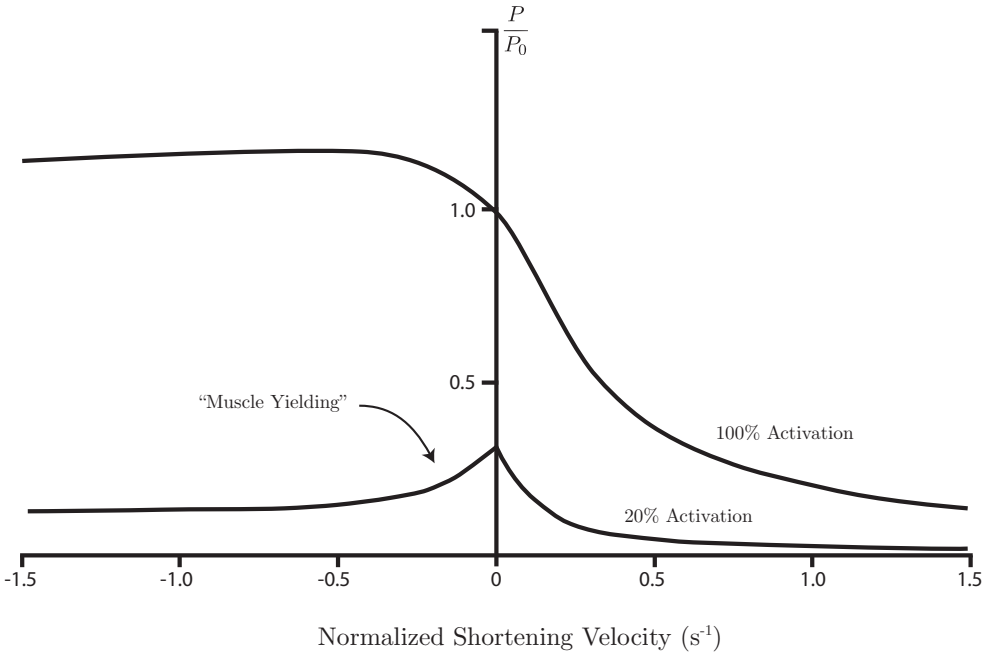

Figure 2.35: Muscle yielding phenomena not explicitly accounted for in Hill. Adapted from Zahalak (1990).

With the exception of the force-length relationship, very little attention is given to the events in muscular contraction at the cellular level. Acquisition of the functional forms of the force-length and force-velocity relationships are almost entirely based on approximations to laboratory results of maximally stimulated muscles (Zahalak, 1990). Despite these theoretic limitations, the Hill model has enjoyed widespread use in biomechanical modelling (Delp et al., 2007; Hatze, 1977; Lloyd and Besier, 2003; McGill and Brown, 1992; Panzer et al., 2011; Zajac, 1989).

In inverse-dynamics modelling, simply using Equation 2.22 is sufficient since obtaining muscle lengths from kinematics is a matter of geometry, however, in forward dynamics, Equation 2.22 is solved for the rate-of-change of the contractile element's length, $\dot{L}_{CE}$, and is then integrated along with Newton's equations (Buchanan et al., 2014; Delp et al., 2007; Zajac, 1989). Originally, inverting f_v was a process easily done algebraically (Hatze, 1977), however, the discovery and implementation of the phenomenon of the muscle "yielding" (Figure 2.35) (Joyce and Rack, 1969) into the model has created some computational challenges (Millard et al., 2013). Specifically, this is because the force-velocity relationship in this case is not represented by an invertible function.

The Huxley Muscle Model

Huxley's model is a mathematical description of sliding filament theory (Huxley, 1957; Williams, 2011). Huxley considered a single cross-bridge between actin and myosin. The myosin is attached to the thick fillament by an elastic member, which is deformed by amount x from its resting position (Figure 2.36). If the elastic member is stretched (or compressed) a force is exerted on the actin molecule. Further, if it is stretched or compressed beyond a certain threshold, there becomes a high probability that the cross-bridge bond will break. Rather than model each individual acin-myosin bond, it is easier to consider the entire population of actin-myosin bonds as a distribution in the amount they are stretched, denoted $n(x,t)$, with x being the key variable in this problem. An analogy might be an age histogram for a population, only in this case, rather than grouping the population based on age, they are grouped by the amount they are stretched. From these observations, Huxley (1957) derived the partial differential equation:

$$\frac{\partial n}{\partial t} - v\frac{\partial n}{\partial x} = f(x)\left(\alpha(t) - n(x,t)\right) - g(x)n(x,t) \tag{2.23}$$

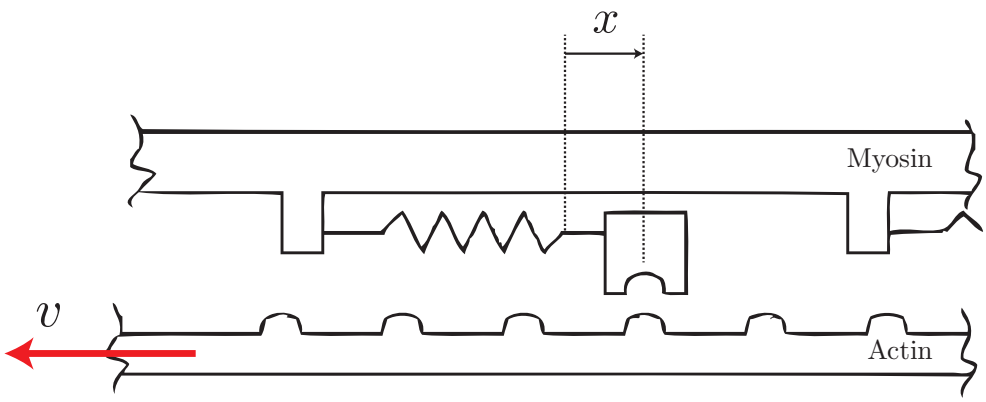

Figure 2.36: The Huxley Model. Adapted from Williams (2011).

Where the function f describes the affinity of a bond to form between actin and myosin if the myosin needs to deform by amount x, and the function g describes the probability of a bond breaking for a cross-bridge stretched by amount x. α represents the number of available binding sites for actin-myosin cross-bridges. Huxley originally proposed the functions which are plotted in Figure 2.37.

Although the added mechanistic nature of the Huxley model is desirable from a modelling point-of-view, its use in biomechanics has been rather limited (Williams, 2011; Zahalak, 1990), owing to the complexity of solving a partial differential equation over the ordinary differential equation of Hill. Furthermore, the cross-bridge distribution function, $n(x,t)$ is not easily (if at all) measurable, and does not have a physically meaningful interpretation. Additionally, the choice of attachment and detachment rate functions adds a layer of phenomenology to the model, despite the fact that they are subject to some level of thermochemical constraints (Ma and Zahalak, 1991).

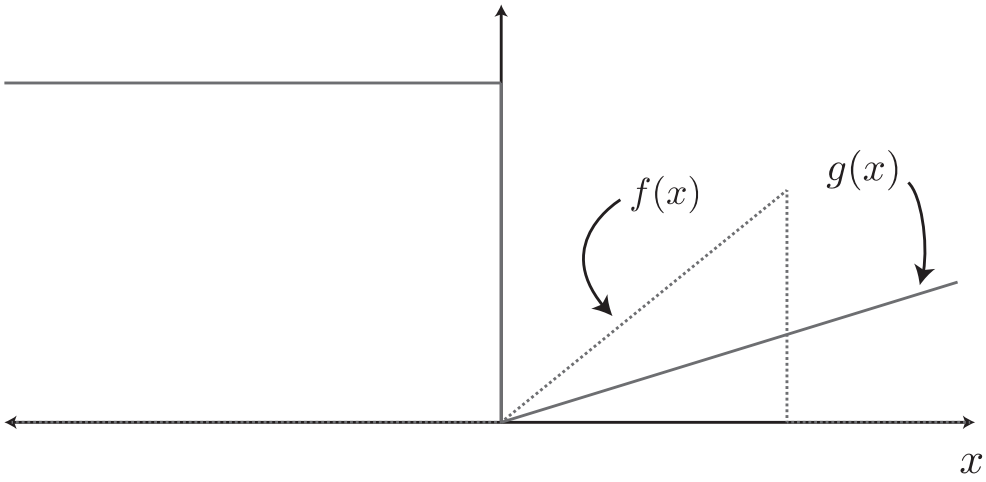

Figure 2.37: The attachment and detachment rate functions originally proposed by Huxley (1957). Adapted from Williams (2011).

The Distribution Moment Approximation

The distribution moment approximation to Huxley's model addresses almost all of the limitations of Huxley's model. Rather than solving a partial differential equation, Huxley's model is reduced to a system of five nonlinear ordinary differential equations in quantities that have physical interpretations (Ma and Zahalak, 1991; Zahalak, 1990). If the spring component of the cross-bridges denoted in Figure 2.36 are assumed to be Hookean with spring-constant k, then the force in that spring would be kx. Further, the force through the entire muscle would be the sum of the forces in every cross bridge, written mathematically:

$$\text{Total Force} = F = \overbrace{\int_{-\infty}^{\infty}}^{\text{sum over } x} \underbrace{kx}_{\substack{\text{force per cross-bridge} \\ \text{stretched by } x}} \overbrace{n(x,t)dx}^{\substack{\text{number of cross-bridges} \\ \text{stretched by } x}}$$

More cleanly:

$$F = k \int_{-\infty}^{\infty} x\, n(x,t) dx \tag{2.24}$$

What appears naturally is that the force is proportional to a quantity that Ma and Zahalak (1991) term Q_1, what statisticians would call the *first raw moment* of the distribution $n(x,t)$. In general the λ^{th} moment is defined as:

$$Q_\lambda = \int_{-\infty}^{\infty} x^\lambda n(x,t) dx \tag{2.25}$$

Ma and Zahalak (1991) began by multiplying Equation 2.23 by x^λ, integrating over the real numbers, and simplifying. To make the resulting integrals tractable, they assumed that $n(x,t)$ obeys a normal distribution, and, to include activation dynamics, they modelled flux of calcium through the cell. The result was a reduction of the Huxley model to just five ordinary differential equations:

$$\dot{\Lambda} = \kappa(Q_1)\dot{Q}_1 - \gamma u(t) \tag{2.26}$$

$$\dot{C} = \rho\left(1 - \frac{c}{c^*}\right) - \tau_0^{-1}\frac{c}{c + k_m} \tag{2.27}$$

$$\dot{Q}_0 = \alpha r \beta_0 - \Phi_0(Q_0, Q_1, Q_2) \tag{2.28}$$

$$\dot{Q}_1 = \alpha r \beta_1 - \Phi_1(Q_0, Q_1, Q_2) - v(t)Q_0 \tag{2.29}$$

$$\dot{Q}_2 = \alpha r \beta_2 - \Phi_2(Q_0, Q_1, Q_2) - v(t)Q_1 \tag{2.30}$$

where:

$$C = c + 2bQ_0 + r\left(2 + \frac{\mu}{c}\right)(1 - bQ_0) \tag{2.31}$$

$$r(c) = \frac{c^2}{c^2 + \mu c + \mu^2} \tag{2.32}$$

Where Q_0, Q_1, and Q_2 are the first three raw moments of the distribution $n(x,t)$ representing the instantaneous stiffness, force, and stored potential energy respectively, $v(t)$ is the shortening velocity. The Φ_k and β_k functions arise from the series of simplifications made my Zahalak (Ma and Zahalak, 1991, 1988; Zahalak, 1990), and α is the number of available binding sites for actin-myosin interactions, and κ is a constant. The constants ρ, τ_0, k_m, μ and c^* are parameters arising from the modeling of calcium dynamics. In this expression, $u(t)$ is the neural input function taking the form of a chain of neural impulses (such as rectified EMG).

There are a number of advantages to using the distribution moment approximation, the first of which is that the mechanistic nature of the Huxley model is obtained in terms of three physically meaningful quantities (Zahalak, 1990). The second is that the complexity of solving a partial differential equation is now reduced to solving five coupled ordinary differential equations, which can be done through numerical techniques (Cholewicki and McGill, 1995). A downside is the complexity in implementing numerical representations of the β_k and Φ_k functions, which involves numerically computing complicated integrals (Ma and Zahalak, 1988). Despite these challenges, there are some advantages to using the distribution moment model. For one, muscle stiffness is directly obtainable from the model with minimal effort. Additionally, it has been shown to agree with experimental data in predicting accurate force-stiffness relationships (Cholewicki and McGill, 1995) as well as

the muscle yielding phenomenon described earlier (Ma and Zahalak, 1988).

2.4 Previous Cervical Spine Models

Broadly speaking there are two main ways to model dynamics in biomechanics: forward and inverse dynamics. Forward dynamics begins with forces as inputs, and integrates the equations of motion to predict kinematics. On the other hand, inverse dynamics begins with the kinematics, and ascertains the net forces that are responsible for the motion. A further distinction is made between multi-body dynamic (MB) simulations and finite element (FE) ones. Briefly, MB simulations integrate the familiar Newton-Euler equations of motion from mechanics while FE simulations solve the field equations of continuum mechanics. Both modelling frameworks can be further subdivided into dynamic and quasi-static, where dynamic models account for inertial and viscous properties of the materials, while quasi-static simulations do not.

To this author's knowledge, the first mathematical head-neck model was developed during Bruce Bowman's Ph.D. at the University of Michigan, to investigate injury mechanisms during car accidents (Bowman, 1971). The model consisted of three segments: the head, the neck, and the torso, which were modelled, by hand, using Lagrangian Mechanics. It even included passive muscle contributions, modelled as Maxwell elements, although ligaments, and IVDs were lumped in with the passive responses of the joints modelled.

Williams and Belytschko (1983) created a model that used a multibody methodology, with muscles that were activated by the stretch reflex. Their incorporation of active muscle components into the model was unique, although completely non-standard – taking mus-

cles to be Kelvin bodies with material properties that changed with muscular activation. Activation was modelled using a linear first-order differential equation, similar to that of Winters and Stark (1985). These authors found that excluding muscle activation resulted in poor agreement between model predictions and experiment.

The models of Deng, Goldsmith, and Merrill began with a multibody simulation, which treated the intervertebral joints as lumped parameter joints, with passive muscle contributions (Merrill et al., 1984). Later, in a two part series, they developed both a physical and numerical model, both of which included muscle activation (Deng and Goldsmith, 1987a,b). Muscle activation was included in the physical model using syringes that were evacuated with air to simulate muscle contraction, while the numeric model used passive muscle stresses identical to the earlier model of Merrill et al. (1984), but included a single via-point in order to mimic muscle wrapping (Deng and Goldsmith, 1987b). Their subsequent finite element model improved the cervical vertebrae geometry and material properties of ligaments (Deng et al., 1999). It was the first finite element model of the cervical spine to use nonlinear, viscoelastic elements to represent the behaviour of the soft tissues, while also implementing Hill-type muscle elements with a single via point to account for muscle wrapping, in the same manner as their previous MB model (Deng and Goldsmith, 1987b). The geometry of the model was adapted by Panzer and Cronin (2009), who developed a comprehensive finite element model of the cervical spine (Panzer et al., 2011). It was later enhanced to include more biofidelic injury mechanics in the ligaments and improved material properties (DeWit and Cronin, 2012; Fice et al., 2011). The finite element model includes the viscoelastic material properties of ligaments into the failure region, a vast array of musculature modelled using a Hill-type approach, and even a thin

layer cortical bone on each cervical vertebrae. To improve efficiency, it can be adapted to treat the bones as rigid segments (DeWit and Cronin, 2012).

Moroney et al. (1988a) was the first inverse dynamic model of the cervical spine, and was used to elucidate the loads in the neck during quasi-static loads. It used an optimization approach to determine muscle forces by minimizing the contraction effort of the muscles to balance the external moment about C4. A similar model by Winters and Peles (1990) considered the neck as an inverted double pendulum, divided into the upper and lower cervical spine. They used the sum of square muscle-stresses as an objective function. Snijders et al. (1991) presented another inverse dynamic model of the cervical spine intended for ergonomic use. It included a simplified cervical spine consisting of three segments (upper, middle, and lower cervical spine), and 7 muscles bilaterally. Muscle forces were obtained via optimization by minimizing the joint reaction forces. It was later used to evaluate the forces on the neck of F-16 pilots (Hoek van Dijke et al., 1993).

One of the more innovative cervical spine models was that of de Jager (1996), which seems to be the first model to include muscle activation, which was accomplished by means of a Hill model. The model certainly is not without limitations, most notably since with the absence of muscle wrapping in a frontal impact scenario, where neck extensor muscles were able to pass through the vertebrae and act as neck flexors. Despite this, de Jager's model was packaged in MADYMO's impact simulation software (Stemper et al., 2004), and paved the ground for more the more advanced models of Yamazaki et al. (2000) and van der Horst (2002); van der Horst et al. (1997), who updated the model to include muscle wrapping by using via points, and more realistic soft tissue properties. It was further improved by van Lopik, who added more physiologic intervertebral discs and ligaments to the model

(van Lopik and Acar, 2007). Its final rendition was a hybrid FE-MB model by Esat and Acar (2009), which uses the finite element method to model the intervertebral discs, and multibody dynamics for the bones and other soft-tissues for increased efficiency.

Camacho et al. (1997) created a multibody head-neck model with a finite-element skull, which was later improved by Van Ee and Chancey to include realistic muscle anatomy (Chancey et al., 2003; Van Ee et al., 2000). The model used optimization to determine the initial tension in muscles needed to stabilize the head prior to a sudden tensile load. It was then used to show that muscle activation was protective against distraction of the head-neck during tensile loading situations (Van Ee et al., 2000).

A neck model was developed and made available in OpenSim (Vasavada et al., 1998). The model features the typical OpenSim style of ligament (nonlinear elastic) and muscle properties, inheriting from Zajac (1989). Recently the model was found to have some significant challenges when being driven by EMG, which the investigators using the model believed to be due to nonlinearities in force generation that were not previously considered (Netto et al., 2008). A similar EMG-driven neck model was developed by Huber as a Master's thesis project at The Ohio State University (Huber, 2013). It has a number of limitations, for one, only three muscles were modelled with no via points for muscle wrapping. Huber's EMG processing techniques were questionable, and the description of the entire modelling process was quite vague.

Models employing the finite element method in the cervical spine began to appear in the early 1990's, with Kleinberger (1993) representing the first. This model was the first to separate contributions of joint mechanics between the intervertebral disc and ligaments, but lacked any representation of muscles.

Brolin and Halldin developed a finite element model with a highly detailed upper cervical spine region (Brolin and Halldin, 2004; Brolin et al., 2008). The model is extremely comprehensive, like that of Panzer and Cronin (2009), consisting of viscoelastic elements for the soft tissues along with Hill-type muscle elements for the muscles.

Another finite element model developed by Zhang was used to determine the loads on the soft tissues during range general loading conditions (Zhang, 2005; Zhang et al., 2006). This model was adapted from a previous model in Teo and Ng (2001a,b), which was designed to model injury to the bones of the upper cervical spine, and soft tissues of the lower cervical spine. A similar model developed by del Palomar et al. (2008) for quasi-static analysis was an improvement over previous quasi-static finite element models (Kumaresan et al., 1999b,a) in terms of more realistic bone geometry. Another model by Meyer et al. (2005) was a finite element model of a whole seated occupant consisted of a very realistic geometry, viscoelastic ligaments and (homogeneous) intervertebral discs, with active muscle involvement (Meyer et al., 2013). Östh (2010) developed a finite element model of the entire spinal column during a vehicular accident with Hill type muscle elements driven by optimization, although used linear spring elements for ligaments and linear solid elements for the intervertebral disc.

All of these models suffer from their non-physiologic treatment of muscles. When muscles are included they are activated to 100% at the onset of impact, in an effort to simulate the reflexive contractions. In addition, with the exception of del Palomar et al. (2008), none of these models are particularly well suited for modelling quasi-static loading over an extended period of time. The majority of whole cervical spine models employ the finite element method, which is well suited to study impacts spanning a small duration, how-

ever, it is its computational complexity that renders it undesirable for long-term exposure modelling. All of these models are summarized in Table 2.17.

Table 2.17: Summary of cervical spine models in the literature.

Study	Type	IVD Model	Ligament Model	Muscle Model	Purpose
Bowman (1971)	MB, Forward	Lumped, 6 DOF Voigt		Passive: Maxwell Elements	Vehicle Collisions
Williams and Belytschko (1983)	MB, Forward	Linear 6 DOF Spring	Nonlinear Spring Elements	Active: Winters and Stark (1985) No explicit contraction	Vehicle Collisions
Merrill et al. (1984)	MB, Forward	Lumped, 6 DOF Voigt		Passive: Nonlinear Spring	Vehicle Collisions
Deng and Goldsmith (1987a,b)	MB, Forward	Lumped, 6 DOF Voigt with coupling		Passive: Nonlinear Springs	Vehicle Collisions
Moroney et al. (1988a)	MB, Inverse	Lumped 6 DOF Voigt		Optimization Minimum contraction intensity	Quasi-static postures
Winters and Peles (1990)	MB, Inverse	3 DOF Voigt Ball-and-Socket		Optimization Minimum squared stress	Voluntary neck movement
Snijders et al. (1991)	MB, Inverse	Lumped 6 DOF QLV Voigt		Optimization Minimize net joint moment	Loads in F-16 Pilots
Kleinberger (1993)	FE, Forward	Isotropic linear elements	Isotropic solid elements		Vehicle Collisions
Dauvilliers et al. (1994)	FE, Forward	Linear composite (truss)	Linear spring/damper		Vehicle Collisions
de Jager et al. (1996)	MB, Forward	Lumped, 6 DOF Linear Voigt with coupling		Passive: Nonlinear Spring Active: Hill type model	Vehicle Collisions
Vasavada et al. (1998)	MB, Forward	Lumped, 6 DOF Bushing Element		Zajac (1989)	OpenSim
Camacho et al. (1997) Camacho et al. (1999)	MB, Forward	Lumped, 6 DOF QLV Voigt		Hill	Tensile Load
Van Ee et al. (2000) Chancey et al. (2003)	MB, Forward	Lumped, 6 DOF QLV Voigt		Hill	Tensile Load
Kumaresan et al. (1999a,b)	FE, Forward (Quasi-static)	AF: Rebar elements NP: incompressible fluid	Nonlinear cable elements		Medical Simulation
Deng et al. (1999) Deng and Fu (2002)	FE, Forward	Isotropic nonlinear (AF) Viscoelastic NP	Linear viscoelastic membrane elements	Hill	Vehicle Collisions
Brolin and Halldin (2004) Brolin et al. (2008)	FE, Forward	Linear Shell elements (AF) Isotropic Linear (NP)	Bilinear Cables	Hill	Vehicle Collisions
Yamazaki et al. (2000)	MB, Forward	6 DOF QLV Voigt		Hill	Vehicle Collisions
Choi and Vanderby (1999) Choi and Vanderby Jr (2000)	MB, Inverse			EMG-Driven Hill	Maximal Contractions

Continued on next page

Table 2.17 – continued from previous page

Study	Type	IVD Model	Ligament Model	Muscle Model	Purpose
van der Horst et al. (1997) van der Horst (2002)	MB, Forward	6 DOF Linear Voigt		Winters and Stark (1985)	
Meyer et al. (2005) Meyer et al. (2013)	FE, Forward	Isotropic Linear IVD	Nonlinear cable	Passive Springs	Vehicle Collisions
Ahn (2005)	MB, Forward	6 DOF QLV Voigt	Nonlinear, tensile viscoelastic springs		Medical Simulation
Teo and Ng (2001a,b) Zhang (2005) Zhang et al. (2006)	FE, Inverse (Quasi-static)	Isotropic Linear IVD	Nonlinear cable		
Panzer et al. (2011) DeWit and Cronin (2012) Fice et al. (2011)	FE, Forward	AF: Shell elements NP: Viscoelastic fluid	Nonlinear viscoelastic cables with failure region	Winters and Stark (1985)	Whiplash investigations
van Lopik and Acar (2007)	MB, Forward	6 DOF Springs	Nonlinear Viscoelastic	Zajac (1989)	Whiplash investigations
Esat and Acar (2009)	MB/FE, Forward	8 Node Elements (FE)	Nonlinear Viscoelastic	Zajac (1989)	Whiplash investigations
del Palomar et al. (2008)	FE, Forward	AF: nonlinear, anisotropic solid NP: viscoelastic fluid	Nonlinear cable		Quasi-Static Exposure
Netto et al. (2008)	MB, Inverse	6 DOF Bushing Element	Nonlinear Cable	EMG-Driven Hill	Validation of EMG-Driven techniques
Östh (2010)	FE, Forward		Linear Springs	Hill	Whiplash
Huber (2013)	MB, Inverse	6 DOF Bushing Element			
Present Investigation	MB, Inverse	Nonlinear Rotational Springs	Nonlinear Springs	EMG-Driven Hill	Ergonomics

2.5 Gaps in the Literature

Currently, cervical spine models are forward models that are well suited for simulating vehicular accidents and predicting whiplash injuries from them. Unfortunately, very few are readily adaptable for inverse dynamics, which limits their use outside of car accident modelling (Moroney et al., 1988a; Snijders et al., 1991; Vasavada et al., 1998). Additionally, most implementations use the finite element method which is computationally demanding and difficult to apply in scenarios of prolonged exposure. Their computational efficiency can be improved by using a quasi-static assumption, at the cost of the ability to describe viscous effects like creep or stress-relaxation. The inability to do so depreciates their value in injury prediction, since creep has been implicated as a possible pathway for the development of workplace related musculoskeletal disorders (Solomonow, 2004; Solomonow et al., 2003). There is need for a musculoskeletal model which can address viscoelastic effects outside of collision scenarios.

There are very few studies modelling the cervical spine with the aid of EMG. The earliest cases are the analyses by Moroney et al. (1988a) and Winters and Peles (1990), which used EMG as a means of validating activation functions derived from optimization. Currently, only two models have been developed that use EMG to drive a musculoskeletal muscle. One is the OpenSim model by Vasavada et al. (1998) in conjunction with some EMG-driving techniques developed for OpenSim (Netto et al., 2008; Sartori et al., 2012). The other is a multibody EMG-driven simulation by Huber (2013). The Huber model has a number of limitations, for one, only three muscles (sternocleidomastoid, semispinalis capitis, and trapezius) were modelled. While these are the largest muscles which span the entire cervical

spine, it leaves the vast majority of the musculature unaccounted for. The methodology of processing EMG used in the Huber model was only given a cursory discussion, and it is not clear whether the EMG driving the model was linear enveloped, or even normalized to a reference contraction. Despite these limitations, Huber observed a reasonable amount of agreement between experimental neck moments calculated from inverse dynamics, and the net moment calculated from their forward model of a cervical spine actuated by only three EMG-driven muscles. Both Vasavada et al. (1998) and Huber (2013) use an underlying forward model driven by EMG which they compare to experimental data; at present, there are no EMG-driven models which exclusively use inverse dynamics methods.

Unfortunately, there are only a handful of studies investigating the viscoelastic properties of ligaments and intervertebral discs, with most attention focused on their strain-rate dependent nature (Bass et al., 2007; Mattucci et al., 2013, 2012), and not enough on creep and stress relaxation. A prime example of the deficiencies in this area are the damping coefficients originally used by de Jager et al. (1996), which have propagated through to subsequent models (van der Horst, 2002; van Lopik and Acar, 2007). These values are the work of pure conjecture from de Jager because no study had yet quantified the viscoelastic properties of the cervical spine intervertebral discs. Currently. investigators are beginning to examine the viscoelastic properties of spinal ligaments in detail (Troyer and Puttlitz, 2011; Troyer et al., 2012b,a). Perhaps the striking lack of research in this area is the reason why models have not explicitly taken into account viscoelastic properties outside of strain-rate dependence, and to this end, there has not been an investigating characterizing how viscoelastic creep affects the joint mechanics of the cervical spine.

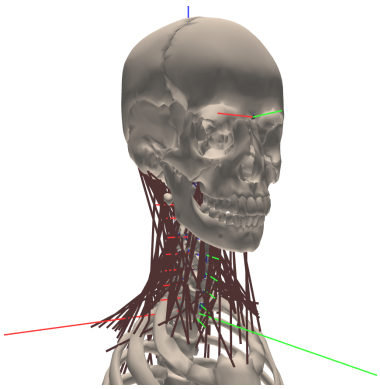

Chapter 3

Model Description

This is the first EMG-driven model of the entire cervical spine, and one of the first which can be used to evaluate the bone-on-bone forces at each joint level. It was programmed using the Python programming language, a completely free and open sourced language, using the `pyglet` package for visualization and the `CVXPY` package for optimization (Diamond and Boyd, 2016). This chapter describes the various tissue properties used to create the model, how the model handles inverse dynamics, and how information flows through the model.

It took two tries to make this model. The first iteration was entirely based on muscle coordinate data reported by three different sources. The inconsistently defined coordinate systems and lack of reference to other anatomical landmarks made combining databases a complicated task, which inevitably lead to a very poor representation of the cervical spine. While the first iteration of this model will not be discussed much in this document, the lessons learned from it were invaluable in the second iteration.

3.1 Anatomy and Kinematics

3.1.1 Anatomical Data

The BodyParts3D project provided the visualizations for this model (Mitsuhashi et al., 2009). However, the model scales the geometry of the vertebrae so that the dimensions of the vertebrae match those dimensions of a 50^{th} percentile male, as presented in Tables 2.1, 2.2, and 2.3. Originally I was going to use anatomical data for origin and insertion points presented in Chancey et al. (2003) and Winters and Woo (1990), however, since neither database provided a means of locating the edges of the vertebral body, prescribing the location of the joint centres of rotation, as reported in Dvorak et al. (1991), proved to be difficult. The resulting model had a qualitatively poor representation of the lordotic curvature of the cervical spine, and so, I manually digitized the origin and insertion points from Mitsuhashi et al. (2009).

Local coordinate systems for the vertebrae are defined using some key landmarks on the vertebral body and transverse process. The positive x-axis points to the right, y anteriorly along the inferior surface of the vertebra, and the positive z-axis is determined from the cross product between the $\hat{i}$ and $\hat{j}$ unit vectors. For the skull, the local coordinate system is coincident with the global coordinate system when the head is in a neutral position. An advantage of manually digitizing these anatomical data is that the user can input a percentile, which the model converts to a series of lengths (using the means and standard deviations in Tables 2.1, 2.2, and 2.3) and attempts to find scaling factors along each axis to best match the model to the specified percentile. More formally, the objective is to find

scaling factors, c_x, c_y and c_z, to minimize:

$$J(c_x, c_y, c_z) = \sum_{n=1}^{N} \left(\ell_n - \left(\bar{\ell}_n + z\sigma_n\right)\right)^2 \tag{3.1}$$

With:

$$\ell_n = \sqrt{c_x^2(\Delta x_n)^2 + c_y^2(\Delta y_n)^2 + c_z^2(\Delta z_n)^2} \tag{3.2}$$

Where N is the number of dimensions to use when rescaling the model, ℓ_n is the n^{th} length from the model z is the z-score for the desired percentile, and $\bar{\ell}_n$ and σ_n are the reported mean and standard deviation for this length. For example, the typical cervical vertebrae used the width between transverse processes, vertebral body height anteriorly and posteriorly, vertebral body width, and vertebral body depth both superiorly and inferiorly. By assuming that Dvorak et al. (1991) reported centres of rotation of 50^{th} percentile individuals, their locations were added to the model with relative ease. The final data file which contains all of this information is a comma separated file with the means and standard deviations of dimensions for scaling reported as a distance between two landmarks. The same file contains the surface mesh used to animate the segment.

3.1.2 Muscle and Ligament Coordinates

In total there are 218 muscle elements representing some 58 muscles in the cervical spine (Figure 3.1). To digitize the muscle's origin, insertion and via points were digitized manually from the BodyParts3D meshes on the left and right sides. These were then

averaged to enforce bilateral symmetry. Similarly there are 482 ligament elements for 32 ligaments spanning from C7-T1 to those at the base of the skull.

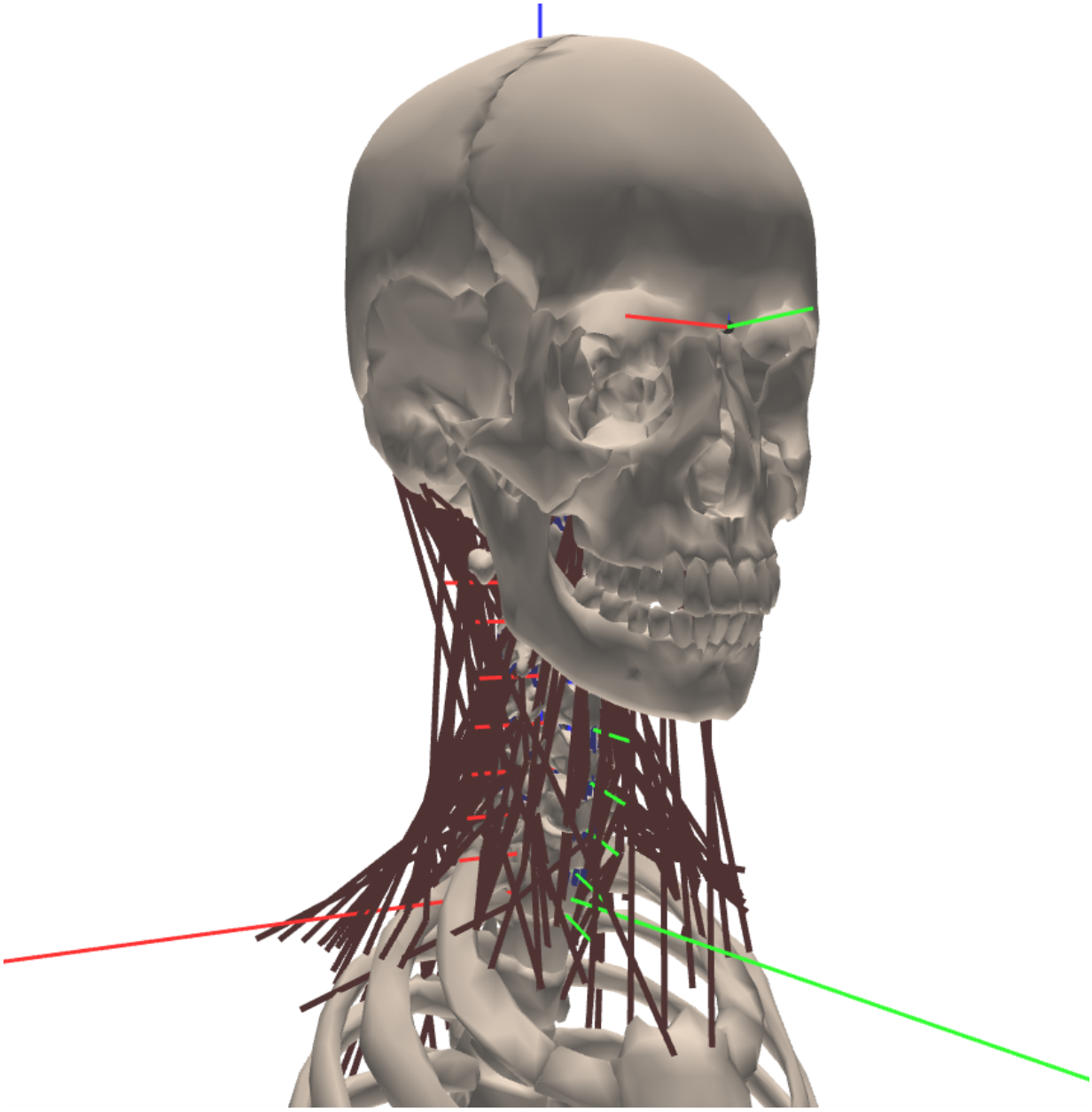

Figure 3.1: The full model with all of the muscles present.

3.1.3 Bones

The model consists of the seven cervical vertebrae, T1 (and ribcage), and a skull, the inertial properties of each are displayed in Table 3.1. The position of which is determined by the joints connecting the segments. Starting with the origin of T1 coincident with the origin of the global coordinate system, the position of C7 is chosen so that the centre of rotation for the C7-T1 joint is the same for both T1 and C7. The position of C6 is determined in a similar manner, and so on until the skull's position has been determined. The joints in the model store the three rotational degrees of freedom, which are approximated from the total head-thorax angle.

Table 3.1: Inertial properties of the segments in the model. Adapted from de Jager et al. (1996).

		Moment of Inertia (kg cm^2)			
Body	**Mass (kg)**	I_{xx}	I_{yy}	I_{zz}	I_{xy}
C7	0.22	2.2	4.3	2.2	–
C6	0.24	2.4	4.7	2.4	–
C5	0.23	2.3	4.5	2.3	–
C4	0.23	2.3	4.4	2.3	–
C3	0.24	2.4	4.6	2.4	–
C2	0.25	2.5	4.8	2.5	–
C1	0.22	2.2	4.2	2.2	–
Occiput	4.69	181	173	236	71.0

Centers of Rotation and Partitioning of Angles

To establish where the vertebrae are in space, the angle difference between the head and thorax is partitioned between each vertebrae, weighted by the fraction of their range

of motion in each direction (Tables 2.14, 2.15, and 2.16). The algorithm for partitioning the angles is based on McGill's method for partitioning lumbar angles between the lumbar vertebrae (McGill and Norman, 1986). The process begins by calculating the total angular difference between the head and trunk:

$$\begin{aligned}\mathcal{U}_{\text{head}}^{T}\mathcal{U}_{\text{trunk}} &= \mathbf{R}_{\phi}\mathbf{R}_{\theta}\mathbf{R}_{\psi} \\ &= \begin{bmatrix}1 & 0 & 0\\ 0 & \cos\phi & \sin\phi\\ 0 & -\sin\phi & \cos\phi\end{bmatrix}\begin{bmatrix}\cos\theta & 0 & -\sin\theta\\ 0 & 1 & 0\\ \sin\theta & 0 & \cos\theta\end{bmatrix}\begin{bmatrix}\cos\psi & \sin\psi & 0\\ -\sin\psi & \cos\psi & 0\\ 0 & 0 & 1\end{bmatrix}\end{aligned} \tag{3.3}$$

Where $\mathcal{U}_{\text{head}} = \begin{bmatrix}\hat{i}_H & \hat{j}_H & \hat{k}_H\end{bmatrix}$, and $\mathcal{U}_{\text{trunk}} = \begin{bmatrix}\hat{i}_T & \hat{j}_T & \hat{k}_T\end{bmatrix}$ are the direction cosine matrices of the head and thorax respectively. The product $\mathcal{U}_{\text{head}}^{T}\mathcal{U}_{\text{trunk}}$ is a rotation matrix describing the relative rotation between the thorax and the head, and it is decomposed into rotations about the cardinal axes such that ψ is a flexion-extension angle (about the z-axis), θ is an axial rotation angle (about the y-axis), and ϕ is the lateral bending angle (about the x-axis). Each of these are decomposed so that:

$$\psi_k = \alpha_k\psi \tag{3.4}$$
$$\theta_k = \beta_k\theta \tag{3.5}$$
$$\phi_k = \gamma_k\phi \tag{3.6}$$

Where α_k, β_k and γ_k are the weightings of each rotation for the k^{th} vertebrae ($k = 8$ is the head) based on range of motion (Table 3.2). The product of the rotation matrices $\mathbf{R}_{\phi}$, $\mathbf{R}_{\theta}$, and $\mathbf{R}_{\psi}$, after the partition, can be computed:

$$\mathbf{R}_\phi \mathbf{R}_\theta \mathbf{R}_\psi = \left(\prod_{k=1}^{N} \mathbf{R}_{\phi_k}\right)\left(\prod_{k=1}^{N} \mathbf{R}_{\theta_k}\right)\left(\prod_{k=1}^{N} \mathbf{R}_{\psi_k}\right) \tag{3.7}$$

Which yields a formula for computing the direction cosine matrix, $\mathcal{U}_K$, for the K^{th} cervical vertebrae in terms of the trunk.

$$\mathcal{U}_K = \mathcal{U}_{\text{trunk}}\left[\left(\prod_{k=1}^{K} \mathbf{R}_{\phi_k}\right)\left(\prod_{k=1}^{K} \mathbf{R}_{\theta_k}\right)\left(\prod_{k=1}^{K} \mathbf{R}_{\psi_k}\right)\right]^T \tag{3.8}$$

With $\mathcal{U}_{\text{trunk}}$ being the direction cosine matrix for the trunk, as before. Note that when $K = 8$ this will compute the direction cosine matrix of the head. By defining the rotation sequences in this way, the relative rotation between vertebrae can also be computed as:

$$\mathcal{U}_{K+1}^T \mathcal{U}_K = \mathbf{R}_{\phi_{K+1}} \mathbf{R}_{\theta_{K+1}} \mathbf{R}_{\psi_{K+1}} \tag{3.9}$$

Table 3.2: Coefficients for partitioning the Euler Angles based on the range of motion study of Ivancic (2013).

Joint	**Flexion-Extension** α_k	**Axial-Rotation** β_k	**Lateral Bending** γ_k
C0-C1 ($k = 8$)	0.242	0.090	0.177
C1-C2 ($k = 7$)	0.156	0.553	0.161
C2-C3 ($k = 6$)	0.083	0.051	0.119
C3-C4 ($k = 5$)	0.103	0.065	0.104
C4-C5 ($k = 4$)	0.105	0.066	0.117
C5-C6 ($k = 3$)	0.129	0.063	0.101
C6-C7 ($k = 2$)	0.114	0.054	0.104
C7-T1 ($k = 1$)	0.069	0.058	0.117

Overall, this method seems to capture a physiologically accurate range of motion 3.2b.

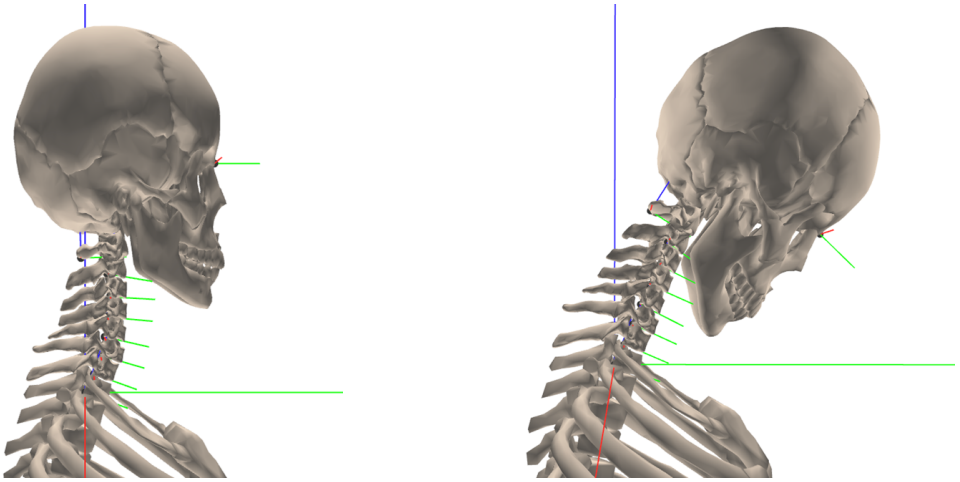

(a) Sagittal view of a neutral posture. (b) Sagittal view of 45° of flexion

Figure 3.2: An Example of the kinematics of the model in flexion.

Computing Angular Velocities

The angular velocity vector was computed by exploiting the property that the time-derivative of a rotation matrix is related to the angular velocity vector, $\vec{\omega}$, in the following manner (Goldstein et al., 1950):

$$\frac{d}{dt}\,\mathcal{U}_K = \begin{bmatrix} 0 & -\omega_z & \omega_y \\ \omega_z & 0 & -\omega_x \\ -\omega_y & \omega_x & 0 \end{bmatrix} \mathcal{U}_K \tag{3.10}$$

This can be rearranged for the skew-symmetric matrix whose components depend only on $\vec{\omega}$ by simple post-multiplication by $\mathcal{U}_K^T$ with the time derivative of $\mathcal{U}_K$, leaving the components of $\vec{\omega}$ to be simply read off. The downside to this method is that storing and differentiating the rotation matrix is less space-efficient and time-efficient – nine numbers need to be stored and differentiated for each local coordinate system in the model. The

most efficient method is to use a generalization of the complex numbers, quaternions, to represent the rotation. This method reduces the computation on nine numbers to just four. As this is a lengthy discussion, it is omitted from this document for brevity.

3.2 Tissue Properties

3.2.1 Ligaments

Tissue properties from ligaments were modelled as nonlinear springs with material properties obtained from Mattucci (2011). In particular, their constitutive expression is:

$$F(\xi) = \frac{k\sigma}{\sqrt{2\pi}} \exp\left(-\frac{(\mu+\xi)^2}{2\sigma^2}\right) + \frac{k(\mu+\xi)}{2}\left(\operatorname{erf}\left(\frac{\mu+\xi}{\sqrt{2}\sigma}\right)+1\right) \tag{3.11}$$

Where ξ is the deformation of the ligament, k is the effective collagen stiffness for the ligament, and μ and σ are the mean and standard deviation for the distribution of collagen fibre slack lengths. This comes from a simplification of a mechanistic ligament model (in preparation) when breakage is ignored. The above expression captures the toe and linear regions of the ligament's force-deflection curve. Using the scaling factors presented by Mattucci (2011), the force-deflection curves can be scaled differently for sex, or spinal level using scaling factors a_{force} and a_{disp} for the force and deflection respectively, so that the force given by a ligament element is given by:

$$F_L(\ell) = \frac{a_{\text{force}}}{n} F\left(a_{\text{disp}}\left(\ell - \ell_0\right)\right) \tag{3.12}$$

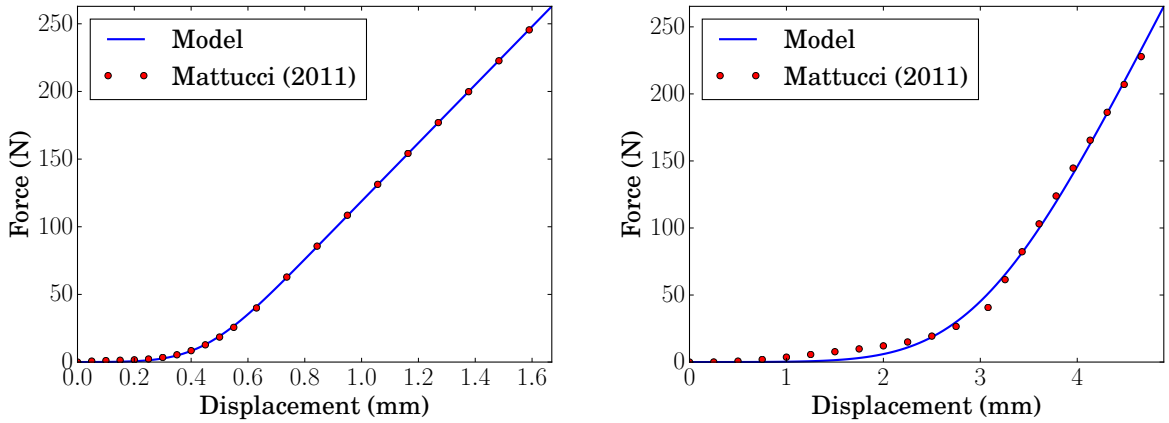

(a) Posterior Longitudinal Ligament.

(b) Ligamentum Flavum.

Figure 3.3: Comparison of force-deflection curves to Mattucci (2011) for two example ligaments.

Where ℓ is the current length of the ligament, ℓ_0 is the slack length (set to 1.05 times the length of the ligament in a neutral posture), and $F(\xi)$ in Equation 3.12 refers to the function defined in Equation 3.11, whose parameters are fitted to the average curves reported by Mattucci (2011). The additional factor, n refers to the number of elements which make up the ligament in the model. Since Mattucci (2011) reported force-deflection curves for whole ligaments, the average curves reported there reflect the entirety of the ligament. Unfortunately, incorporating viscoelastic effects into the model was never completed, so investigating into how stress-relaxation may affect joint kinetics is a potential future investigation.

Equation 3.11 fits the average curves reported by Mattucci (2011) very well, and some examples are given below (Figure 3.3). Parameters in Table 3.3.

Table 3.3: Summary of ligament parameters.

Ligament	Level	Parameter k (N/mm)	σ (mm)	μ (mm)	a_{force}	a_{disp}
ISL	C2 – C3	13.4	0.590	-1.18	0.94	0.87
	C4 – C6				0.83	0.78
	C7 – T1				1.27	1.4
LF	C2 – C3	140	0.813	-3.00	0.90	0.75
	C4 – C6				0.84	0.90
	C7 – T1				1.38	1.51
CL	C2 – C3	85.8	0.229	-0.621	1.056	0.86
	C4 – C6				1.045	1.03
	C7 – T1				1.22	1.21
PLL	C2 – C3	215	0.148	-0.44	1.0	1.23
	C4 – C6				1.17	0.905
	C7 – T1				1.0	1.15
ALL	C2 – C3	140	0.33	-1.01	1.32	0.845
	C4 – C6				0.955	0.757
	C7 – T1				1.184	1.012
AAOM	—	160	0.363	-1.29	1	1
TM	—	220	0.358	-0.978	1	1
TL	—	186	0.303	-2.12	1	1
PAOM	—	69.3	0.226	-1.10	1	1

3.2.2 The Intervertebral Disc

Intervertebral discs were modelled using a non-linear restoring moment dependent on the joint's rotational degrees of freedom using the constitutive expression:

$$M(\phi) = B(e^{A\phi} - 1) \tag{3.13}$$

These coefficients were fit to the nonlinear load-displacement curves obtained from de Jager et al. (1996), and are presented in Table 3.4.

Table 3.4: Summary of stiffness-coefficients for the simplified intervertebral disc model.

Direction	**Segment Level**					
	C2-C3	**C3-C4**	**C4-C5**	**C5-C6**	**C6-C7**	**C7-T1**
			***A*-Coefficient (1/rad)**			
Flexion	0.66	0.66	0.66	0.66	0.66	0.66
Extension	0.11	0.11	0.11	0.11	0.11	0.11
Lateral Bending	0.22	0.22	0.22	0.22	0.22	0.22
Axial Rotation	0.22	0.22	0.22	0.22	0.22	0.22
			***B*-Coefficient (Nm)**			
Flexion	2.1×10^{-4}	2.1×10^{-4}	2.1×10^{-4}	2.1×10^{-4}	2.1×10^{-4}	2.1×10^{-4}
Extension	0.27	0.27	0.27	0.27	0.27	0.27
Lateral Bending	0.17	0.17	0.17	0.17	0.17	0.17
Axial Rotation	0.23	0.23	0.23	0.23	0.23	0.23

3.2.3 Muscle Model

EMG was detrended, full-wave rectified, and low-pass filtered with a single pass critically damped second order filter (Winter, 1976) in order to obtain the activation function for the subsequent Hill muscle model. Cut-off frequencies were different for each muscle involved based on their electromechanical delays (Table 3.5) (Almosnino et al., 2009). In the case where an electromechanical delay was not available, it was assumed to be 40 ms, giving a cut-off frequency of 4.0 Hz. This value is similar to the electromechanical delay reported by Almosnino et al. (2009) for the cervical spine extensor muscles, and has also been used in processing cervical spine musculature EMG in previous studies (Callaghan et al., 2014; Lu and Bishop, 1996).

Table 3.5: Electromechanical delays, mean (standard deviation), of a few cervical spine muscles. Adapted from Almosnino et al. (2009). The computed cut-off frequencies for these muscles are also included.

Muscle	**Electromechanical Delay**	**Cutoff Frequency**
Splenius Capitis	32.2 ms (5.1)	4.9 Hz
Upper Trapezius	38.1 ms (3.3)	4.2 Hz
Sternocleidomastoid	70.3 ms (4.6)	2.3 Hz

Parameters for the Hill Model

The passive force-length relationship can be represented by the exponential function (Delp et al., 2007; Thelen, 2003; Winters and Woo, 1990):

$$F_{PE} = \frac{\exp\left(\frac{k_{PE}}{\ell_{\max}}\left(\frac{\ell}{\ell_{\text{rest}}} - 1\right)\right)}{\exp(k_{PE}) - 1} \tag{3.14}$$

Where F_{PE} was the normalized force, k_{PE}, $\ell_{\max}$ and ℓ_{rest} were shape-parameters dictating the slope of the exponential function, and ℓ was the length of the contractile element of the Hill model. The active force-length was represented by the Gaussian function (Thelen, 2003; Winters, 1990):

$$f_{\ell}(\ell) = e^{-S_K(\ell-\ell_0)^2} \tag{3.15}$$

Where ℓ is the length of the contractile element, and S_K and ℓ_0 are parameters that specify the shape of the curve. Finally, the force-velocity relationship has been proposed to obey the expression (Winters, 1995, 1990):

$$f_v(v) = \frac{1 - \frac{v}{v_{\max}}}{1 + \frac{v}{a_f v_{\max}}} \tag{3.16}$$

For concentric contractions, and:

$$f_v(v) = \frac{1 - \frac{v}{v_{\max}} \cdot \frac{\alpha}{\beta}}{1 - \frac{v}{v_{\max}} \cdot \frac{1}{\beta}} \tag{3.17}$$

For eccentric contractions. Here, v is the shortening velocity of the contractile element, $v_{\max}$ is the maximum shortening velocity, and α, β and a_f are shape parameters. While Winters and Woo (1990) present parameters for these equations, they omit the parameter β, which will be taken to guarantee continuity between the concentric and eccentric contractions: a technique borrowed from Panzer (2006). Parameter values are summarized in Table 3.6.

Table 3.6: Parameters that will be used for the Hill model in the active and passive force-length and force-velocity equations.

Parameter	**Range**	**Value**	**Reference**
$\sigma_{\max}$	25 – 100 MPa	35 MPa	Zajac (1989)
k_{PE}		3	Winters (1995)
ℓ_{rest}	From muscle origin/insertion points		
$\ell_{\max}$	0.6 – 0.7	0.6	Winters (1995)
S_k		6.25	Winters and Woo (1990)
ℓ_0		1.05	Winters and Woo (1990)
$v_{\max}$	Slow twitch: 2 ℓ_{rest}/s Fast twitch: 8 ℓ_{rest}/s	5 ℓ_{rest}/s	Winters and Woo (1990)
a_f	Slow twitch: 0.1 – 1.0 Fast twitch: 0.1 – 0.25	0.55	Winters and Woo (1990)
α	1.1 – 2.0	1.3	Winters and Woo (1990)
β	For continuity: $\beta = \frac{a_f(\alpha-1)}{a_f+1}$	0.1065	Panzer (2006)

3.3 Inverse Dynamics

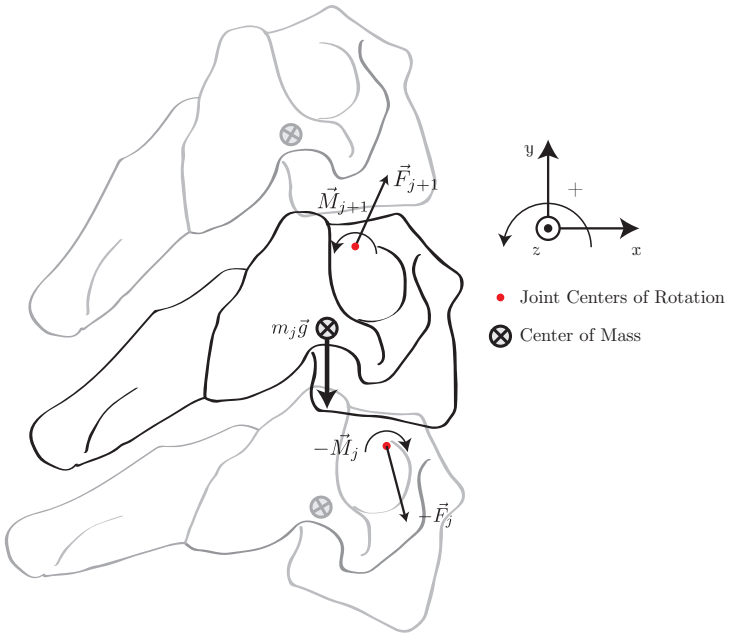

Figure 3.4: Free Body Diagram of an individual cervical spine vertebra. Note that this assumes that there is no external force.

The inverse dynamics functionality is at the core of the model, which computes the net joint moments and forces acting at the joint centres of rotation. The model uses the recursive Newton-Euler algorithm to solve for the net joint forces and moments (Featherstone, 2008). Using the free-body diagram in Figure 3.4, the equilibrium equations for the j^{th} segment can be written ($j = 1, \ldots, 8$ where $j = 1$ is the skull, $j = 2, \ldots, 7$ is C1 through C6, and $j = 8$ is C7):

$$m_j\vec{a}_j = m_j\vec{g} + \vec{F}_{j+1} - \vec{F}_j \tag{3.18}$$

$$\mathbf{I}_j\dot{\vec{\omega}}_j + \vec{\omega}_j \times \mathbf{I}_j\vec{\omega}_j = \vec{r}_{j,j+1} \times \vec{F}_{j+1} - \vec{r}_{j,j} \times \vec{F}_j + \vec{M}_{j+1} - \vec{M}_j \tag{3.19}$$

Where $\vec{r}_{j,j}$ and $\vec{r}_{j,j+1}$ are the moment arms for the j^{th} and $(j+1)^{\text{th}}$ joint centres of rotation to the centre of mass in reference frame j; m_j is the mass of the segment j; $\mathbf{I}_j$ is the inertia tensor of segment j in the global coordinate system about the segment's centre of mass; $\vec{\omega}_j$ is the angular velocity of segment j; $\vec{F}_j$ and $\vec{M}_j$ are the reaction forces and moments at the superior joint center of segment j (with $\vec{F}_1 = \vec{0}$ and $\vec{M}_1 = \vec{0}$ at the head).

Equations 3.18 and 3.19 are recursively solved for $\vec{M}_j$ and $\vec{F}_j$ until a base-case is reached (in this case, the head). Then the algorithm collapses down to find the reaction forces and moments at C7-T1, solving each joint along the way. While it is true that it is possible to start immediately at the head and work down to C7-T1 (the so-called top-down approach), implementing the algorithm in this recursive manner is better suited to handling more complicated model geometries than kinematic chains. In particular, model geometries that branch outward can be added with minimal adjustments of the code. In this way, future revisions of the model could include shoulders that branch from the torso, and with one call to the recursive function all of the net joint moments and forces can be computed with the same underlying inverse-dynamics code. Such an investigation may be undertaken to investigate the complicated interactions between cervical spine and shoulder injuries observed in the workplace (Bao, 1995).

3.4 Indeterminacy

The net joint moment is the sum of contributions from muscles, ligaments and intervertebral discs, each of which applies a force at one segment and another at a distal one with equal and opposite magnitude. Partitioning the moment is easiest to understand beginning

with the head, where the net-joint moment is the result of muscle and ligament action. Here:

$$\vec{M}_1 = \sum_{k \in \mathcal{M}} \vec{r}_{1,k} \times \vec{F}_{1,k} + \sum_{\ell \in \mathcal{L}} \vec{r}_{1,\ell} \times \vec{F}_{1,\ell} \tag{3.20}$$

Here $\mathcal{M}$ is the set of all muscles in the model, and k serving as an index over this set; similarly, $\mathcal{L}$ is the set of all ligaments in the model, with ℓ indexing over them. $\vec{F}_{1,k}$ and $\vec{F}_{1,\ell}$ are the forces from the muscles and from the ligaments respectively. When there is a disc present, it is included as an extra term in this expression. In general:

$$\vec{M}_j = \sum_{k \in \mathcal{M}} \vec{r}_{j,k} \times \vec{F}_{j,k} + \sum_{\ell \in \mathcal{L}} \vec{r}_{j,\ell} \times \vec{F}_{j,\ell} + \vec{M}_{d,j} \tag{3.21}$$

Where $\vec{M}_{d,j}$ is the restorative moment from the intervertebral disc between segments j and $j-1$, calculated from the moment-rotation relationship described earlier. Because of the many multi-joint muscles in the cervical spine, all 8 equations in Equation 3.21 need to be balanced. Unfortunately, this problem is under-determined since there are more unknowns than equations. In an EMG-driven model, the forces calculated from the muscle model needs to be balanced in this equation. Often times, the balance is poor, and the muscle forces need to be adjusted in order to balance the moment done through EMG-assisted optimization (Cholewicki and McGill, 1994; McGill and Norman, 1986). Finally, since the magnitude of the muscle force is the same at each joint and only changes direction with the line of action, Equation 3.21 can be rewritten:

$$\vec{M}_j = \sum_{m \in \mathcal{M}} F_m \vec{r}_{j,m} \times \hat{u}_{j,m} + \sum_{\ell \in \mathcal{L}} F_\ell \vec{r}_{j,\ell} \times \hat{u}_{j,\ell} + \vec{M}_{d,j} \tag{3.22}$$

Where $\hat{u}_{j,m}$ is the line of action of muscle element m as it passed by joint j. Finally, it is convenient to define the **moment-arm vector** as $\vec{d}_{j,m} = \vec{r}_{j,m} \times \hat{u}_{j,m}$ for muscles and $\vec{q}_{j,m} = \vec{r}_{j,\ell} \times \hat{u}_{j,\ell}$ for ligaments. This vector's components represent the minimal perpendicular distance from the muscle's line of action to the j^{th} joint centre. Under this definition, Equation 3.21 can be written compactly as:

$$\vec{M}_j = \sum_{m \in \mathcal{M}} F_m \, \vec{d}_{j,m} + \sum_{\ell \in \mathcal{L}} F_\ell \, \vec{q}_{j,\ell} + \vec{M}_{d,j} \tag{3.23}$$

These equations can even be further condensed by stacking them vertically and using matrix notation. Doing so:

$$\begin{bmatrix} \vec{M}_1 \\ \vdots \\ \vec{M}_K \end{bmatrix} = \begin{bmatrix} \vec{d}_{1,1} & \vec{d}_{1,2} & \dots & \vec{d}_{1,M} \\ \vec{d}_{2,1} & \vec{d}_{2,2} & \dots & \vec{d}_{2,M} \\ \vdots & \vdots & \ddots & \vdots \\ \vec{d}_{K,1} & \vec{d}_{K,2} & \dots & \vec{d}_{K,M} \end{bmatrix} \begin{bmatrix} F_1 \\ \vdots \\ F_M \end{bmatrix} + \begin{bmatrix} \vec{q}_{1,1} & \vec{q}_{1,2} & \dots & \vec{q}_{1,L} \\ \vec{q}_{2,1} & \vec{q}_{2,2} & \dots & \vec{q}_{2,L} \\ \vdots & \vdots & \ddots & \vdots \\ \vec{q}_{K,1} & \vec{q}_{K,2} & \dots & \vec{q}_{K,L} \end{bmatrix} \begin{bmatrix} F_1 \\ \vdots \\ F_L \end{bmatrix} + \begin{bmatrix} \vec{M}_{d,1} \\ \vdots \\ \vec{M}_{d,K} \end{bmatrix} \tag{3.24}$$

Finally, these can be consolidated to:

$$\vec{\mathcal{M}} = \mathbf{J}_m^T \vec{F}_m + \mathbf{J}_L^T \vec{F}_L + \vec{M}_d \tag{3.25}$$

Where $\mathbf{J}_m$ and $\mathbf{J}_L$ are the **Muscle Jacobian** and **Ligament Jacobian**, respectively (Zatsiorsky and Prilutsky, 2002). These are $M \times 3K$ and $L \times 3K$ matrices. $\vec{F}_m$ and $\vec{F}_L$ are obtained by vertically stacking the muscle and ligament forces, while $\vec{M}_d$ is obtained in a similar manner but for those moments from the intervertebral disc. To populate the entries of the muscle and ligament Jacobian matrices, one needs to compute the

smallest perpendicular distance to the muscle or ligament's line of action. Fortunately, an efficient method for calculating these matrices can be found using the Tendon Excursion Method:

$$\mathbf{J}_{ij} = \frac{\partial \ell_i}{\partial \theta_j} \tag{3.26}$$

Where ℓ_i is the length of the i^{th} tissue, muscle for the muscle Jacobian and ligament for the ligament Jacobian, and j represents the number of degrees of freedom. In this case, $j = 1$ represents C0-C1 flexion-extension, $j = 2$ for C0-C1 lateral bend, and so on until $j = 24$ is C7-T1 axial twist. On each frame, joint angles are sequentially perturbed, and the change in length of each muscle element computed. The ratio of the length change in the i^{th} element to a perturbation in the j^{th} degree of freedom is the element of the corresponding Jacobian matrix. To compute the contributions of muscles and ligaments in shear and compression, a related matrix is computed:

$$\mathbf{P}_{ij} = \frac{\partial \ell_i}{\partial x_j} \tag{3.27}$$

In this case, the denominator is a shear perturbation. Perturbations in this manner isolate the elements of $\hat{u}$, the line of action of the tissue. This takes some algorithmic complexity out of computing the lines of action of tissues as they cross specific joints. Instead, on each frame, the joints are perturbed in a translational direction and the change in length of the muscles computed. Finally, the net compression and shear can be computed as:

$$\vec{C} = \vec{R} - \mathbf{P}_m^T \vec{F}_m - \mathbf{P}_L^T \vec{F}_L \tag{3.28}$$

Using these Jacobian formulations of the moment-balance requirements also proves useful for programming optimization schemes, for instance, EMG assisted optimization.

3.4.1 Generalized EMG-Assisted Optimization

The major problem with naïvely implementing EMG-Assisted Optimization as in Cholewicki and McGill (1994) is that it only balances one moment at a time. Balancing moments down the kinetic chain, beginning with the head, quickly runs into issues, since the solution of one optimization routine is dependent on all of the previous solutions. A more robust solution might try to adjust all of the muscle gains to balance all of the net-joint moments simultaneously. From the outset, the generalization should have two important properties:

1. When applied to a single-joint problem it should reduce to the originally proposed EMG-Assisted Optimization

2. It should maintain the originally proposed reasoning, which is that muscle forces should be minimally adjusted to balance the net joint moment.

Property (1) will be relaxed. In particular, the choice of cost function will not be proportional to the magnitude of the moment produced by the muscle, but to its estimated force. This was briefly mentioned by Cholewicki and McGill (1994) as a possible alternative to their proposed objective function.

To begin with, Equations 3.25 can be used to derive the balance restrictions for the optimization routine. Let there be M-muscles in the model spanning K-joints. For simplicity, call $\vec{M}_k$ the resulting moment at joint k once the ligamentous and disc contributions have been accounted for. After applying the gains, these equations can be written:

$$\vec{M}_k = \sum_{m=1}^{M} g_m F_m \vec{d}_{k,m} \tag{3.29}$$

This represents $3K$ simultaneous equations in M unknowns, the gains for each muscle fascicle. Like before, these equations can be combined into a global equation by stacking them:

$$\vec{\mathcal{M}} = \mathbf{J}_m^T \left(\vec{g} \diamond \vec{F}_m \right) \tag{3.30}$$

Where $\vec{\mathcal{M}}$ is a $3K \times 1$ vector obtained by appending the joint moments together; $\mathbf{J}_m$ is the muscle Jacobian, a $M \times 3K$ matrix or $M \times K$ block-matrix, where each j, mi block is given by $\vec{d}_{j,m}^T$, each of which are 1×3 vectors representing the moment arm vector on joint j for the m^{th} muscle; and $\vec{g}$ is a vector of all of the muscle gains appended together, and $\vec{F}_m$ is the same with forces; the notation $\vec{g} \diamond \vec{F}_m$ is meant to indicate element-wise multiplication. The generalized EMG-assisted optimization is obtained using these moment-balance equations with a modified objective function like the one in Cholewicki and McGill (1994):

$$\begin{aligned}
\text{Minimize:} \quad & \Theta(\vec{g}) = \sum_{m=1}^{M} (1 - g_m)^2 F_m && (3.31)\\
\text{Subject to:} \quad & \mathbf{J}_m^T \left(\vec{g} \diamond \vec{F}_m \right) = \vec{\mathcal{M}} && \text{(Moment Balance Constraint)}\\
& g_m \geq 0, \quad \text{for all } m = 1, \ldots, M && \text{(Non-negativity Constraint)}
\end{aligned}$$

Note that the resulting objective function is a linear combination of quadratic programming problems analogous to Cholewicki and McGill (1994), and it is the Moment Balance Constraint which ultimately couples solutions at every joint. A very similar method was presented by Gagnon et al. (2011), although the above formulation with muscle Jacobians is better described. These authors also impose a more stringent non-negativity constraint, forcing the gains to fall within 50% of the activation level obtained from the electromyogram.

3.5 Model Development

The model development, done in Python, was made as modular as possible, in three new modules: a general use biomechanics function library, a modelling specific library, and a `model` object which oversees the model geometry, motion capture, and EMG data, as well as handle any kinematic constraints (for instance, the partitioning of inter-segmental angles) (Figure 3.5). Lastly, the `viewer` module handles actually drawing the model to the screen.

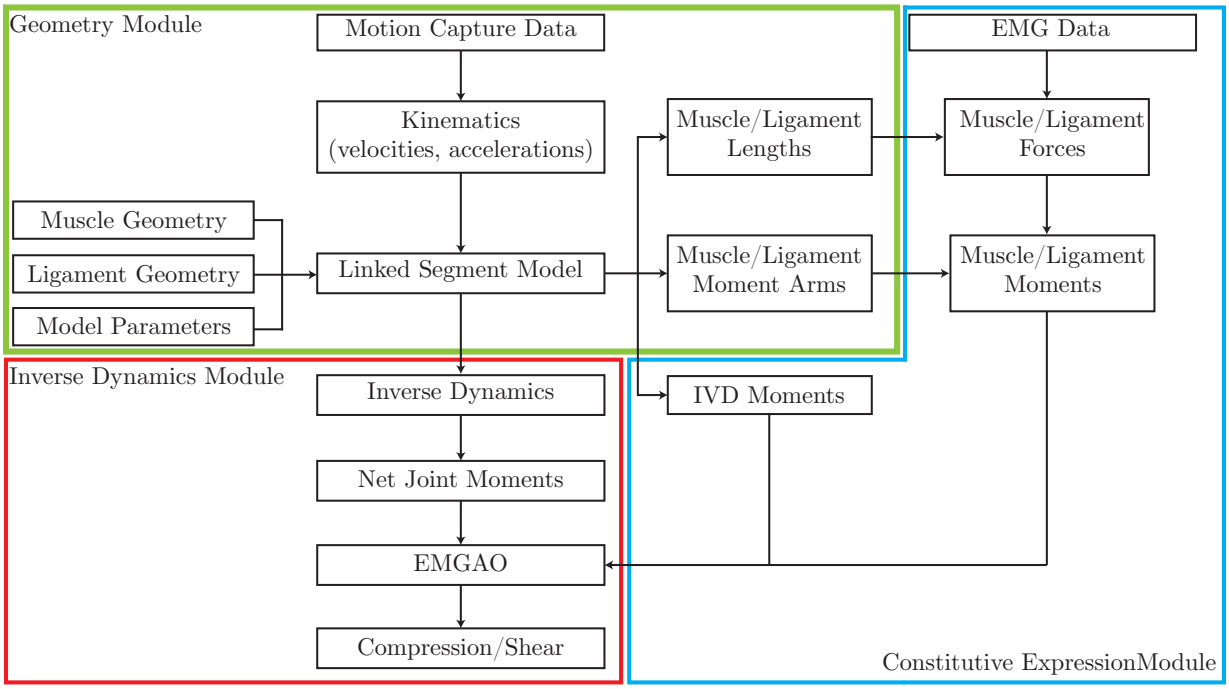

Figure 3.5: Flow diagram of data through the proposed model.

3.5.1 The PyBiomech Module

The `PyBiomech` Module (developed here) consists of a collection of functions which are useful for processing EMG and motion capture data. The intention is to be an easy to use module for the linear enveloping of EMG and processing of joint angles. As far as kinematics go, it contains functions to convert between Euler angle conventions, between Euler angles and rotation matrices and quaternions, and computing angular velocities. For EMG, this module contains functions which are useful for linear enveloping EMG data and computing a series of co-contraction metrics. Thus far, this module contains many more functions that were needed for the completion of this project, the hope is to make this module a freely available open-source code-base.

3.5.2 The Modeller Module

The `Modeller` module (also developed here) contains a mix of functions and objects which are generally useful for modelling, specializing in linked-segment modelling and resolving indeterminacy. A linked segment model can be made by instantiating two or more `segment` objects, and attaching them together with a joint object. `Segment` objects consist of the inertial properties of the joint, as well as an initial orientation matrix, and has the option of storing a triangular surface mesh so that it can be drawn in 3D space. The `segment` object contains all of the logic for animating and rescaling the segment. The joint object is generally a 6 degree-of-freedom joint, and is subclassed into a rotary joint, which isolates the three rotational degrees of freedom. This `RotaryJoint` object is subclassed into an IVD (Intervertebral disc) joint, which takes parameters for calculating a restorative moment depending on the three rotational degrees of freedom in the joint.

A `tissue` class contains a list of points together with the `segment` within which they reside. The `tissue` class calculates lengths and shortening velocities. The `tissue` class is subclassed by the `ligament` and `muscle` classes, which house the necessary parameters for computing force depending on the length and shortening velocity of the tissue. The `muscle` class also contains an activation-array which is obtained from the linear envelope of the EMG.

The rest of the module consists of two functions for resolving indeterminacy. `emg_optimization` takes an array of net-joint moments, the muscle Jacobian matrix, an array of estimated muscle forces, and an array of muscle physiological cross-sectional areas. It returns an array of gains for each muscle fascicle in a time-varying manner. `crowninshield_optimization`

takes the same parameters and returns the gains by minimizing the sum of cubed muscle forces normalized to the physiological cross sectional areas, originally proposed by Crowninshield and Brand (1981). In order to solve these optimization problems, the program makes extensive use of the `CVXPY` package (Diamond and Boyd, 2016).

3.5.3 The Viewer Module

The `Viewer` module contains methods for creating a graphics window so that the animation can be displayed to the user. It contains a `camera` object, which manages where the camera is in three dimensional space, the field of view, and necessary projective mappings. Currently, control of the camera is done using the keyboard and mouse, which give the user a detailed 6 degree of freedom control over the position and orientation of the camera. The `viewer` object instantiates a viewing window and gives the user control over the camera. This graphical component makes extensive use of an external Python package called `pyglet`, which allows Python to interface with OpenGL, an open-sourced graphical library.

3.5.4 The CSpine2016 Module

This module contains an object which reads in anatomical data, instantiates the linked-segment model, and computes the necessary Jacobians to be used with the `modeller` module. It also contains several graphing methods, and is responsible for instantiating the viewer window which displays the model. This is where the majority of the abstraction occurs.

3.6 Verification

The most straightforward way to verify a model is to check the model outputs to analytic solutions of the equations. Unfortunately, documenting this procedure has not been well-addressed in the literature, and many authors prefer to stick to the use of commercial software (Hicks et al., 2014). Using commercial software provides an avenue of subverting this discussion, since it is assumed to have endured rigorous verification. With the proposed model there are three major components that need to be verified: (*i*) the geometry of the kinematics, (*ii*) the computation of net joint moments and forces, or inverse dynamics, and (*iii*) balancing the net joint moments with muscle forces.

Verification was done throughout development. The geometry of the model was checked by visual inspection of plotted marker and cervical spine trajectories. The inverse dynamics net joint forces and moments were checked, for a variety of postures, against hand calculations. To avoid calculating these moments at every joint level, they were done just about C7-T1, using the position of the whole cervical spine's center of mass, and assuming that it was rigid.

Angular velocities were verified by computing them three different ways: (*i*) with the derivatives of the joint angles and using the relationships in Goldstein et al. (1950), (*ii*) by differentiation of the direction cosine matrices (the preferred method), and (*iii*) by converting the direction cosine matrices to quaternions and computing them with quaternions. In all cases, angular velocity calculations were in perfect agreement.

The muscle forces computed following the EMG assisted optimization matched joint re-

action moments exactly, additionally, the Lagrange multipliers returned from the CVXPY package certified that these solutions achieved the minimum value of the objective function under the Karush–Kuhn–Tucker (KKT) conditions.

Chapter 4

Model Validation

4.1 Introduction

Validation asks 'am I solving the correct equations?' whereas verification asks 'am I solving the equations correctly?' Any model proposition would be incomplete without a discussion of how these terms apply to the proposed model. Verification was previously described and examined regularly throughout the development process. Validation is much more difficult to accomplish, and must be done by comparing model outputs to experimentally measured results. This adds a level of complexity to this thesis, since neck loads have never been rigorously quantified *in-vivo*. Fortunately, there have been some comparable modeling efforts which have had similar goals to the proposed model which offer opportunity for comparison.

Validation of linked segment models of the whole body have been done previously by

comparing top-down and bottom-up approaches (Kingma et al., 1996). Additionally, since forward multibody dynamic models of the cervical spine have been successful in predicting the kinematics seen in whiplash events (DeWit and Cronin, 2012; Esat and Acar, 2009; van der Horst et al., 1997; van Lopik and Acar, 2007), it stands to reason that an inverse dynamic model of the cervical spine may be successful in predicting the internal forces from kinematics. Of course, the success of previous models does not validate the current model, whose validation is contingent on the prediction of forces and moments similar to those obtained experimentally under similar conditions.

The validation procedure of the model was based on three criteria: (*i*) a detailed evaluation of muscle gains, (*ii*) comparing compression and shear values calculated during maximal voluntary contractions and comparing values to previously published results, and (*iii*) by performing a sensitivity analysis in order to determine if the model is overly sensitive to specific parameters. The analysis of muscle gains offers insight into how physiologically plausible the predicted muscle forces are. If a muscle needs to be gained by a substantial amount, then the force predicted from EMG was unreasonably small. Conversely, should it need to be substantially gained down, then the predicted force was too large. The second goal, comparing predicted compression and shear to previously published values, is a classic undertaking in validation studies, as it gives a model some criterion validity. Finally, a sensitivity analysis can determine if a model is overly sensitive to certain parameters. If a model provides estimates which are ultimately governed by a small number of parameters, then it is especially important that those parameters be accurate.

4.2 Methods

The experimental data presented in this chapter directly follows from a previous study conducted at the University of Waterloo (Callaghan et al., 2014). Therefore, what follows is a brief synopsis of what was described there.

4.2.1 Data Collection

Participants

Eight healthy males (mean age: 21.3 ± 1.7 years; height: 177.9 ± 6.8 cm; body mass: 79.7 ± 11.5 kg) with no previous history of neck, shoulder, or upper back pain participated in the study.

Maximum Voluntary Exertions

Following a brief, 5-minute, warm-up of neck and trunk stretching with submaximal exertions, participants were strapped to a chair with Velcro^{TM} straps while wearing a Canadian Armed Forces CH146 Griffon Helicopter helmet. The helmet was mounted on a robotic arm (HP50 with NX100 Controller, Yakasawa Motoman Robotics, 3530 Laird Road, Unit 3, Mississauga, ON), with a 6 degree-of-freedom load cell (MC3A-6-500, Advanced Mechanical Technology Inc., USA) positioned between the helmet and robotic arm. Participants performed maximal voluntary isometric exertions in a neutral posture: pushing their heads forward (flexion), backward (extension), or to their right (lateral bend).

Data from the load cell were sampled at 1500 Hz.

Electromyography

Surface electromyography (EMG) electrodes, placed 2 cm apart, evaluated the level of muscular activation of 10 muscles (5 bilaterally): splenius capitis, sternocleidomastoid, levator scapulae, the cervical erectors, and upper trapezius. A 16-channel Noraxon Telemyo 2400T G2 Telemetry electromyography system (Noraxon U.S.A. Inc, Scottsdale, AZ) amplified the signals, and fed them to a 16-bit analog to digital card which sampled the data at 1500 Hz. The resulting surface EMG signal was detrended, full-wave rectified and linear enveloped with a single pass critically damped digital filter with cut-off frequencies chosen based off the electromechanical delay of the muscles (*c.f.* Table 3.5). The resulting smoothed signals were normalized to the maximum activation among all of the MVE trials on a channel-by-channel basis using the maximum activation over the time-series.

Motion Capture

Kinematic data from a passive motion capture system (Vicon MX, Vicon Motion Systems Ltd, Los Angeles, CA) were sampled at 50 Hz from a total of 9 markers. Markers on the xyphoid process, acromion processes, and C7 spinous process were used to make a local coordinate system (LCS) for the trunk, while the markers over the ear covers of the helmet and the most superior point of the helmet were used to make a LCS for the head-segment. Both of these LCSs were defined to be consistent with ISB standards, and the relative rotation between these two coordinate systems quantifies the head-trunk angle which was used as an input into the cervical spine model.

Participants moved from a neutral posture to one of 7 target postures, which they held for 15 seconds before returning to a neutral posture. In addition to the change in posture, participants wore a helicopter helmet in one of three configurations: just the helmet (hOnly), the helmet with night vision goggles (hNVG), and the helmet with the NVG and a counterweight (hCW + NVG). In total there were 84 trials analyzed for each participant, performing each helmet and posture combination three times. The model processed EMG and motion capture data using the methods described above and resolved the compression and shear forces acting on each joint level throughout the cervical spine. Note that data from the helmet trials were not analyzed in this study, but were in the subsequent one.

4.2.2 Driving the Model

The collected EMG drove the activation profiles of several muscles, which are listed below:

1. The levator scapula channels drove the anterior, middle, and posterior scalenes in addition to levator scapula. This was mainly based on the image of the levator scapula electrode placement in Callaghan et al. (2014): it looks like there could plausibly be cross-talk between the scalenes and the levator scapula.

2. The cervical erector spinae channels drove longissimus cervicis, longissimus capitis, semispinalis capitis and cervicis, and splenius cervicis. The rationale for driving these muscles was that they originate from a similar location and have similar functionality as extensors of the cervical spine.

3. The sternocleidomastoid channels drove the sternocleidomastoid, sternohyoid and longus colli muscles. Vitti et al. (1973) showed that there seems to be some synergy between the sternocleidomastoid muscle and the longus colli muscles, while Siegmund et al. (2007) demonstrated the synergistic relationship between the sternocelidomastoid and the sternohyoid muscle.

4. The splenius capitis channels drove splenius capitis. Siegmund et al. (2007) showed that splenius capitis displays subject specific, sometimes paradoxical, activation patterns that are not representative of posterior cervical spine muscles in general.

5. The upper trapezius channels drove the upper trapezius

4.2.3 Analysis of Muscle Gains

The gains computed from the EMG-assisted optimization routine for all postures in the un-helmeted condition were used as a performance measure of the model. Ideally these gains are close to unity, indicating that the constitutive expression for muscle force fits well with the net joint moments computed from the inverse dynamics module and EMG measured from the subject; otherwise the gains serve as correction factors to the parameters used in the model (*e.g.* specific tension of muscles, or the physiological cross-sectional areas). The median fascicle gain over time gives an indication of the average amount of gain for the fascicle, which is then averaged over all fascicles in a muscle to give a muscle gain. The analysis of muscle gains was performed using the postural trials from the non-helmeted condition and were compared to a performance corridor of 0.5 – 1.5. Outside of this range they were flagged for potential issues. This performance corridor was

chosen based on discussions with others who have used EMG-assisted optimization before (Dr. Ed Cambridge and Jordan Cannon from Dr. Stuart McGill's lab).

4.2.4 Comparison to Published Results

To test the criterion validity of the current model, compression and shear values at C4-C5 in maximal voluntary contraction (MVC) trials were compared to a previously published model's response (Choi and Vanderby, 1999). This model also used EMG assisted optimization with a similar experimental protocol for MVC trials. Participants in a neutral posture maximally and isometrically exerted against a force-transducer in flexion, extension and bidirectional lateral bending. Using the corresponding MVE trials collected in the present study, compression and shear forces at the C4-C5 levels were compared to see how the model's response compares to previously published results.

The study by Forde et al. (2011) used the joint reaction forces and moments calculated about C7-T1 as surrogate measurements for compression and shear values. Because these reaction forces omit muscle activation, compression and shear values reported there are incommensurable with those reported here. With the exception of Choi and Vanderby (1999) and Forde et al. (2011), no other studies have attempted to quantify the compression and shear loads on the *in-vivo* cervical spine.

4.2.5 Sensitivity Analysis

A sensitivity analysis was conducted by incrementally changing a parameter-value, running a simulation, and comparing the effect of the changed parameter on an outcome

variable (van Griensven et al., 2006). Such a method is called a "local sensitivity analysis," and it is performed by computing the partial derivative of an outcome variable with respect to an input parameter. The normalized sensitivity coefficient, or relative sensitivity coefficient, is then defined as:

$$S_p = \frac{\partial C}{\partial p} \frac{p}{C} \tag{4.1}$$

When normalized in this way, the sensitivity coefficient, S_p, quantifies the percent by which the outcome variable C will change for a percent change in the parameter p. For the sensitivity analysis in this document, C was either the compression or shear values. The parameters in question which were tested using this sensitivity analysis were:

1. Muscle and Ligament origin, insertion and via points
2. All of the parameters in the muscle's hill model
3. All of the parameters in the ligament model

And the outcome variable was the median compression and shear values over the trial. The data used for the sensitivity analysis came from three trials from a single subject, were repeatedly analyzed with small changes in each parameter: (i) a neutral posture, (ii) a flexed and rotated posture, both at 45°, and (iii) laterally bent to the left by 20°. In total, this analysis examined the sensitivity of compression and shear values at each cervical level to the 9,833 parameters used in the model.

To gauge the sensitivity of the model to a given muscle or ligament force generating parameter, the absolute value of the compression and shear sensitivities were averaged to

obtain an 'overall' sensitivity to a specific ligament or muscle parameter. Then, these were summed over all the ligaments or muscles in the model.

4.3 Results

4.3.1 Muscle Gains with Posture

Time varying gains for each muscle fascicle are presented in the appendix, as they are roughly constant in the deviated posture only the median gain for each trial need be considered in this analysis. On average, most muscle gains were close to unity (Figures 4.1 to 4.7), however, some exceeded the performance margin of (0.5, 1.5), and, in a few notable cases, even exceeded a value of 3.0. These levels of gain are quite concerning, and speak to a possible issue with the collected EMG or with the model itself. It should be said that the muscles with the most dramatic gains were typically deeper musculature, like the longus colli or illiocostalis capitis muscles, or those whose EMG were driven from a neighbouring muscle, like the sternohyoid muscle. This implies, to some extent, that the dramatic increase or decrease in muscle gain may be the result of poor representation of the actual neural drive being sent to those muscles.

By and large, the best performance was in the neutral posture, where average muscle gains rarely left the performance margins (Figure 4.1). Conversely, the worst was in extension (with or without axial twist) and lateral bending, where the gain in the sternohyoid muscle were in excess of 3.0. Large activity in this muscle is to be expected, since the hyoid group is well positioned to generate the necessary flexion moment to counterbalance the weight of the head. Similarly, in lateral bending, the vast majority of the musculature in the cervical spine is posterior to the spinal column, and those on the posterolateral side would also inadvertently produce an extensor moment.

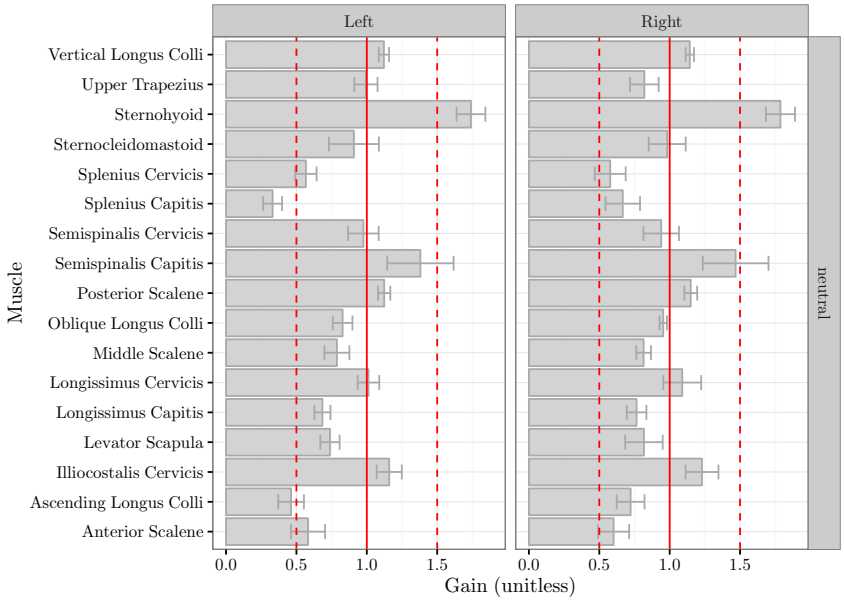

Figure 4.1: Average gains across muscle in a neutral posture. The dotted red lines represent the performance margin (0.5 – 1.5)

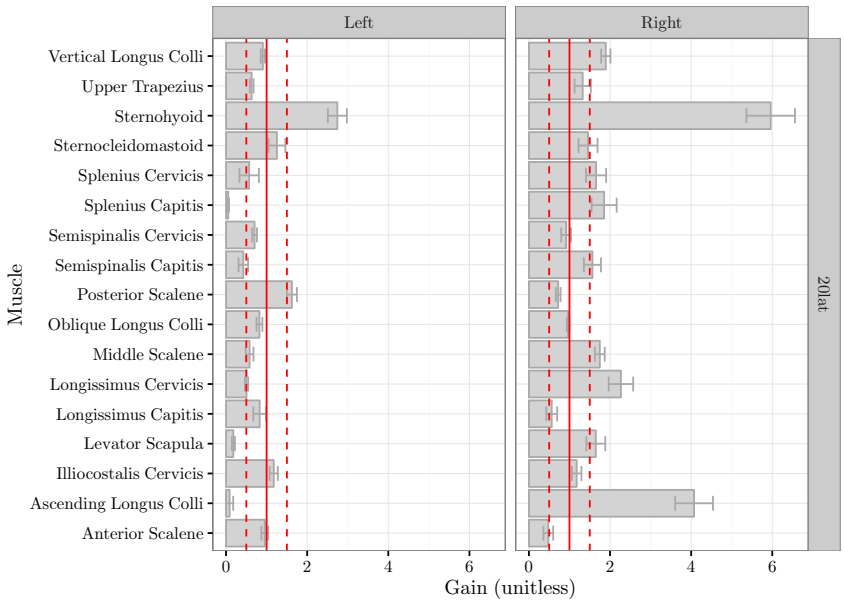

Figure 4.2: Average gains (means ± standard errors) across muscle in 20° of lateral bending to the subject's left. The dotted red lines represent the performance margin (0.5 – 1.5).

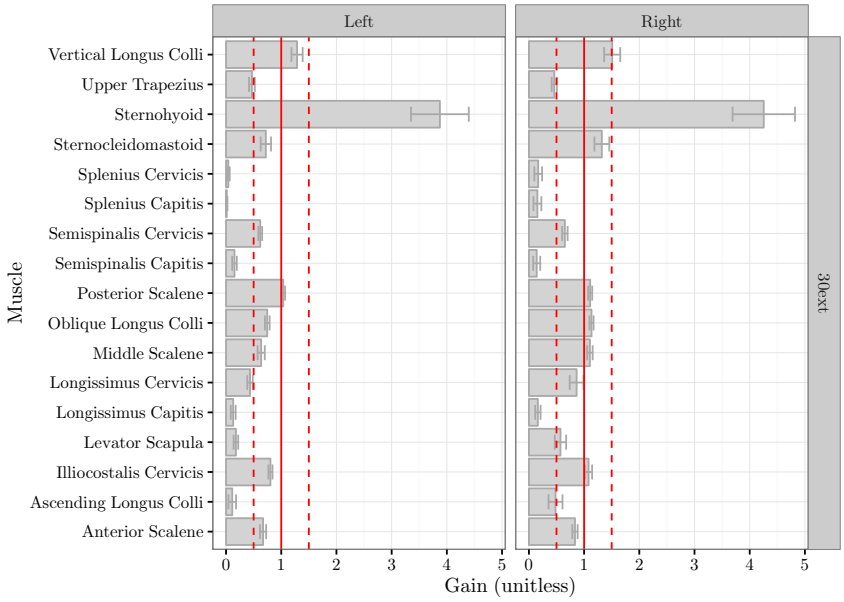

Figure 4.3: Average gains across muscle in 30° of extension. The dotted red lines represent the peformance margin (0.5 – 1.5)

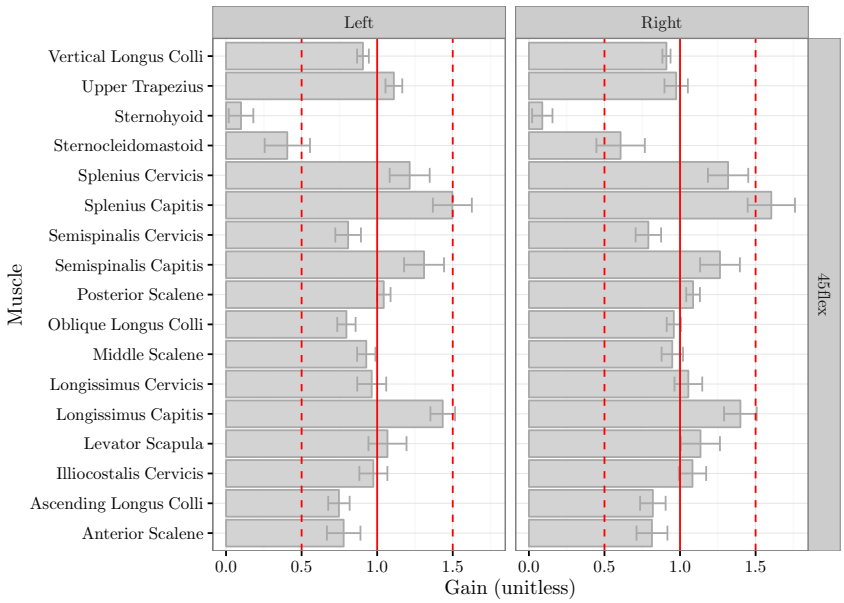

Figure 4.4: Average gains across muscle in 45° of flexion. The dotted red lines represent the performance margin (0.5 – 1.5)

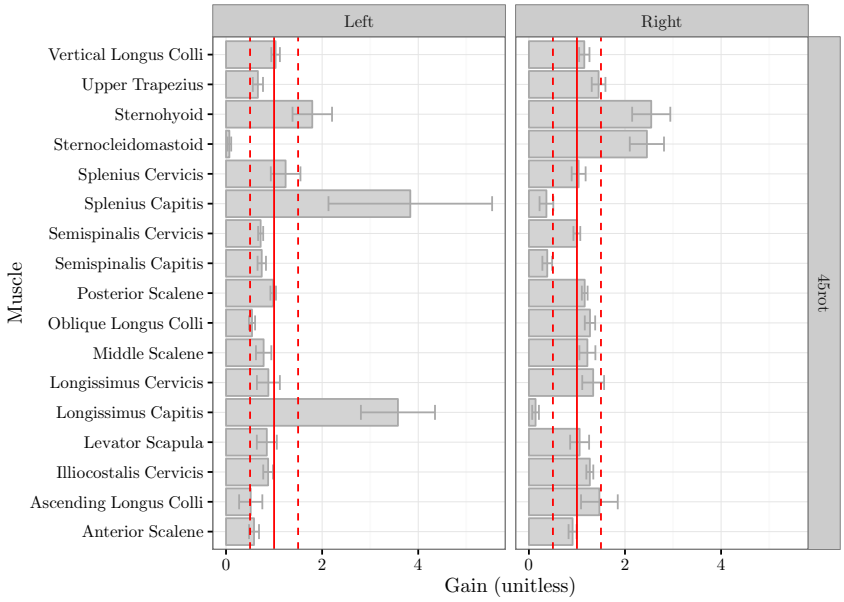

Figure 4.5: Average gains across muscle in 45° of axial rotation to the subject's left. The dotted red lines represent the performance margin (0.5 – 1.5)

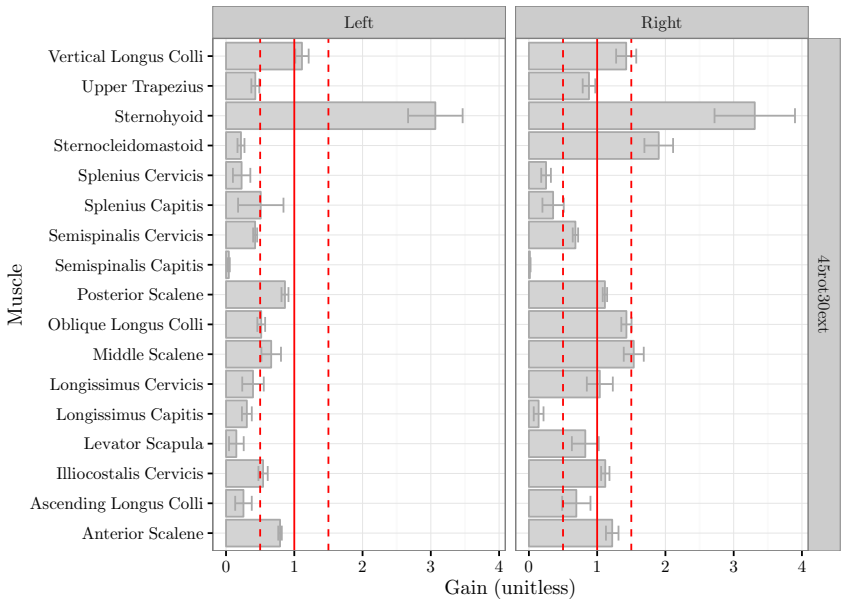

Figure 4.6: Average gains across muscle in a combination of leftward 45° axial rotation, with 30° of extension. The dotted red lines represent the performance margin (0.5 – 1.5)

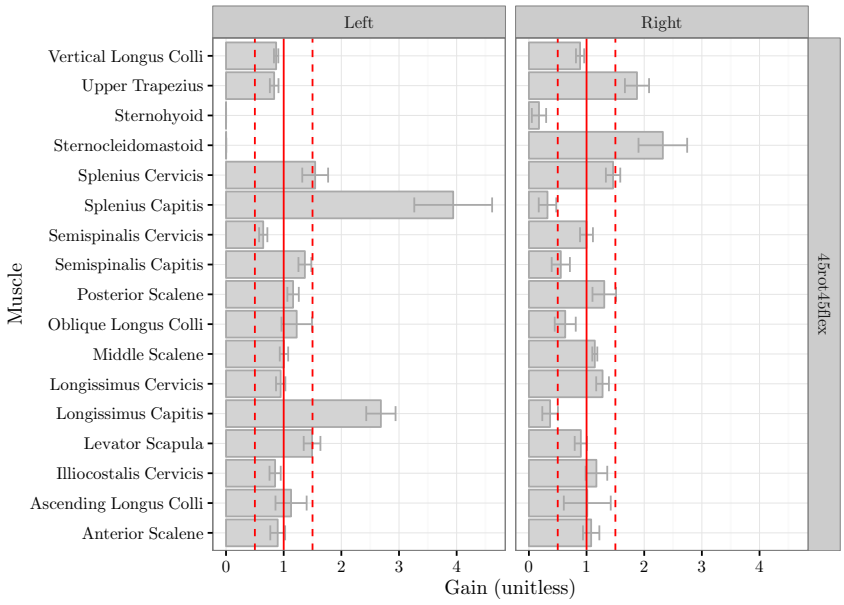

Figure 4.7: Average gains across muscle in a combination of leftward 45° of axial rotation and 45° of flexion. The dotted red lines represent the performance margin (0.5 – 1.5)

Of course, an even more considerable number of muscles have a gain less than 0.5, forming a secondary mode in the gain histogram (Figure 4.8). These represent muscles that the EMG-assisted optimization routine is turning off. In general these were muscles whose actions would have been 'agonists' for the motion being performed, for instance, the extensors when the cervical spine went into extension.

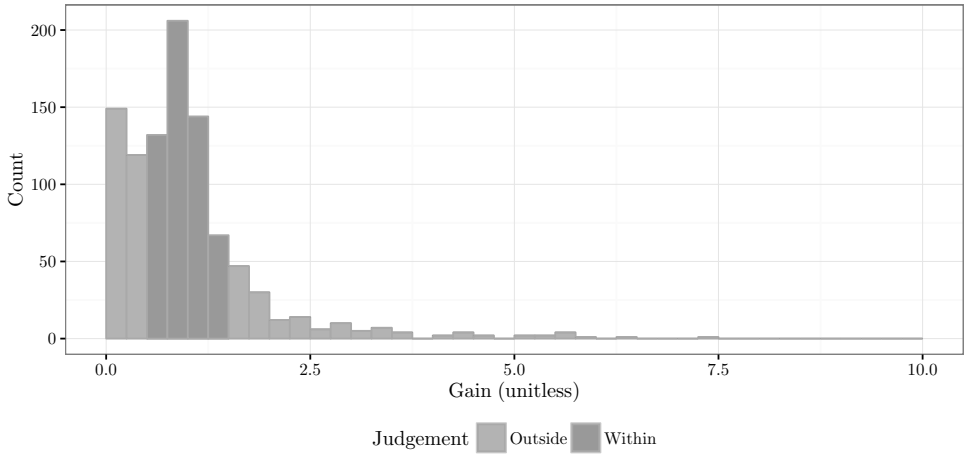

Figure 4.8: A muscle gain histogram over all trails.

4.3.2 Compression and Shear at C4-C5 in MVC Trials

A similar model by Choi and Vanderby (1999); Choi and Vanderby Jr (2000) approximated the loads at C4/C5 using EMG assisted optimization. Their EMG placement was reminiscent of Moroney et al. (1988a). In addition, their model contained roughly half as many muscles as the current model (28 muscles total versus 58 here). Nevertheless, it offers a chance to compare computed shear and compression values to previously published results.

Compression

With the exception of lateral bending there is good agreement between this study and that of Choi and Vanderby (1999) in compression, where predicted compression levels are within 30% of each-other (Figure 4.9). In extension, the current model predicted 20% more compression than that of Choi and Vanderby (1999), a 348 N difference. Conversely in a flexion MVC trial, this model predicts 30% more compression, an absolute difference of 690 N. Lastly, in lateral bending, the current model predicts 60% more compression than Choi and Vanderby (1999), representing an absolute difference of 1400 N.

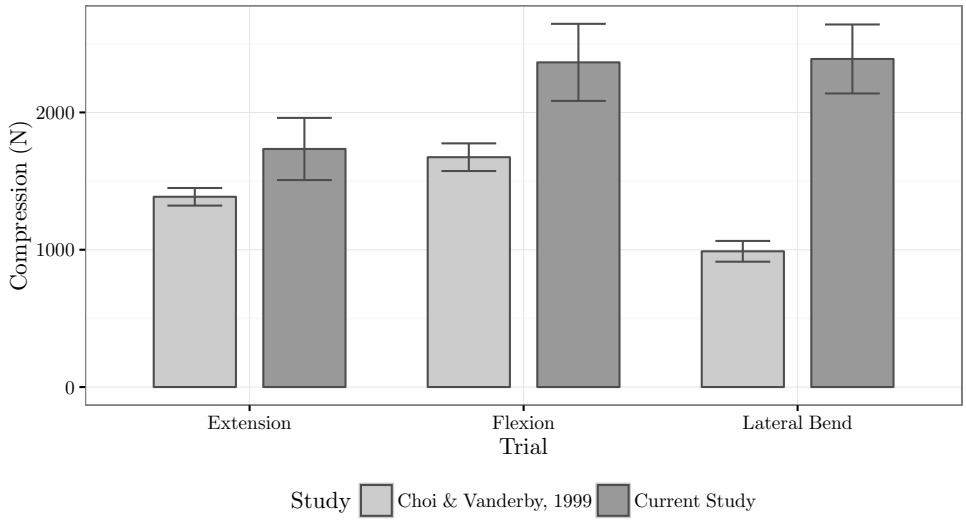

Figure 4.9: Comparison of compression forces at C4-C5 between this study and Choi and Vanderby (1999)

Shear Forces

The most dramatic differences between the two models was observed in the anteroposterior shear axis, where the current model predicts much less anterior-posterior shear than Choi and Vanderby (1999) (Figure 4.10). Choi and Vanderby (1999) predicts almost nine times as much shear in an extension trial, representing an absolute difference of 162 N. In flexion, the absolute difference is 128 N, characterizing a threefold larger prediction from Choi and Vanderby (1999). Lastly, in a lateral bending trial, the difference in shear was 29 N, where their predicted compression was 150% greater than what was predicted by the current model.

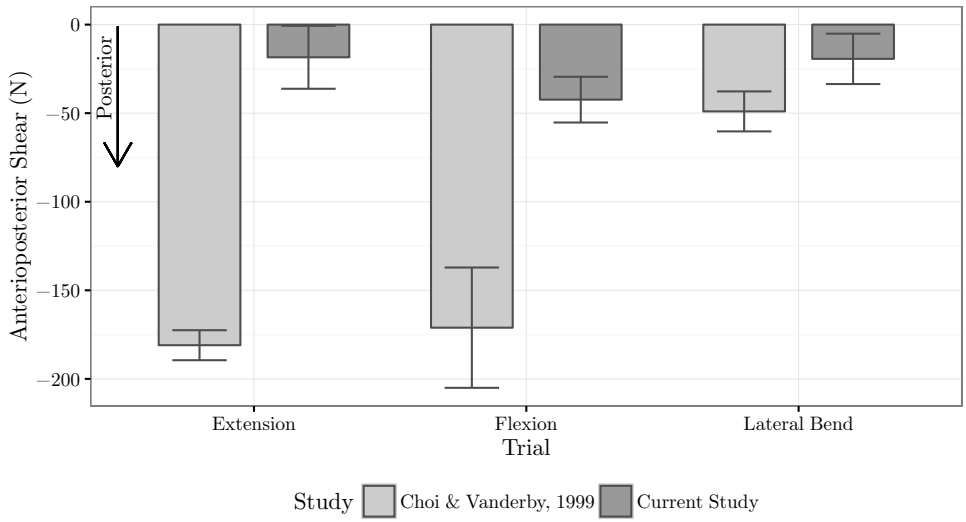

Figure 4.10: Comparison of anterioposterior shear forces at C4-C5 between this study and Choi and Vanderby (1999)

Lateral shear values are comparable across models (Figure 4.11). In extension, the difference in mediolateral shear was 13.5 N between models, representing a 70% difference.

In flexion, the worst match between models, the difference was 41.5 N, or a 178% difference – even differing in the polarity of the shear. The best agreement between the two models was mediolateral shear in the lateral bending trials, where the difference in force was only 5.6 N, or a 7.1% difference.

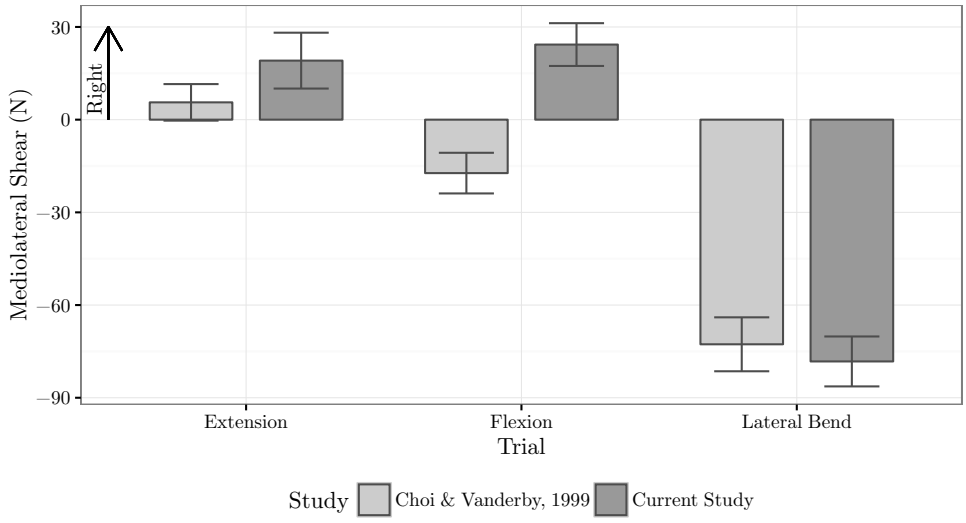

Figure 4.11: Comparison of mediolateral shear forces at C4-C5 between this study and Choi and Vanderby (1999)

4.3.3 Sensitivity Analysis

Compression

The model is much more responsive to changes in anatomical geometry than to changes in the force-deflection relationships which define the tissues. For instance, the largest compression sensitivity coefficient associated with a geometric parameter was larger by an order of magnitude than the largest coefficient among non-geometric parameters (Figures 4.12

and 4.13). Here a geometric parameter is defined as one which governs the line of action of the muscle or ligament, whereas a non-geometric parameter would be those which appear in the force calculating equations.

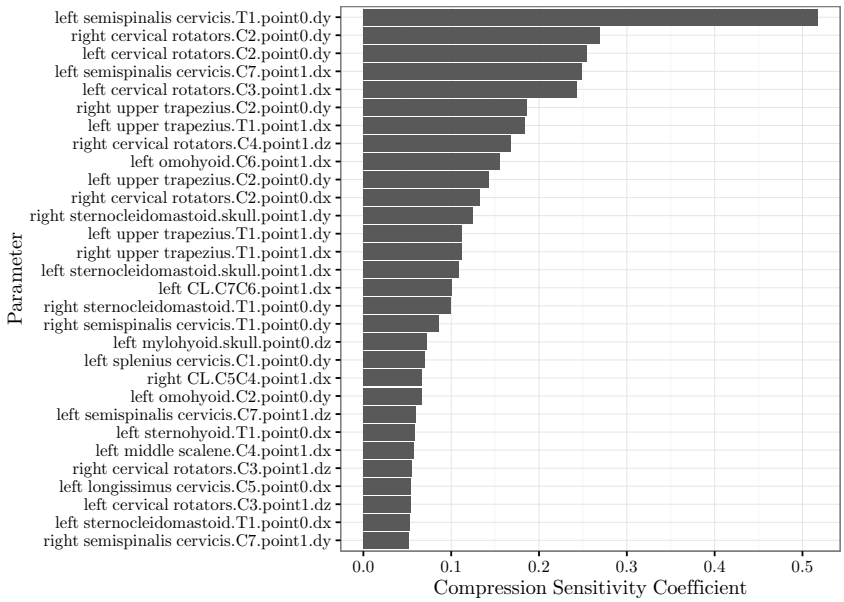

Figure 4.12: The thirty greatest normalized sensitivity coefficients of the model. This shows the abundance of sensitivity to geometric parameters like origin and insertion points.

In Figure 4.12, the parameter name nomenclature is the muscle name, the segment that it is on, then the point number (0 for origin, 1 for insertion) and the direction of perturbation in the sensitivity analysis (dx for the x-position, or mediolateral position; dy for anterior-posterior and dz for superior-inferior). Perturbations in the mediolateral (x) and anteroposterior (y) directions have the largest effects on changing the median compression, likely because these directions have the largest effect on changing the muscle's line of action. Neck extensors are more sensitive to changes anterior-posteriorly and superior-inferiorly, while the neck flexors are more responsive to changes in the superior-inferior direction. The

sensitivity of these specific muscles in these directions is intuitive: the perturbations in the positive y direction moved the origin or insertion point anteriorly toward the joint centers of rotation, which would increase the force required to balance the external moment.

Once geometric parameters like origin and insertion points are removed from the analysis, the model's sensitivity was greatest to muscle and ligament slack lengths and parameters which define the exponential shape of the passive parallel elastic component (like L_{opt} and ℓ_0). The sensitivity to muscle slack lengths is perhaps not a surprising one considering that they are modeled as exponential springs: a small change in these slack lengths may result in substantially larger forces. Ligaments, on the other hand, are modeled roughly linearly, so their appearance in the 30 most sensitive parameters is somewhat surprising.

Overall, in compression, the model's response is very robust to changes in parameter values. A 1% change in any parameter value results in at most a 0.5% change in estimated compression values. With regards to tissue properties, a 1% change in any parameter yields a less than 0.05% change in the estimated compression.

Mediolateral and Anteroposterior Shear

For the most part, the interpretation of the anteroposterior (and mediolateral) shear sensitivity analysis is the same as that of compression: the model is much more sensitive to changes in anatomical data than muscle or ligament force-length parameters, exhibiting the same order of magnitude increase in sensitivity coefficients. Detailed graphs showing this can be found in the appendix, although they are not much different from those of compression (Figures A.2 and A.3 for AP shear, and Figures A.4 and A.5 for mediolateral).

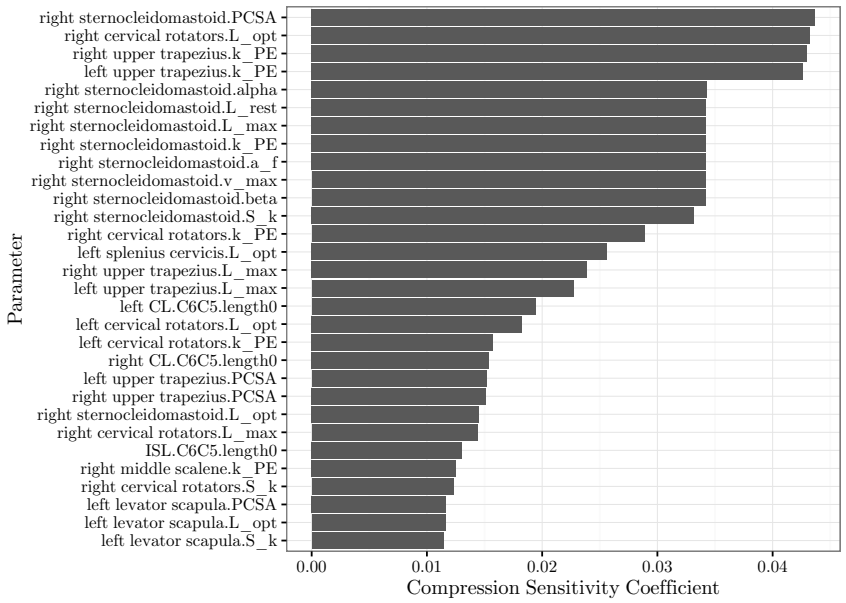

Figure 4.13: The thirty greatest normalized sensitivity coefficients of the model once geometric parameters were excluded. As anticipated, the ligament slack lengths are among the most sensitive coefficients.

Because the mediolateral shear is typically very small at C6 — T1, only the sensitivity coefficients for the joints of the upper and middle cervical spine were used in that sensitivity analysis. With the low levels of shear at C6 — T1, the relative sensitivity coefficients are volatile since they end up being a very small number divided by another small number. Once these aberrant values were removed, the sensitivity coefficients told a similar story: the model is generally more sensitive to geometric data than to force-deflection.

Holistic Sensitivity

While the above sensitivity analysis does highlight some very specific key parameters, it does not provide insight into which family of parameters the model is the most sensitive

to. By summing the parameters of a given family, for instance the k_{PE} of muscles, a more compact metric of the model's sensitivity can be achieved. To define these, the absolute value of the sensitivities in compression, AP shear and ML shear, were collapsed across parameter.

Muscle Parameters: These are parameters which define the force-length, force-velocity, and EMG-to-force prediction. As one would expect, the model is most sensitive to muscle parameters which govern the parallel elastic component (Figure 4.14). Here, a 1% change in the parameters k_{PE} or L_{opt} result in a 1.9% or 1.3% change in the outcome bone-on-bone forces, respectively. Similarly, for the cross-sectional area, a 1% change results in a 1.04% change, on average, in compression or shear values.

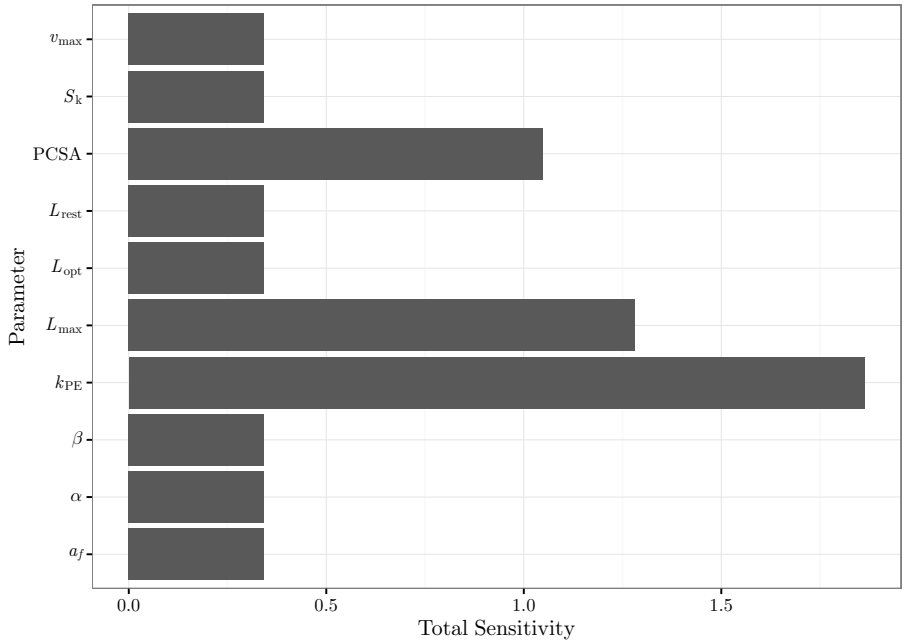

Figure 4.14: The overall sensitivity coefficient of each muscle parameter.

Ligament Parameters: These are the parameters used in Equations 3.11 and 3.12. A similar observation can be made with regards to ligaments (Figure 4.15). Here, the a 1% change in each ligament's slack length results in a 1.9% change in the estimated bone-on-bone forces. The model was surprisingly insensitive to changes in σ, which had an overall sensitivity coefficient of 0.0037, the lowest of any observed between muscle and ligament parameters.

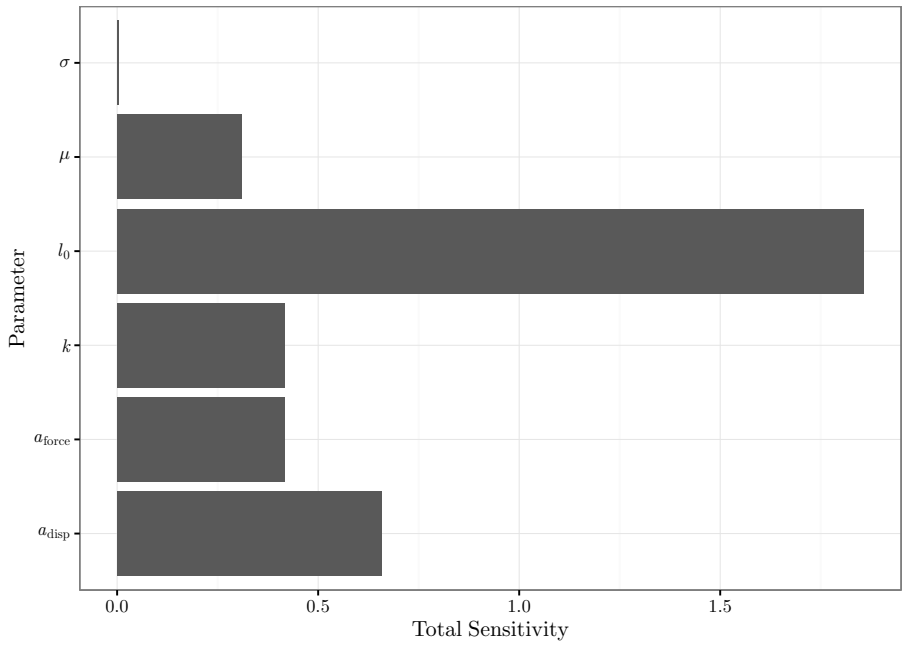

Figure 4.15: The overall sensitivity coefficient of each muscle parameter.

4.4 Discussion

The objective of this chapter was to present evidence that the current model is making predictions which are mechanically accurate and physiologically plausible. This was done by showing that the model predicts a reasonable amount of muscle force by analyzing the gains; by showing that the model's predicted compression and shear values were comparable to the literature; and by showing that these predictions are not entirely governed by a small subset of parameters used.

4.4.1 The Role of Deeper Cervical Musculature

A few of the average muscle gains were far outside the range of 'acceptable' gain values (between 0.5 and 1.5). With the exception of the trapezius, the muscles whose gains were significantly outside of this range were typically deep muscles or those driven from another muscle. These errors are most notable for the longus colli muscle, which was driven from the sternocleidomastoid EMG channel.

A simple explanation may be that, at low levels of activation, these deep muscles of the cervical spine do not produce a signal strong enough to be picked up by surface electrodes or are masked by cross-talk with the superficial musculature. Therefore, when the overall level of activation is low, the contribution of these muscles to balancing the external moment is grossly underestimated by surface EMG. This is surprising for a few reasons: deeper muscles tend to have smaller moment arms, and so using them to balance the external moment, as opposed to superficial muscles, would result in higher compressive forces. The

exception might be splenius cervicis, whose insertion onto the transverse process of the atlas, the widest of the cervical vertebrae, afford it a rather substantial moment arm in terms of lateral bending and axial twist. A study utilizing in-dwelling electrodes to the deep muscles of the posterior cervical spine may be useful in falsifying this hypothesis. Should the deep cervical musculature, in particular splenius cervicis, play a minor role in balancing the gravitational moment from the head, then the predictions from this model should be called into question. While there have been studies investigating the role of semispinalis cervicis and splenius capitis, there has yet to be one investigating the activation of splenius cervicis (Siegmund et al., 2007; Takebe et al., 1974).

4.4.2 Low Gains

As mentioned, some muscles gains were substantially lower than unity. This may speak to a potential issue with the objective function used in EMG assisted optimization. Gains are multiplicative factors, and unfortunately the current objective function does not reflect that. In particular, the cost of gaining down a muscle is smaller than gaining up a muscle the reciprocal amount. For instance, a gain of 1/3 carries the same 'cost' as a gain of 5/3 in the objective function when it should be more comparable to 3, as both are adjusting the muscle force by a factor of 3. Mathematically, this is the statement that the objective function should have the property that $\Theta(x) = \Theta(\frac{1}{x})$ for all positive x. One can construct many functions which satisfy this requirement, the simplest being $\Theta(x) = |\log x|$[1]. A convex function with this property is $\Theta(x) = \max\left\{(1-x)^2, \left(1-\frac{1}{x}\right)^2\right\}$, which keeps its squared agitation to gains which exceed unity. Future investigations might explore this

[1]Note: This function is not convex, and would therefore not be compatible with the `CVXPY` package.

type of cost function as opposed to the standard quadratic form originally proposed by Cholewicki and McGill (1994).

4.4.3 Comparison to Previous Models

Currently there are very few criteria to compare the model's predictions against, aside from failure loads of functional spinal unit tests. Performance corridors for cervical spine models reported in the literature are typically specialized for whiplash events, with very little consideration given for low magnitude loads and muscular activation. This lack of experimental criteria makes validation of inverse dynamics models like the one presented a daunting task. This is in part to blame for the rather unorthodox validation study undertaken here: from an analysis of muscle gains to a sensitivity analysis.

The current model contains dramatically more anatomical detail than that of Choi and Vanderby (1999), whose anatomical data was inherited from Moroney et al. (1988a). There, transverse sectional anatomical drawings were used to produce a cardboard cutout of each muscle, and the cardboard used to scale and calculate centroids for muscle lines of action. The current method uses the centroid path obtained from MRI to guide the muscle line of action with via points. The differences in anatomical detail may account for the dramatic differences in anteroposterior shear between models. It is possible that the muscle line of actions used by Choi and Vanderby (1999) to be angled in a way that does not buttress against shear, although, they did not publish their line of action details.

Both models agree to a certain extent when it comes to mediolateral shear, with the exception of flexion trials. This may have been simply due to experimental set-up; in a

flexion MVC trial there is no reason to expect any degree of mediolateral shear, and both models predict only a modest magnitude. In lateral bend, where one would expect the amount of mediolateral shear to be significant, both models agree with one another almost exactly.

The differences in compression may be explained by the observation that the participants in the current study were able to produce a larger moment than in Choi and Vanderby (1999). It may also be due to differences in experimental set up. In the present study, participants were strapped in to a helicopter helmet and performed maximal exertions against a robot outfitted with a force transducer. The size of this helmet may have allowed participants some freedom to move their head during the MVC trial. In contrast, Choi and Vanderby (1999) strapped the participants to a force transducer with Velcro straps which were able to prevent the participants' heads from moving. The possible motion in the current study may pose some violation to the assumption that the force was applied precisely at the occipital protuberance, and may contribute to error in the estimated shear and compressive forces.

Both models produced bone-on-bone forces that carry with them some face validity. It takes 500 N of shear to fail a cervical functional spinal unit, and 3000 N of compression (Yoganandan et al., 2000), indicating that both models yield a physiologically plausible level of force. While this does not validate either model, it does not preclude either from a providing a plausible amount of compression and shear for possible future *in vitro* work wishing to apply physiological loads to cervical functional spinal units.

4.4.4 The Importance of Accurate Anatomical Data

The sensitivity analysis revealed that, of all the parameters in the model, origin and insertion points of muscles and ligaments, have the greatest influence on the predicted compression and shear values. This sensitivity was further evidenced by the failed first attempt of the model, where anatomical data came from combining inconsistent databases between three different authors. Muscle via points were estimated from straight lines connecting origin and insertion points in a neutral position which most likely over-estimated the moment arms of the extensor muscles (Vasavada et al., 1998). In addition, a qualitatively poor representation of the lordotic curvature of the cervical spine made some of the muscle lines of action appear to be on the wrong side of the joint center of rotation, which translated to poor reports of compression and shear values. In addressing these limitations, anatomical landmarks were manually digitized, which also provided an avenue for making the geometry of the model scalable for different percentiles and sexes. The new anatomical dataset represents a dramatic improvement over the previous endeavor.

The Hyoid Muscles

As discussed earlier, the hyoid group is a small group muscles situated on the anterior aspect of the neck. While they possess a modest physiological cross-sectional area, they also have the largest moment arm of any neck flexor. In addition, their insertion onto the hyoid bone, then the suprahyoid muscle's insertion onto the mandible, grant them the ability to flex the entire cervical column. This is in contrast to the longus colli muscle, the deep neck flexor, whose physiological cross sectional area is larger than that of the hyoid muscles, but

whose moment arm is significantly less. Originally the hyoid group was to be excluded in this model, as their moment generating capacity is often called into question. However, in their absence, when a participant went into extension, the model had tremendous difficulty balancing the resulting flexor moment. Eventually, if the convex optimization solver was even able to find a feasible solution, the muscle gain in the sternocleidomastoid and longus colli muscles was in excess of 100, and over 1500 N of compression and 500 N of shear were being generated throughout the column. Seeing as this level of shear force is enough to fail a functional spinal unit it seemed unlikely that the models response was indeed physiological.

Once the hyoid muscles were included in the model, they were able to balance this flexor moment with remarkably low activation and the resulting shear and compressive forces were in a physiological range. The natural conclusion is that the hyoid muscles seem to have a much more significant role in generating moments in the cervical spine than previously thought; a finding that is in agreement with electromyography studies of these muscles (Siegmund et al., 2007), which showed that they seem to be active when the sternocleidomastoid muscle was active. It may seem that these muscles have roles to play aside from their usually assumed role in breathing (King, 1939), speaking (Ohala and Hirose, 1970), and swallowing (Palmer et al., 1992).

4.4.5 Slack Lengths

The sensitivity analysis also revealed that the model is especially sensitive to both ligament and muscular slack lengths. A similar observation has been made in analyzing the

sensitivity of a Hill-type muscle model in gait studies (Scovil and Ronsky, 2006; Xiao and Higginson, 2010). There, sensitivity coefficients of muscle slack lengths varied between 0.26 in running and 10^5 in walking, several orders of magnitude higher than what was reported here. The large discrepancy between the current model and those of Scovil and Ronsky (2006) and Xiao and Higginson (2010) is best explained by the very different amount of motion which occurred in the cervical spine versus the lower limb during gait. Muscle lengths observed here resided in a region of the force-length curve where the exponential term was not very steep, which explains why the sensitivity to these muscle slack lengths was not several orders of magnitude larger. Previous studies have also noted the sensitivity of biomechanical models to ligament slack lengths (Li et al., 1999; Delp et al., 1990), although no previous local sensitivity analysis has been conducted.

4.4.6 Model Limitations

Via points, the muscle wrapping technique used here, has been criticized for its unfortunate ability to produce discontinuities in length calculations (Garner and Pandy, 2000). Since the muscle Jacobian computation requires that muscle lengths be differentiable, a stronger condition than continuity, this is cause for concern. Unfortunately, the vertebrae do not lend themselves well to geometric approximations like spheres or cylinders, and therefore pose a challenge for more sophisticated muscle wrapping techniques like those used in Dickerson et al. (2007). Via points have worked exceptionally well in previous cervical spine models, and no such discontinuity manifested in this investigation.

At present, there is no representation of the cervical viscera in the model. As the

neck moves, these structures are deformed, and would supply a restoring force due to their viscoelasticity. Additionally, the inertial properties of the viscera are largely ignored. In addition, some geometric features of the vertebrae themselves are ignored in this modelling paradigm, namely, the facet joints and the uncovertebral joints. These are known to have a profound effect in inducing coupling between motions in the cervical spine (Clausen et al., 1997; Panjabi et al., 2001b). While the moment of inertial values are derived from geometric simplifications of segments of the neck to a cylinder (de Jager et al., 1996), the coupling of motions is reliant on the partitioning of the head-thorax angle being an accurate approximation to the true motion. Similarly, there is no explicit attention given to the facet or uncovertebral joints. Their contributions are lumped together with the compressive and shear forces tolerated at the level of the intervertebral disc.

There are a number of muscles of the cervical spine which insert onto the scapula and clavicle, thereby coupling the mechanics of the neck with that of the shoulder. The motion of the scapula and clavicle can be approximated from the position of the humerus as presented in Dickerson et al. (2007), which may be a straightforward improvement to the model down the road. It was not included in this iteration of the model, primarily because the helicopter pilot study did not collect humeral angle.

Kinematics

Linearly partitioning the neck-thorax angle over the cervical spine immediately runs into some issues: there is more than one way to move a neck. In addition to the complicated, sometimes paradoxical motion between C1-C2, it is possible for someone to flex their lower cervical spine while extending the upper cervical spine. This posture, which is often

assumed by individuals using a computer, cannot be accommodated by the current model without manually prescribing the angles at each individual joint. At present this would not be impossible, just tedious. Using inverse kinematics may be a possible avenue for exploration, where an optimization routine is carried out to minimize the error between the model's position and experiment.

Ligaments

The ligament representation seems to be reasonable in the middle and lower cervical spine, however, more work should go into improving the ligament representation in the upper cervical spine. Perhaps this is not surprising, since the majority of cervical spine motion, at least in rotation, comes from the complicated arrangement of osteoligamentous structures between the occiput, C1, and C2. The force-deflection curves from Mattucci (2011) in this area come from one or two specimens each, and no attention was given to measuring their approximate slack length. There is need for improved upper cervical spine ligament force-deflection curves.

Additionally, the nuchal ligament has yet to undergo rigorous materials testing, despite its well established role in resisting flexion. Takeshita et al. (2004a) used a cadaveric model to show that resection of the nuchal ligament decreased rotational 'tangent stiffness' by 27% and increased range of motion by 28%. Fielding et al. (1976) showed that it is rich in nerve supply and may play a role in proprioception and motor control of the head. Follow-up studies examining, in detail, the biomechanical properties would be beneficial, and allow the addition of the nuchal ligament to the present model. The ligament itself poses a considerable modelling challenge as it is unlike any other in the cervical spine. It

has two histologically distinct regions (Figure 2.7), with fibres from the lamellar section spanning the fibrous funicular region to the spinous processes of every cervical vertebrae. In order to model this section accurately, one would either need to resort to the finite element method or have ligament attachment sites which track with another ligament.

Aside from these ligaments, those of the middle and lower cervical spine have had their slack lengths arbitrarily set to 5% more than their anatomical length. This is to conservatively underestimate the ligament force; although, the results of the sensitivity analysis seem to conclude that this 5% change in the slack length of ligaments does not contribute significantly to the compression and shear. Regardless there does not seem to be much in the way of quantifying the slack length of cervical ligaments in the literature.

Both failure and the viscoelastic properties of ligaments are ignored in the current model. Adding more detail here would have been ideal, however, since the trials used for this investigation were quasi-static, the viscous term would be negligible. Additionally, by ignoring stress-relaxation in the postures examined, the model may over-estimate the amount of compression at each of the joints.

Lastly, while the constitutive expression used for the ligaments does, in general, provide an accurate, biofidelic force-deflection curve, it does a remarkably poor job representing the ligamenta flava. Since it is derived from the simplification of a mechanistic model involving only collagen, this inaccuracy may be due to the ligamenta flava violating the assumption of purely collagenous ligaments. Future work should improve this model for elastin-rich ligaments, like the ligamenta flava.

Muscles

Currently, muscles are represented in the model by a Hill-type muscle model, the limitations of which were discussed in great detail previously. Such a model is phenomenological, and gives no consideration to any underlying mechanisms in muscular force generation beyond the superficial observations of the force-length and force-velocity relationships. To this end, there are a number of phenomena that have yet to be addressed, for instance, the phenomenon of muscle yielding for submaximal eccentric contractions (Joyce and Rack, 1969), or the sensitivity of the force-length relationship to levels of muscular activation (Roszek et al., 1994). Many limitations of the Hill model are addressed by the more sophisticated Distribution Moment model, which may provide an avenue for future model improvements.

Aside from the basic phenomenology of the Hill model, muscles in this model act as independent linear actuators of rotary joints. As of yet, there is no modelling paradigm for addressing the connective tissues, like fascia the complicated intramuscular force transmission pathways, which link muscular elements together (Yucesoy et al., 2003).

It was the deeper muscles which, in general, experienced the largest gains, indicating that the neural drive from the superficial muscles is not representative of their action. Future work with fine-wire electrodes may uncover some more rigorous muscle synergies between cervical spine muscles, which this model could take advantage of.

Intervertebral Joints and Disc

The modelling of the intervertebral discs done here is, like the muscle model, phenomenological. In addition, there is little attention given to the uncovertebral or facet joints outside of the same phenomenology that governs the intervertebral disc, both of which, detract from the apparent bio-fidelity of the current model. By all accounts these are parts of the model that could be addressed for future improvements, perhaps a hybrid approach where the intervertebral disc is modelled using the finite element method, as has been done in the past, may be useful (van Lopik and Acar, 2007). The uncovertebral and facet joints represent a substantial challenge, as bony contact mechanics are incredibly complicated. Nevertheless these are avenues that could be explored in order to improve the model in the future.

4.5 Conclusion

While there are certainly limitations to the current model, its predicted muscle, compression and shear forces have been shown to be physiologically plausible. Furthermore, model predictions are not overly sensitive to any one parameter, although, as a family of parameters, those which govern the trajectory of muscle lines of action have the most impact on the resulting shear and compression values. In terms of non-geometric parameters, ligament slack lengths are the greatest cause for the most concern. To date, this is the most anatomically detailed, EMG-driven cervical spine model, and the results from this validation study forecast a promising future.

Chapter 5

Posture, Helmets, and Joint Kinetics

5.1 Introduction

In the Canadian civilian population, both the incidence and prevalence of chronic neck pain are alarmingly high. Cross-sectional epidemiological studies have shown that in any 6-month time-frame, 54% of Canadian adults suffer from neck pain (Côté et al., 1998). Additionally, cohort studies have estimated the annual incidence of neck pain to be approximately 18% (Croft et al., 2001). These staggering numbers pale in comparison to those reported by the Canadian Armed forces, where between 43 and 97% of helicopter pilots report chronic neck pain (Adam, 2004; Lange et al., 2011; van den Oord et al., 2010; Bridger et al., 2002). Since neck pain has been shown to be chronic and episodic, with sufferers rarely experiencing a full remission from their symptoms (Côté et al., 2004), there is a substantial benefit to understanding its root cause and preventing it.

For helicopter pilots in the Canadian military, the risk for chronic neck pain skyrockets when night vision goggles (NVG) are worn during night flights (Forde et al., 2011), a quandary whose mechanism is thought to be the forward positioned mass of the NVG system inducing a flexor moment. The classical solution is to add a counter-weight to the posterior of the helmet in order to supplement the extensor moment the posterior neck muscles need to produce to balance the anteriorly oriented weight.

To date, investigations into chronic neck pain have been limited to EMG studies of both the superficial and deep musculature. The current hypothesis is that there is a trade-off of muscular demands from the deep to superficial musculature (Falla et al., 2007, 2004). However, these authors have yet to link their hypothesis to mechanical risk factors, for instance, neck length and amount of time flexed (Ariens et al., 2000). The latter two risk factors can be explained in terms of mechanics, although, to date, no detailed cervical spine model has attempted to quantify the loads experienced in the neck in a flexed posture.

Therefore, the purpose of this study was twofold: (*i*) quantify the loads in the cervical spine in a neutral versus flexed posture, and (*ii*) to quantify the compression and shear forces in individuals wearing a helmet. Since disc herniations are more common in the lower cervical spine, it was hypothesized that at those levels there would be more compression and shear. For the second investigation, compression and shear forces were compared at C5-C6, as this is the most common site of posterior disc prolapse (Matsumoto et al., 1998).

5.2 Methods

5.2.1 Data Collection

The same data were used in this investigation as in the last chapter, so the data collection procedure is identical to what was described previously. To establish the role that joint level and posture had on the intervertebral joint kinetics the trials where participants were non-helmeted were used. On the other hand, trials where participants wore a helmet only (hOnly), night vision goggles (hNVG) or both night vision goggles and the counterweight (hCW + NVG) were used to approximate the joint kinetics in helicopter pilots.

5.2.2 Helmet Center of Mass

The helmet's center of mass relative to the ear canal, obtained from Forde et al. (2011) and presented in Table 5.1, was used to place an additional force in the head segment when the participant was wearing a helmet in one of the configurations. The weight of the helmet alone was 14 N, with the night vision goggles was 25 N and with the night vision goggles and the counterweight was 36 N. Forde et al. (2011) note this change in helmet weight from 14 N to 36 N, with the addition of the NVG and counterweight; it was assumed here that half of the 22 N increase in weight comes from the night vision goggles and the other half from the counterweight. In the head's local coordinate system, the projection of the ear-canal on the sagittal plane, or the location of the ear-canal from which the helmet's center of mass is offset, was $(0.0, -7.96, -2.27)^T$ cm.

Table 5.1: Position of the helmet's center of mass relative to the ear canal of the pilot in the head's local coordinate system. Adapted from Forde et al. (2011).

	Offset (cm)		
Condition	**Mediolateral**	**Anteroposterior**	**Superior-Inferior**
No Helmet	0.0	0.0	0.0
hOnly	0.0	-0.5	7.0
hNVG	0.0	6.3	9.2
hCW +NVG	0.0	1.2	2.8

5.2.3 Statistics

An *a priori* level of significance was set at $\alpha = 0.05$ for all statistical tests. Each analysis was done in RStudio (version 0.99.491) (RStudio Team, 2015) using the R statistical programming language (R Core Team, 2015), using the `lme4` package to fit the generalized linear models (Bates et al., 2015), and the `lsmeans` package to perform any post-hoc tests on the least-squares means with a Bonferroni adjustment (Lenth, 2016).

Analysis of Neck Loads in Flexion

Generalized linear models (GLM) were used to analyze the effect that a flexed posture and joint level (2 postures $\times$ 8 joint levels) had on the computed compression and anteroposterior shear. This was done using neutral and flexed postures and joint level as factors in the model, with repeated measures on both. Mediolateral shear was not included in this analysis since it was extremely small in both a neutral and flexed posture.

Analysis of Helicopter Neck Loads

A similar approach, using a GLM with posture and helmet condition (7 postures $\times$ 4 helmet conditions) as factors with repeated measures on both was used to evaluate the effect that each had on the compression and shear forces at C5-C6.

5.3 Results

5.3.1 Cervical Spine Loads with Posture

Compression

There was a significant interaction effect between joint level and posture ($p < 0.001$). As expected, compression generally increases as one moves down the vertebral column but does not change signficantly after the C4-C5 joint ($p > 0.05$). At every joint level, the compression is significantly higher in flexion than a neutral ($p < 0.05$) (Figure 5.1). In flexion, the compression is larger at C1-C2 than at C0-C1 ($p < 0.001$), however, in a neutral posture they are not statistically significantly different ($p = 0.9394$).

Anteroposterior Shear

Like compression, there was a significant interaction effect of level by posture ($p < 0.001$). In this case, the interaction is significantly more complicated than compression. From C0-C1 until C4-C5, the magnitude of anteroposterior shear is significantly larger

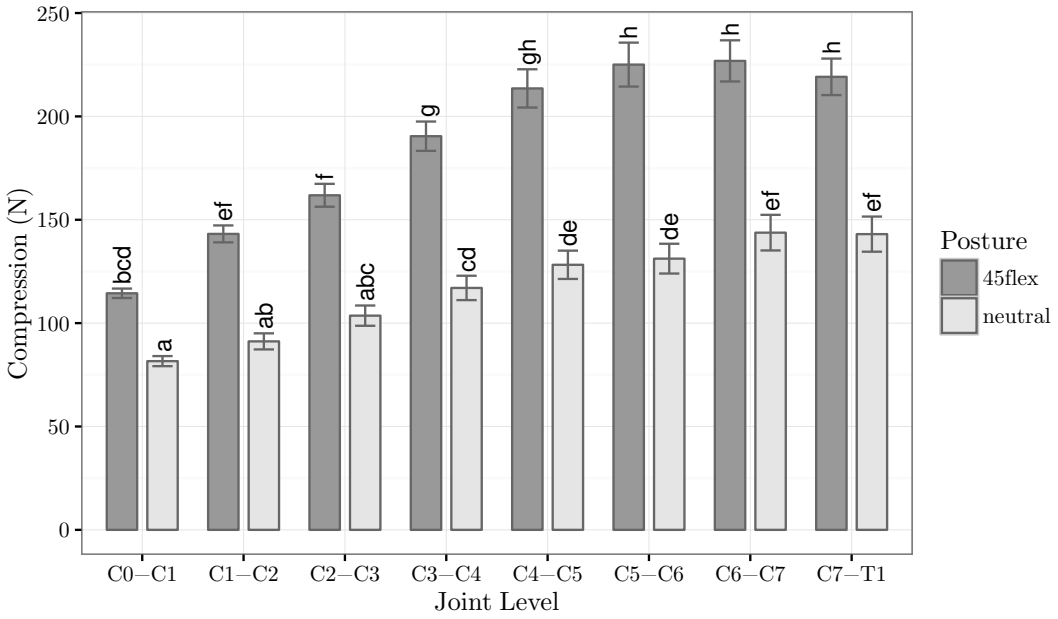

Figure 5.1: Compression in the cervical spine in a non-helmeted condition by joint level in various postures. Positive values indicate higher levels of compression.

in flexion ($p < 0.001$), is the same at C5-C6 ($p = 0.49$), then is, surprisingly, smaller in magnitude for C6-C7 and C7-T1 ($p < 0.001$). In a neutral posture, the highest amount of anteroposterior shear was at C2-C3 ($p < 0.05$), whereas the rest of the vertebral column was mostly constant, with C0-C1 being slightly larger than C5-C6 ($p = 0.031$). In flexion the distribution of anteroposterior shear changed substantially (Figure 5.2), with C0-C1 overtaking the largest amount of shear ($p < 0.05$), followed closely, but significantly, by C2-C3 ($p < 0.001$). After C2-C3, there is a decrease in the magnitude of anteroposterior shear down the vertebral column ($p < 0.05$), which, surprisingly, reaches a positive value at C7-T1. With the exception of C7-T1 in a flexed posture, most shear forces were directed posteriorly, which speaks to possible overcompensation of musculature.

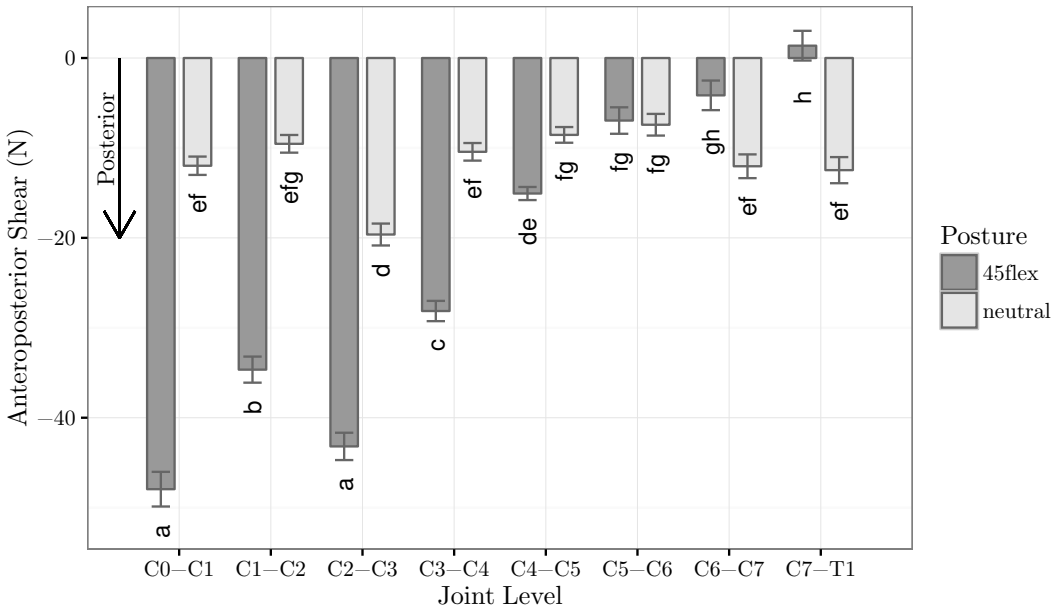

Figure 5.2: Anteroposterior shear across spinal level in a netural versus flexed posture, here the positive y-axis is oriented anteriorly.

5.3.2 Cervical Spine Loads in Helicopter Pilots

Compression

There was no significant interaction effect between posture and helmet condition ($p = 0.17$), however, there were both main effects of posture ($p < 0.001$) and helmet condition ($p < 0.001$) on compression at the C5-C6 level. Compression at this level did not change when the counterweight was added to the back of the helmet ($p = 0.66$); however, adding the night vision goggles to the helmet significantly increased the compressive forces compared to the helmet alone ($p < 0.001$), which was also significantly larger than not wearing a helmet at all ($p < 0.001$) (Figure 5.3).

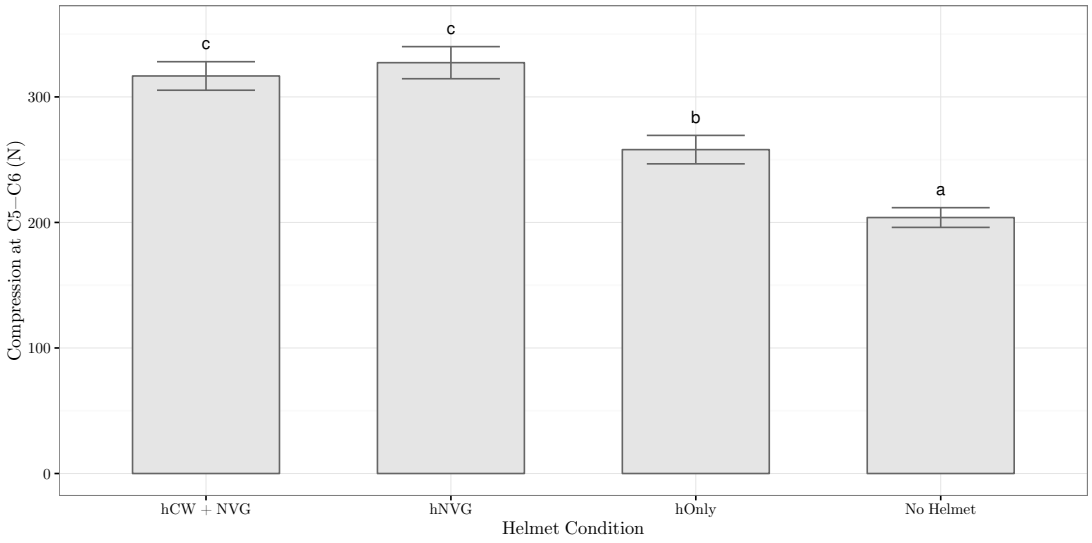

Figure 5.3: Main effect of helmet on compressive forces at C5-C6.

All deviated postures had significantly more compression than a neutral posture ($p < 0.001$) (Figure 5.4). Additionally, 45° of flexion combined with 45° of axial rotation had

significantly more compressive force than any other posture ($p < 0.001$). There we no significant differences between 20° of lateral bending, 30° of extension, and 45° of axial rotation ($p > 0.38$). Nor were there significant differences between 45° of flexion and 45° of extension with 45° of axial rotation ($p = 0.98$). 45° of flexion, as well as a combination of rotation and extension experienced similar compression values ($p = 0.9997$), which were significantly higher than all other postures ($p < 0.01$) except for flexion and rotation ($p < 0.001$).

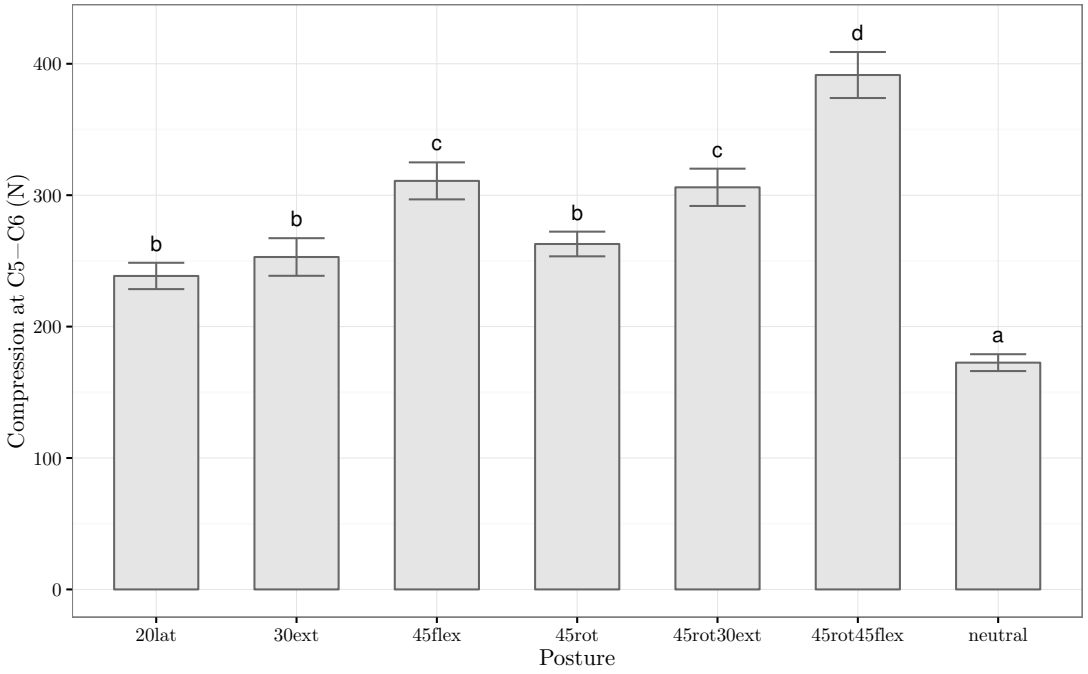

Figure 5.4: Main effect of posture on compressive forces at C5-C6.

Anteroposterior Shear

There was a significant interaction effect between posture and helmet condition on anteroposterior shear ($p < 0.001$). For most postures, helmet configuration did not influence the amount of anteroposterior shear ($p > 0.05$), with the exception of an extended and rotated posture, where the helmet and night vision goggles yielded a significant increase in anteroposterior shear ($p < 0.05$). For these postures, which seem to be driving the interaction effect, the addition of the counterweight was enough to return the amount of shear to the non-helmeted condition. In addition, assuming a rotated, extended, or extended and rotated posture significantly increased the amount of anteroposterior shear ($p < 0.05$) (Figure 5.5). Interestingly, with lateral bending, the addition of a counterweight is enough to reduce the amount of shear down to the same levels as a neutral posture ($p > 0.05$).

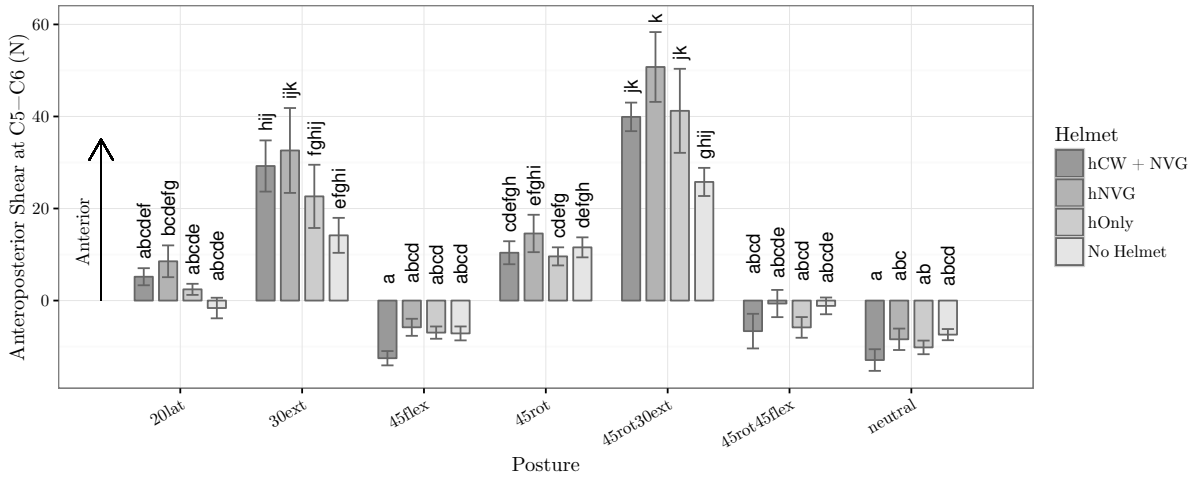

Figure 5.5: The interaction between posture and helmet condition on anteroposterior shear. Here, significance is only shown within each posture.

Mediolateral Shear

As with anteroposterior shear, mediolateral shear showcased a significant interaction effect between helmet condition and posture ($p < 0.001$). The combination of axial twist with flexion dramatically increased the amount of mediolateral shear, highest with the night vision goggles deployed, but not significantly higher than when the counterweight was added ($p = 0.081$). In pure axial rotation, the night vision goggles significantly increased the amount of mediolateral shear compared to the non-helmeted condition ($p < 0.05$), and the counterweight seemed to be effective in partly decreasing the shear forces down to non-helmeted levels. In general the mediolateral shear was quite low, roughly 5% of what was observed in the compressive axis (Figure 5.6).

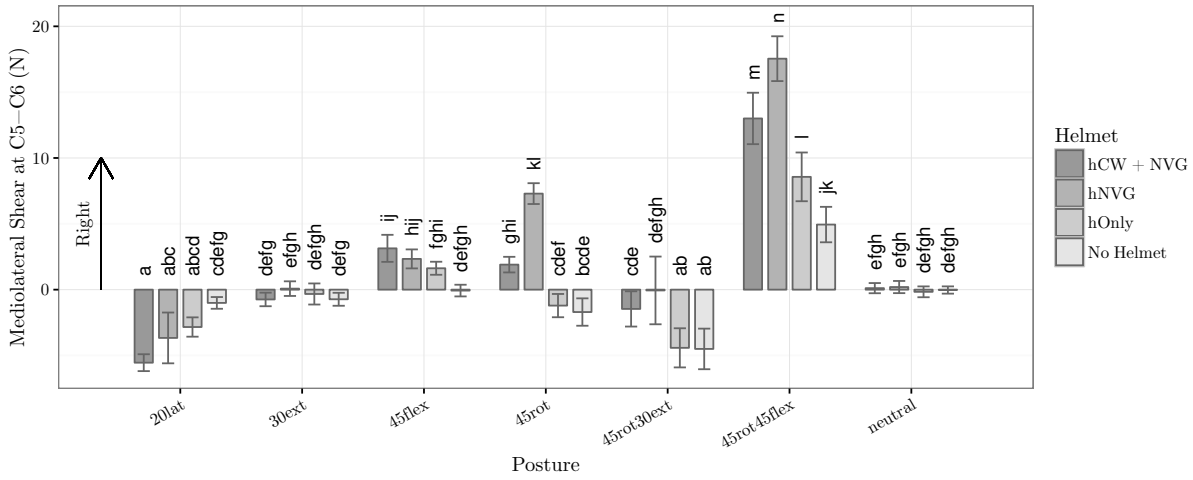

Figure 5.6: The interaction between posture and helmet condition on mediolateral shear. Here, significance is only shown within each posture.

Surprisingly, lateral bending did not experience the expected increase in mediolateral shear ($p > 0.05$). In most cases, the addition of the helmet and counterweight had no

affect on the computed mediolateral shear.

5.4 Discussion

5.4.1 Joint Kinetics in Flexion

In terms of compressive forces, the loads on the cervical spine vary down the column in a predictable way: joints further down the column experience greater compression. This effect levels off at C4-C5. The subsequent joints do not experience a significant increase in joint compression. This effect is accentuated with flexion, where the compression measured at each vertebral level increases almost twofold. This may help explain why a flexed posture has been flagged as a risk factor for the development of chronic neck pain (Ariens et al., 2000). The injury mechanism most likely implicates the intervertebral disc, much in the same way the pathomechanics of disc herniation has been described in the lumbar spine (Callaghan and McGill, 2001; Tampier et al., 2007). The two injury mechanisms are likely quite analogous: the flexed posture, coupled with axial compression, serve to pressurize and push the nucleus pulposis posteriorly against the annulus fibrosis, which, with repeated exposure, may induce injury.

In a neutral posture the amount of posterior shear is roughly constant throughout the vertebral column: around 18 N. This is due to the action of the neck extensors in supporting the upright head. Not surprisingly, the magnitude of posterior shear increases in the upper cervical spine almost fourfold with flexion, however, decreases at the lower cervical spine. Large amounts of anteroposterior shear have been implicated as a risk factor for disc

herniations (Schmidt et al., 2013), however, an insurmountable degree of anteroposterior shear does not seem to be the case in the cervical spine. Interestingly, in flexion, around the C6-C7 spinal level, the shear forces shift from being posteriorly to anteriorly directed. Perhaps this local shift in direction down the column has implications in the development of chronic neck pain more-so than the actual magnitude of shear forces. Differing amounts of shear superiorly and inferiorly would naturally serve to torque the intervening vertebra. If the intervertebral tissues allowed for additional motion, the resulting flexion may play into the repeated flexion injury mechanism discussed previously.

5.4.2 The Pathomechanics of Helicopter Helmets

Even before night vision goggles are worn and the counterweight added, the added mass from the helmet is enough to significantly increase the amount of compression acting at the C5-C6 level (Figure 5.3). Since chronic neck pain is also a complaint of F-16 pilots (De Loose et al., 2008), who typically do not wear NVG, it stands to reason that this increase in joint kinetics may be enough to induce chronic neck pain. It seems even a modest increase in the mass of the head-segment is problematic once awkward postures and duration of flight are considered. The increased loads just from the weight of the helmet seems to imply that the scapegoat for chronic neck pain among pilots may not simply be NVG on their own. Future engineering designs would ignore the mass of their prototypes at their peril.

It should be noted that the magnitudes of compression and shear observed here are well below the forces required to fail a functional spinal unit: it takes roughly 3.9 kN of

compression and 500 N of shear for failure to occur (Pintar et al., 1998; Shea et al., 1991). This implicates a mechanism of cumulative load, sustained over the hours of flight-time that helicopters endure during training or completing missions (Forde et al., 2011). For instance, in the Canadian military it is the helicopter pilots with greater than 150 flight-hours who experience the highest prevalence of chronic neck pain (Adam, 2004). It is also difficult to attribute the aetiology of neck pain to only the mechanical variables measured here, as it has been shown to be a multifaceted issue (Côté et al., 2009, 1998).

Night Vision Goggles

With the addition of night vision goggles, there is a corresponding significant increase in compression (Figures 5.3), which is further increased with flexion and axial rotation (Figure 5.4). Coincidentally, these would be the postures helicopter pilots undertake when looking at the ground from their cockpit, indicating that the increased mass from the NVG is a significant problem. The addition of the counterweight, the current solution, seems to only exacerbate this issue. The combination of flexion and axial rotation might be particularly troublesome, since this is where mediolateral shear values were also greatest (Figure 5.6). In axial rotated, extended posture, the amount of anteroposterior shear is also increased (Figure 5.5).

The Counterweight

Presented here is considerable evidence that the counterweight positioned on the posterior helmet does not generally prevent the increase in joint kinetics. This solution works

on a theoretical basis if a static neck posture is assumed, however, undertaking awkward postures is a crucial element of a helicopter pilots' job (Forde et al., 2011). For instance, in a flexed posture, the mass of the counterweight is no longer positioned posterior to the vertebral column. As a result, this added mass ends up producing a flexor moment, which is ironically what it is intended to prevent. This runs counter to Thuresson et al. (2003) who evaluated the EMG of pilots wearing a helmet, night vision goggles and counterweight in various trunk and neck flexion angles. They concluded that the required muscle activity was negligibly affected by the additional weight of the head, and was more strongly determined by the amount of flexion. While the surface electromyogram may not have been affected by the additional weight, the joint kinetics most certainly are.

This effect is evidenced in the present study by examining bone-on-bone forces. The counterweight failed to significantly reduce the amount of compression at C5-C6 (Figure 5.3), independent of posture. When analyzed, it clearly supported the hypothesis that a deviated posture significantly changed the joint kinetics at this spinal level (Figure 5.4). The addition of the counterweight was not able to significantly decrease the amount of anteroposterior shear in any posture over the NVG alone, however, in an extended posture was able to slightly reduce its magnitude to similar levels as an un-helmeted condition. The same slight reduction was observed in assessing mediolateral shear in a flexed and axially rotated position, however, the magnitude of mediolateral shear was modest in almost all conditions (Figures 5.6). Overall, there seems to be significant evidence here that the counterweight is not a feasible solution to the problem of reducing the bone-on-bone forces experienced by helicopter pilots.

The Toucan

The problem of an anteriorly placed mass has a precedence in nature, which comes with its own intuitive solution. A toucan is a tropical bird from South America whose beak is tremendously large given its small head and long neck (Seki et al., 2005). The toucan's solution is simple: their beaks are made of extremely light material. Perhaps rather than re-engineering a new helmet around the NVG, inspired by the toucan, the NVG could be re-designed to produce significantly lower neck loads simply by being made out of lighter material. Seeing as the intention of NVG is not to protect the user from ballistics, there is no reason it should be made out of heavy, military-grade material. This report offers strong evidence that adding mass to the helmet only amplifies the potentially pathological joint mechanics: perhaps its time to explore the removal of mass.

5.4.3 Limitations

Inertial Forces

The helicopter's cockpit, a frame which undergoes significant rotational and translational accelerations, was not explicitly modelled in this collection. Participants were recreating postures in a static room. Because of this, the three inertial forces were not included; namely the Coriolis, Euler, and Centrifugal, forces. Since all of these forces are proportinal to m, it stands to reason that their magnitude on the head is proportional to the mass of the helmet. Despite this limitation, the model does provide an avenue of simulating these forces outside of the lab. It is noteworthy that the magnitude of these

forces are typically very small relative to the gravitational force, so ignoring them may be an appropriate abstraction to make. Such claims are, of course, unsubstantiated without measuring the velocities and accelerations of the helicopters in the field.

Model Limitations

As was addressed in the validation chapter, the model may suffer from significantly under-estimating the amount of anteroposterior shear. This may explain why the magnitude of these forces were so low when examining the flexed, non-helmeted posture. Unfortunately, these forces have never been quantified *in-vivo*, so it is difficult to know how accurate the predictions of the model are. This model provides a lower bound on what the anteroposterior shear forces could be, which may still be useful for ergonomic applications.

5.5 Conclusion

The loads on the cervical spine in flexion were successfully quantified using an EMG-driven cervical spine model. This revealed that the compressive forces increase twofold with 45° of flexion, while the anteroposterior shear forces tend to increase fourfold in the upper-cervical spine, return to neutral posture levels by C5-C6, and continue decrease in magnitude further down to C7-T1.

Additionally, the loads acting on the C5-C6 cervical level while wearing a helmet were also quantified for a variety of conditions. This analysis revealed that the additional weight from the night vision goggles and counterweight may be doing more harm than good. This

suggests exploring the use of lighter materials for the manufacture of night vision goggles, and the reconsideration of ballistic requirements on helicopter pilot helmets.

Chapter 6

Conclusion and Recommendations

The purpose of this research project was to develop the first EMG-driven cervical spine model for investigating joint kinetics in occupational settings. The model attempted to represent the geometry of the cervical spine that is mechanically accurate from the level of kinematics, tissue properties, and muscle mechanics, while also preserving the neurological activation patterns obtained from EMG.

6.1 Validation

The model underwent a rigorous validation procedure. As no previous investigator has quantified the loads in the cervical spine *in-vivo*, this proved to be a challenging task. In analyzing the muscle gains during various postural movements, comparing the predicted compression and shear forces at C4-C5 against previously published models, and conducting a thorough sensitivity analysis, the model has undergone a fairly diverse and

relatively unorthodox set of validation protocols.

Muscle gains obtained from the EMG assisted optimization were within an acceptable range for most postures: the exception being the deep musculature and trapezius. Future work using fine-wire electrodes may quantify, in better detail, the synergistic relationship between the superficial and deep musculature in order to more closely drive the deep muscles. Counter-intuitively, the force profile of trapezius, the most superficial of the posterior neck muscles, was poorly represented. Inclusion of a mobile scapula and clavicle with glenohumeral angle may improve its realism, or perhaps a more representative electrode placement should be used.

The compression and mediolateral shear values obtained from the model compared very well with the previous model of Choi and Vanderby (1999), whereas the anteroposterior shear values were significantly lower. Without experimental data to compare these estimates to, it is difficult to say which model is doing a better job predicting the amount of anteroposterior shear. In either case, both models present physiologically plausible values, although it is tempting to favour the current model due to the improved anatomical detail.

Finally, the sensitivity analysis revealed that the model is sensitive to the slack lengths of ligaments and muscles. While the model's sensitivity to these parameters is markedly lower than what is reported in the literature, it does flag some potential sources of error that should be investigated. Slack lengths are by no means trivial to acquire. Should an effective method arise, it would prove immeasurably useful.

Overall, the model outputs physiologically plausible compression and shear values, and is capable of predicting muscle forces within a reasonable tolerance.

6.2 Postural Loads on the Cervical Spine

The model has shown that compressive forces throughout the cervical spine increase twofold with flexion, with the largest compressive forces at the lower cervical spine. Interestingly enough, compression seems to plateau at the C4-C5 level, which possibly explains why damage to that level is quite common. Conversely, the analysis of anteroposterior shear revealed that shear values are typically around 18 N posteriorly in a neutral spine configuration, but can increase fourfold in the upper cervical spine with flexion. Surprisingly, the amount of anteroposterior shear decreases significantly toward the C6-C7 joint, ultimately changing directions at that level. Both the analysis of shear and compression may have implications in the pathomechanics of chronic neck pain.

6.3 Reducing Loads for Pilots

Balancing the anteriorly directed mass of the night vision goggles with a posteriorly placed counterweight, the classic solution offered by the military, is not conducive to reducing bone-on-bone forces in the cervical spine. Indeed, it seems even the mass of the helmet alone in flexion is enough to induce significantly greater amounts of compression and shear. While an obvious outcome of this research, and by no means a trivial exercise in design change, the mass of the helmet system had significant impact on joint loading and would be a prime target to alter pilot exposure.

References

Adam, J. (2004). Results of nvg-induced neck strain questionnaire study in ch-146 griffon aircrew. Technical report, DTIC Document.

Ahn, H. S. (2005). *A Virtual Model of the Human Cervical Spine for Physics-based Simulation and Applications*. Ph.d. thesis, The University of Tennessee.

Alexander, R. M. (2003). Modelling approaches in biomechanics. *Philosophical transactions of the Royal Society of London. Series B, Biological sciences*, 358(1437):1429–1435.

Almosnino, S., Pelland, L., Pedlow, S. V., and Stevenson, J. M. (2009). Between-day reliability of electromechanical delay of selected neck muscles during performance of maximal isometric efforts. *Sports medicine, arthroscopy, rehabilitation, therapy & technology : SMARTT*, 1(1):22.

Anderst, W., Donaldson, W., Lee, J., and Kang, J. (2015). Cervical Spine Disc Deformation During In Vivo Three-Dimensional Head Movements. *Annals of biomedical engineering*.

Ariens, G. A., Van Mechelen, W., Bongers, P. M., Bouter, L. M., and Van Der Wal, G. (2000). Physical risk factors for neck pain. *Scandinavian journal of work, environment & health*, pages 7–19.

Babuska, I. and Oden, J. (2004). Verification and validation in computational engineering and science: basic concepts. *Computer Methods in Applied Mechanics and Engineering*, 193(36-38):4057–4066.

Bao, S. (1995). *Shoulder-neck exposure from assembly work and the significance of rationalization*. Doctoral thesis, Luleå University of Technologyy.

Basmadjian, D. U. o. T. (1999). *The Art of Modeling in Science and Engineering with Mathematica - CRC Press Book*.

Bass, C. R., Lucas, S. R., Salzar, R. S., Oyen, M. L., Planchak, C., Shender, B. S., and Paskoff, G. (2007). Failure properties of cervical spinal ligaments under fast strain rate deformations. *Spine*, 32(1):E7–E13.

Bates, D., Mächler, M., Bolker, B., and Walker, S. (2015). Fitting linear mixed-effects models using lme4. *Journal of Statistical Software*, 67(1):1–48.

Belytschko, T., Kulak, R., a.B. Schultz, and Galante, J. (1974). Finite element stress analysis of an intervertebral disc. *Journal of Biomechanics*, 7:277–285.

Benzel, E., Currier, B., Dormans, J., Dvorak, J., and Clark, C. R. (2004). *The Cervical Spine*. Lippincott Williams & Wilkins.

Bethard, J. D. and Seet, B. L. (2013). Sex Determination from the Second Cervical Vertebra: A Test of Wescott's Method on a Modern American Sample. *Journal of Forensic Sciences*, 58(1):101–103.

Bogduk, N. and Mercer, S. (2000). Biomechanics of the cervical spine. I: Normal kinematics. *Clinical biomechanics (Bristol, Avon)*, 15(9):633–648.

Bonney, R. a. and Corlett, E. N. (2002). Head posture and loading of the cervical spine. *Applied ergonomics*, 33(5):415–7.

Bowman, B. M. (1971). *An analytical model of a vehicle occupant for use in crash simulations*. Doctor of philosophy (engineering mechanics), University of Michigan.

Box, G. E. P. and Draper, N. R. (1987). *Empirical Model-Building and Response Surfaces*.

Bridger, R. S., Groom, M. R., Jones, H., Pethybridge, R. J., and Pullinger, N. (2002). Task and postural factors are related to back pain in helicopter pilots. *Aviation, space, and environmental medicine*, 73(8):805–11.

Broberg, K. (1993). Slow deformation of intervertebral discs. *Journal of Biomechanics*, 26(4-5):501–512.

Brolin, K. and Halldin, P. (2004). Development of a finite element model of the upper cervical spine and a parameter study of ligament characteristics. *Spine*, 29(4):376–385.

Brolin, K., Hedenstierna, S., Halldin, P., Bass, C., and Alem, N. (2008). The importance of muscle tension on the outcome of impacts with a major vertical component. *International Journal of Crashworthiness*, 13(5):487–498.

Bruehlmann, S. B., Rattner, J. B., Matyas, J. R., and Duncan, N. A. (2002). Regional variations in the cellular matrix of the annulus fibrosus of the intervertebral disc. *Journal of anatomy*, 201(2):159–71.

Buchanan, T. (1995). Evidence that maximum muscle stress is not a constant: differences in specific tension in elbow flexors and extensors. *Medical Engineering & Physics*, 17(7):529–536.

Buchanan, T. S., Lloyd, D. G., Manal, K., and Besier, T. F. (2014). Neuromusculoskeletal Modeling: Estimation of Muscle Forces and Joint Moments and Movements From Measurements of Neural Command. *Journal of Applied Biomechanics*, 20(4):367–395.

Callaghan, J., Laing, A., and Dickerson, C. (2014). The Influence of Neck Posture and Helmet Configuration on Neck Muscle Demands. Technical report, Research and Defence Development Canada, Toronto, Ontario.

Callaghan, J. P. and McGill, S. M. (2001). Intervertebral disc herniation: studies on a porcine model exposed to highly repetitive flexion/extension motion with compressive force. *Clinical Biomechanics*, 16(1):28–37.

Calvert, T. W. and Chapman, a. E. (1977). The relationship between the surface EMG and force transients in muscle: simulation and experimental studies. *Proceedings of the IEEE*, 65(5):682–689.

Camacho, D. L., Nightingale, R. W., Robinette, J. J., Vanguri, S. K., Coates, D. J., and Myers, B. S. (1997). Experimental Flexibility Measurements for the Development of a Computational Head-Neck Model Validated for Near-Vertex Head Impact.

Camacho, D. L. a., Nightingale, R. W., and Myers, B. S. (1999). Surface friction in near-vertex head and neck impact increases risk of injury. *Journal of Biomechanics*, 32(3):293–301.

Carter, D. R. and Wong, M. (2003). Modelling cartilage mechanobiology. *Philosophical transactions of the Royal Society of London. Series B, Biological sciences*, 358(1437):1461–1471.

Cassidy, J. J., Hiltner, a., and Baer, E. (1989). Hierarchical structure of the intervertebral disc. *Connective tissue research*, 23(1):75–88.

Cavanaugh, J., Ozaktay, A., H.T., Y., and King, A. (1996). Lumbar Facet Pain: Biomechanics, Neuroanatomy and Neurophysiology. *Journal of biomechanics*, 29(9):1117–1129.

Chancey, V. C., Nightingale, R. W., Van Ee, C. a., Knaub, K. E., and Myers, B. S. (2003). Improved estimation of human neck tensile tolerance: reducing the range of reported tolerance using anthropometrically correct muscles and optimized physiologic initial conditions. *Stapp car crash journal*, 47(October):135–53.

Chandrashekar, N., Hashemi, J., Slauterbeck, J., and Beynnon, B. D. (2008). Low-load behaviour of the patellar tendon graft and its relevance to the biomechanics of the reconstructed knee. *Clinical biomechanics (Bristol, Avon)*, 23(7):918–25.

Chang, H., Gilbertson, L. G., Goel, V. K., Winterbottom, J. M., Clark, C. R., and Patwardhan, A. (1992). Dynamic response of the occipito-atlanto-axial (C0-C1-C2) complex in right axial rotation. *Journal of Orthopaedic Research*, 10(3):446–453.

Chazal, J., Tanguy, a., Bourges, M., Gaurel, G., Escande, G., Guillot, M., and Vanneuville, G. (1985). Biomechanical properties of spinal ligaments and a histological study of the supraspinal ligament in traction. *Journal of Biomechanics*, 18(3):167–176.

Choi, H. and Vanderby, R. (1999). Comparison of biomechanical human neck models: muscle forces and spinal loads at c4/5 level. *Journal of Applied Biomechanics*, 15:120–138.

Choi, H. and Vanderby Jr, R. (2000). Muscle forces and spinal loads at c4/5 level during isometric voluntary efforts. *Medicine and science in sports and exercise*, 32(4):830–838.

Cholewicki, J. and McGill, S. M. (1994). EMG assisted optimization: A hybrid approach for estimating muscle forces in an indeterminate biomechanical model. *Journal of Biomechanics*, 27(10):1287–1289.

Cholewicki, J. and McGill, S. M. (1995). Relationship Between IVIuscle Force and Stiffness in tlie Wliole IVIammalian IVIuscle : A Simulation Study. *Journal of Biomechanical Engineering*, 117(August 1995):1993–1996.

Cholewicki, J. and McGill, S. M. (1996). Mechanical stability of the in vivo lumbar spine: Implications for injury and chronic low back pain. *Clinical Biomechanics*, 11(1):1–15.

Christophy, M., Curtin, M., Faruk Senan, N. A., Lotz, J. C., and O'Reilly, O. M. (2013). On the modeling of the intervertebral joint in multibody models for the spine. *Multibody System Dynamics*, 30:413–432.

Clausen, J. D., Goel, V. K., Traynelis, V. C., and Scifert, J. (1997). Uncinate processes and Luschka joints influence the biomechanics of the cervical spine: quantification using a finite element model of the C5-C6 segment. *Journal of orthopaedic research : official publication of the Orthopaedic Research Society*, 15(3):342–7.

Corcos, D. M., Gottlieb, G. L., Latash, M. L., Almeida, G. L., and Agarwal, G. C. (1992). Electromechanical delay: An experimental artifact. *Journal of electromyography and kinesiology : official journal of the International Society of Electrophysiological Kinesiology*, 2(2):59–68.

Côté, P., Cassidy, D. J., Carroll, L. J., and Kristman, V. (2004). The annual incidence and course of neck pain in the general population: a population-based cohort study. *Pain*, 112(3):267–273.

Côté, P., Cassidy, J. D., and Carroll, L. (1998). The Saskatchewan Health and Back Pain Survey. *Spine*, 23(15):1689–1698.

Côté, P., Kristman, V., Vidmar, M., Van Eerd, D., Hogg-Johnson, S., Beaton, D., and Smith, P. M. (2009). The Prevalence and Incidence of Work Absenteeism Involving Neck Pain. A Cohort of Ontario Lost-Time Claimants. *Journal of Manipulative and Physiological Therapeutics*, 32(2):219–226.

Crisco, J. J., Panjabi, M. M., and Dvorak, J. (1991). A model of the alar ligaments of the upper cervical spine in axial rotation. *Journal of biomechanics*, 24(7):607–14.

Croft, P. R., Lewis, M., Papageorgiou, A. C., Thomas, E., Jayson, M. I., Macfarlane, G. J., and Silman, A. J. (2001). Risk factors for neck pain: a longitudinal study in the general population. *Pain*, 93(3):317–325.

Crosby, P. a. (1978). Use of surface electromyogram as a measure of dynamic force in human limb muscles. *Medical & biological engineering & computing*, 16(5):519–524.

Crowninshield, R. D. and Brand, R. A. (1981). A physiologically based criterion of muscle force prediction in locomotion. *Journal of biomechanics*, 14(11):793–801.

Dauvilliers, F., Bendjellal, F., Weiss, M., Lavaste, F., and Tarrière, C. (1994). Development of a Finite Element Model of the Neck.

de Jager, M. (1996). *Mathematical Head-Neck Models for Acceleration Impacts*. PhD thesis, Eindhoven University of Technology.

de Jager, M., Sauren, A., Thunnissen, J., and Wismans, J. (1996). A Global and a Detailed Mathematical Model for Head-Neck Dynamics.

De Loose, V., Van den Oord, M., Burnotte, F., Van Tiggelen, D., Stevens, V., Cagnie, B., Witvrouw, E., and Danneels, L. (2008). Individual, work-, and flight-related issues in f-16 pilots reporting neck pain. *Aviation, space, and environmental medicine*, 79(8):779–783.

De Luca, C. J. (1979). Physiology and mathematics of myoelectric signals. *IEEE transactions on bio-medical engineering*, 26(6):313–325.

del Palomar, a. P., Calvo, B., and Doblaré, M. (2008). An accurate finite element model of the cervical spine under quasi-static loading. *Journal of biomechanics*, 41(3):523–31.

Delp, S. L., Anderson, F. C., Arnold, A. S., Loan, P., Habib, A., John, C. T., Guendelman, E., and Thelen, D. G. (2007). OpenSim: Open-source software to create and analyze dynamic simulations of movement. *IEEE Transactions on Biomedical Engineering*, 54(11):1940–1950.

Delp, S. L., Loan, J. P., Hoy, M. G., Zajac, F. E., Topp, E. L., and Rosen, J. M. (1990). An interactive graphics-based model of the lower extremity to study orthopaedic surgical procedures. *IEEE Transactions on Biomedical engineering*, 37(8):757–767.

Deng, Y.-C. and Fu, J. (2002). Simulation and Identification of the Neck Muscle Activities During Head and Neck Flexion Whiplash.

Deng, Y. C. and Goldsmith, W. (1987a). Response of a human head/neck/upper-torso replica to dynamic loading–I. Physical model. *Journal of biomechanics*, 20(5):471–486.

Deng, Y. C. and Goldsmith, W. (1987b). Response of a human head/neck/upper-torso replica to dynamic loading–II. Analytical/numerical model. *Journal of biomechanics*, 20(5):487–497.

Deng, Y.-C., Li, X., and Liu, Y. (1999). Modeling of the Human Cervical Spine Using Finite Element Techniques.

DeWit, J. a. and Cronin, D. S. (2012). Cervical spine segment finite element model for traumatic injury prediction. *Journal of the Mechanical Behavior of Biomedical Materials*, 10:138–150.

Diamond, S. and Boyd, S. (2016). CVXPY: A Python-embedded modeling language for convex optimization. *Journal of Machine Learning Research*, 17(83):1–5.

Dibblee, J., Worthy, P., Farrell, P., Hetzler, M., Reid, S., Stevenson, J., and Fischer, S. (2015). Evaluating a prototype device designed to alleviate night vision goggle induced neck strain among military personnel. *Ergonomics*, 0139(November):1–11.

Dickerson, C. R., Chaffin, D. B., and Hughes, R. E. (2007). A mathematical musculoskeletal shoulder model for proactive ergonomic analysis. *Computer methods in biomechanics and biomedical engineering*, 10(6):389–400.

DiSilvestro, M. R. and Suh, J. K. F. (2001). A cross-validation of the biphasic poroviscoelastic model of articular cartilage in unconfined compression, indentation, and confined compression. *Journal of Biomechanics*, 34:519–525.

Doherty, B. J. and Heggeness, M. H. (1994). The Quantitative Anatomy of the Atlas. *SPINE*, 19(Supplement):2497–2500.

Doherty, B. J. and Heggeness, M. H. (1995). Quantitative Anatomy of the Second Cervical Vertebra. *Spine*, 20(5):513–517.

Dvorak, J., Panjabi, M. M., Gerber, M., and Wichmann, W. (1987). CT-Functional Diagnostics of the Rotatory Instability of Upper Cervical Spine. *Spine*, 12(3):197–205.

Dvorak, J., Panjabi, M. M., Novotny, J. E., and Antinnes, J. a. (1991). In vivo flexion/extension of the normal cervical spine. *Journal of Orthopaedic Research*, 9(4):828–834.

Dvorak, J., Schneider, E., Saldinger, P., and Rahn, B. (1988). Biomechanics of the Craniocervical Region: the Alar and Transverse Ligaments. *Journal of orthopaedic research : official publication of the Orthopaedic Research Society*, 6(3):452–461.

Ebara, S., Iatridis, J. C., Setton, L. A., Foster, R. J., Mow, V. C., and Weidenbaum, M. (1996). Tensile Properties of Nondegenerate Human Lumbar Anulus Fibrosus. *Spine*, 21(4):452–461.

Elliott, D. M. and Setton, L. A. (2001). Anisotropic and Inhomogeneous Tensile Behavior of the Human Anulus Fibrosus: Experimental Measurement and Material Model Predictions. *Journal of Biomechanical Engineering*, 123(3):256.

Esat, V. and Acar, M. (2009). Viscoelastic finite element analysis of the cervical intervertebral discs in conjunction with a multi-body dynamic model of the human head and neck. *Proceedings of the Institution of Mechanical Engineers. Part H, Journal of engineering in medicine*, 223(2):249–262.

Falla, D., Bilenkij, G., and Jull, G. (2004). Patients with chronic neck pain demonstrate altered patterns of muscle activation during performance of a functional upper limb task. *Spine*, 29(13):1436–1440.

Falla, D., Farina, D., Dahl, M. K., and Graven-Nielsen, T. (2007). Muscle pain induces task-dependent changes in cervical agonist/antagonist activity. *Journal of applied physiology (Bethesda, Md. : 1985)*, 102(2):601–9.

Farina, D. and Negro, F. (2012). Accessing the neural drive to muscle and translation to neurorehabilitation technologies. *IEEE Reviews in Biomedical Engineering*, 5:3–14.

Featherstone, R. (2008). *Rigid Body Dynamics Algorithms*.

Feynman, R. (1963). *The Feynman Lectures on Physics*, volume I. Addison-Wesely.

Fice, J. B., Cronin, D. S., and Panzer, M. B. (2011). Cervical spine model to predict capsular ligament response in rear impact. *Annals of Biomedical Engineering*, 39(8):2152–2162.

Fielding, J. W., Burnstein, A. H., and Frankel, V. H. (1976). The Nuchal Ligament. *Spine*, 1(1):3–14.

Forde, K. A., Albert, W. J., Harrison, M. F., Neary, J. P., Croll, J., and Callaghan, J. P. (2011). Neck loads and posture exposure of helicopter pilots during simulated day and night flights. *International Journal of Industrial Ergonomics*, 41(2):128–135.

Forsberg, C.-M., Hellsing, E., Linder-Aronson, S., and Sheikholeslam, a. (1985). EMG activity in neck and masticatory muscles in relation to extension and flexion of the head. *The European Journal of Orthodontics*, 7(3):177–184.

Francis, C. C. (1955). Variations in the articular facets of the cervical vertebrae. *The Anatomical Record*, 122(4):589–602.

Frigg, R. and Hartmann, S. (2012). Models in Science. In Zalta, E., editor, *The Stanford Encyclopedia of Philosophy*. Fall 2012 edition.

Fuglevand, a. J., Winter, D. a., and Patla, a. E. (1993). Models of recruitment and rate coding organization in motor-unit pools. *Journal of neurophysiology*, 70(6):2470–2488.

Fuglevand, A. J., Winter, D. A., Patla, A. E., and Stashuk, D. (1992). Detection of motor unit action potentials with surface electrodes: influence of electrode size and spacing. *Biological cybernetics*, 67(2):143–53.

Fung, Y. C. (1967). Elasticity of soft tissues in simple elongation. *The American journal of physiology*, 213(6):1532–1544.

Gagnon, D., Arjmand, N., Plamondon, A., Shirazi-Adl, A., and Larivière, C. (2011). An improved multi-joint EMG-assisted optimization approach to estimate joint and muscle forces in a musculoskeletal model of the lumbar spine. *Journal of biomechanics*, 44(8):1521–9.

Galante, J. O. (1967). Tensile properties of the human lumbar annulus fibrosus. *Acta orthopaedica Scandinavica*, 100:Suppl 100:1–91.

Garner, B. A. and Pandy, M. G. (2000). The obstacle-set method for representing muscle paths in musculoskeletal models. *Computer methods in biomechanics and biomedical engineering*, 3(1):1–30.

Gilad, I. and Nissan, M. (1986). A Study of Vertebra and Disc Geometric Relations of the Human Cervical and Lumbar Spine. *Spine*, 11(2):154–157.

Gilsanz, V., Kovanlikaya, a., Costin, G., Roe, T. F., Sayre, J., and Kaufman, F. (1997). Differential effect of gender on the sizes of the bones in the axial and appendicular skeletons. *The Journal of clinical endocrinology and metabolism*, 82(5):1603–7.

Goel, V. K., Clark, C. R., Gallaes, K., and Liu, Y. K. (1988a). Moment-rotation relationships of the ligamentous occipito-atlanto-axial complex. *Journal of biomechanics*, 21(8):673–680.

Goel, V. K., Clark, C. R., Harris, K. G., and Schulte, K. R. (1988b). Kinematics of the cervical spine: Effects of multiple total laminectomy and facet wiring. *Journal of Orthopaedic Research*, 6(4):611–619.

Goel, V. K., Clark, C. R., McGowan, D., and Goyal, S. (1984). An in-vitro study of the kinematics of the normal, injured and stabilized cervical spine. *Journal of biomechanics*, 17(5):363–76.

Goel, V. K. and Clausen, J. D. (1998). Prediction of load sharing among spinal components of a C5-C6 motion segment using the finite element approach.

Goldstein, H., Poole, C., and Safko, J. (1950). *Classical Mechanics*. Addison-Wesely, Flushing, New York, NY, USA, third edition.

Gordon, A. M., Huxley, A. F., and Julian, F. J. (1966). The variation in isometric tension with sarcomere length in vertebrate muscle fibres. *The Journal of Physiology*, 184(1):170–192.

Gray, H. (1918). *Anatomy of the Human Body*. Bartleby.com, New York, NY, 20 edition.

Green, T., Adams, M., and Dolan, P. (1993). Tensile properties of the annulus fibrosus. *European Spine Journal*, 2:209–214.

Gregory, D. E. and Callaghan, J. P. (2011). A comparison of uniaxial and biaxial mechanical properties of the annulus fibrosus: a porcine model. *Journal of biomechanical engineering*, 133(2):024503.

Gregory, D. E., Veldhuis, J. H., Horst, C., Wayne Brodland, G., and Callaghan, J. P. (2011). Novel lap test determines the mechanics of delamination between annular lamellae of the intervertebral disc. *Journal of Biomechanics*, 44(1):97–102.

Guimaraes, a. C., Herzog, W., Allinger, T. L., and Zhang, Y. T. (1995). The EMG-force relationship of the cat soleus muscle and its association with contractile conditions during locomotion. *The Journal of experimental biology*, 198(Pt 4):975–987.

Hatze, H. (1977). A myocybernetic control model of skeletal muscle. *Biological cybernetics*, 25(2):103–119.

Hayes, a. J., Benjamin, M., and Ralphs, J. R. (2001). Extracellular matrix in development of the intervertebral disc. *Matrix Biology*, 20:107–121.

Hayes, W. and Mockros, L. (1971). Some viscoelastic properties of human articular cartilage. *Journal of APplied Physiology*, 31(4):562–538.

Heller, J. G., Alson, M. D., Schaffler, M. B., and Garfin, S. R. (1992). Quantitative Internal Dens Morphology. *Spine*, 17(8):861–866.

Herzog, W., Sokolosky, J., Zhang, Y. T., and Guimarães, a. C. S. (1998). EMG-force relation in dynamically contracting cat plantaris muscle. *Journal of Electromyography and Kinesiology*, 8:147–155.

Hicks, J. L., Uchida, T. K., Seth, a., Rajagopal, a., and Delp, S. (2014). Is my model good enough? Best practices for verification and validation of musculoskeletal models and simulations of human movement. *Journal of Biomechanical Engineering*, 137(February).

Hill, A. (1949). The abrupt transition from rest to activity in muscle. *Proceedings of the Royal Society of London. Series B, Containing papers of a Biological character. Royal Society (Great Britain)*, 136(884):399–420.

Hill, a. V. (1938). The Heat of Shortening and the Dynamic Constants of Muscle. *Proceedings of the Royal Society B: Biological Sciences*, 126(843):136–195.

Hoek van Dijke, G. A., Snijders, C. J., Roosch, E. R., and Burgers, P. I. (1993). Analysis of biomechanical and ergonomic aspects of the cervical spine in F-16 flight situations. *Journal of biomechanics*, 26(9):1017–1025.

Hof, a. L. and Van den Berg, J. (1981a). EMG to force processing I: An electrical analogue of the Hill muscle model. *Journal of biomechanics*, 14(11):747–758.

Hof, a. L. and Van den Berg, J. (1981b). EMG to force processing II: Estimation of parameters of the Hill muscle model for the human triceps surae by means of a calfergometer. *Journal of biomechanics*, 14(11):759–770.

Hof, a. L. and Van den Berg, J. (1981c). EMG to force processing III: Estimation of model parameters for the human triceps surae muscle and assessment of the accuracy by means of a torque plate. *Journal of biomechanics*, 14(11):771–785.

Hof, a. L. and Van den Berg, J. (1981d). EMG to force processing IV: Eccentric-concentric contractions on a spring-flywheel set up. *Journal of biomechanics*, 14(11):787–792.

Holm, L. W., Carroll, L. J., Cassidy, J. D., Hogg-Johnson, S., Côté, P., Guzman, J., Peloso, P., Nordin, M., Hurwitz, E., van der Velde, G., Carragee, E., and Haldeman, S. (2008). The Burden and Determinants of Neck Pain in Whiplash-Associated Disorders After Traffic Collisions. *European Spine Journal*, 17(Suppl 1):52–59.

Holzapfel, G. A., Schulze-Bauer, C. A. J., Feigl, G., and Regitnig, P. (2005). Single lamellar mechanics of the human lumbar anulus fibrosus. *Biomechanics and Modeling in Mechanobiology*, 3(3):125–140.

Huber, Z. E. (2013). *Creation and Evaluation of a Dynamic, EMG-Driven Cervical Spine Model*. Master of science, The Ohio State University.

Humzah, M. D. and Soames, R. W. (1988). Human intervertebral disc: Structure and function. *The Anatomical Record*, 220(4):337–356.

Huxley, A. F. (1957). Muscle structure and theories of contraction. *Prog Biophys Biophys Chem*, 7:255–318.

Huxley, A. F. and Simmons, R. M. (1971). Proposed Mechanism of Force Generation in Striated Muscle. *Nature*, 233(5321):533–538.

Iatridis, J. C., Setton, L. a., Foster, R. J., Rawlins, B. a., Weidenbaum, M., and Mow, V. C. (1998). Degeneration affects the anisotropic and nonlinear behaviors of human anulus fibrosus in compression. *Journal of Biomechanics*, 31(6):535–544.

Iatridis, J. C., Setton, L. A., Weidenbaum, M., and Mow, V. C. (1997a). Alterations in the mechanical behavior of the human lumbar nucleus pulposus with degeneration and aging. *Journal of Orthopaedic Research*, 15(2):318–322.

Iatridis, J. C., Setton, L. A., Weidenbaum, M., and Mow, V. C. (1997b). The viscoelastic behavior of the non-degenerate human lumbar nucleus pulposus in shear. *Journal of Biomechanics*, 30(10):1005–1013.

Iatridis, J. C., Weidenbaum, M., Setton, L. A., and Mow, V. C. (1996). Is the Nucleus Pulposus a Solid or a Fluid? Mechanical Behaviors of the Nucleus Pulposus of the Human Intervertebral Disc. *Spine*, 21(10):1174–1184.

Inoue, H. (1981). Three-Dimensional Architecture of Lumbar Intervertebral Discs. *Spine*, 6(2):139–146.

Ivancic, P. C. (2013). Effects of orthoses on three-dimensional load-displacement properties of the cervical spine. *European Spine Journal*, 22(1):169–177.

Jaumard, N. V., Welch, W. C., and Winkelstein, B. A. (2011). Spinal Facet Joint Biomechanics and Mechanotransduction in Normal, Injury and Degenerative Conditions. *Journal of Biomechanical Engineering*, 133(7):071010.

Johnson, E. F., Chetty, K., Moore, I. M., Stewart, a., and Jones, W. (1982). The distribution and arrangement of elastic fibres in the intervertebral disc of the adult human. *Journal of Anatomy*, 135(Pt 2):301–9.

Johnson, G. M., Zhang, M., and Jones, D. G. (2000). The fine connective tissue architecture of the human ligamentum nuchae. *Spine*, 25(1):5–9.

Joyce, G. C. and Rack, P. M. (1969). Isotonic lengthening and shortening movements of cat soleus muscle. *The Journal of Physiology*, 204(2):475–491.

Jull, G. a. (2000). Deep cervical flexor muscle dysfunction in whiplash. *J Musculoskelet Pain*, 8(1-2):143–154.

Jull, G. a., O'Leary, S. P., and Falla, D. L. (2008). Clinical Assessment of the Deep Cervical Flexor Muscles: The Craniocervical Flexion Test. *Journal of Manipulative and Physiological Therapeutics*, 31(7):525–533.

Kamibayashi, L. K. and Richmond, F. J. (1998). Morphometry of Human Neck Muscles. *Spine*, 23(12):1314–1323.

Kandel, R. a., Hamilton, D., Séguin, C., Li, S.-Q., Arana, C., and Pilliar, R. (2007). An in vitro tissue model to study the effect of age on nucleus pulposus cells. *European spine journal : official publication of the European Spine Society, the European Spinal Deformity Society, and the European Section of the Cervical Spine Research Society*, 16:2166–2173.

Kapandji, A. (2008). *The Physiology of the Joints, volume III*.

Karajan, N., Röhrle, O., Ehlers, W., and Schmitt, S. (2013). Linking continuous and discrete intervertebral disc models through homogenisation. *Biomechanics and Modeling in Mechanobiology*, 12(3):453–466.

Kelsey, J., Githens, P., Walter, S., Southwick, W., Weil, U., Holford, T., Ostfeld, A., Calogero, J., O'Connor, T., and White, A. (1984). An epidemiological study of acute prolapsed cervical intervertebral disc. *The Journal of bone and joint surgery*, 66(6):907–914.

Kenedi, R. M., Gibson, T., Evans, J. H., and Barbenel, J. C. (1975). Tissue mechanics. *Physics in Medicine and Biology*, 20(5):001.

King, B. T. (1939). New and function-restoring operation for bilateral abductor cord paralysis: preliminary report. *journal of the American Medical Association*, 112(9):814–823.

Kingma, I., De Looze, M. P., Toussaint, H. M., Klijnsma, H. G., and Bruijnen, T. B. M. (1996). Validation of a full body 3-D dynamic linked segment model. *Human Movement Science*, 15(6):833–860.

Kleinberger, M. (1993). Application of Finite Element Techniques to the Study of Cervical Spine Mechanics.

Koebke, J. and Brade, H. (1982). Morphological and functional studies on the lateral joints of the first and second cervical vertebrae in man. *Anatomy and Embryology*, 164(2):265–275.

Kumaresan, S., Yoganandan, N., and Pintar, F. a. (1999a). Finite element analysis of the cervical spine: a material property sensitivity study. *Clinical Biomechanics*, 14(1):41–53.

Kumaresan, S., Yoganandan, N., Pintar, F. a., and Maiman, D. J. (1999b). Finite element modeling of the cervical spine: Role of intervertebral disc under axial and eccentric loads. *Medical Engineering and Physics*, 21(10):689–700.

Lange, B., Torp-Svendsen, J., and Toft, P. (2011). Neck pain among fighter pilots after the introduction of the JHMCS helmet and NVG in their environment. *Aviation Space and Environmental Medicine*, 82(5):559–563.

Lautrup, B. (2005). *Physics of Continuous Matter*.

Lenth, R. V. (2016). Least-squares means: The R package lsmeans. *Journal of Statistical Software*, 69(1):1–33.

Li, G., Gil, J., Kanamori, A., and Woo, S.-Y. (1999). A validated three-dimensional computational model of a human knee joint. *Journal of biomechanical engineering*, 121(6):657–662.

Lin, H. S., Liu, Y. K., Ray, G., and Nikravesh, P. (1978). Systems identification for material properties of the intervertebral joint. *Journal of biomechanics*, 11:1–14.

Lin, Y.-C., Walter, J. P., Banks, S. A., Pandy, M. G., and Fregly, B. J. (2010). Simultaneous prediction of muscle and contact forces in the knee during gait. *Journal of Biomechanics*, 43(5):945–952.

Lippold, O. C. J. (1952). The relation between integrated action potentials in a human muscle and its isometric tension. *The Journal of Physiology*, 117(4):492–499.

Little, J. S. and Khalsa, P. S. (2005). Material properties of the human lumbar facet joint capsule. *J Biomech Eng*, 127(1):15–24.

Lloyd, D. G. and Besier, T. F. (2003). An EMG-driven musculoskeletal model to estimate muscle forces and knee joint moments in vivo. *Journal of Biomechanics*, 36(6):765–776.

Lu, W. W. and Bishop, P. J. (1996). Electromyographic activity of the cervical musculature during dynamic lateral bending.

Lu, Y., Chen, C., Kallakuri, S., Patwardhan, A., and Cavanaugh, J. M. (2005). Neurophysiological and biomechanical characterization of goat cervical facet joint capsules. *Journal of Orthopaedic Research*, 23(4):779–787.

Lucas, S., Bass, C., Salzar, R., Shender, B. S., and Paskoff, G. (2006). High-rate viscoelastic properties of human cervical spinal intervertebral discs. In *Annual Meeting of the American Society of Biomechanics*. American Society of Biomechanics.

Lucas, S. R., Bass, C. R., Crandall, J. R., Kent, R. W., Shen, F. H., and Salzar, R. S. (2009). Viscoelastic and failure properties of spine ligament collagen fascicles. *Biomechanics and Modeling in Mechanobiology*, 8(6):487–498.

Ma, S. and Zahalak, G. I. (1988). Activation dynamics for a distribution-moment model of skeletal muscle. *Mathematical and Computer Modelling*, 11(1):778–782.

Ma, S. and Zahalak, G. I. (1991). A distribution-moment model of energetics in skeletal muscle. *Journal of Biomechanics*, 24(1):21–35.

Maak, T. G., Tominaga, Y., Panjabi, M. M., and Ivancic, P. C. (2006). Alar, transverse, and apical ligament strain due to head-turned rear impact. *Spine*, 31(6):632–638.

Marchand, F. and Ahmed, A. M. (1990). Investigation of the Laminate Structure of Lumbar Disc Anulus Fibrosus. *Spine*, 15(5):402–410.

Marlow, E. J. and Pastor, R. F. (2011). Sex determination using the second cervical vertebra–A test of the method. *Journal of forensic sciences*, 56(1):165–9.

Martonosi, A. N. (2000). Animal electricity, Ca2+ and muscle contraction. A brief history of muscle research. *Acta Biochimica Polonica*, 47(3):493–516.

Matsumoto, M., Fujimura, Y., Suzuki, N., Nishi, Y., Nakamura, M., Yabe, Y., and Shiga, H. (1998). Mri of cervical intervertebral discs in asymptomatic subjects. *Bone & Joint Journal*, 80(1):19–24.

Mattucci, S. F., Moulton, J. a., Chandrashekar, N., and Cronin, D. S. (2012). Strain rate dependent properties of younger human cervical spine ligaments. *Journal of the Mechanical Behavior of Biomedical Materials*, 10:216–226.

Mattucci, S. F. E. (2011). *Strain rate dependent properties of younger human cervical spine ligaments.* Master's thesis, University of Waterloo.

Mattucci, S. F. E., Moulton, J. a., Chandrashekar, N., and Cronin, D. S. (2013). Strain rate dependent properties of human craniovertebral ligaments. *Journal of the Mechanical Behavior of Biomedical Materials*, 23:71–79.

McGill, S. M. (1992). A myoelectrically based dynamic three-dimensional model to predict loads on lumbar spine tissues during lateral bending. *Journal of Biomechanics*, 25(4):395–414.

McGill, S. M. and Brown, S. (1992). Creep response of the lumbar spine to prolonged full flexion. *Clinical Biomechanics*, 7:43–46.

McGill, S. M. and Norman, R. W. (1986). Partitioning of the L4-L5 dynamic moment into disc, ligamentous, and muscular components during lifting. *Spine*, 11(7):666–78.

Mengoni, M., Luxmoore, B. J., Wijayathunga, V. N., Jones, A. C., Broom, N. D., and Wilcox, R. K. (2015). Derivation of inter-lamellar behaviour of the intervertebral disc annulus. *Journal of the Mechanical Behavior of Biomedical Materials*, 48:164–172.

Mercer, S. and Bogduk, N. (1993). Intra-articular inclusions of the cervical synovial joints. *Br J Rheumatol*, 32(8):705–10.

Mercer, S. R. and Bogduk, N. (2001). Joints of the cervical vertebral column. *The Journal of orthopaedic and sports physical therapy*, 31(4):174–182; discussion 183.

Merrill, T., Goldsmith, W., and Deng, Y. C. (1984). Three-dimensional response of a lumped parameter head-neck model due to impact and impulsive loading. *Journal of biomechanics*, 17(2):81–95.

Meyer, F., Bourdet, N., Gunzel, K., and Willinger, R. (2013). Development and validation of a coupled head-neck FEM application to whiplash injury criteria investigation. *International Journal of Crashworthiness*, 18(1):40–63.

Meyer, F., Bourdet, N., and Willinger, R. (2005). Experimental and numerical modal analysis of the human head-neck system - a new finite element model validation method. *International Journal of Vehicle Safety*, 1(1/2/3):145.

Millard, M., Uchida, T., Seth, A., and Delp, S. L. (2013). Flexing Computational Muscle: Modeling and Simulation of Musculotendon Dynamics. *Journal of Biomechanical Engineering*, 135(2):021005.

Milner-Brown, H. S., Stein, R. B., and Yemm, R. (1973). Changes in firing rate of human motor units during linearly changing voluntary contractions. *The Journal of physiology*, 230(2):371–390.

Mitsuhashi, N., Fujieda, K., Tamura, T., Kawamoto, S., Takagi, T., and Okubo, K. (2009). Bodyparts3d: 3d structure database for anatomical concepts. *Nucleic acids research*, 37(suppl 1):D782–D785.

Moore, K. and Dalley, A. (2005). *Clinically Oriented Anatomy*. Lippincott Williams & Wilkins, Philadelphia, 5 edition.

Moroney, S. P., Schultz, a. B., and Miller, J. a. (1988a). Analysis and measurement of neck loads. *Journal of orthopaedic research : official publication of the Orthopaedic Research Society*, 6(5):713–720.

Moroney, S. P., Schultz, a. B., Miller, J. a., and Andersson, G. B. (1988b). Load-displacement properties of lower cervical spine motion segments. *Journal of biomechanics*, 21(9):769–779.

Mow, V. C. and Guo, X. E. (2002). Mechano-Electrochemical Properties Of Articular Cartilage: Their Inhomogeneities and Anisotropies. *Annual Review of Biomedical Engineering*, 4(1):175–209.

Myklebust, J. B., Pintar, F., Yoganandan, N., Cusick, J. F., Maiman, D. J., Myers, T. J., and Sances, A. (1988). Tensile Strength of Spinal Ligaments. *Spine*, 13(5):528–531.

Nachemson, A. L. and Evans, J. H. (1968). Some mechanical properties of the third human lumbar interlaminar ligament (ligamentum flavum). *Journal of Biomechanics*, 1:211–220.

Netto, K. J., Burnett, A. F., Green, J. P., and Rodrigues, J. P. (2008). Validation of an EMG-driven, graphically based isometric musculoskeletal model of the cervical spine. *Journal of biomechanical engineering*, 130(3):031014.

Newton, I. (1687). *Philosophiae Naturalis Principia Mathematica*.

Nightingale, R. W., Carol Chancey, V., Ottaviano, D., Luck, J. F., Tran, L., Prange, M., and Myers, B. S. (2007). Flexion and extension structural properties and strengths for male cervical spine segments. *Journal of biomechanics*, 40(3):535–542.

Nightingale, R. W., Winkelstein, B. a., Knaub, K. E., Richardson, W. J., Luck, J. F., and Myers, B. S. (2002). Comparative strengths and structural properties of the upper and lower cervical spine in flexion and extension. *Journal of biomechanics*, 35(6):725–732.

Nissan, M. and Gilad, I. (1984). The cervical and lumbar vertebrae an anthropometric model. *ARCHIVE: Engineering in Medicine 1971-1988 (vols 1-17)*, 13(3):111–114.

Oda, J., Tanaka, H., and Tsuzuki, N. (1988). Intervertebral Disc Changes with Aging of Human Cervical Vertebra. *Spine*, 13(11):1205–1211.

Ohala, J. and Hirose, H. (1970). The function of the sternohyoid muscle in speech. *Annual Bulletin, Research Institute of Logopedics and Phoniatrics*, 4:41–44.

Olney, S. J. and Winter, D. a. (1985). Predictions of knee and ankle moments of force in walking from EMG and kinematic data. *Journal of biomechanics*, 18(1):9–20.

Östh, J. (2010). *Active Muscle Responses in a Finite Element Human Body Model*. PhD thesis, Chalmers University of Technology.

Pal, G. (2001). The orientation of the articular facets of the zygapophyseal. *The Journal of Anatomy*, 198:431–441.

Palmer, J. B., Rudin, N. J., Lara, G., and Crompton, A. W. (1992). Coordination of mastication and swallowing. *Dysphagia*, 7(4):187–200.

Panjabi, M. M., Chen, N., Shin, E., and Wang, J. (2001a). The cortical shell architecture of human cervical vertebral bodies. *Spine*, 26(22):2478–2484.

Panjabi, M. M. and Courtney, T. W. (2001). High-speed subfailure stretch of rabbit anterior cruciate ligament: changes in elastic, failure and viscoelastic characteristics. *Clinical biomechanics (Bristol, Avon)*, 16(4):334–40.

Panjabi, M. M., Crisco, J. J., Lydon, C., and Dvorak, J. (1998). The Mechanical Properties of Human Alar and Transverse Ligaments at Slow and Fast Extension Rates. *Clinical Biomechanics*, 13(2):112–120.

Panjabi, M. M., Crisco, J. J., Vasavada, A., Oda, T., Cholewicki, J., Nibu, K., and Shin, E. (2001b). Mechanical Properties of the Human Cervical Spine as Shown by Three-Dimensional LoadDisplacement Curves. *Spine*, 26(24):2692–2700.

Panjabi, M. M., Duranceau, J., Goel, V., Oxland, T., and Takata, K. (1991a). Cervical Human Vertebrae Quantitative Three-Dimensional Anatomy of the Middle and Lower Regions. *Spine*, 16(8):861–869.

Panjabi, M. M., Dvorak, J., Crisco, J. J., Oda, T., Wang, P., and Grob, D. (1991b). Effects of Alar Ligament Transection on Upper Cervical Spine Rotation. *Journal of orthopaedic research : official publication of the Orthopaedic Research Society*, 9(17):584–593.

Panjabi, M. M., Dvorak, J., Duranceau, J., and Yamamoto, I. (1988). Three-Dimensional Movements of the Upper Cervical Spine. pages 370–377.

Panjabi, M. M., Dvorak, J., and III, J. C. (1991c). Flexion, Extension, and Lateral Bending of the Upper Cervical Spine in Response to Alar Ligament Transections. *Journal of SPINAL DISORDERS*, 4(2):157–167.

Panjabi, M. M., Oxland, T., and Parks, E. (1991d). Quantitative anatomy of cervical spine ligaments. Part I. Upper cervical spine.

Panjabi, M. M., Oxland, T., and Parks, E. (1991e). Quantitative Anatomy of Cervical Spine Ligaments. Part II. Middle and Lower Cervical Spine. *Journal of Spinal Disorders*, 4(3):277–285.

Panjabi, M. M., Oxland, T., Takata, K., Goel, V., Duranceau, J., and Krag, M. (1993). Articular Facets of the Human Spine Quantitative Three-Dimensional Anatomy. *Spine*, 18(10):1298–1310.

Panzer, M. B. (2006). *Numerical Modelling of the Human Cervical Spine in Frontal Impact*. Master's thesis, University of Waterloo.

Panzer, M. B. and Cronin, D. S. (2009). C4-C5 segment finite element model development, validation, and load-sharing investigation. *Journal of Biomechanics*, 42(4):480–490.

Panzer, M. B., Fice, J. B., and Cronin, D. S. (2011). Cervical spine response in frontal crash. *Medical Engineering and Physics*, 33(9):1147–1159.

Pearson, W. G., Langmore, S. E., Zumwalt, A. C., Pearson Jr., W. G., Langmore, S. E., Zumwalt, A. C., and Pearson, W. G. (2010). Evaluating the Structural Properties of Suprahyoid Muscles and their Potential for Moving the Hyoid. *Dysphagia*, 26(4):345–51.

Penning, L. (1978). Normal movements of the cervical spine. *American Journal of Roentgenology*, 130(2):317–326.

Penning, L. (1988). Differences in anatomy, motion, development and aging of the upper and lower cervical disk segments. *Clinical biomechanics (Bristol, Avon)*, 3(1):37–47.

Penning, L. and Wilmink, J. T. (1987). Rotation of the Cervical Spine. *Spine*, 12(8):732–738.

Pintar, F. A., Yoganandan, N., and Voo, L. (1998). Effect of age and loading rate on human cervical spine injury threshold. *Spine*, 23(18):1957–1962.

Pooni, J., Hukins, D., Harris, P., Hilton, R., and Davies, K. (1986). Comparison of the structure of human intervertebral discs in the cervical, thoracic and lumbar regions of the spine. *Surgical and Radiologic Anatomy*, 8(3):175–182.

Popper, K. (1959). *The logic of scientific discovery*, volume 268.

Provenzano, P., Heisey, D., Hayashi, K., Lakes, R., and Vanderby, R. (2002). Subfailure damage in ligament: a structural and cellular evaluation. *Journal of applied physiology (Bethesda, Md. : 1985)*, 92(1):362–371.

Provenzano, P., Lakes, R., Keenan, T., and Vanderby, Jr., R. (2001). Nonlinear Ligament Viscoelasticity. *Annals of Biomedical Engineering*, 29(10):908–914.

Przybylski, G. J., Carlin, G. J., Patel, P. R., and Woo, S. L. Y. (1996). Human anterior and posterior cervical longitudinal ligaments possess similar tensile properties. *Journal of Orthopaedic Research*, 14(6):1005–1008.

Przybylski, G. J., Patel, P. R., Carlin, G. J., and Woo, S. L.-Y. (1998). Quantitative Anthropometry of the Subatlantal Cervical Longitudinal Ligaments. *Spine*, 23(8):893–898.

Puttlitz, C. M., Rousseau, M. A., Xu, Z., Hu, S., Tay, B. K.-B., and Lotz, J. C. (2004). Intervertebral disc replacement maintains cervical spine kinetics. *Spine*, 29(24):2809–2814.

R Core Team (2015). *R: A Language and Environment for Statistical Computing*. R Foundation for Statistical Computing, Vienna, Austria.

Richter, M., Wilke, H. J., Kluger, P., Claes, L., and Puhl, W. (2000). Load-displacement properties of the normal and injured lower cervical spine in vitro. *European spine journal : official publication of the European Spine Society, the European Spinal Deformity Society, and the European Section of the Cervical Spine Research Society*, 9(2):104–8.

Rigby, B. J., Hirai, N., Spikes, J. D., and Eyring, H. (1959). The Mechanical Properties of Rat Tail Tendon. *J Gen Physiol*, 43(2):265–83.

Roberts, S., Menage, J., Duace, V., Wotton, S., and Ayad, S. (1991). 1991 Volvo Award in Basic Sciences. *Spine*, 16(9):1030–1038.

Roberts, S., Menage, J., and Urban, J. P. G. (1989). Biochemical and Structural Properties of the Cartilage End-Plate and its Relation to the Intervertebral Disc. *Spine*, 14(2):166–174.

Robertson, D. E. and Dowling, J. J. (2003). Design and responses of Butterworth and critically damped digital filters. *Journal of Electromyography and Kinesiology*, 13(6):569–573.

Roszek, B., Baan, G. C., and Huijing, P. A. (1994). Decreasing stimulation frequency-dependent length-force characteristics of rat muscle. *Journal of Applied Physiology*, 77(5):2115–2124.

Roughley, P. J. (2004). Biology of intervertebral disc aging and degeneration: involvement of the extracellular matrix. *Spine*, 29(23):2691–2699.

RStudio Team (2015). *RStudio: Integrated Development Environment for R*. RStudio, Inc., Boston, MA.

Sargent, R. (1998). Verification and validation of simulation models. *1998 Winter Simulation Conference. Proceedings (Cat. No.98CH36274)*, 1.

Sartori, M., Reggiani, M., Farina, D., and Lloyd, D. G. (2012). EMG-Driven Forward-Dynamic Estimation of Muscle Force and Joint Moment about Multiple Degrees of Freedom in the Human Lower Extremity. *PLoS ONE*, 7(12):e52618.

Schmidt, H., Bashkuev, M., Dreischarf, M., Rohlmann, A., Duda, G., Wilke, H. J., and Shirazi-Adl, A. (2013). Computational biomechanics of a lumbar motion segment in pure and combined shear loads. *Journal of Biomechanics*, 46(14):2513–2521.

Schollum, M. L., Robertson, P. a., and Broom, N. D. (2008). ISSLS Prize Winner: Microstructure and Mechanical Disruption of the Lumbar Disc Annulus. *Spine*, 33(25):2702–2710.

Schollum, M. L., Robertson, P. A., and Broom, N. D. (2010). How age influences unravelling morphology of annular lamellae - a study of interfibre cohesivity in the lumbar disc. *Journal of Anatomy*, 216(3):310–319.

Schulte, K., Clark, C. R., and Goel, V. K. (1989). Kinematics of the Cervical Spine Following Discectomy and Stabilization. *Spine*, 14(10):1116–1121.

Scovil, C. Y. and Ronsky, J. L. (2006). Sensitivity of a hill-based muscle model to perturbations in model parameters. *Journal of biomechanics*, 39(11):2055–2063.

Seki, Y., Schneider, M. S., and Meyers, M. A. (2005). Structure and mechanical behavior of a toucan beak. *Acta materialia*, 53(20):5281–5296.

Shao, Q., Bassett, D. N., Manal, K., and Buchanan, T. S. (2009). An EMG-driven Model to Estimate Muscle Forces and Joint Moments in Stroke Patients. *Computer Methods in Biology and Medicine*, 39(12):1083–1088.

Shea, M., Edwards, W., White, A., and Hayes, W. (1991). Variations of stiffness and strength along the human cervical spine. *Journal of biomechanics*, 24(2):95–107.

Shim, V. P. W., Liu, J. F., and Lee, V. S. (2006). A Technique for Dynamic Tensile Testing of Human Cervical Spine Ligaments. *Experimental Mechanics*, 46(1):77–89.

Siegmund, G. P., Blouin, J.-S., Brault, J. R., Hedenstierna, S., and Inglis, J. T. (2007). Electromyography of superficial and deep neck muscles during isometric, voluntary, and reflex contractions. *Journal of biomechanical engineering*, 129(1):66–77.

Sivan, S. S., Hayes, A. J., Wachtel, E., Caterson, B., Merkher, Y., Maroudas, A., Brown, S., and Roberts, S. (2014). Biochemical composition and turnover of the extracellular matrix of the normal and degenerate intervertebral disc. *European Spine Journal*, 23(SUPPL. 3):344–353.

Snijders, C., Hoek van Dijke, G., and Roosch, E. (1991). A biomechanical model for the analysis of the cervical spine in static postures. *Journal of Biomechanics*, 24(9):783–792.

Solomonow, M. (2004). Ligaments: a source of work-related musculoskeletal disorders. *Journal of Electromyography and Kinesiology*, 14(1):49–60.

Solomonow, M., Baratta, R. V., Zhou, B. H., Burger, E., Zieske, a., and Gedalia, a. (2003). Muscular dysfunction elicited by creep of lumbar viscoelastic tissue. *Journal of Electromyography and Kinesiology*, 13(4):381–396.

Spilker, R. L., Jakobs, D. M., and Schultz, a. B. (1986). Material constants for a finite element model of the intervertebral disk with a fiber composite annulus. *Journal of biomechanical engineering*, 108(1):1–11.

Standring, S. (2008). *Gray's Anatomy: The Anatomical Basis of Clinical Practice*. 40 edition.

Stemper, B. D., Yoganandan, N., and Pintar, F. a. (2004). Validation of a head-neck computer model for whiplash simulation. *Medical & biological engineering & computing*, 42(3):333–338.

Takebe, K., Vitti, M., and Basmajian, J. V. (1974). The functions of semispinalis capitis and splenius capitis muscles: an electromyographic study. *The Anatomical Record*, 179(4):477–480.

Takeshita, K., Peterson, E. T., Bylski-Austrow, D., Crawford, A. H., and Nakamura, K. (2004a). The nuchal ligament restrains cervical spine flexion. *Spine*, 29(18):E388–E393.

Takeshita, K., Peterson, E. T. K., Bylski-Austrow, D., Crawford, A. H., and Nakamura, K. (2004b). The nuchal ligament restrains cervical spine flexion. *Spine*, 29(18):388–93.

Tampier, C., Drake, J. D. M., Callaghan, J. P., and McGill, S. M. (2007). Progressive disc herniation: an investigation of the mechanism using radiologic, histochemical, and microscopic dissection techniques on a porcine model. *Spine*, 32(25):2869–2874.

Teo, E. C. and Ng, H. W. (2001a). Evaluation of the role of ligaments, facets and disc nucleus in lower cervical spine under compression and sagittal moments using finite element method. *Medical Engineering and Physics*, 23:155–164.

Teo, E. C. and Ng, H. W. (2001b). First cervical vertebra (atlas) fracture mechanism studies using finite element method. *Journal of Biomechanics*, 34:13–21.

Thelen, D. G. (2003). Adjustment of Muscle Mechanics Model Parameters to Simulate Dynamic Contractions in Older Adults. *Journal of Biomechanical Engineering*, 125(1):70.

Thuresson, M., Linder, J., Harms-Ringdahl, K., et al. (2003). Neck muscle activity in helicopter pilots: effect of position and helmet-mounted equipment. *Aviation, space, and environmental medicine*, 74(5):527–532.

Trajkovski, A., Omerovic, S., Krasna, S., and Prebil, I. (2014). Loading rate effect on mechanical properties of cervical spine ligaments. *Acta of bioengineering and biomechanics / Wrocław University of Technology*, 16(3):13–20.

Troyer, K. L., Estep, D. J., and Puttlitz, C. M. (2012a). Viscoelastic effects during loading play an integral role in soft tissue mechanics. *Acta Biomaterialia*, 8(1):234–243.

Troyer, K. L. and Puttlitz, C. M. (2011). Human cervical spine ligaments exhibit fully nonlinear viscoelastic behavior. *Acta biomaterialia*, 7(2):700–709.

Troyer, K. L., Puttlitz, C. M., and Shetye, S. S. (2012b). Experimental Characterization and Finite Element Implementation of Soft Tissue Nonlinear Viscoelasticity. *Journal of Biomechanical Engineering*, 134(11):114501.

Tubbs, R. S., Grabb, P., Spooner, A., Wilson, W., and Oakes, W. J. (2000). The apical ligament: anatomy and functional significance. *Journal of Neurosurgery*, 92(2 Suppl):197–200.

Urban, J. P. G. and Roberts, S. (2003). Degeneration of the intervertebral disc. *Arthritis research & therapy*, 5(3):120–130.

van den Oord, M. H. a. H., De Loose, V., Meeuwsen, T., Sluiter, J. K., and Frings-Dresen, M. H. W. (2010). Neck pain in military helicopter pilots: prevalence and associated factors. *Military medicine*, 175(1):55–60.

van der Horst, M. J. (2002). *Human Head Neck Response in Frontal , Lateral and Rear End Impact Loading - modelling and validation -*. PhD thesis.

van der Horst, M. J., Thunnissen, J. G. M., Happee, R., van Haaster, R. M. H. P., and Wismans, J. S. H. M. (1997). The Influence of Muscle Activity on Head-Neck Response During Impact.

Van Ee, C. a., Nightingale, R. W., Camacho, D. L., Chancey, V. C., Knaub, K. E., Sun, E. a., and Myers, B. S. (2000). Tensile properties of the human muscular and ligamentous cervical spine. *Stapp car crash journal*, 44(1972):85–102.

van Griensven, A., Meixner, T., Grunwald, S., Bishop, T., Diluzio, M., and Srinivasan, R. (2006). A global sensitivity analysis tool for the parameters of multi-variable catchment models. *Journal of Hydrology*, 324(1-4):10–23.

van Lopik, D. W. and Acar, M. (2007). Development of a multi-body computational model of human head and neck.

Vasavada, A. N., Danaraj, J., and Siegmund, G. P. (2008). Head and neck anthropometry, vertebral geometry and neck strength in height-matched men and women. *Journal of Biomechanics*, 41(1):114–121.

Vasavada, a. N., Li, S., and Delp, S. L. (1998). Influence of muscle morphometry and moment arms on the moment-generating capacity of human neck muscles. *Spine*, 23(4):412–422.

Vasseljen, O., Woodhouse, A., Bjørngaard, J. H., and Leivseth, L. (2013). Natural course of acute neck and low back pain in the general population: The HUNT study. *Pain*, 154(8):1237–1244.

Villas, C., Arriagada, C., and Zubieta, J. L. (1999). Preliminary CT study of C1-C2 rotational mobility in normal subjects. *European Spine Journal*, 8(3):223–228.

Vitti, M., Fujiwara, M., Basmajian, J. V., and Iida, M. (1973). The integrated roles of longus colli and sternocleidomastoid muscles: an electromyographic study. *The Anatomical Record*, 177(4):471–484.

Voo, L. M., Pintar, F. A., Yoganandan, N., and Liu, Y. K. (1998). Static and dynamic bending responses of the human cervical spine. *Journal of biomechanical engineering*, 120(6):693–6.

Wade, K. R., Robertson, P. a., and Broom, N. D. (2012). On the extent and nature of nucleus-annulus integration. *Spine*, 37(21):1826–33.

Wagner, D. R. and Lotz, J. C. (2004). Theoretical model and experimental results for the nonlinear elastic behavior of human annulus fibrosus. *Journal of Orthopaedic Research*, 22(4):901–909.

Wang, Q. M., Mohan, A. C., Oyen, M. L., and Zhao, X. H. (2014). Separating viscoelasticity and poroelasticity of gels with different length and time scales. *Acta Mechanica Sinica/Lixue Xuebao*, 30(1):20–27.

Wen, N., Lavaste, F., Santin, J. J., and Lassau, J. P. (1993). Three-dimensional biomechanical properties of the human cervical spine in vitro. *European Spine Journal*, 2(1):2–11.

Wheeldon, J. a., Pintar, F. a., Knowles, S., and Yoganandan, N. (2006). Experimental flexion/extension data corridors for validation of finite element models of the young, normal cervical spine. *Journal of Biomechanics*, 39(2):375–380.

White, a. a. and Panjabi, M. M. (1990). *Clinical Biomechanics of the Spine Volume 2*. Lippincott Company, Philadelphia.

Williams, J. L. and Belytschko, T. B. (1983). A three-dimensional model of the human cervical spine for impact simulation. *Journal of biomechanical engineering*, 105(4):321–31.

Williams, W. O. (2011). Huxley ' s Model of Muscle Contraction with Compliance. *Journal of Elasticity*, pages 1–22.

Winkelstein, B. a., Nightingale, R. W., Richardson, W. J., and Myers, B. S. (2000). The cervical facet capsule and its role in whiplash injury: a biomechanical investigation. *Spine*, 25(10):1238–1246.

Winter, D. (1976). Biomedical model relating emg to changing isometric tension.

Winter, D. (1990). *Biomechanics and motor control of human movement*. John Wiley & Sons Inc.

Winters, J. M. (1990). Hill-based muscle models: a systems engineering perspective. *Multiple Muscle Systems*, pages 69–93.

Winters, J. M. (1995). How detailed should muscle models be to understand multi-joint movement coordination? *Human Movement Science*, 14(95):401–442.

Winters, J. M. and Peles, J. D. (1990). Neck muscle activity and 3-D head kinematics during quasi-static and dynamic tracking movements. In *Multiple Muscle Systems*, chapter 28, pages 431–480. Springer New York, New York, NY.

Winters, J. M. and Stark, L. (1985). Analysis of fundamental human movement patterns through the use of in-depth antagonistic muscle models. *IEEE transactions on biomedical engineering*, 32(10):826–839.

Winters, J. M. and Woo, S. L.-Y. (1990). *Multiple Muscle Systems*.

Wu, H. C. and Yao, R. F. (1976). Mechanical behavior of the human annulus fibrosus. *Journal of biomechanics*, 9:1–7.

Xiao, M. and Higginson, J. (2010). Sensitivity of estimated muscle force in forward simulation of normal walking. *Journal of applied biomechanics*, 26(2):142.

Yamazaki, K., Ono, K., and Kaneoka, K. (2000). A Simulation Analysis of Human Cervical Spine Motion During Low Speed Rear-End Impacts.

Yoganandan, N., Knowles, S. a., Maiman, D. J., and Pintar, F. a. (2003). Anatomic study of the morphology of human cervical facet joint. *Spine*, 28(20):2317–2323.

Yoganandan, N., Kumaresan, S., and Pintar, F. a. (2000). Geometric and Mechanical Properties of Human Cervical Spine Ligaments. *Journal of Biomechanical Engineering*, 122(6):623.

Yoganandan, N., Kumaresan, S., and Pintar, F. a. (2001). Biomechanics of the cervical spine. Part 2. Cervical spine soft tissue responses and biomechanical modeling. *Clinical Biomechanics*, 16(1):1–27.

Yoganandan, N., Pintar, F. a., Butler, J., Reinartz, J., Sances, A., and Larson, S. J. (1989). Dynamic Response of Human Cervical Spine Ligaments. *Spine*, 14(10):1102–1110.

Yoganandan, N., Pintar, F. a., Maiman, D. J., Cusick, J. F., Sances, a., and Walsh, P. R. (1996). Human head-neck biomechanics under axial tension. *Medical engineering & physics*, 18(4):289–94.

Yu, J., Fairbank, J. C. T., Roberts, S., and Urban, J. P. G. (2005). The elastic fiber network of the anulus fibrosus of the normal and scoliotic human intervertebral disc. *Spine*, 30(16):1815–1820.

Yu, J., Tirlapur, U., Fairbank, J., Handford, P., Roberts, S., Winlove, P. P., Cui, Z., and Urban, J. (2007). Microfibrils, elastin fibres and collagen fibres in the human intervertebral disc and bovine tail disc. *Journal of Anatomy*, 210(4):460–471.

Yu, S. W., Sether, L., and Haughton, V. M. (1987). Facet joint menisci of the cervical spine: correlative MR imaging and cryomicrotomy study. *Radiology*, 164(1):79–82.

Yucesoy, C. A., Koopman, B. H., Baan, G. C., Grootenboer, H. J., and Huijing, P. A. (2003). Effects of inter-and extramuscular myofascial force transmission on adjacent synergistic muscles: assessment by experiments and finite-element modeling. *Journal of biomechanics*, 36(12):1797–1811.

Zahalak, G. (1990). Modeling muscle mechanics (and energetics). In *Multiple muscle systems: Biomechanics and Movement Organization*, pages 1–23.

Zajac, F. E. (1989). Muscle and tendon: properties, models, scaling, and application to biomechanics and motor control.

Zatsiorsky, V. and Prilutsky, B. (2002). *Biomechanics of skeletal muscles*.

Zhang, Q. H. (2005). Development and Validation of A C0C7 FE Complex for Biomechanical Study. *Journal of Biomechanical Engineering*, 127(5):729.

Zhang, Q. H., Teo, E. C., Ng, H. W., and Lee, V. S. (2006). Finite element analysis of moment-rotation relationships for human cervical spine. *Journal of Biomechanics*, 39(1):189–193.

Zuniga, E. N. and Simons, E. G. (1969). Nonlinear relationship between averaged electromyogram potential and muscle tension in normal subjects.

Appendices

Appendix A

Appendix

A.1 Anatomical Data

Raw muscle and ligament anatomical data are available for download as supplemental material.

A.2 More on Muscle Gains

Contains some more detailed muscle gains resulting from the sensitivity analysis, facet wrapped by muscle.

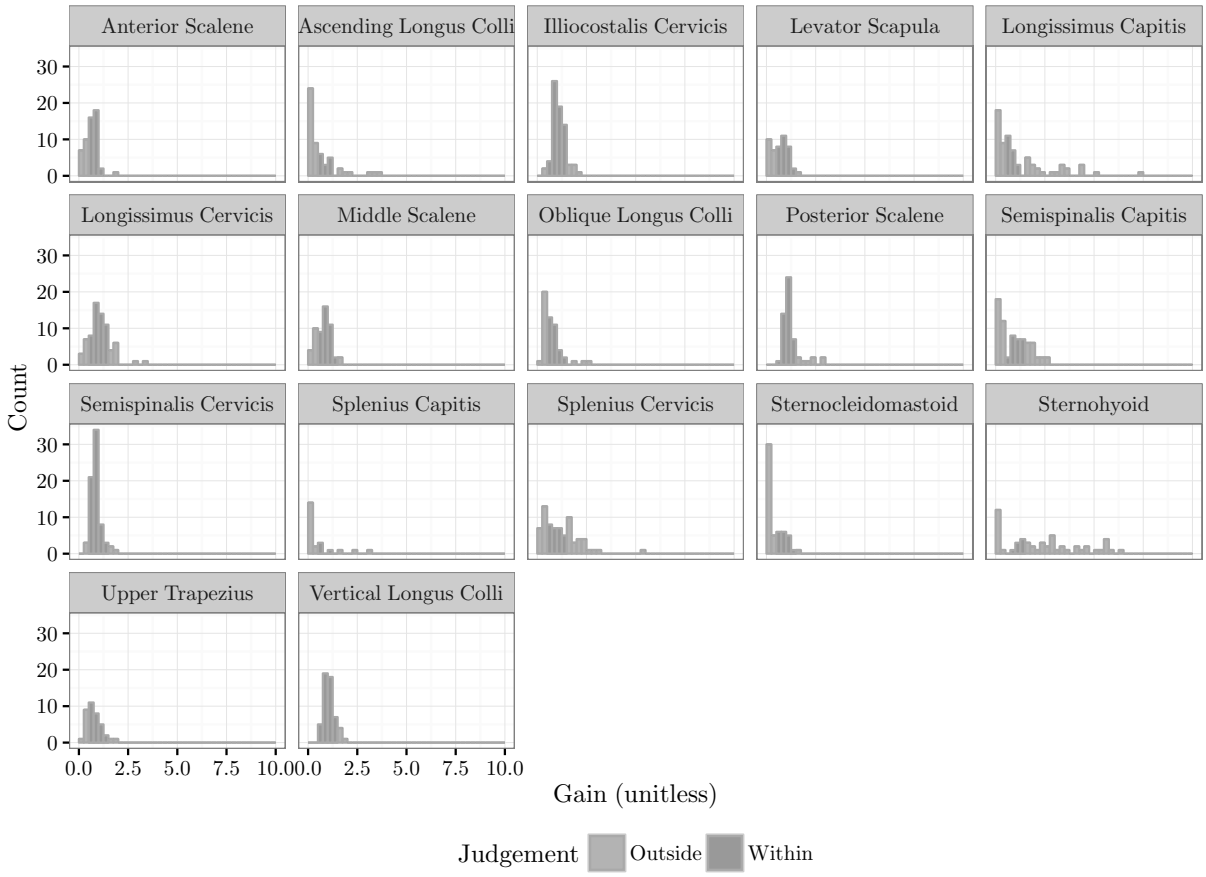

Figure A.1: Muscle gain histograms for each individual muscle, collapsed across side.

A.3 Sensitivity Analysis for Mediolateral and Anteroposterior Shear

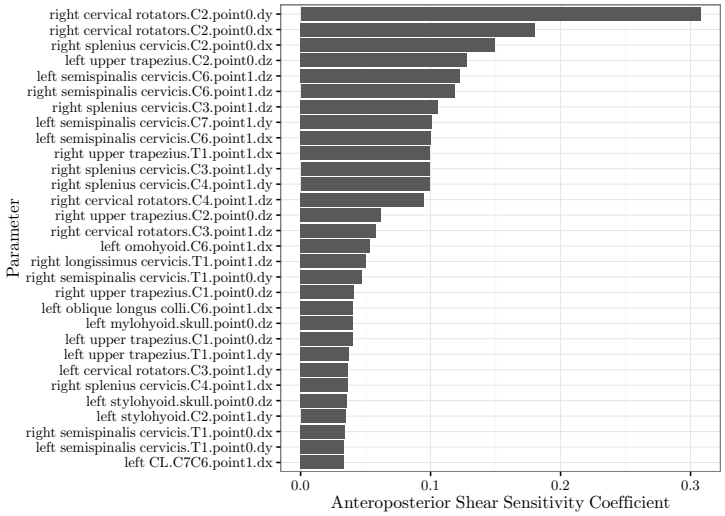

Figure A.2: The thirty greatest normalized sensitivity coefficients for the model in anteroposterior shear.

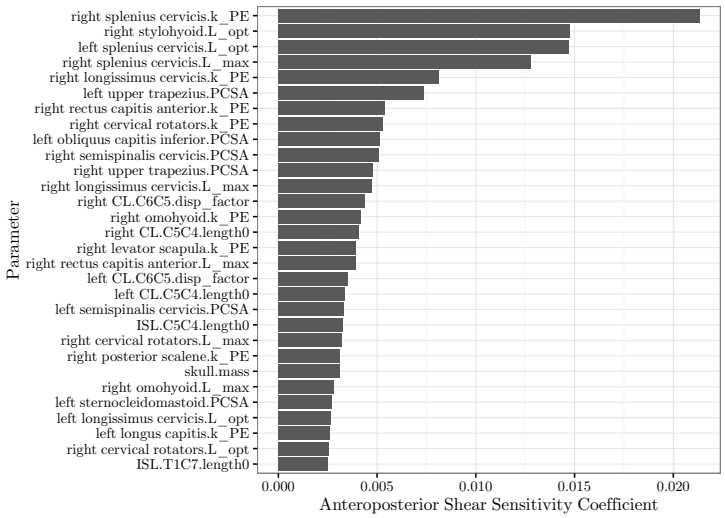

Figure A.3: The thirty greatest normalized sensitivity coefficients of the model once geometric parameters were excluded. As anticipated, the ligament slack lengths are among the most sensitive coefficients.

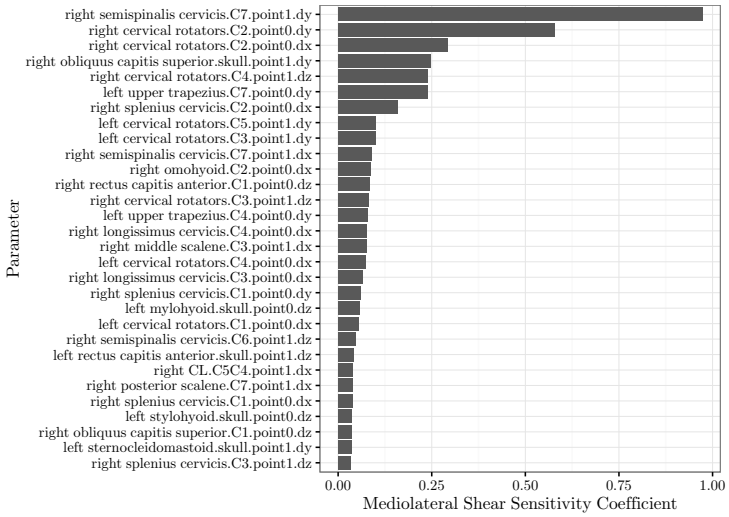

Figure A.4: The thirty greatest normalized sensitivity coefficients for the model in mediolateral shear.

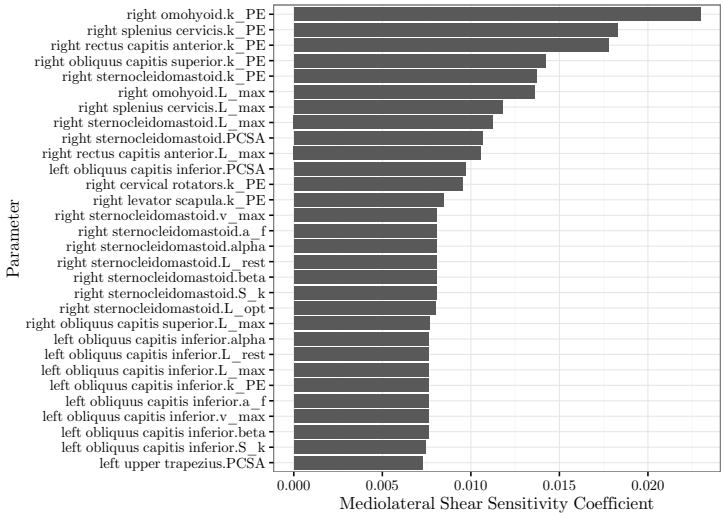

Figure A.5: The thirty greatest relative sensitivity coefficients of the model in mediolateral shear once geometric parameters were excluded. As anticipated, the ligament slack lengths are among the most sensitive coefficients.

A.4 Joint Loads by Level, Posture, and Time

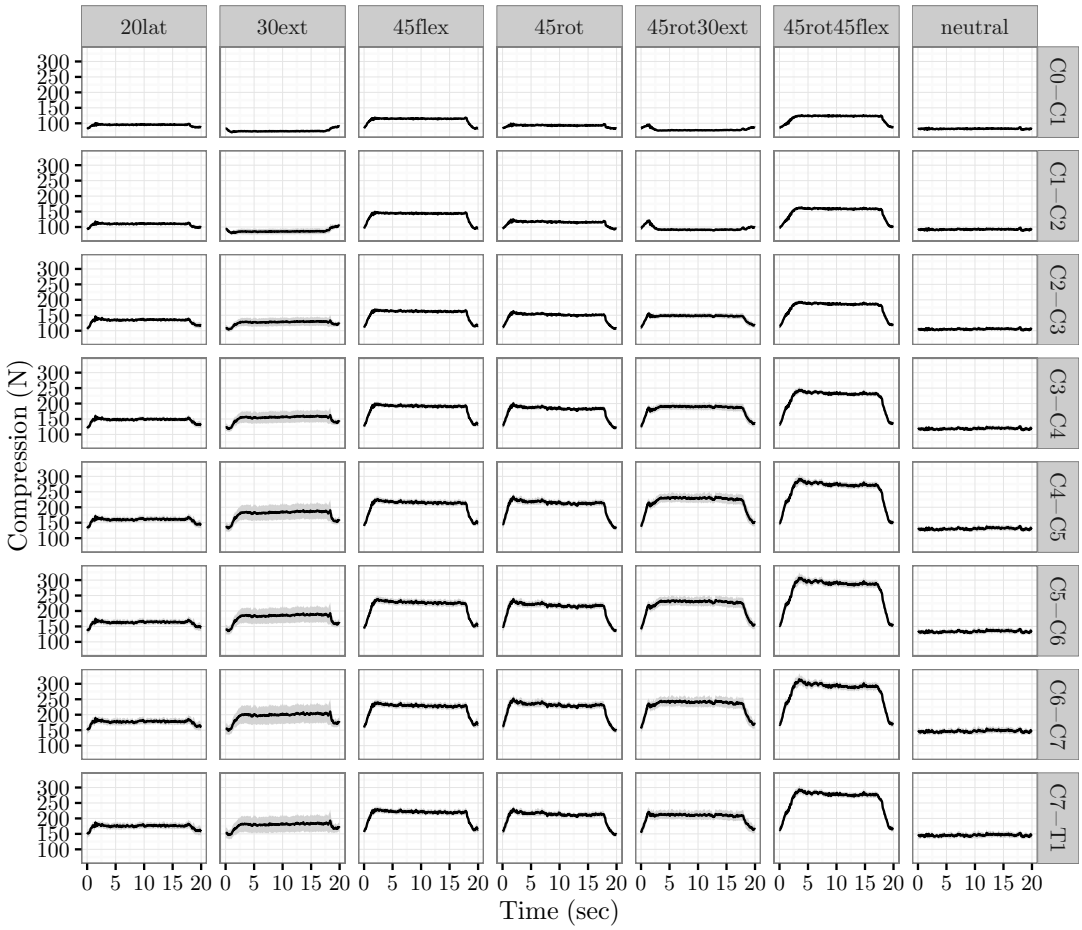

Figure A.6: Timeseries of compression by posture at each spinal level. Curves are mean, with the shaded region representing the standard error.

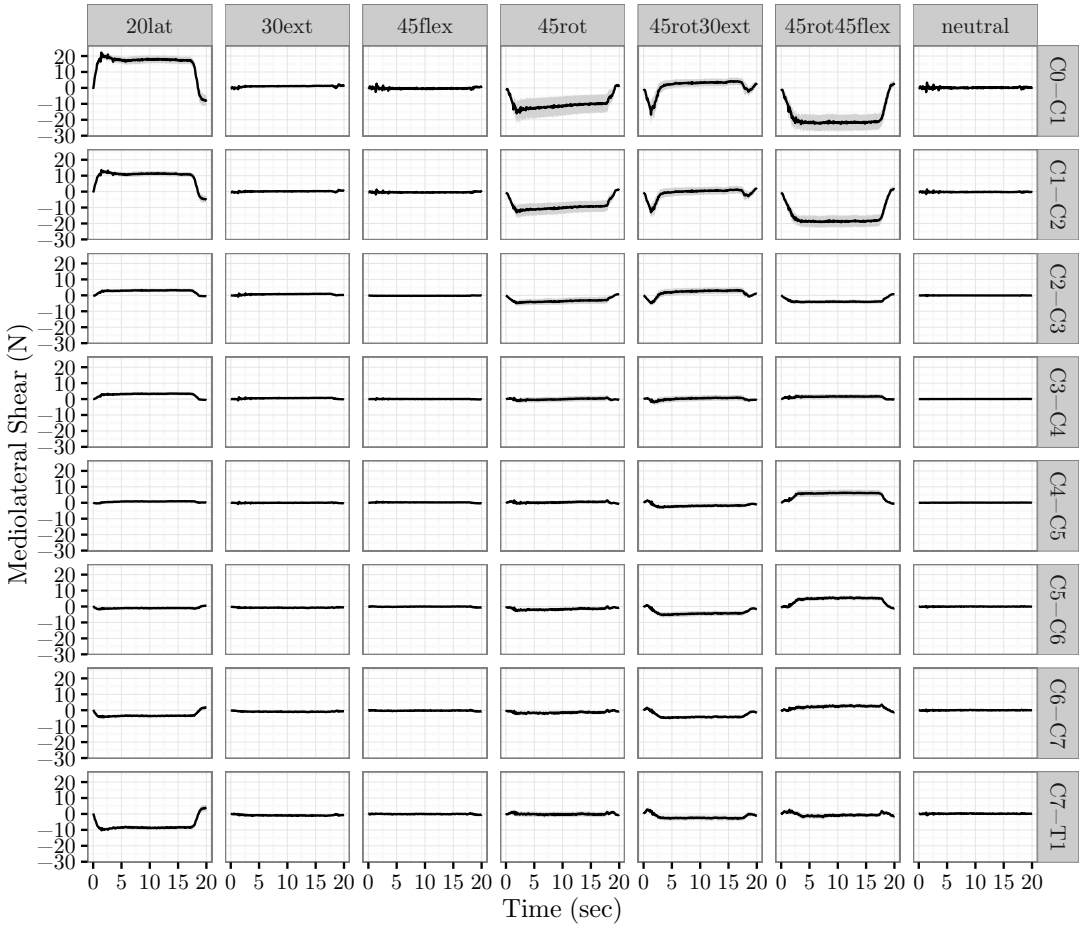

Figure A.7: Timeseries of mediolateral shear by posture at each spinal level. Curves are mean, with the shaded region representing the standard error. Positive values indicate the rightward direction.

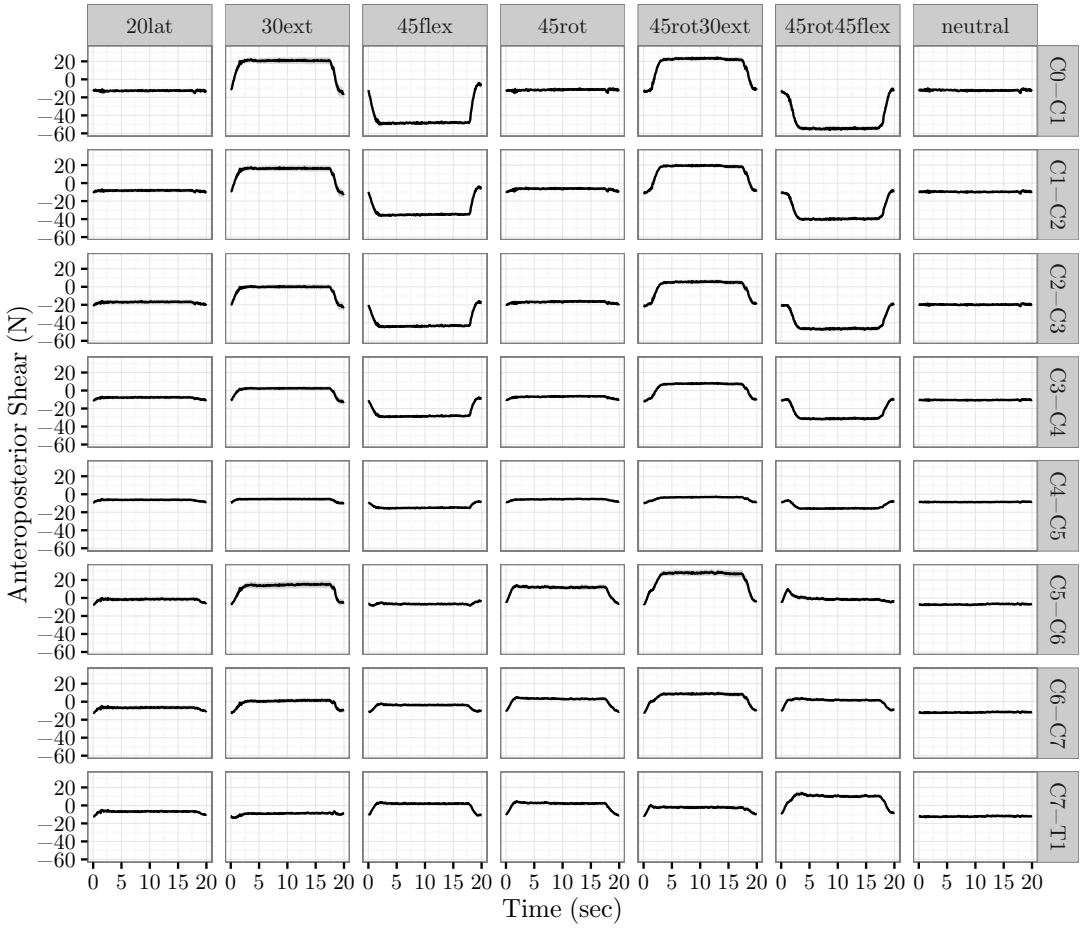

Figure A.8: Timeseries of anterior-posture shear by posture at each spinal level. Curves are mean, with the shaded region representing the standard error. Positive values indicate the foreward direction.